Advances in Structure Research by Diffraction Methods

Fortschritte der Strukturforschung mit Beugungsmethoden

Volume 3

Edited by
R. BRILL and R. MASON

with contributions of

A. AUTHIER · K. KAMBE / K. MOLIÈRE
R. HOSEMANN / A. SCHÖNFELD / W. WILKE · A. I. KITAJGORODSKIJ

With 77 Figures

Pergamon Press
Oxford · London · Edinburgh
New York · Toronto · Sydney · Paris

Friedr. Vieweg + Sohn
Braunschweig

Pergamon Press Ltd., Headington Hill Hall, Oxford
4 & 5 Fitzroy Square, London W. 1

Pergamon Press (Scotland) Ltd., 2 & 3 Teviot Place, Edinburgh 1

Pergamon Press Inc., Maxwell House, Fairview Park, Elmsford, New York 10523

Pergamon of Canada Ltd., 207 Queen's Quay West, Toronto 1

Pergamon Press (Aust.) Pty. Ltd., 19a Boundary Street, Rushcutters Bay, N.S.W. 2011, Australia

Pergamon Press S.A.R.L., 24 rue des Écoles, Paris 5e

Vieweg + Sohn GmbH, Burgplatz 1, Braunschweig

Editorial Assistance: *Werner Schröder*

1970

All rights reserved

Copyright © 1970 by Friedr. Vieweg + Sohn GmbH, Verlag, Braunschweig

Library of Congress Catalog Card No. 73–99027

Set by Friedr. Vieweg + Sohn GmbH, Braunschweig

Bookbinder: W. Langelüddecke, Braunschweig

Printed in Germany

08 017543 0 Pergamon Press

8113 Vieweg

A. Authier *)

Ewald Waves in Theory and Experiment (Dynamical Theory of X-Ray Diffraction)

With 33 figures

I Bases of the dynamical theory

I-1 Introduction

Although the bases of the dynamical theory were laid very soon [1, 2] after the first diffraction experiment by a crystal [3], more than fifty years ago, relatively little work, experimental or theoretical, was done in application of this theory until some 20 years ago. The main reason is that the approximate, kinematical theory suffices to account for the intensities diffracted by very imperfect crystals and that was enough for structure determinations.

The first developments of the theory occured in the forties and fifties with the discovery of anomalous absorption, or Borrmann effect [4, 5, 6] and its interpretation [7, 8] and with the study of the X-ray energy propagation [9] to [14].

The discovery of techniques for growing perfect single crystals such as silicon and germanium and the development of X-ray topographic techniques for the observation of single dislocation lines induced further studies of the propagation of real waves inside a crystal. This led to the evaluation of the energy distribution on the exit surface of the crystal [15, 16].

Actually, real waves are not plane and the classical dynamical theory had to be generalized to account for the propagation of spherical waves [17] or any kind of waves [18].

The basic concept of the classical dynamical theory is that of *wave-fields* or Ewald-waves and we shall show how it explains all the absorption and propagation properties of X-rays at the Bragg setting in a perfect crystal. Although they were at first introduced as a mathematical expression, they are a physical reality as was shown by the existence of the Borrmann effect or that of Pendellösung fringes [19, 17] and directly demonstrated by the observation of the double refraction of X-rays [20, 21].

Many general papers were devoted to the classical dynamical theory [15, 21] to [29]. The aim of this paper is to compare the classical and generalized dynamical theories of X-rays.

*) Faculte des Sciences, Paris, Frankreich.

I-2 Maxwell's equations

There are two possible starting points to derive the dynamical theory. One is to use the Fresnel zone calculations and Darwin's reccurence formulae [1]. This is usually done for the Bragg case but has been recently extended to the Laue case [30, 31]. The other, and more widely used, starting point is given by Maxwell's equations. The foundations of corresponding theory were laid by *P. P. Ewald* [2] and the final form was given by *M. von Laue* [32]. *Ewald's* theory is microscopic and *v. Laue's* is a macroscopic approach. They lead to the same result if the same physical model is used [85].

M. von Laue's theory will be discussed here. His fundamental hypothesis is that one can define at each point of the crystal the electric field and the electric displacement, the electric susceptibility and the other electric or magnetic quantities. They are related by Maxwell's equations:

$$\text{curl } \mathbf{E} = -\frac{\partial \mathbf{B}}{\partial t} \qquad \text{curl } \mathbf{H} = \frac{\partial \mathbf{D}}{\partial t}$$

$$\text{div } \mathbf{D} = 0 \qquad \text{div } \mathbf{B} = 0 \tag{I-2-1}$$

The local charge and current density are taken to be equal to zero. The justification for the assumed local neutrality is that since the nucleus does not contribute to the scattering, its charge may be expanded over the volume occupied by the electron cloud to compensate the negative charge.

Boundary conditions are:

$$\begin{aligned} \mathbf{E}_{T_1} - \mathbf{E}_{T_2} &= 0 \qquad & \mathbf{D}_{N_1} - \mathbf{D}_{N_2} &= 0 \\ \mathbf{H}_{T_1} - \mathbf{H}_{T_2} &= 0 \qquad & \mathbf{B}_{N_1} - \mathbf{B}_{N_2} &= 0 \end{aligned} \tag{I-2-2}$$

T and N indicate tangential and normal components, respectively.

We shall throughout consider incoming monochromatic electromagnetic waves with frequency ν:

$$\mathbf{E}\, e^{2\pi i \nu t}, \qquad \mathbf{H}\, e^{2\pi i \nu t}.$$

$\mathbf{S} = R\, \mathbf{E} \times \mathbf{H}^*$ is the Poynting vector of such a wave. Its time average is equal to:

$$\bar{\mathbf{S}} = \frac{1}{2} R\, \mathbf{E} \times \mathbf{H}^* \qquad (R \text{ means real part of}) \tag{I-2-3}$$

and the intensity, that is the energy flow per square meter (fig.1), is equal, for a plane wave, to:

$$I = |\bar{\mathbf{S}}| = \frac{1}{2} c \epsilon_0 |\mathbf{E}|^2 \tag{I-2-4}$$

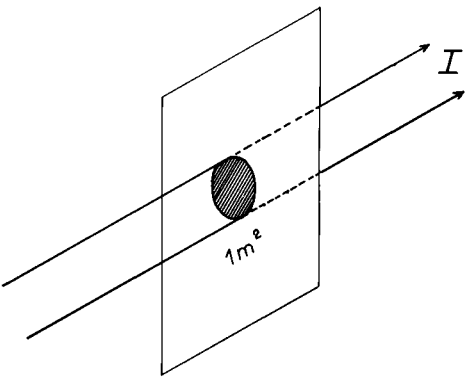

Fig. 1

I-3 Wave propagation in an homogeneous dielectric medium

Let ϵ and χ be the dielectric constant and susceptibility of the medium, respectively, ϵ_0 the dielectric permittivity and μ_0 the magnetic permeability of the vacuum. There comes:

$$\mathbf{D} = \epsilon\ \mathbf{E} = \epsilon_0\,(1+\chi)\mathbf{E}\ ; \qquad \mathbf{B} = \mu_0\mathbf{H}\ ;\ \ \epsilon_0\mu_0 = \frac{1}{c^2} \tag{I-3-1}$$

The propagation equation is:

$$\Delta\mathbf{E} = \frac{1+\chi}{c^2}\,\frac{\partial^2\mathbf{E}}{\partial t^2} \tag{I-3-2}$$

of which the simplest solution is a plane wave:

$$\mathbf{E} = \mathbf{E}_0\, e^{2\pi i(\nu t - \mathbf{K}\cdot\mathbf{r})}\ ; \qquad \mathbf{K} = k\sqrt{1+\chi} = nk$$

n is the refractive index, k the wave number in vacuum ($k = 1/\lambda = \nu/c$). χ is very small in the case of X-rays and we can write:

$$n = 1 + \frac{\chi}{2} \tag{I-3-3}$$

I-4 Wave propagation in an homogeneous absorbing dielectric medium

The absorption is taken into account in a phenomenological way by introducing an imaginary part to the electric susceptibility and therefore to the wave vectors:

$$\chi = \chi^r + i\chi^i\ ; \quad \mathbf{K} = \mathbf{K}^r + i\mathbf{K}^i\ ; \qquad k\chi^i/2 = \mathbf{K}^i\cos(\mathbf{K}^r, \mathbf{K}^i) \tag{I-4-1}$$

The expression of the wave becomes:

$$\mathbf{E} = \mathbf{E}_0\, e^{2\pi k\,\frac{\chi^i}{2\cos(\mathbf{K}^r,\mathbf{K}^i)}\,x}\ e^{2\pi i(\nu t - \mathbf{K}^r\cdot\mathbf{r})} \tag{I-4-2}$$

x is the path of the wave in the medium in the direction of $\mathbf{K}_i$.

I-5 Electric susceptibility for the electron-photon interaction

a) classical computation. When an electromagnetic wave falls on an electron, it will oscillate becoming an emitting dipole. Due to the electric moment of all the electrons, the medium becomes polarised. If ρ is the electron density, one finds for the electric polarisation:

$$\mathbf{P} = -\frac{e^2}{m}\frac{1}{4\pi^2\nu^2}\rho\,\mathbf{E}$$

and, for the electric susceptibility:

$$\chi = -\frac{e^2}{mc^2}\frac{1}{4\pi\epsilon_0}\frac{\lambda^2}{\pi}\rho = -R\frac{\lambda^2}{\pi}\rho \qquad \text{(I-5-1)}$$

where R is the classical radius of the electron.

In a crystal, the electron density is triply periodic and the susceptibility can be expanded in Fourier series:

$$\chi = \sum_{\mathbf{h}} \chi_{\mathbf{h}}\, e^{2\pi i\mathbf{h}\cdot\mathbf{r}} \qquad \text{with } \chi_{\mathbf{h}} = -\frac{R}{\pi}\frac{\lambda^2}{V}F_{\mathbf{h}} \qquad \text{(I-5-2)}$$

where $\mathbf{h}$ is a reciprocal lattice vector, $F_{\mathbf{h}}$ the structure factor, V the volume of the unit cell.

$\chi_{\mathbf{h}}$ is of the order of 10^{-6} and negative.

b) The electric susceptibility in the absorbing case. The quantum mechanical treatment leads to the same result, χ_n, as the classical treatment with two additionnal terms, usually called anomalous dispersion corrections. They are due to two effects:

- during the absorption of the photon by the atom in the intermediary stages of the scattering event, the atom transfers to an excited state; this leads to a real correction term χ_a
- photoelectric absorption; this leads to an imaginary term χ^i

The electric susceptibility can thus be written:

$$\chi = \chi^r + i\chi^i \quad \text{with } \chi^r = \chi_n + \chi_a \qquad \text{(I-5-3)}$$

The imaginary part is also triply periodic and can be expanded in Fourier series:

$$\chi^i = \sum_{\mathbf{h}} \chi^i_{\mathbf{h}}\, e^{-2\pi i\mathbf{h}\cdot\mathbf{r}} \qquad \text{(I-5-4)}$$

with

$$\chi^i_0 = -\frac{\mu}{2\pi k} \qquad (\mu \text{ linear absorption coefficient}) \qquad \text{(I-5-5)}$$

The Fourier coefficients of χ_r and χ_i obey the following relations:

$$\chi^r_{\bar{\mathbf{h}}} = \chi^{r*}_{\mathbf{h}}; \qquad \chi^i_{\bar{\mathbf{h}}} = \chi^{i*}_{\mathbf{h}} \qquad (* \text{ means complex conjugate}) \qquad \text{(I-5-6)}$$

Let φ be the phase angle between χ_h^i and χ_h^r. The following expressions valid for small values of $|\chi_h^i|$ only will be useful later:

$$\left|\frac{\chi_h}{\chi_{\bar{h}}}\right| = 1 - 2\left|\frac{\chi_h^i}{\chi_h^r}\right| \sin\varphi\,; \quad \sqrt{\chi_h \chi_{\bar{h}}} = \left|\chi_h^r\right| + i\left|\chi_h^i\right| \cos\varphi \qquad \text{(I-5-7)}$$

The phase angle φ is equal to $k\pi$ in the case of a centrosymmetric crystal. The first relation (I-5-7) shows the failure of Friedel's law in the case of an absorbing non centrosymmetric crystal.

c) Influence of the thermal vibrations. Because of the thermal agitation, the atoms are not at rest and the observed electron density is an average. This effect can be taken into account by multiplying the Fourier components of the electric susceptibility by the Debye-Waller factor. This is true as well for the real part [33, 34, 35], and the imaginary part [36, 37, 38]. In the remaining of this paper, χ_h^r and χ_h^i will *always* be assumed to *include* the exp-M factor.

I-6 Propagation equation in a crystalline medium- wave-fields

In a crystalline medium χ is not constant, as we have seen. The propagation equation, deduced from Maxwell's equations (I-2-1) is therefore more complicated than equation (I-3-2). One obtains, for a monochromatic wave:

$$\Delta \mathbf{D} + \text{curlcurl}\, \chi \mathbf{D} + 4\pi^2 k^2 \mathbf{D} = 0 \qquad \text{(I-6-1)}$$

with $k = \nu/c$.

The solution will be a linear combination of partial solutions, combination which is determined by the boundary conditions.

Since χ is triply periodic, we shall look for a solution which has the same periodicity. We must consider here two cases:

- the incident wave is any wave, the crystal is limited or eventually slightly distorted.
- The incident wave is a plane wave, the crystal has no lateral boundaries and is perfect.

In the later case, we shall try as a solution a *Bloch wave:*

$$\mathbf{D}_j = e^{2\pi i(\nu t - \mathbf{K}_0 \cdot \mathbf{r})} \sum_h \mathfrak{D}_{hj}\, e^{2\pi i \mathbf{h} \cdot \mathbf{r}} \qquad \text{(I-6-2)}$$

Subscript j denotes the particular solution. (I-6-2) can also be written:

$$\mathbf{D}_j = e^{2\pi i \nu t} \sum_h \mathfrak{D}_{hj}\, e^{-2\pi i \mathbf{K}_{hj} \cdot \mathbf{r}} \qquad \text{(I-6-3)}$$

with

$$\mathbf{K}_{hj} = \mathbf{K}_{oj} - \mathbf{h}\,. \qquad \text{(I-6-4)}$$

This Bloch wave is interpreted as a *wave-field* constituted of an infinite number of plane waves with wave-vectors $\mathbf{K}_{hj}$ and amplitudes $\mathfrak{D}_{hj}$. Following Professor Borrmann's suggestion, we shall call it an Ewald wave since *Ewald* was the first to introduce it in the X-ray case. In practice, this number is finite and, for X-rays, usually equal to 2, sometimes to 3 or 4. All the wave vectors of a given wave-field drawn from the various reciprocal lattice points, define a *tie-point (Anregungspunkt)* P_j characteristic of the wave-field (fig. 2).

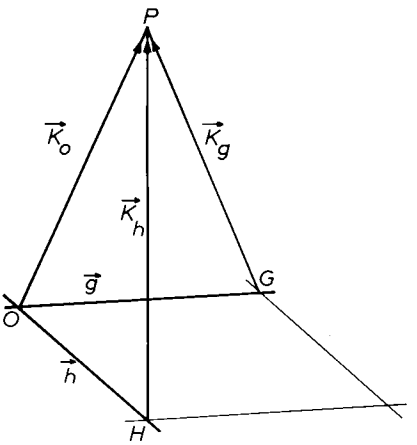

Fig. 2
P : tie-point characterizing a given wave-field
O, H, G : reciprocal lattice points.

The notion of wave-fields is very important because all their wave components have common properties which enable to describe completely the propagation of an X-ray plane wave in a perfect crystal. For example, in an absorbing crystal, the wave vectors are complex. Relation (I-6-4) shows that the wave vectors of a given wave field all have the same imaginary parts:

$$\mathbf{K}^i_{hj} = \mathbf{K}^i_{oj}$$

and that all the waves belonging to the same wave-field have the same attenuation factor. We shall show that they also have the same propagation direction.

What is more, the different wave-fields excited by an incident wave can be separated and isolated, demonstrating that the Bloch wave is not simply a mathematical way of describing the solution but has a physical reality.

In the development (I-6-2), both the wave-vector $\mathbf{K}_{oj}$ and the amplitudes $\mathfrak{D}_{hj}$ are constants. They are unknown, and we shall show in II how they are determined. We are only interested in the case where the Bragg condition is practically fullfilled for one or several families of lattice planes. Let L_a or Laue point be the center of the

Ewald sphere passing through the corresponding reciprocal lattice points. It is obvious that $\mathbf{OP}_j = \mathbf{K}_{oj}$ will be close to $\mathbf{OL}_a$ (fig. 3). P_j lies on a certain surface called the *dispersion surface* [1]), and its exact position is determined by the boundary conditions.

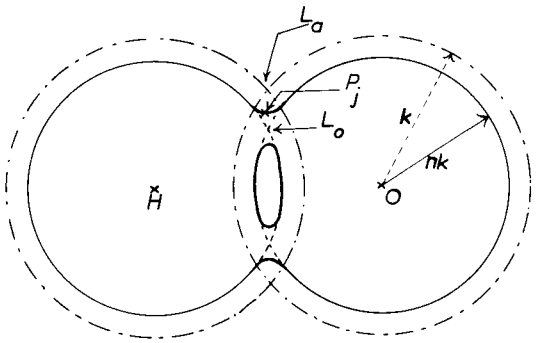

Fig. 3
Dispersion surface (solid curve).
L_a: Laue point,
L_o: Lorentz point.

When the incident wave is not a plane wave, or the crystal is finite or slightly distorted, the solution can no more have the simple form (I-6-2); in particular, $\mathbf{K}_{oj}$ and $\mathfrak{D}_{hj}$ are not constants anymore but functions of the position within the crystal. Since real waves are never plane but usually spherical, it is highly important to solve the problem in this case. However, up to about 10 to 15 years ago, there was not much interest in the actual propagation of X-rays, the plane wave theory giving good enough results for rocking curves and integrated intensities. In particular, we shall show that spherical waves and plane waves give the same integrated intensities. But, as soon as the actual propagation was studied, an answer to the problem was sought.

There are two main ways to study the propagation of real waves.

One is to consider the incident wave as a sum of plane waves and to use the well known results of the plane wave theory. By simply considering that the whole dispersion surface is excited, many experimental results can be explained, as has been shown by *G. Borrmann* [15] and *N. Kato* [16]. It is however more rigourous to expand the incident spherical wave in plane waves by means of a Fourier integral and to actually compute the integral (*N. Kato* [17]). This is necessary to obtain the exact position of the interference fringes which are always observed in a not too absorbing crystal, as it has been confirmed experimentally [39, 87].

---

[1]) We shall through out in this paper use wave vectors drawn *away* from the reciprocal lattice points (and not pointing towards them). The dispersion surface has been called *„Ausbreitungsfläche"* by *E. Fues* [86] in this particular case. We shall however keep the usual term of dispersion surface, *although* with a different convention for the orientation of wave vectors.

Another way to solve the problem is to let aside altogether the plane wave theory and to generalise it. This has been done in a very elegant way by *S. Takagi* [18]. We mentionned above that both $\mathbf{K}_o$ and $\mathfrak{D}_h$ in (I-6-2) now vary with the position within the crystal. $\mathbf{K}_o$ will always remain close to $\mathbf{OL}_a$ and to avoid carrying two types of variables, we shall assume $\mathbf{K}_o$ to have an arbitrarily set value and write the solution as a modified Ewald wave:

$$\mathbf{D} = e^{2\pi i\nu t} \sum \mathfrak{D}_h(\mathbf{r})\, e^{-2\pi i \mathbf{K}_h \cdot \mathbf{r}}$$

with

$$\mathbf{K}_h = \mathbf{K}_o - \mathbf{h} \; ; \qquad |\mathbf{K}_o| = nk \; . \tag{I-6-5}$$

The rapid oscillations of the phase will thus be contained in the $\exp -2\pi i \mathbf{K}_h \cdot \mathbf{r}$ factors while its slower variations will be contained in the amplitudes $\mathfrak{D}_h(\mathbf{r})$ which we shall assume to be a *slowly varying* function of $\mathbf{r}$; in particular, we shall neglect $\Delta\mathfrak{D}_h$. This is the main assumption of the Takagi theory.

The modified Ewald wave can not be interpreted as a wave-field and we also loose the useful geometrical support of the dispersion surface. However, in simple cases, such as that of a spherical wave falling on a perfect crystal [40] or a perfect crystal containing a stacking fault [41], one obtains by a simple analytical integration the same results as with *Kato's* spherical wave theory. In the general case of a complicated incident wave or a deformation such as that introduced by a thermal gradient [42] or a dislocation line [43, 44, 45], the results can be obtained by numerical integration. In these more complicated cases, Takagi's theory proves to be the most powerful one.

I-7 Properties of wave-fields

A certain number of properties of wave-fields can be deduced from their definition (I-6-3).

The electric field, magnetic field and induction can be expanded in a similar way to the electric induction. We shall write:

$$\begin{aligned} \mathbf{E}_j &= e^{2\pi i\nu t} \sum_h \mathfrak{E}_{hj}\, e^{-2\pi i \mathbf{K}_{hj} \cdot \mathbf{r}} \\ \mathbf{H}_j &= e^{2\pi i\nu t} \sum_h \mathfrak{H}_{hj}\, e^{-2\pi i \mathbf{K}_{hj} \cdot \mathbf{r}} \\ \mathbf{B}_j &= e^{2\pi i\nu t} \sum_h \mathfrak{B}_{hj} e^{-2\pi i \mathbf{K}_{hj} \cdot \mathbf{r}} \end{aligned} \tag{I-7-1}$$

From Maxwell's equations it is possible to show that:

$$\mathbf{K}_{hj} \cdot \mathfrak{D}_{hj} = 0$$

$$\mathfrak{H}_{hj} = \frac{\nu}{K_{hj}^2} \mathbf{K}_{hj} \times \mathfrak{D}_{hj} \tag{I-7-2}$$

$$\mathfrak{E}_{hj} = \frac{1}{\epsilon_0} (\mathfrak{D}_{hj} - \sum_{h'} \mathfrak{D}_{h'j} \chi_{h-h'}) \ .$$

This shows that $\epsilon_0 \mathfrak{E}_{hj}$ and $\mathfrak{D}_{hj}$ are practically equal and that the waves which build up a wave-field are transverse waves.

The Poynting vector of a wave-field is given from equation (I-2-3):

$$\bar{\mathbf{S}}_j = \frac{1}{2} \Re \mathbf{E}_j \times \mathbf{H}_j^* \ . \tag{I-7-3}$$

From (I-7-1) there comes:

$$\bar{\mathbf{S}}_j = \frac{1}{2} e^{4\pi \mathbf{K}_{oj}^i \cdot \mathbf{r}} \sum_h \sum_{h'} (\mathfrak{E}_{hj} \mathfrak{H}_{h'j}^* e^{-2\pi i (\mathbf{h}-\mathbf{h}') \cdot \mathbf{r}} \ . \tag{I-7-4}$$

Those terms of this expansion for which $\mathbf{h} \neq \mathbf{h}'$, oscillate very rapidly in real space. If we take the average over the unit cell, we get:

$$\bar{\mathbf{S}}_j = \frac{1}{2} e^{4\pi \mathbf{K}_{oj} \cdot \mathbf{r}} \sum_h (\mathfrak{E}_{hj} \times \mathfrak{H}_{hj}^* \tag{I-7-5}$$

and, from (I-7-2):

$$\bar{\mathbf{S}}_j = \frac{c}{\epsilon_0} e^{4\pi \mathbf{K}_{oj}^i \cdot \mathbf{r}} \sum_h s_h \left| \mathfrak{D}_{hj} \right|^2 \tag{I-7-6}$$

where s_h is a unit vector in the direction $\mathbf{K}_h$.

I-8 Fundamental equations of the dynamical theory

Let us now put the expansions (I-5-2) of χ and the modified Ewald wave expansion of $\mathbf{D}$ in the propagation equation (I-6-1). We thus obtain an equation containing an infinite number of terms. It is possible to show that it is equivalent to an infinite set of equations which can be written, neglecting such terms as $\partial \chi_h / \partial x$, $\Delta \mathfrak{D}_h$, $\chi_h \partial \mathfrak{D}_h / \partial x$, etc.:

$$\frac{(\mathbf{K}_h \cdot \mathbf{grad}) \mathfrak{D}_h}{k^2 - K_h^2} + i\pi \mathfrak{D}_h + i\pi \frac{K_h^2}{k^2 - K_h^2} \sum_{h'} \chi_{h-h'} \mathfrak{D}_{h'[h]} = 0 \tag{I-8-1}$$

where $\mathfrak{D}_{h'[h]}$ is the projection of $\mathfrak{D}_{h'}$ on a plane normal to $\mathbf{K}_h$.

The terms we have neglected are all second-order terms since χ_h is of the order of 10^{-6} and we have assumed $\mathfrak{D}_h$ to be a slowly varying function.

In practical cases, a finite number of terms only in expansion (I-6-5) have a non negligible amplitude. They correspond to the p reciprocal lattice points nearest to the Ewald sphere and to the *resonance factors* $K_h^2/(K_h^2 - k^2)$ which take very large values.

In usual X-ray cases, p is equal to 2. In electron diffraction, p is seldom as low as 2. In the following, we shall limit ourselves to $p = 2$.

The system (I-8-1) is thus reduced to p vector equations. In the electron case, we would have simply p scalar equations since we deal in that case with scalar waves. The p vector equations are equivalent to $3p$ scalar equations. This number can be reduced to $2p$ independant equations since we know that each $\mathfrak{D}_h$ lies in a plane normal to the corresponding wave vector $\mathbf{K}_h$ and that the direction of the wave vectors of a wave-field is determined to a small angular uncertainty, which is nothing else but the very narrow range of reflection.

When p is equal to 2, the system reduces to 4 equations. It is convenient to decompose $\mathfrak{D}_h$ into its components normal and parallel to the $\mathbf{K}_0, \mathbf{K}_h$ plane. The 4 equations then combine into two independant subsystems, one for the components polarized normal to the $\mathbf{K}_0, \mathbf{K}_h$ plane, the other for the components polarized in this plane.

By successively projecting equations (I-8-1) on the normal to the $\mathbf{K}_0, \mathbf{K}_h$ plane and on that plane, we obtain the *generalised fundamental equations* of the dynamical theory:

$$\begin{aligned} \mathbf{s}_0 \cdot \mathbf{grad}\, \mathfrak{D}_0 &= \frac{\partial \mathfrak{D}_0}{\partial s_0} = -i\pi k C \chi_{\bar{h}}\, \mathfrak{D}_h \\ \mathbf{s}_h \cdot \mathbf{grad}\, \mathfrak{D}_h &= \frac{\partial \mathfrak{D}_h}{\partial s_h} = -i\pi k \left[C \chi_h \mathfrak{D}_0 - 2\beta_h \mathfrak{D}_h\right] \end{aligned} \qquad \text{(I-8-2)}$$

where s_0 and s_h are the unit vectors in the incident and reflected directions, respectively. The system is identical for both directions of polarisation with the convention: $C = 1$ when $\mathfrak{D}_0$ and $\mathfrak{D}_h$ are normal to the $\mathbf{K}_0, \mathbf{K}_h$ plane, $C = \cos 2\theta$ when they are parallel to that plane.

$$\beta_h = \frac{|\mathbf{K}_h|^2 - |\mathbf{K}_0|^2}{2k^2} \cong \frac{K_h - k(1 + \frac{1}{2}\chi_0)}{k} \qquad \text{(I-8-3)}$$

Let L_0 or Lorentz point be the center of a sphere going through the reciprocical lattice points O and H and with radius nk, T_0 and T_h the asymptotes in L_0 to the spheres with the same radius and centered in O and H. From the definition given above, the end-point P_T of $\mathbf{K}_0$ lies on T_0 (fig. 4) and the geometrical interpretation of β_h is:

$$\beta_h = -\frac{\overline{L_0 P_T}}{k} \sin 2\theta \ . \qquad \text{(I-8-4)}$$

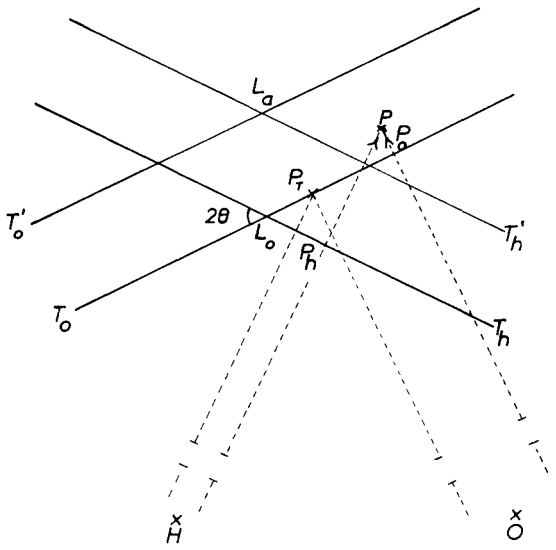

Fig. 4
Reciprocal space – neighbourhood of the Laue and Lorentz points.
P : tie-point used in the classical theory ;
P_T : tie-point used in Takagi's theory.

We shall show further on that the system (I-8-2) can be solved analytically if β_h can be taken equal to 0. This is the case for a perfect crystal or a crystal containing a stacking fault. For a deformed crystal, it is in general not possible and the system must be solved numerically on a computer.

II Plane wave case

II-1 Dispersion surface in the two beam case

When the incident wave is plane, the solution of the propagation equation is an *Ewald* wave (I-6-3) where the wave vectors

$$\mathbf{OP} = \mathbf{K}_0 \; ; \quad \mathbf{HP} = \mathbf{K}_h$$

are unknowns. The modified *Ewald* wave (I-6-5) can also be used, writing the amplitude in the following way

$$\begin{aligned} \mathfrak{D}_0(\mathbf{r}) &= \mathfrak{D}_0 \exp - 2\pi i \mathbf{P_T P} \cdot \mathbf{r} \\ \mathfrak{D}_h(\mathbf{r}) &= \mathfrak{D}_h \exp - 2\pi i \mathbf{P_T P} \cdot \mathbf{r} \end{aligned} \qquad \text{(II-1-1)}$$

P_T is an arbitrary point on T_0, P is the real tie-point of the wave-field.

If we put the amplitudes (II-1-1) in the system (I-8-2), there comes:

$$\begin{aligned} \overline{P_0 P}\, \mathfrak{D}_0 &= X_0 \mathfrak{D}_0 = \frac{1}{2} kC \chi_{\bar{h}} \mathfrak{D}_h \\ \overline{P_h P}\, \mathfrak{D}_h &= X_h \mathfrak{D}_h = \frac{1}{2} kC \chi_h \mathfrak{D}_0 \end{aligned} \qquad \text{(II-1-2)}$$

where P_0 and P_h are the projections of P on T_0 and T_h respectively (fig. 4). $\overrightarrow{\mathbf{OP}}$ and $\overrightarrow{\mathbf{HP}}$ are oriented towards P. X_0 and X_h are therefore positive for branch 1 and negative for branch 2.

This system is identical to the fundamental equations of the classical dynamical theory (e.g.v. *Laue* [22], eq. 27–5).

In the classical theory, both the amplitudes and $\mathbf{K}_0$, that is the position of the tie point P, are unknowns. The system (II-1-2) beeing linear and homogeneous in $\mathfrak{D}_0$, $\mathfrak{D}_h$, it has a non trivial solution only when its determinant is equal to zero:

$$X_0 X_h = \frac{1}{4} k^2 C^2 \chi_h \chi_{\bar{h}} \qquad \text{(II-1-3)}$$

This equation is that of a surface, locus of the possible positions of the tie-point, usually called *dispersion surface.* Its intersection with the $\mathbf{K}_0, \mathbf{K}_h$ plane is a hyperbola asymptotic to T_0 and T_h (fig. 5).

The wave-fields which can propagate through the crystal have their tie-points on the dispersion surface. The ratio of the amplitudes of their waves is deduced from equations (II-1-2):

$$R_{hj} = \frac{\mathfrak{D}_{hj}}{\mathfrak{D}_{0j}} = \frac{2X_{0j}}{kC\chi_{\bar{h}}} \qquad \text{(II-1-4)}$$

From fig. 5, it can be seen that this ratio has opposite signs for tie-points lying on branchs 1 and 2 of the hyperbola. It is negative for branch 1. At the summits it is equal to ± 1.

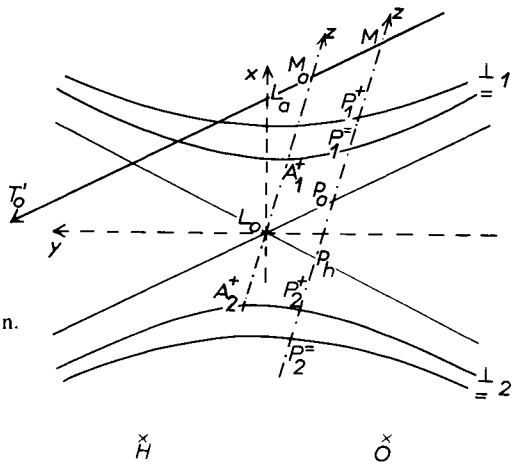

Fig. 5
Dispersion surface at a large magnification.
⊥: polarization normal to the incidence plane;
=: polarization parallel to the incidence plane

II-2 Relation between the Poynting vector and the dispersion surface

From (I-7-6), the expression of the Poynting vector is, in the two beam case:

$$\bar{\mathbf{S}}_j = \frac{c}{\epsilon_0} e^{4\pi \mathbf{K}^i_{0j} \cdot \mathbf{r}} (s_0 |\mathfrak{D}_{0j}|^2 + s_h |\mathfrak{D}_{hj}|^2) \qquad \text{(II-2-1)}$$

Figure 6 shows the geometrical construction of the Poynting vector. Let α_j be the angle between the lattice planes and $\mathbf{S}_j$. It can readily be seen that:

$$\operatorname{tg}\alpha_j = \frac{|\mathfrak{D}_{0j}|^2 - |\mathfrak{D}_{hj}|^2}{|\mathfrak{D}_{0j}|^2 + |\mathfrak{D}_{hj}|^2} \operatorname{tg}\theta = \frac{1 - R^2_{hj}}{1 + R^2_{hj}} \operatorname{tg}\theta \qquad \text{(II-2-2)}$$

Let us choose two orthonormal coordinates axes, L_0x parallel to the lattice planes and L_0y parallel to OH (fig. 5). One has:

$$\begin{aligned} X_0 &= x\cos\theta + y\sin\theta \\ X_h &= x\cos\theta - y\sin\theta \end{aligned} \qquad \text{(II-2-3)}$$

The equation (II-1-3) of the hyperbola can also be written:

$$x^2\cos^2\theta - y^2\sin^2\theta = \frac{k^2}{4} C^2 \chi_h \chi_{\bar{h}} \qquad \text{(II-2-4)}$$

The slope of the normal to the dispersion surface at the tie-point is equal to:

$$\operatorname{tg}\alpha_j = \frac{dx}{dy} = \frac{y\sin^2\theta}{x\cos^2\theta} = \frac{X_h - X_0}{X_h + X_0} \operatorname{tg}\theta = \frac{1 - R^2_{hj}}{1 + R^2_{hj}} \operatorname{tg}\theta \qquad \text{(II-2-5)}$$

This shows that the Poynting vector is normal to the dispersion surface.

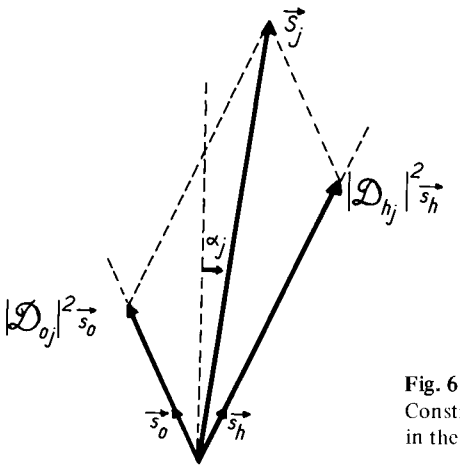

Fig. 6
Construction of the Poynting vector. N.B. α_j is negative in the case represented

II-3 Boundary conditions for the wave vectors

The above derivation tells us *which* wave fields can propagate in a crystal and the *boundary conditions* for the wave vectors tell us which particular ones are excited in a given problem. The boundary conditions for the amplitudes will give us the absolute values of the amplitudes of the waves in each wave field.

The boundary condition for the wave vectors is that of the *continuity of the tangential component* of the wave vector. Let **Mz** be the normal to the entrance surface drawn from the tie-point M of the incident wave towards the inside of the crystal. It cuts the two sheets of the dispersion surface in four points: $P_1^{\perp}$, $P_2^{\perp}$; $P_1^{=}$, $P_2^{=}$ (fig. 5); four wave fields and eight waves are therefore excited in the crystal.

We must distinguish two cases depending on the orientation of the normal **Mz** with respect to the asymptotes (fig. 7). Let ψ_0 and ψ_h be the angles between **Mz** and the incident and reflected directions $\mathbf{s}_0$ and $\mathbf{s}_h$ respectively:

a) reflection or Bragg case:

$$-\frac{\pi}{2} < \psi_0 < 2\theta - \frac{\pi}{2}; \qquad \gamma_0 = \cos\psi_0 > 0$$

$$-\frac{\pi}{2} - 2\theta < \psi_h < -\frac{\pi}{2}; \qquad \gamma_h = \cos\psi_h < 0$$

P_1 and P_2 lie on the *same* branch of the dispersion surface

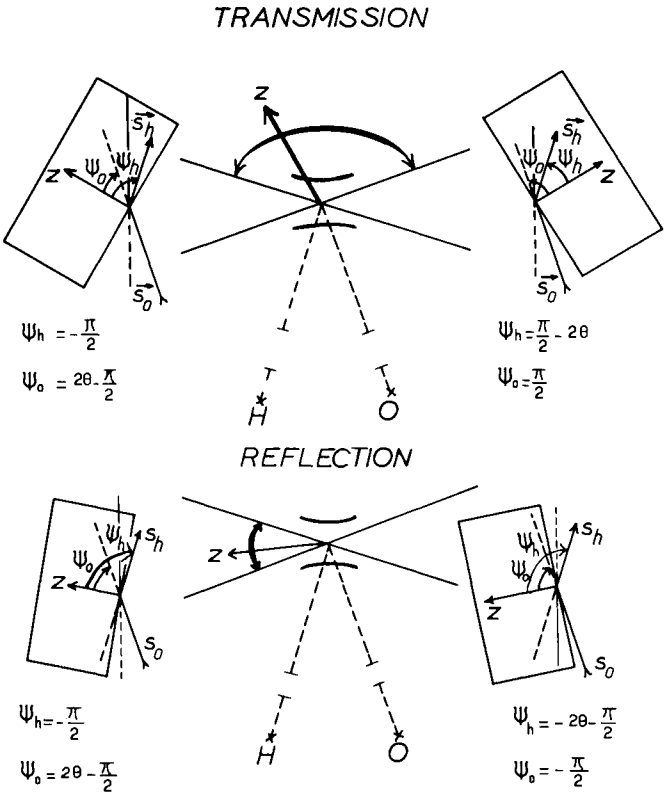

Fig. 7
Bragg and Laue settings: *Transmission (Laue)*: $2\theta - \pi/2 < \psi_0 < \pi/2$; $-\pi/2 < \psi_h < \pi/2 - 2\theta$;
Reflection (Bragg): $-\pi/2 < \psi_0 < -\pi/2 + 2\theta$; $-\pi/2 - 2\theta < \psi_h < -\pi/2$

b) transmission or Laue case:

$$2\theta - \frac{\pi}{2} < \psi_0 < \frac{\pi}{2}; \qquad \gamma_0 > 0$$

$$-\frac{\pi}{2} < \psi_h < \frac{\pi}{2} - 2\theta; \qquad \gamma_h > 0$$

P_1 and P_2 lie on *different* branches of the dispersion surface.

II-4 Tie points of the excited wave-fields

Let T_0' be the tangent to the circle centered at the origin of the reciprocal lattice and with radius k. The center L_a of the Ewald sphere and the extremity of the wave-vector

$$\mathbf{OM} = \mathbf{K}_0^{(a)}$$

of the incident wave lie on T_0' (fig. 5). We shall call the angle

$$\Delta\theta = \frac{\overline{L_a M}}{k} \tag{II-4-1}$$

departure from Bragg's law of the incident wave.

Let M_0 be the intersection of a parallel L_0z to the normal to the crystal surface with T_0', p_0 and p_h those of MP with T_0 and T_h (fig. 5). We can write $\overline{p_0 p_h}$ in two ways, thus obtaining the equation of the normal Mz to the entrance surface:

$$\overline{p_0 p_h} = \frac{X_0}{\gamma_0} - \frac{X_h}{\gamma_h} = \overline{M_0 M}\,\frac{\sin 2\theta}{\gamma_h} = \frac{k(\Delta\theta - \Delta\theta_0)\sin 2\theta}{\gamma_h} \tag{II-4-2}$$

with

$$\Delta\theta_0 = \frac{\overline{L_a M_0}}{k}$$

The tie point P lies as the intersection of the dispersion surface and Mz. Its co-ordinates satisfy both (II-1-3) and (II-4-2). Let us introduce a parameter:

$$\eta = \Lambda_0\,\overline{p_0 p_h} \tag{II-4-3}$$

where

$$\Lambda_0 = \overline{A_1 A_2} = \frac{\lambda\sqrt{\gamma_0 |\gamma_h|}}{|C|\sqrt{\chi_h \chi_{\bar{h}}}} \tag{II-4-4}$$

is the diameter of the dispersion surface parallel to Mz (fig. 5). It is sometimes called the *extinction distance* or the *Pendellösung fringe distance*, for reasons which will become clear further on. In the Bragg case, the diameter is pure imaginary and equal to $i\Lambda_0$.

There comes:

$$\begin{aligned} X_0 &= \frac{1}{2}\Lambda_0^{-1}\gamma_0\,\frac{\gamma_h}{|\gamma_h|}\left(\eta \pm \sqrt{\eta^2 + \frac{\gamma_h}{|\gamma_h|}}\right) \\ X_h &= \frac{1}{2}\Lambda_0^{-1}|\gamma_h|\left(-\eta \pm \sqrt{\eta^2 + \frac{\gamma_h}{|\gamma_h|}}\right) \end{aligned} \tag{II-4-5}$$

The upper sign corresponds to j = 1.

The ratio of the amplitudes of the two waves of the wave-field corresponding to the tie-point P is, using (II-1-4), (II-4-4) and (II-4-5):

$$\left(R_{hj} = \frac{\mathfrak{D}_{hj}}{\mathfrak{D}_{0j}} = \frac{|C|}{C}\sqrt{\frac{\chi_h}{\chi_{\bar{h}}}}\sqrt{\frac{\gamma_0}{|\gamma_h|}}\,\frac{\gamma_h}{|\gamma_h|}\right)\left(\eta \pm \sqrt{\eta^2 + \frac{\gamma_h}{|\gamma_h|}}\right) \qquad \text{(II-4-6)}$$

II-5 Boundary conditions for the amplitudes in the Laue case

From what we have seen in last section, an incident plane wave falling on a crystal in the Laue case excites two wave-fields inside the crystal. We must now find the absolute amplitudes of the waves of these wave-fields.

The boundary conditions of Maxwell's equations are given by (I-2-2).

Since $\mathbf{E}_j$ differs only very slightly from $\mathbf{D}_j/\epsilon_0$, they can be approximately replaced by:

$$\mathfrak{D}_0^{(a)} = \Sigma_j \mathfrak{D}_j$$

Using (I-6-3), there comes:

$$\mathfrak{D}_0^{(a)} e^{-2\pi i \mathbf{K}_0^{(a)} \cdot \mathbf{r}_s} = \Sigma \mathfrak{D}_{0j} e^{-2\pi i \mathbf{K}_{0j} \cdot \mathbf{r}_s} + \Sigma \mathfrak{D}_{hj} e^{-2\pi i \mathbf{K}_{hj} \cdot \mathbf{r}_s} \qquad \text{(II-5-1)}$$

$\mathfrak{D}_0^{(a)}$ is the amplitude and $\mathbf{K}_0^{(a)}$ the wave vector of the incident wave; $\mathbf{r}_s$ is the position vector of a point in the surface of the crystal. There is one equation (II-3-2) for each direction of polarization (parallel or normal to the incidence plane). Using the continuity of the tangential component of wave vectors it is readily seen that:

$$\mathfrak{D}_0^{(a)} = \mathfrak{D}_{01} + \mathfrak{D}_{02}\,; \qquad 0 = \mathfrak{D}_{h1} + \mathfrak{D}_{h2} \qquad \text{(II-5-2)}$$

Expression (II-4-6) is written, in the Laue case:

$$R_{hj} = \frac{\mathfrak{D}_{hj}}{\mathfrak{D}_{0j}} = -\frac{|C|}{C}\sqrt{\frac{\chi_h}{\chi_{\bar{h}}}}\sqrt{\frac{\gamma_0}{|\gamma_h|}}\,(\eta \pm \sqrt{1+\eta^2}) \qquad \text{(II-5-3)}$$

From(II-5-2) and (II-5-3), we calculate the absolute values of the amplitudes of the two wave-fields:

$$\mathfrak{D}_{0j} = \frac{\sqrt{1+\eta^2} \mp \eta}{2\sqrt{1+\eta^2}}\,\mathfrak{D}_0^{(a)}$$

$$\mathfrak{D}_{hj} = \mp \frac{|C|}{C}\sqrt{\frac{\chi_h}{\chi_{\bar{h}}}}\sqrt{\frac{\gamma_0}{\gamma_h}}\,\mathfrak{D}_0^{(a)}/2\sqrt{1+\eta^2} \qquad \text{(II-5-4)}$$

The upper sign corresponds to $j = 1$.

The elongations of the waves are:

$$D_{0j} = \mathfrak{D}_{0j}\, e^{-2\pi i\, \mathbf{K}_{0j}\cdot\mathbf{r}} = \mathfrak{D}_{0j}\, e^{-2\pi i\, (\overline{MP}_j z + \mathbf{K}_0^{(a)}\cdot\mathbf{r})}$$

$$D_{hj} = \mathfrak{D}_{hj}\, e^{-2\pi i\, \mathbf{K}_{hj}\cdot\mathbf{r}} = \mathfrak{D}_{hj}\, e^{-2\pi i\, (\overline{MP}_j z + \mathbf{K}_0^{(a)}\cdot\mathbf{r} + \mathbf{h}\cdot\mathbf{r})} \qquad \text{(II-5-5)}$$

$j = 1, 2$.

$\mathbf{r}$ is the position vector of the point within the crystal where the amplitudes of the wave-field are studied; z is the depth of this point.

Fig. 8 shows the variation of the amplitudes (II-5-4) with parameter η that is with the departure from Bragg's law in a non absorbing crystal.

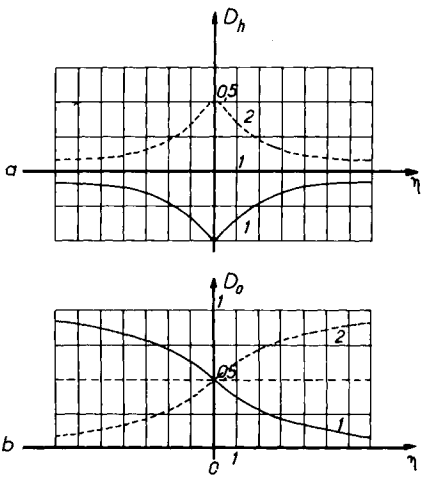

Fig. 8
Variations of the reflected and refracted amplitudes for wave-fields of type 1 (*solid curves*) and 2 (*broken curves*) in a non absorbing crystal.

II-6 Anomalous absorption in the Laue case

When the crystal is absorbing, the wave vectors and the dispersion surface are complex. The conditions of the continuity of the tangential components show that the imaginary parts of all wave vectors are parallel and normal to the entrance surface. There is thus no difficulty in the derivation of these imaginary parts.

One can write:

$$\mathbf{K}_{0j} = \mathbf{OP}_j = \mathbf{OM} + \mathbf{MP}_j = \mathbf{K}_0^{(a)} + \mathbf{MP}_j$$

and, from fig. 5,

$$\overline{MP}_j = (X_{0j} + k\,\chi_0/2)/\gamma_0$$

The imaginary parts of the two sides of this equation are equal to:

$$K^i_{0j} = K^i_{hj} = \overline{MP_j}^i = \frac{1}{\gamma_0}\left(X^i_{0j} + \frac{1}{2}k\chi^i_0\right) = \frac{1}{\gamma_h}\left(X^i_{hj} + \frac{1}{2}k\chi^i_0\right) \qquad \text{(II-6-1)}$$

The attenuation factor for the *intensities* is given, from (II-5-5) or (I-7-6) and (II-6-1) by:

$$e^{4\pi K^i_{0j} z} = e^{-(\mu + 2\chi^i_0)z/\gamma_0} = e^{-\mu_e z/\gamma_0} \qquad \text{(II-6-2)}$$

where μ_e is the effective absorption coefficient of the wave-field near the Bragg setting:

$$\mu_e = -4\pi K^i_0 \gamma_0 = \mu(1 + 2X^i_0/k\chi^i_0) \qquad \text{(II-6-3)}$$

Using (II-4-5), we finally obtain, for small values of $|\chi^i|$

$$\mu_e = \gamma_0\mu\left\{\frac{1}{2}\left(\frac{1}{\gamma_0} + \frac{1}{\gamma_h}\right) \mp \frac{1}{\sqrt{1+\eta_r^2}}\left[\frac{1}{2}\left(\frac{1}{\gamma_0} - \frac{1}{\gamma_h}\right)\eta_r + \right.\right.$$
$$\left.\left. + \frac{|C|}{\sqrt{\gamma_0\gamma_h}}\frac{|\chi^i_h|}{|\chi^i_0|}\cos\varphi\right]\right\} \qquad \text{(II-6-4)}$$

a) symmetric case: $\psi_0 = \psi_h$; $\gamma_0 = \gamma_h = \cos\theta$

Expression (II-6-4) simplifies to:

$$\mu_e = \mu\left(1 \pm \frac{\chi^i_h}{\chi^i_0}\cos\varphi\sqrt{1+\eta_r^2}\right) \qquad \text{(II-6-5)}$$

If φ is equal to $2k\pi$ (k integer), *the effective absorption coefficient is smaller than the normal absorption coefficient for wave-fields corresponding to branch 1 of the dispersion surface. It is bigger than the normal coefficient for wave-fields corresponding to branch 2.* If φ is equal to $k\pi$ (k odd), it will be the reverse. This is for example the case for the 222 reflection on calcite.

This effect is called the *Borrmann effect*, after the name of its discoverer [4, 5]. It can be interpreted physically in the following way [8, 17]. The amplitude of a wave-field can be written, in the two beam case, from (I-6-2):

$$\mathbf{D}_j = \exp 2\pi i(\nu t - \mathbf{K}_{0j}\cdot\mathbf{r})\,(\mathfrak{D}_{0j} + \mathfrak{D}_{hj}\exp -2\pi i\,\mathbf{h}\cdot\mathbf{r}$$

Its intensity is equal to:

$$|\mathbf{D}_j|^2 = |\mathfrak{D}_{0j}|^2 \exp 4\pi\mathbf{K}^i_{0j}\cdot\mathbf{r}\left(1 + \left|\frac{\mathfrak{D}_{hj}}{\mathfrak{D}_{0j}}\right|^2 + 2C\frac{\mathfrak{D}_{hj}}{\mathfrak{D}_{0j}}\cos 2\pi\,\mathbf{h}\cdot\mathbf{r}\right) \qquad \text{(II-6-6)}$$

The wave-field builds up stationnary waves of which the nodes lie on the planes:

$\mathbf{h}\cdot\mathbf{r}$ = constant

For *branch* 1 ($\mathfrak{D}_{hj}/\mathfrak{D}_{0j} < 0$ – see end of (II-1), the *nodes* of the electric field lie on the reflecting planes and the absorption is very small, the smallest for C = 1 (polarization normal to the incidence plane).

For *branch* 2 ($\mathfrak{D}_{hj}/\mathfrak{D}_{0j} > 0$), the *antinodes* of the electric field lie on the reflecting plane and the absorption is very high.

Equations (II-6-6) and (II-6-7) show that the Bormann effect or anomalous absorption effect is maximum for $\eta = 0$ ($\mathfrak{D}_{hj}/\mathfrak{D}_{0j} = \pm 1$), that is in the center of the reflecting range. When $\eta \to \pm\infty$, that is far from the reflecting range, the absorption coefficient tends towards the normal absorption coefficient.

The ratio $|\chi_h^i/\chi_0^i|$ can be calculated easily with Wagenfeld's expressions [46].

We mentionned in I-5 that χ_h^i includes the Debye-Waller factor. The Borrmann effect depends therefore very much on temperature and increases significantly at low temperatures, as has been shown by *G. Borrmann* [47].

II-7 Boundary conditions on the exit surface – Rocking curves in the Laue case

When the wave-fields reach the exit surface, the two waves making up each wave-field have no more reason to propagate together and they split up. Since there are four wave-fields within the crystal for an incident plane wave, we have *eight* out-going plane waves, four in the incident direction, and four in the reflected direction. The wave vectors of these eight waves are obtained by applying the condition of the continuity of the tangential component of the wave vector. Their amplitudes are obtained by applying the boundary conditions (I-2-2):

$$\mathfrak{D}_h^{(d)} e^{-2\pi i \mathbf{K}_h^{(d)} \cdot \mathbf{r}} = \mathfrak{D}_{h1} e^{-2\pi i \mathbf{K}_{h1} \cdot \mathbf{r}} + \mathfrak{D}_{h2} e^{-2\pi i \mathbf{K}_{h2} \cdot \mathbf{r}}$$

$$\mathfrak{D}_0^{(d)} e^{-2\pi i \mathbf{K}_0^{(d)} \cdot \mathbf{r}} = \mathfrak{D}_{01} e^{-2\pi i \mathbf{K}_{01} \cdot \mathbf{r}} + \mathfrak{D}_{02} e^{-2\pi i \mathbf{K}_{02} \cdot \mathbf{r}} \qquad \text{(II-7-1)}$$

$\mathfrak{D}_h^{(d)}$ and $\mathfrak{D}_0^{(d)}$ are the amplitudes and $\mathbf{K}_h^{(d)}$, $\mathbf{K}_0^{(d)}$ the wave vectors of the outgoing waves.

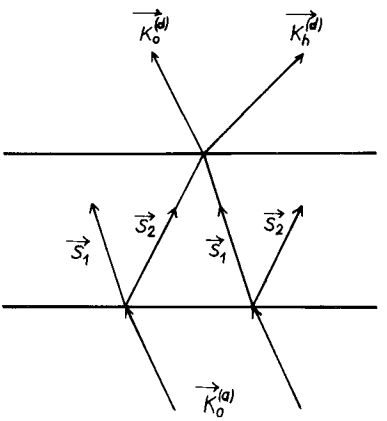

Fig. 9

At any given point of the exit surface, arrive two wave-fields belonging to both branches of the dispersion surface (fig. 9). They interfere as is shown by the expressions (II-7-1) of the amplitudes of the total reflected and refracted waves. Their intensities are:

$$\left|\mathfrak{D}_h^{(d)}\right|^2 = \left|\frac{\chi_h}{\chi_{\bar{h}}}\right| \frac{\gamma_0}{\gamma_h} \frac{\exp -\frac{1}{2}\mu z\left(\frac{1}{\gamma_0}+\frac{1}{\gamma_h}\right)}{2(1+\eta_r^2)} \left|\mathfrak{D}_0^{(a)}\right|^2 \left\{ \mathrm{ch}\left[z\left(\tau^{-1} + \mu\eta_r\left(\frac{1}{\gamma_0}-\frac{1}{\gamma_h}\right)\right)\Big/\sqrt{1+\eta_r^2}\right] - \cos\left(2\pi z\sqrt{1+\eta_r^2}/\,t\right)\right\} \tag{II-7-2}$$

$$\left|\mathfrak{D}_0^{(d)}\right|^2 = \frac{\exp -\frac{1}{2}\mu z\left(\frac{1}{\gamma_0}+\frac{1}{\gamma_h}\right)}{2(1+\eta_r^2)} \left|\mathfrak{D}_0^{(a)}\right|^2 \left\{ \mathrm{ch}\left[2v + z\left(\tau^{-1} + \mu\eta_r\left(\frac{1}{\gamma_0}-\frac{1}{\gamma_h}\right)\right)\Big/\sqrt{1+\eta_r^2}\right] + \cos\left[\left(2\pi z\sqrt{1+\eta_r^2}/\,t\right) + 2\eta_i/\sqrt{1+\eta_r^2}\right]\right\}$$

where τ^{-1} and C^{-1} are the real and imaginary parts of Λ_0^{-1}, respectively, $v = \mathrm{arg\,sh}\,\eta_r$, η_i and η_r are the real and imaginary parts of η.

The hyperbolic cosine term in each expression is equal to one and *ch 2v*, respectively, when there is no absorption; the cosine term is due to the interference between wave-fields 1 and 2. It can be seen that the intensities of the reflected and transmitted beams are sinusoidal functions of the thickness z of the crystal and that they are in opposition: there is continuous transfer of energy from one beam to the other. *Ewald* has given to this oscillation of the energy the name of *Pendellösung*. Its period is equal to

$$\Lambda = \frac{t}{\sqrt{1+\eta_r^2}} = P_1 P_2$$

The rocking curves deduced from (II-7-2) have been checked experimentally, among others, by *Schwarz* and *Rogosa* [48], *Brogren* and *Addell* [49], *Authier* [21]. Figures 10a and 10b show examples of the shapes of these rocking curves for silicon crystals 0.7 mm and 2.5 mm thick, respectively [1]).

[1]) The oscillation due to the cosine term can only be observed with an incident plane wave. This has been done recently by *S. Kikuta* and *K. Kohra* [90] and by *C. Malgrange* and *M. Lefeld-Sosnowska* [91].

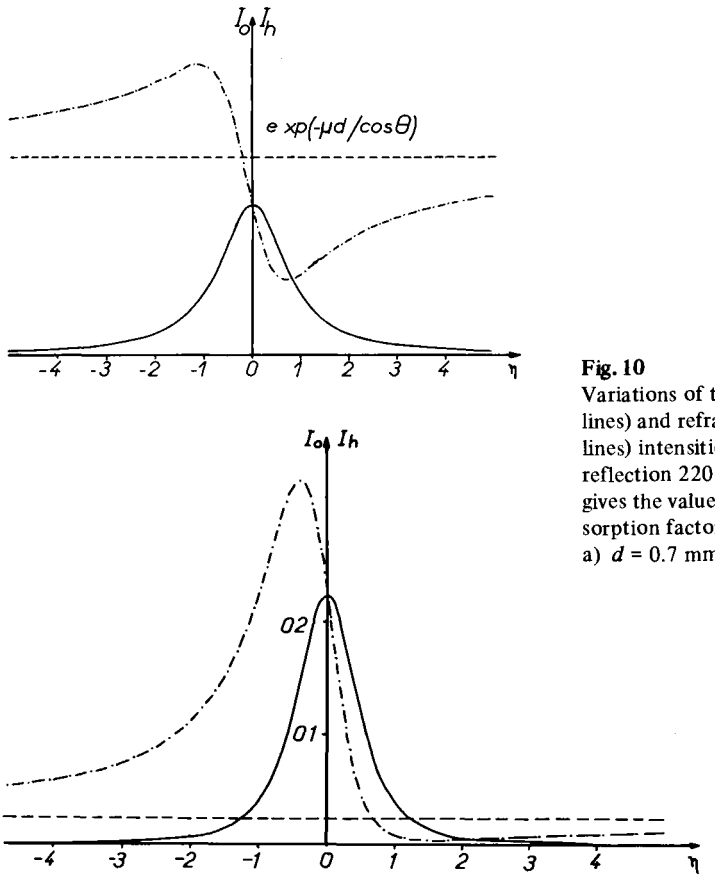

Fig. 10
Variations of the reflected (solid lines) and refracted (interrupted lines) intensities. Silicon crystals, reflection 220. The broken line gives the value of the normal absorption factor.
a) d = 0.7 mm b) d = 2,5 mm

The integrated intensity for the reflected beam is proportional to the area under its rocking curve. It is possible to show [50] that it is equal to:

$$I_{hi} = \left|\frac{\chi_h}{\chi_{\bar{h}}}\right| \sqrt{\frac{\gamma_h}{\gamma_0}} \frac{\pi |C|\, |\chi_h^r|}{2 \sin 2\theta} e^{-\frac{1}{2}\mu d \left(\frac{1}{\gamma_0} + \frac{1}{\gamma_h}\right)} \left[I_0(\zeta) - 1 + \int_0^{2\pi d/t} J_0(z)\,dz \right] \quad \text{(II-7}$$

where d is the thickness of the crystal, $J_0(z)$ the zero order Bessel function, $I_0(\zeta)$ the zero order modified Bessel function and:

$$\zeta = \frac{\mu d}{\sqrt{\gamma_0 \gamma_h}} \sqrt{|C|^2 \left|\frac{\chi_h^i}{\chi_0^i}\right|^2 \cos\varphi + \frac{1}{4} \frac{(\gamma_h - \gamma_0)^2}{\gamma_0 \gamma_h}}$$

I_{hi} is an oscillating function of thickness. Its pseudo period is t.

II-8 Boundary conditions in the Bragg case

a) infinitely thick crystals

In the Bragg case, the normal to the entrance surface, drawn from the extremity of the incident wave vector

$$\mathbf{OM} = \mathbf{K}_0^{(a)}$$

cuts the dispersion surface in two points lying on the *same* branch (II-3). Fig. 11 shows that the propagation directions of the corresponding wave-fields, which are normal to the dispersion surface, are from the outside towards the inside of the crystal for one point, but from the inside towards the outside for the other point. In the latter case, the wave-field must have been reflected from the back surface of the crystal, but due to absorption, always present, even if small, it will be completely absorbed out in an infinitely thick crystal.

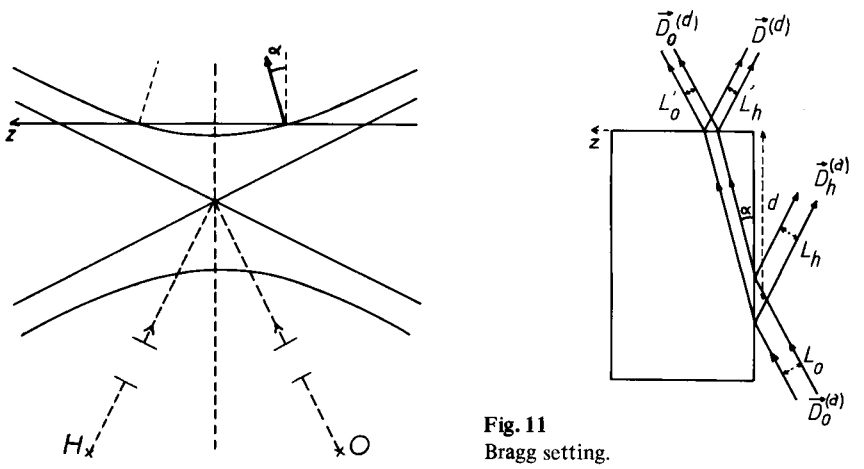

Fig. 11
Bragg setting.

In this case, therefore, only *one* wave-field per direction of polarization is excited at the surface of the crystal. The ratio of the amplitudes of its waves is given by (II-4-6), remembering that γ_h is negative in the Bragg case:

$$R_h = \frac{\mathfrak{D}_h}{\mathfrak{D}_0} = -\frac{|C|}{C}\sqrt{\frac{\chi_h}{\chi_{\bar{h}}}}\sqrt{\frac{\gamma_0}{|\gamma_h|}}\ (\eta \pm \sqrt{\eta^2 - 1}) \qquad \text{(II-8-1)}$$

The boundary conditions are simply:

$$\mathfrak{D}_{0j} = \mathfrak{D}_0^{(a)}\ ; \qquad \mathfrak{D}_{hj} = \mathfrak{D}_h^{(a)}$$

Let L_0 and L_h be the cross sections of the incident and reflected beams, respectively. Fig. 11 shows that

$$\frac{L_0}{L_h} = \frac{\gamma_0}{|\gamma_h|}$$

The reflecting power is:

$$I_h = \frac{L_h}{L_0} \frac{|\mathfrak{D}_h^{(a)}|^2}{|\mathfrak{D}_0^{(a)}|^2} = \left| \frac{\chi_h}{\chi_{\bar{h}}} \right| \left| \eta \pm \sqrt{\eta^2 - 1} \right|^2 \qquad \text{(II-8-2)}$$

– Non absorbing case

For $|\eta| < 1$, R_h is a complex number, even for a non absorbing crystal. It is easy to show that in this case:

$$I_h = 1$$

There is *total reflection.* The total reflection range corresponds to the values of the departures from Bragg's law such that the normal to the surface of the crystal drawn from M cuts the dispersion surface in imaginary points (fig. 11), that is to:

$$-1 < \eta < +1$$

or, using (II-4-2), to:

$$|\Delta\theta - \Delta\theta_0| < \frac{\lambda|\gamma_h|}{\Lambda_0 \sin 2\theta} \qquad \text{(II-8-3)}$$

This shows that the width of the total reflection range is equal to:

$$\frac{2\lambda|\gamma_h|}{\sin 2\theta} = \frac{2|C|\sqrt{\chi_h \chi_{\bar{h}}}\left(\sqrt{\frac{|\gamma_h|}{\gamma_0}}\right)}{\sin 2\theta} = \frac{2R\lambda^2 e^{-M}}{\pi V \sin 2\theta} \sqrt{\frac{|\gamma_h| F_h F_{\bar{h}}}{\gamma_0}}$$

It is proportional to the structure factor, the square of the wave-length and the Debye-Waller factor. It is therefore expected that the width of the rocking curve should become narrower with increasing temperature. This has been proved experimentally by *B. W. Batterman.* The width also depends on the angle between the surface of the crystal and the net planes. Using a very asymmetric reflection is a way to get a very narrow rocking curve.

(II-8-3) shows also that the middle of the total reflection range does not correspond to the exact Bragg setting. It differs from it by an angle:

$$\Delta\theta_0 = \frac{|\chi_0|}{2 \sin 2\theta}\left(1 + \frac{|\gamma_h|}{\gamma_0}\right) = \frac{1-\eta}{\sin 2\theta}\left(1 + \frac{|\gamma_h|}{\gamma_0}\right) \qquad \text{(II-8-4)}$$

It is proportional to the difference between the refractive index and one.

The attenuation factor within the total reflecting range can be calculated in the same way as in section II-6. One can show that the effective absorption distance, here called extinction distance, is equal to:

$$\mu_e^{-1} = \frac{\Lambda_e}{2\pi} = \frac{\sqrt{\gamma_0 |\gamma_h|}}{2\pi k |C| |\chi_h|} \qquad \text{(II-8-5)}$$

in the symmetrical case, one has simply:

$$\Lambda_e = \frac{\lambda \sin\theta}{|C| |\chi_h|} \qquad \text{(II-8-6)}$$

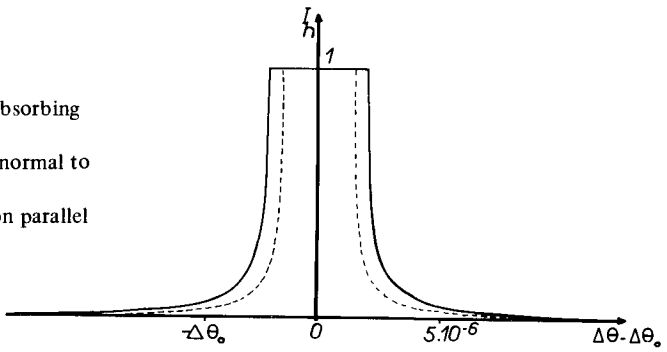

Fig. 12
Rocking curve for a non absorbing crystal (Bragg case)
solid curve: polarization normal to the plane of incidence;
broken curve: polarization parallel to the plane of incidence

Figure 12 shows a rocking curve $I_h(\Delta\theta)$. It is possible to show [22] that the integrated intensity, proportional to the area under the rocking curve, is equal to:

$$I_{hi} = \frac{8}{3} |C| \frac{\chi_h}{\sin 2\theta} \sqrt{\frac{|\gamma_h|}{\gamma_0}} \qquad \text{(II-8-7)}$$

– *Absorbing case.*

When the crystal is absorbing, η is complex, and anomalous absorption occurs. As in Laue cases, it is lower than usual absorption for branch 1 of the dispersion surface and higher for branch 2. Figure 13 shows a typical rocking curve for an absorbing case. One can notice that the total reflection range has disappeared and the curve has become asymmetrical: on the small angles side, the excited wave-field belongs to branch 1 and the intensity is high, on the high angles side, on the contrary excited wave-field belongs to branch 2 and the energy is more absorbed.

b) thin crystals

In the case of a thin crystal, the wave-field created at the entrance surface of the crystal with tie-point P_1 is reflected back at the other face of the crystal (fig. 14).

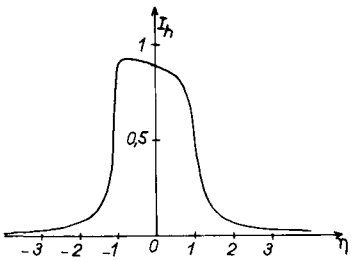

Fig. 13
Rocking curve for an absorbing crystal (Germanium, 111, Cu $K\alpha_1$)-Bragg case.

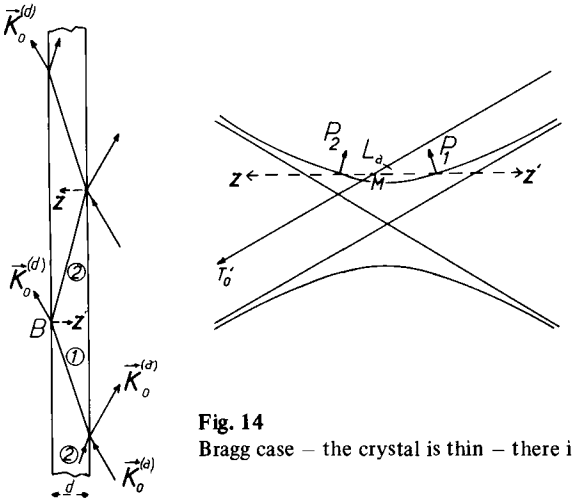

Fig. 14
Bragg case – the crystal is thin – there is partial reflection at the back surface.

The tie-point of the reflected wave-field is P_2. The boundary conditions must therefore be written at both surfaces and take into account both wave-fields:

Front surface:

$$\mathfrak{D}_0^{(a)} = \mathfrak{D}_{01} + \mathfrak{D}_{02} \; ; \qquad \mathfrak{D}_h^{(a)} = \mathfrak{D}_{h1} + \mathfrak{D}_{h2} \tag{II-8-8}$$

Back surface:

$$0 = \mathfrak{D}_{h1}\, e^{-2\pi i \mathbf{K}_{h1} \cdot \mathbf{r}} + \mathfrak{D}_{h2}\, e^{-2\pi i \mathbf{K}_{h2} \cdot \mathbf{r}}$$

$$\mathfrak{D}_0^{(d)}\, e^{-2\pi i \mathbf{K}_0^{(d)} \cdot \mathbf{r}} = \mathfrak{D}_{01}\, e^{-2\pi i \mathbf{K}_{01} \cdot \mathbf{r}} + \mathfrak{D}_{02}\, e^{-2\pi i \mathbf{K}_{02} \cdot \mathbf{r}} \tag{II-8-9}$$

$\mathfrak{D}_0^{(d)}$ and $\mathbf{K}_0^{(d)}$ are the amplitude and wave vector of the transmitted wave out of the back surface. The wave vector is related to the wave vectors inside the crystal and

at the front surface by the boundary conditions, that is the continuity of the tangential component of the wave vectors. If the crystal is a plane parallel slab, we have:

$$\mathbf{K}_0^{(d)} = \mathbf{K}_{01} + \mathbf{MP}_1 = \mathbf{K}_{02} + \mathbf{MP}_2 = \mathbf{K}_0^{(a)} \tag{II-8-10}$$

Using (II-8-10) and remembering that $\mathbf{MP}_j$ is normal to the crystal faces, (II-8-9) can be written:

$$\begin{aligned} \mathfrak{D}_0^{(d)} &= \mathfrak{D}_{01}\, e^{-2\pi i \overline{MP}_1 d} + \mathfrak{D}_{02}\, e^{-2\pi i \overline{MP}_2 d} \\ 0 &= \mathfrak{D}_{h1}\, e^{-2\pi i \overline{MP}_1 d} + \mathfrak{D}_{h2}\, e^{-2\pi i \overline{MP}_2 d} \end{aligned} \tag{II-8-11}$$

d is the crystal thickness.

From (II-8-1), (II-8-8) and (II-8-11), it is possible to calculate the reflecting power of the crystal. We get, when absorption can be neglected:

$$I_h = \frac{|\gamma_h|}{\gamma_0} \frac{\left|\mathfrak{D}_h^{(a)}\right|^2}{\left|\mathfrak{D}_0^{(a)}\right|^2} = \frac{1}{\eta^2 + (\eta^2 - 1)\,\mathrm{cotg}^2\left(\frac{\pi}{\Lambda_0}\, d\, \sqrt{\eta^2 - 1}\right)} \tag{II-8-12}$$

for $|\eta| > 1$

and

$$I_h = \frac{1}{\eta^2 + (1 - \eta^2)\coth^2\left(\frac{\pi}{\Lambda_0}\, d\, \sqrt{1 - \eta^2}\right)}$$

for $|\eta| < 1$.

Figure 15 shows a typical rocking curve of I_h versus η.

One can see that there is no more total reflection.

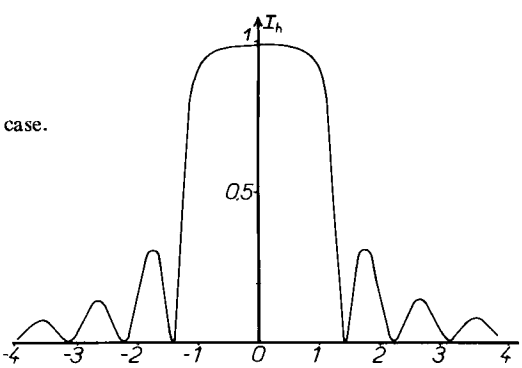

Fig. 15
Rocking curve for a thin crystal – Bragg case.

The oscillating term of I_h for $|\eta| > 1$ gives rise to fringes. They are due to the interference between the two wave-fields propagating within the crystal and can be considered as Pendellösung fringes, but it must be noted that the interfering wave-fields correspond to the same branch of the dispersion surface (fig. 14). These oscillations have first been observed by *Batterman* and *Hildebrandt* [51] (fig. 16), [87].

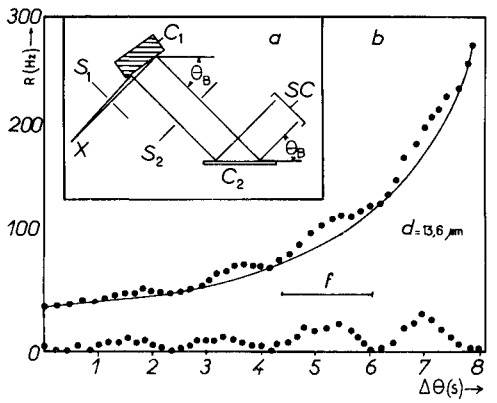

Fig. 16
Pendellösung in the Bragg case-after [51]
a) ***experimental arrangements;*** X : X-ray source (Cu Kα) C_1, C_2 : silicon crystals; $\theta_B = \theta_{333}$
b) ***observed fringes*** Crystal thickness 13.6 μm - f is the predicted angular fringe spacing (1.72 s. of arc).

The integrated intensity

$$I_{hi} = \int_{-\infty}^{+\infty} I_h \, d(\Delta\theta) \qquad \text{(II-8-13)}$$

has been shown by *v. Laue* [22] to be equal to:

$$I_{hi} = \frac{\pi |C|\,|\chi_h|}{\sin 2\theta} \left(\sqrt{|\gamma_h|/\gamma_0}\right) \text{th}\,(\pi d/\Lambda_0) \qquad \text{(II-8-14)}$$

When the ratio d/Λ_0 decreases, this expression tends towards that given by the kinematical theory:

$$I_{hi} = \frac{\pi^2 |C|^2 |\chi_h|^2 d}{\gamma_0 \lambda \sin 2\theta} \qquad \text{(II-8-15)}$$

The dynamical theory thus contains the kinematical theory as an approximation for small thicknesses or small structure factors.

III Propagation of real waves

As we have said earlier, real waves are never plane waves and the incident beam usually excites the whole dispersion surface. We shall describe in this section the consequences of this simple fact on the propagation of X-rays in perfect crystals.

III-1 Angular amplification

It is very interesting to study how the path of the wave-fields vary with the departure from Bragg's law of the plane wave associated with the tie-point of the wave-field.

Let $d(\Delta\theta)$ be the angle between the wave vectors of the plane waves associated with two neighbouring tie-points P and P', and $d\alpha$ the angle between the paths of the corresponding wave-fields (fig. 17). We shall call

$$A = \frac{d\alpha}{d(\Delta\theta)} \qquad \text{(III-1-1)}$$

the angular amplification ratio of the crystal.

From (II-2-2) and (II-4-6), it is possible to show that, in the symmetrical Laue case ($\gamma_0 = \gamma_h = \cos\theta$):

$$\operatorname{tg}\alpha = \frac{\eta}{\sqrt{1+\eta^2}}\ \operatorname{tg}\theta \qquad \text{(III-1-2)}$$

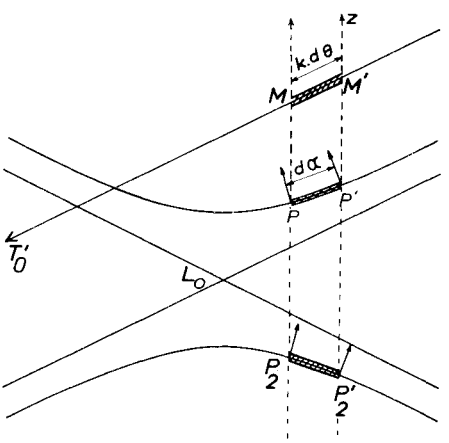

Fig. 17
Domains excited on the dispersion surface by a wave packet MM'.
$d\alpha$ is the angle between the paths of the wave-fields, excited at P and P'.

From (III-1-1), (III-1-2), (II-4-2) and (II-4-3), we obtain:

$$A = \frac{2\sin^2\theta}{\cos\theta}\ \frac{\cos^2\alpha}{(1+\eta^2)^{3/2}}\ \Lambda_0 k \qquad \text{(III-1-3)}$$

If we introduce the radius of curvature $\mathfrak{R}$ of the dispersion surface:

$$\mathfrak{R} = \frac{PP'}{d\alpha} \qquad \text{(III-1-4)}$$

we can show that:

$$A = \frac{\cos\theta}{\cos\alpha} \frac{k}{\mathfrak{R}} \qquad \text{(III-1-5)}$$

Far from Bragg's setting, α is practically equal to $\pm\theta$ and $\mathfrak{R}$ to k, and the amplification ratio is equal to 1.

At the Bragg setting $(\alpha = 0;\ \eta = 0)$:

$$\mathfrak{R}_{Min} = \frac{\Lambda_0^{-1}}{2\,tg^2\theta}$$

$$A_{Max} = \frac{2\sin^2\theta}{\cos\theta} \frac{\Lambda_0}{\lambda} \qquad \text{(III-1-6)}$$

A is proportional to the ratio of the Pendellösung fringe distance to the wave length and is of the order of 10^4. For example, in the case of silicon, reflection 220 and Mo Kα, $A_{Max} = 3.6 \times 10^4$.

At the Bragg setting, the crystal acts therefore as a very powerful angular amplifier. Fig. 18 shows the variation of the angular amplification ratio with the departure from Bragg's law.

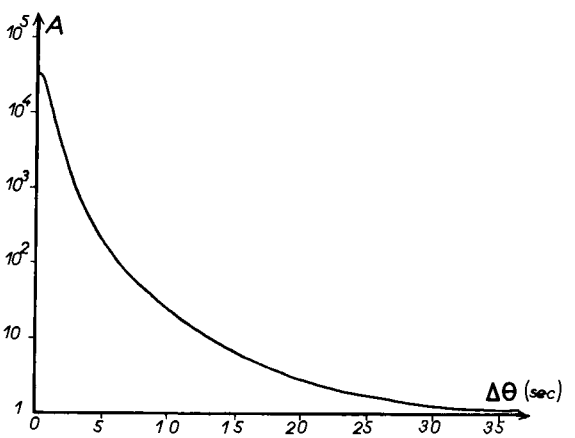

Fig. 18
Variations of the amplification ratio with the departure from Bragg's law.

III-2 Energy distribution on the exit surface

Let us consider a divergent beam emitted by a point or line focus F and falling on a crystal in the Laue setting. Since the width of the rocking curve is very small, the useful part of the incident beam is very narrow and let A be the point where it impinges the surface of the crystal. This beam excites the whole dispersion surface and the propagation directions of the corresponding wave-fields cover the whole angle between the incident and reflected directions AB and AC (fig. 19). The spreading out of the propagation directions in a fan (fig. 19) was first described by *G. Borrmann, G. Hildebrandt* and *H. Wagner* [88]. For this reason, the triangle ABC is called Borrmann fan.

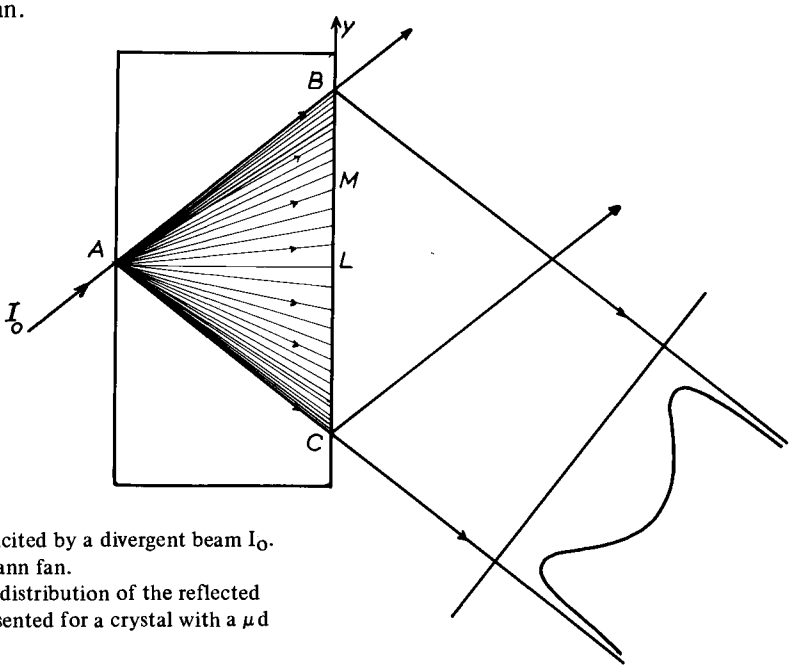

Fig. 19
Wave-fields excited by a divergent beam I_0.
ABC: Borrmann fan.
The intensity distribution of the reflected beam is represented for a crystal with a μd of about 2.5.

Let $I_0(\Delta\theta)$ be the angular distribution of the energy of the beam incident on the crystal, and $I(y)$ be the intensity distribution along the exit surface (fig. 19); y is a position coordinate on the exit surface. The reflecting power is equal to the ratio of the reflected or refracted energy to the incident energy. It can be written in two ways:

$$\frac{I_{mj}(y)\,dy}{I_0(\Delta\theta)\,d(\Delta\theta)} = \frac{\gamma_m \left|\mathfrak{D}_{mj}^{(d)}\right|^2}{\gamma_0 \left|\mathfrak{D}_0^{(a)}\right|^2} \qquad \text{(III-2-1)}$$

$m = 0, h;\ j = 1, 2.$

The intensity distribution is therefore equal to:

$$I_{mj}(y) = \frac{d(\Delta\theta)}{dy} I_0(\Delta\theta) \frac{\gamma_m \left|\mathfrak{D}_{mj}^{(d)}\right|^2}{\gamma_0 \left|\mathfrak{D}_0^{(a)}\right|^2} \qquad \text{(III-2-2)}$$

From (II-5-4) and (III-1-3), we obtain:

$$I_{hj} = \frac{\gamma_0 \sqrt{\gamma_0 \gamma_h}}{2 \sin^2 2\theta} |C| \left|\frac{\chi_h}{\chi_{\bar{h}}}\right| \sqrt{\chi_h \chi_{\bar{h}}} \frac{e^{-\mu_{ej} d/\gamma_0}}{d} \frac{I_0(\Delta\theta)}{(1-Y^2)^{1/2}}$$

$$I_{0j} = \frac{\gamma_0 \sqrt{\gamma_0 \gamma_h}}{2 \sin^2 2\theta} |C| \sqrt{\chi_h \chi_{\bar{h}}} \frac{e^{-\mu_{ej} d/\gamma_0}}{d} \frac{(1+Y)^{1/2}}{(1-Y)^{3/2}} I_0(\Delta\theta) \qquad \text{(III-2-3)}$$

μ_{ej} is given by (II-6-5) and the position of the point M at which the intensity is calculated, is defined by:

$$Y = \frac{\overline{LM}}{\overline{LB}} = \mp \frac{\eta}{\sqrt{1+\eta^2}} \qquad \text{(III-2-4)}$$

L is the mid-point of the base BC of the Bormann fan (see fig. 19).

Expressions (III-2-3) show that there is a considerable energy enhancement on each side of the reflected beam ($Y \to \pm 1$) and on the direct beam side of the refracted beam ($Y \to +1$). This effect, which is predominant for small values of μd, has been called *margin effect* by *Lang* and was calculated by *Kato* [16]. It had in fact been observed by many investigators in the past on Laue spots and often wrongly attributed to surface dammage. The physical reason is that the density of wave-fields propagating on the sides of the Borrmann triangle is very high because of their low angular amplification. Although the energy of each one is small, the total intensity is large: When the crystal is very absorbing, the Borrmann effect becomes predominant and the intensity is maximum in the center of the reflected beam where the anomalous absorption is minimum (see equation (II-6-5). The intensity distributions for a crystal of silicon of 2.7 mm are shown on figure 20.

The intensity distribution in the Bragg case was also calculated by *H. Wagner* [89].

III-3 Double refraction

A plane wave incident on a crystal excites four wave-fields (fig. 5) which have each a different Poynting vector and a different propagation direction. This effect was called *multiple refraction* by *G. Borrmann* [10]. Actually, the paths of wave-fields corresponding to the two directions of polarization are very close and cannot be

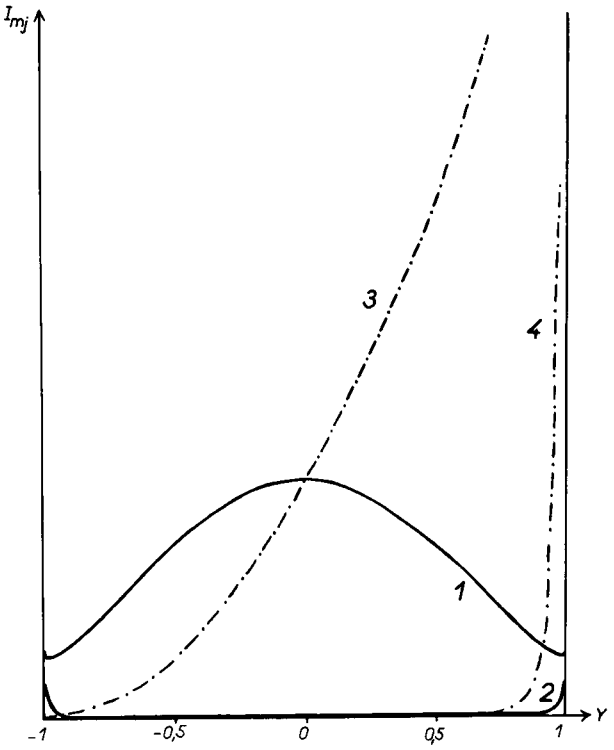

Fig. 20
Intensity distribution on the exit surface - Silicon 220, Mo Kα, d = 2.78 mm
1: reflected beam - branch 1;
2: reflected beam - branch 2;
3: refracted beam - branch 1;
4: refracted beam - branch 2.

separated experimentally. We shall therefore speak of *double* refraction only. This effect would be impossible to observe if a real plane wave existed since it would have an infinite lateral extension. It would also be impossible to observe with an ordinary setting since, as we have seen, the whole dispersion surface is then excited.

It is therefore necessary to have a narrow beam which will excite a small portion only of the dispersion surface, in other words, a beam which is also narrow in reciprocal space. These two conditions are of course contradictory, and it is impossible to obtain a small enough divergence by means of an ordinary setting. With the setting of fig. 21 however, it is possible to obtain a very parallel beam [20, 21]. A long focus is used (8 mm x 20 μm) and the incident beam falls on a first crystal thick enough for wave-fields of type 2 to be absorbed out (~ 3 mm for a silicon crystal and Mo Kα radiation). Since the reflection range is small, the useful part of the incident beam is narrow. It impinges the first crystal at A and excites wave-fields propagating within the *Borrman fan ABC*. The intensity distribution of the reflected beam along the exit surface BC is similar to that represented on fig. 20. In the center of the pattern, the intensity is high, due to the Borrmann effect and the amplification ratio is maximum. If we

put a slit f_1 of about $50\,\mu m$ in the middle of the reflected beam, we isolate a narrow pencil of rays with a very small divergence, of the order of 0.1 s of arc. It corresponds to wave-fields which, in the first crystal, had a path close to AQ (fig. 21).

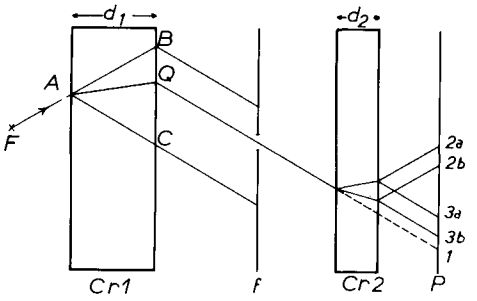

Fig. 21
Experimental set-up to observe the double refraction
F: focus; Cr_1 and Cr_2: first and second crystals; f: slit; P: photographic plate.

This pencil of rays is now incident on a second crystal, identical and practically parallel to the first one. It excites a small portion on each branch of the dispersion surface (fig. 17). Two narrow packets of wave-fields will thus be created. If the mean departure from Bragg's law of the pencil of rays on the second crystal is different from zero, the paths of the two packets of wave-fields will separate at a certain depth. As each wave-field decouples into its two wave components when it reaches the exit surface of the crystal, we expect four traces on a photographic plate P placed beyond the crystal. This is indeed what is observed experimentally [20, 21] and is shown on fig. 22.

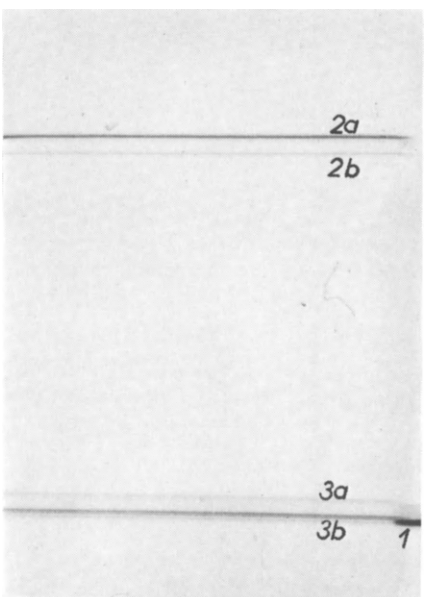

Fig. 22
Double refraction
1: *direct beam;* 2: *reflected beams*
(a: branch 1; b: branch 2)
3: *refracted beams* (a: branch 1; b: branch 2)
Silicon crystals, 220, Mo Kα, d = 0.8 mm.

The pencil of rays isolated by the slit f is of course not a plane wave, but since its angular width (*MM'* in reciprocal space – fig. 17) is very narrow, it can be considered as a good approximation for a plane wave and the experiment *demonstrates the double refraction* of X-rays. It also proves that *the wave-fields have a physical reality* and, so to speak, *materializes the two Ewald waves* which are solutions of the propagation equation (I-6-1).

The same experiment can be done with the second crystal in the Bragg setting and the wave-field described in II-8 isolated [52].

What we have said until now implies that the beams we consider are monochromatic, which is of course not rigorously true. However, if we put the slit symmetrically of the focus with respect to the first crystal, there is a focalization effect and all the pencils isolated by the slit have the same departure from Bragg's law, to the 0.1 s. divergence mentionned above, even if they have different wave-lengths.

Applications

The experiment we have just described is not only interesting from a theoretical point of view, but also has a certain number of applications of which we shall mention two.

a) intrinsic rocking curves

A rocking curve obtained on a double crystal spectrometer is actually a convolution of the intrinsic rocking curves of the two crystals. If we want it to be *intrinsic,* that is identical, or at least as close as possible to that of the second crystal, the width of the rocking curve of the first crystal should be very narrow. This can be achieved using an asymmetrical reflection (see II-8a) [53, 54] or a triple crystal spectrometer [55 to 58].

It can also be achieved, in a very efficient way, with the setting of fig. 21 [59,91], since the divergence of the pencil of X-rays passing through the slit is of 0.1 s. of arc only. Figure 23 shows two examples of rocking curves obtained this way. It can be noticed that their width agrees very well with the theoretical one.

b) measurements of the index of refraction

If a prism of some substance is placed in the path of the pencil of X-rays between the slit and the second crystal, this pencil will be refracted. Since the index of refraction n is always very close to 1 for X-rays, the deviation angle is very small, usually smaller than the width of the rocking curve of the second crystal. When the prism is introduced, the departure from Bragg's law of the pencil of rays for the second crystal is modified, and therefore also the paths of the wave-fields excited in this crystal and the separation of the corresponding traces *2a* and *2b* of the reflected beams on the photograph. The variation of the distance between the traces can easily be measured and the deviation angle of the pencil of rays deduced from it. The value of $n - 1$

can thus be measured to a few percent. The best accuracy is obtained at the minimum deviation angle. For example, this experiment has been done with a prism of aluminium [60]. One finds:

$$\chi_0 \text{ experimental} = 2(n-1) = 3.53 \times 10^{-6} \pm 0.05 \times 10^{-6}$$
$$\chi_0 \text{ theoretical} = 2(n-1) = 3.55 \times 10^{-6}$$

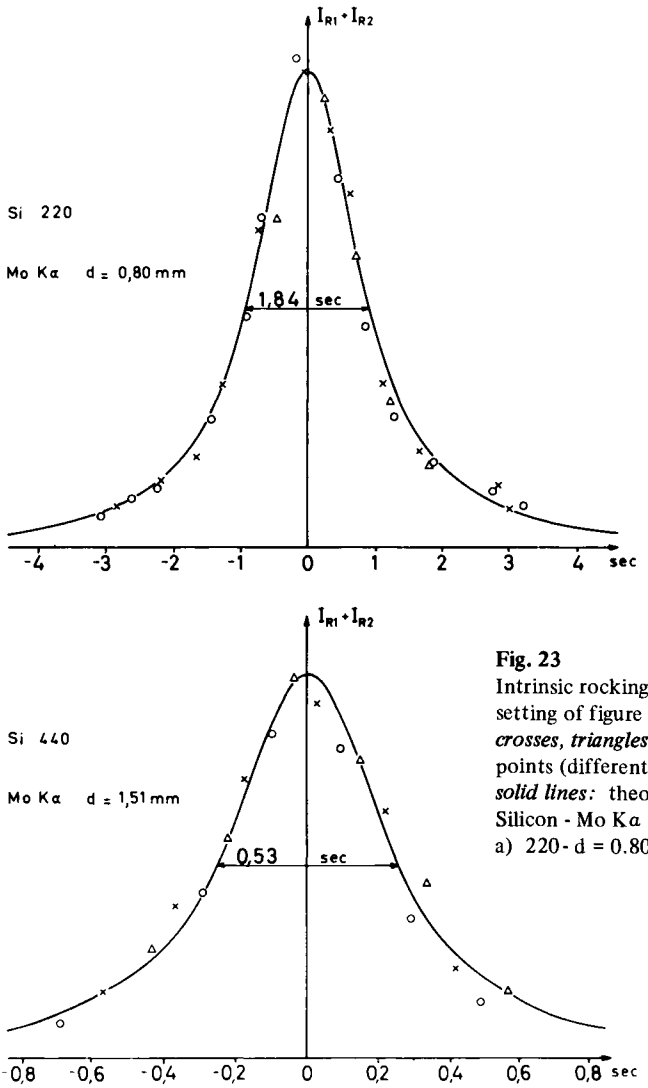

Fig. 23
Intrinsic rocking curves recorded with the setting of figure 21. After [83]
crosses, triangles, circles: experimental points (different runs)
solid lines: theoretical curves.
Silicon - Mo Kα
a) 220 - d = 0.80 mm; b) 440 - d = 1.51 mm.

A similar measurement of the index of refraction of materials for X-rays has been done by *Okkerse* [61] using a single "L" shaped crystal. The vertical bar is used as a first crystal and is very thick; due to the Borrmann effect, a narrow beam only is reflected; it falls on the horizontal bar of the "L" where it undergoes total reflection. The introduction of a prism of plastic on the path of the beam, between both bars, will change very slightly the glancing angle of the beam on the second part of the crystal and the reflected intensity is modified. The index of refraction can be thus measured.

III-4 Pendellösung fringes

a) Plane wave Pendellösung

In II-7, we described the interference between the two wave-fields created by a given plane wave. Equation (II-7-2) shows that there is a periodic exchange of energy between the total reflected and refracted beams when the thickness of the crystal increases. This is the reason why *Ewald* spoke of the *oscillating solution (Pendellösung)* of the propagation equation. This effect can be observed using the setting of fig. 21 with a wedge shaped second crystal. The pencil of X-rays passing through the slit has a certain breadth and the separation of the wave-fields excited in the crystal can only occur after a certain depth (fig. 24). When the thickness is too small for the wave-fields to be separated, the oscillations of the refracted and reflected beams can be observed on the topograph [62] (fig. 25). It can be noticed that they are in opposition for both beams.

Fringes of the same type can also be observed using a single crystal with a gap sawn into it [63].

b) Spherical wave Pendellösung

Let us consider an ordinary beam, that is a spherical wave, falling on a single crystal and the Borrmann fan ABC it excites (fig. 26a). Which wave-fields propagate along any given path AM? They correspond to tie-points where the normal to the dispersion surface is parallel to AM. Fig. 26b shows that there are two such points, lying on a diameter of the hyperbola. Two wave-fields propagate therefore along AM: they are coherent since they are excited by the same spherical wave and they interfere. We shall show in section IV that the equal intensity curves in the plane of incidence are hyperbolae asymptotic to the sides of the Borrmann fan (fig. 26a). Corrresponding fringes can be observed on a photographic plate placed in the reflected or the transmitted beams. They were first observed by *Kato* and *Lang* [19] and explained by *Kato* [17]. It must be remembered that the interfering fields are different from those of the plane-wave Pendellösung fringes.

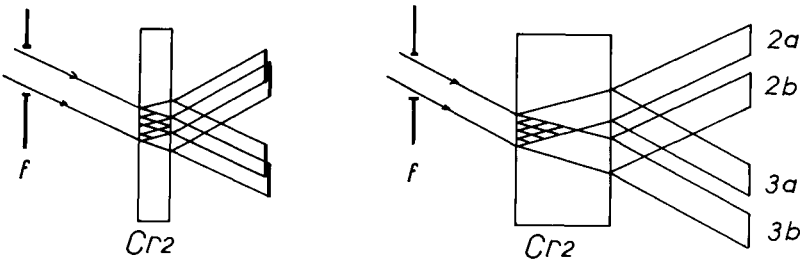

Fig. 24

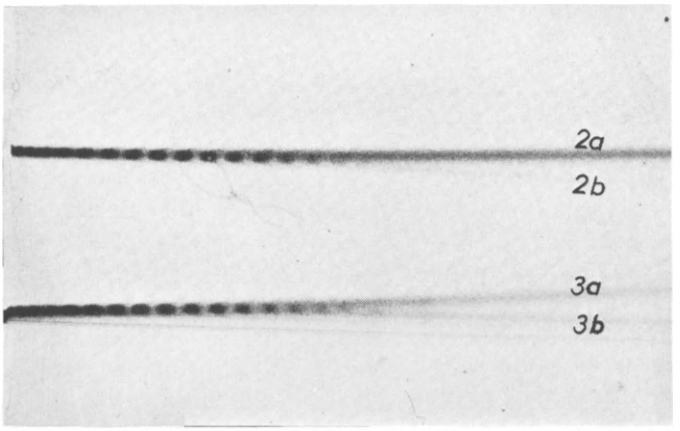

Fig. 25
Plane wave Pendellösung fringes
The second crystal is wedge-shaped. On the left hand side, it is too thin for both wave-fields to be separated (see fig. 24a). The wave-fields interfere. Notice that maxima in the reflected beam (2) correspond to minima in the refracted beam (3). One the right hand side, the crystal is thick enough for the wave fields to be separated and four traces can be seen.

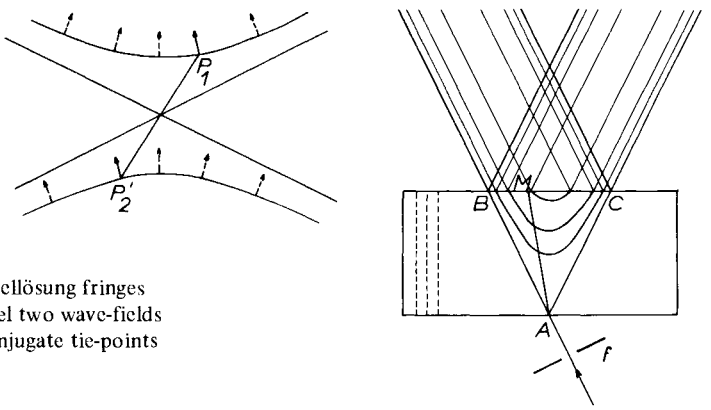

Fig. 26
Spherical wave Pendellösung fringes
Along path AM travel two wave-fields corresponding to conjugate tie-points P_1 and P'_2 .

If one uses a point focus and a narrow slit f parallel to the reflecting planes in front of the crystal (fig. 26a), the equal intensity surfaces are hyperbolic cylinders parallel to the slit. Fringes observed on a photographic plate placed in the reflected beam will be straight lines for a plane parallel crystal (fig. 27) and hyperbolae for a wedge shaped crystal (fig. 28).

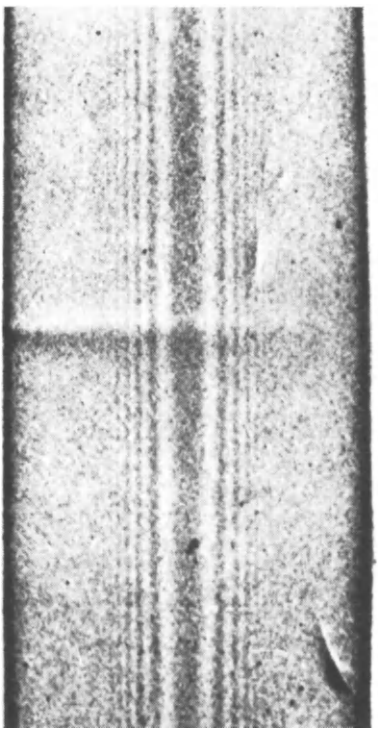

Fig. 27
Spherical wave Pendellösung fringes.
Plane parallel Silicon crystal 0.8 mm thick – Mo Kα-111 - reflection.

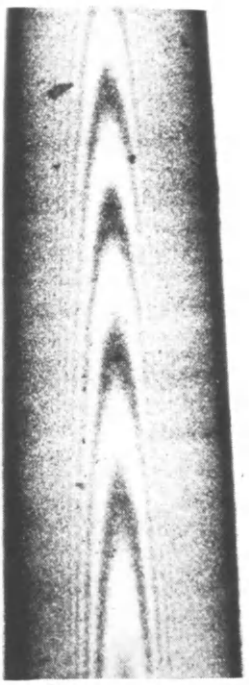

Fig. 28
Spherical wave Pendellösung fringes – wedge shaped $NaNO_3$ crystal. Mo Kα.

IV Generalized Diffraction Theory

The X-ray optics described in section II and III are related to the geometric optics in that they are ray optics. They are inadequate to treat fully the case of an incident spherical wave or that of the diffraction effects due to a slit, for instance. To do that, the equivalent of physical optics is necessary. This can be done either by expanding the incident wave in plane waves by means of a Fourier integral and using the results of the classical theory, which has been done by *Kato* [17] or by solving the generalized equations (I-8-2).

IV-1 Numerical integration of the fundamental equations

In the general case, in particular when β_h is not constant, as in a deformed crystal, there is no simple analytical solution of equations (I-8-2). *S. Takagi* [18] has given the principle of the calculations. Let M be the point where the values of the total amplitudes D_0 and D_h are sought for, P_1 and Q_1 two neighbouring points such that P_1M and Q_1M are respectively parallel to the incident and reflected directions (fig. 29). Using a first order Taylor expansion, it is possible to show that (I-8-2) can be written [42]:

$$D_0(M) = D_0(P_1) + p\,(-i\pi kC\,\chi_{\bar{h}})\,D_h(P_1)$$

$$D_h(M) = D_h(Q_1) + q\,(-i\pi kC\,\chi_h)\,D_0(Q_1) + q\,(2\,i\pi k\beta_h)\,D_h(Q_1) \qquad \text{(IV-1-1)}$$

with $p = P_1M$; $q = Q_1M$.

The amplitudes D_0 and D_h in M are thus given in terms of the values they take in P_1 and Q_1. If their values are known along any straight line parallel to P_1Q_1, they are easy to derive in M by means of a step by step calculation. Since these values are known along the entrance surface, the easiest is to choose P_1Q_1 parallel to it and p/q equal to γ_h/γ_0 (see fig. 29). To have a good accuracy, one should use a large number of steps and a computer is necessary.

IV-2 Analytical solution

An analytical solution of (I-8-2) has been given by *S. Takagi,* but has unfortunately not been published by its author [1]). The principle of his derivation will be summarized here.

---

[1]) It will be published in the May issue of the Tourn of the Phys. Soc. of Japan, 1969.

The system (I-8-2) can easily be transformed into a system of two independant second order partial differential equations:

$$\frac{\partial^2 D_0}{\partial s_0 \partial s_h} - 2i\pi k\beta_h \frac{\partial D_0}{\partial s_0} + \pi^2 k^2 \chi_h \chi_{\bar{h}} D_0 = 0$$
$$\frac{\partial^2 D_h}{\partial s_0 \partial s_h} - 2i\pi k\beta_h \frac{\partial D_h}{\partial s_0} + \pi^2 k^2 \chi_h \chi_{\bar{h}} D_h = 0 \qquad \text{(IV-2-1)}$$

These equations are hyperbolic and an integration method has been given by *Riemann* (see for example [64]). Equations (IV-2-1) are of the form:

$$L[u] \equiv \frac{\partial^2 u}{\partial X \partial Y} + a(X,Y)\frac{\partial u}{\partial X} + b(X,Y)\frac{\partial u}{\partial Y} + c(X,Y) = f(X,Y) \qquad \text{(IV-2-2)}$$

Let us put:

$$M[v] \equiv \frac{\partial^2 v}{\partial X \partial Y} - \frac{\partial (av)}{\partial X} - \frac{\partial (bv)}{\partial Y} + cv \qquad \text{(IV-2-3)}$$

where v, or *Riemann function,* is to be determined. Let us consider the integral of $(vL[u] - uM[v])$ over the area inside a closed curve **C**. There comes, by means of Stokes' theorem:

$$\iint (vL[u] - uM[v])\,dX\,dY = \frac{1}{2}\int_C \left(v\frac{\partial u}{\partial X} - u\frac{\partial v}{\partial X} + 2buv\right)dX - \frac{1}{2}\int_C \left(v\frac{\partial u}{\partial Y} - u\frac{\partial v}{\partial Y} + 2auv\right) \qquad \text{(IV-2-4)}$$

Let us now assume that the curve **C** is made of two segments MP_0 and MQ_0 respectively parallel to the X and Y coordinates axes and of an arc P_0Q_0 such that in no point the tangent to the curve is parallel to either one of the coordinate axes. It is possible to find the solution of (IV-2-2) in M if one knows the value of u, $\partial u/\partial X$, $\partial u/\partial Y$ along P_0Q_0 and if the Riemann function satisfies the following conditions:

$$\begin{aligned} M[v] &= 0 \\ bv &= \partial u/\partial X \text{ along } P_0M \\ av &= \partial u/\partial Y \text{ along } Q_0M \\ v[M] &= 1 \end{aligned} \qquad \text{(IV-2-5)}$$

Let us now choose the coordinates axes respectively parallel to the incident and reflected directions and P_0Q_0 parallel to the surface of the crystal (fig. 29). The boundary conditions will give us the values of the amplitudes and their derivatives along P_0Q_0.

In order to satisfy the continuity of the tangential component of the wave vector, we shall write the incident wave in the following way:

$$\mathbf{D}_0^{(a)} = \mathbf{D}_0^{(a)}(\mathbf{r}) \exp - 2\pi i \mathbf{k}_0 \cdot \mathbf{r} \qquad \text{(IV-2-6)}$$

where $\mathbf{k}_0$ and the wave vector $\mathbf{K}_0$ *chosen* inside the crystal(I-6)have the same component along the surface of the crystal. It is thus the couple of vectors $\mathbf{k}_0, \mathbf{K}_0$ which is arbitrarily chosen and of which depends the value of the parameter β_h, equation (I-8-3).

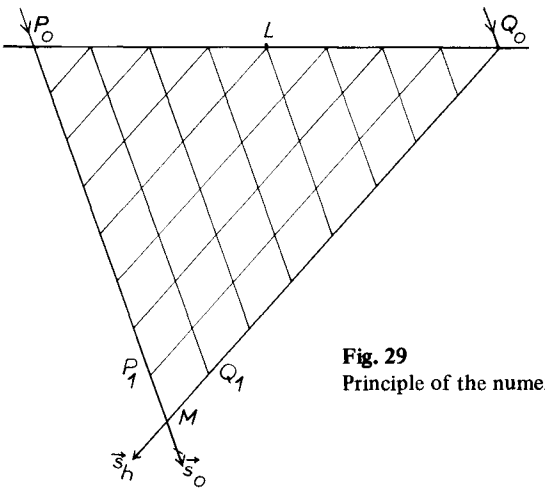

Fig. 29
Principle of the numerical resolution of Takagi's equations.

For example, the amplitude of an incident plane wave of wave vector $\mathbf{K}_0^{(a)}$ would be written:

$$\mathbf{D}_0^{(a)} = \left[\mathfrak{D}_0^{(a)} \exp - 2\pi i \left(\mathbf{K}_0^{(a)} - \mathbf{k}_0\right) \cdot \mathbf{r}\right] \exp - 2\pi i \mathbf{k}_0 \cdot \mathbf{r} \qquad \text{(IV-2-7)}$$

Using this convention, the boundary conditions are, for the amplitudes:

$$D_0 = \mathfrak{D}_0^{(a)} \; ; \; D_h = 0 \text{ along } P_0Q_0 \qquad \text{(IV-2-8)}$$

and, for their derivatives:

$$\left[\frac{\partial D_0}{\partial s_0}\right]_{P_0Q_0} = 0 \; ; \; \left[\frac{\partial D_0}{\partial s_h}\right]_{P_0Q_0} = \frac{\sin 2\theta}{\gamma_0} \left[\frac{\partial \mathfrak{D}_0^{(a)}}{\partial y}\right]_{P_0Q_0}$$

$$\left[\frac{\partial D_h}{\partial s_0}\right]_{P_0Q_0} = -i\pi k \frac{\gamma_0}{\gamma_h} \chi_h \mathbf{D}_0^{(a)} \; ; \; \left[\frac{\partial D_h}{\partial s_h}\right]_{P_0Q_0} = -i\pi k \chi_h \mathfrak{D}_0^{(a)} \qquad \text{(IV-2-9)}$$

y is a coordinate along P_0Q_0.

From (IV-2-4), (IV-2-1), (IV-2-5) and (IV-2-8), (IV-2-9), we obtain an expression for the amplitudes in M in terms of the Riemann function:

$$D_h(M) = -\frac{i\pi k \chi_h \gamma_0}{\sin 2\theta} \int_{P_0Q_0} \mathfrak{D}_0^{(a)}(y)\, v\, dy$$

$$D_0(M) = \frac{1}{2}\left[\mathfrak{D}_0^{(a)}(P_0) + \mathfrak{D}_0^{(a)}(Q_0)\right] \qquad \text{(IV-2-10)}$$

$$- \frac{1}{2\sin 2\theta} \int_{P_0Q_0} \left[\mathfrak{D}_0^{(a)}\left(\gamma_h \frac{\partial v}{\partial s_0} + \gamma_0 \frac{\partial v}{\partial s_h}\right) - \gamma_0 v \frac{\partial \mathfrak{D}_0^{(a)}}{\partial s_h}\right] dy$$

It is possible to show that, when the parameter β_h is equal to zero, which it is always possible to have in a perfect crystal by an appropriate choice of the vectors $\mathbf{k}_0$ and $\mathbf{K}_0$, the Riemann function is equal to:

$$v = J_0\left[G\sqrt{l^2 - y^2}\right] \qquad \text{(IV-2-11)}$$

The origin of the y coordinates is the mid-point L of P_0Q_0,

$$l = LQ_0; \qquad G = 2\pi\gamma_0\gamma_h/\Lambda_0 \sin 2\theta \qquad \text{(IV-2-12)}$$

Λ_0 is defined by (II-4-4).

It is particularly remarquable that the amplitudes D_h and D_0 in M are functions of the values taken by the incident amplitude along the segment P_0Q_0 only of the entrance surface.

IV-3 Solution for an incident spherical wave

The amplitude of a spherical wave can be written, using (IV-2-6):

$$D_0^{(a)}(\mathbf{r}) = \left[D_0^{(a)} \frac{\exp -2\pi i(kr - \mathbf{k}_0 \cdot \mathbf{r})}{4\pi r}\right] \exp -2\pi i \mathbf{k}_0 \cdot \mathbf{r} \qquad \text{(IV-3-1)}$$

If one puts the term between square brackets in (IV-2-10) and integrates by the stationnary phase method, one obtains, for the amplitudes:

$$D_h(M) = -i\frac{\mathfrak{D}_0^{(a)}}{4}\sqrt{\frac{k}{r_0}}\frac{\sqrt{\chi_h\chi_{\bar{h}}}}{\sin 2\theta} e^{-i\pi/4} J_0\left(G\sqrt{l^2 - y_0^2}\right)$$

$$D_0(M) = \frac{\mathfrak{D}_0^{(a)}}{4\pi r_0}\left\{\exp\left[-\pi i k \gamma_0^2 (l - y_0)^2 / r_0\right]\right. \qquad \text{(IV-3-2)}$$

$$\left. - e^{-i\pi/4}\sqrt{kr_0}\sqrt{\chi_h\chi_{\bar{h}}}\sqrt{\frac{\gamma_h}{\gamma_0}}\sqrt{\frac{l + y_0}{l - y_0}} J_1\left(G\sqrt{l^2 - y_0^2}\right)\right\}$$

where y_0 is the abscissa of M relative to a point E of the exit surface defined as follows: let F be the source of the spherical wave, A the point of the entrance surface such that FA satisfies the geometric Bragg condition ($FA = r_0$) and BC the base of the corresponding Borrmann triangle (fig. 30); E is the mid-point of BC and $2l = BC$.

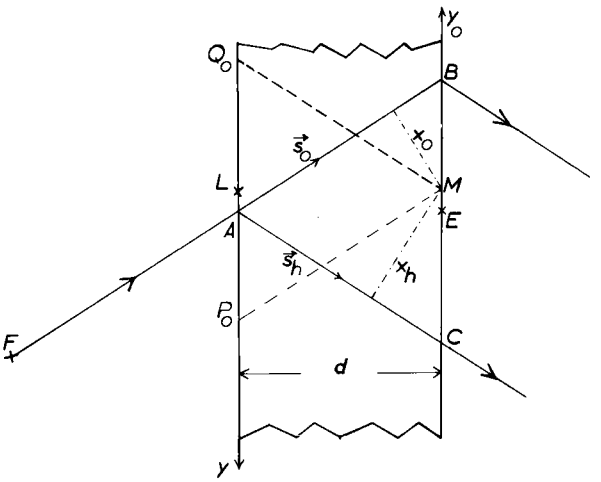

Fig. 30
ABC: Borrmann fan for the incident beam *FA*.
MP_0Q_0: integration triangle for point *M*.

The first term in the curly brackets in the expression of the amplitudes of $D_0(M)$ corresponds to the direct beam AB, that is to that part of the incident beam which is out of Bragg condition.

Both the reflected and the refracted amplitudes contain a Bessel function term and are therefore oscillating. The physical interpretation has been given in section III-4b: these oscillations can be considered as due to the interference of two wave-fields propagating along AM and corresponding to conjugate tie-points on the dispersion surface. This has been shown to be true by *Kato* [17] by interpreting the Fourier expansion of the spherical wave.

The constant amplitude curves are given in the plane of incidence by:

$$G\sqrt{l^2 - y_0^2} = G\sqrt{MB \cdot MC} = \text{constant}$$

$$\frac{G}{\sqrt{\gamma_0 \gamma_h}} \sqrt{x_0 x_h} = \text{constant}$$

where x_0 and x_h are the distances of M from AB and AC (fig. 30). The equal amplitude curves are therefore hyperbolae $x_0 x_h = constant$, asymptotic to the sides of the Borrmann triangle (see figs. 26, 27, 28). This result was first proved by *Kato* [17]. It is directly related to the shape of the dispersion surface. A careful study of

the fringes obtained with a wedge shaped crystal has been made, showing them to be really hyperbolic [65]. This was the first direct proof with X-rays that the dispersion surface is hyperbolic.

When the crystal is absorbing, a similar derivation can be done, using complex Bessel functions. An asymptotic expression can be used when the crystal is thicker than a few extinction distances:

$$I_h \sim |A_h|^2 \exp -\frac{1}{2}\mu d\left[\frac{1}{\gamma_0}+\frac{1}{\gamma_h}-Y\left(\frac{1}{\gamma_0}-\frac{1}{\gamma_h}\right)\right]\frac{\mathrm{sh}^2\left(\pi\frac{d}{\tau}\sqrt{1-Y^2}\right)+\cos^2\pi\left(\frac{d}{t}\sqrt{1-Y^2}-\frac{1}{4}\right)}{1-Y^2} \qquad \text{(IV-3-3)}$$

$$I_0 \sim |A_0|^2 \exp -\frac{1}{2}\mu d\left[\frac{1}{\gamma_0}+\frac{1}{\gamma_h}-Y\left(\frac{1}{\gamma_0}-\frac{1}{\gamma_h}\right)\right]\frac{1-Y}{1+Y}\,\frac{\mathrm{sh}^2\left(\pi\frac{d}{\tau}\sqrt{1-Y^2}\right)+\cos^2\pi\left(\frac{d}{t}\sqrt{1-Y^2}+\frac{1}{4}\right)}{1-Y^2}$$

where
$Y = \overline{EM}/\overline{EB}$, A_0 and A_h are constants t^{-1} and τ^{-1} are the real and imaginary parts of Λ_0^{-1} respectively. Expressions (IV-3-3) show that the contrast of the fringes decrease with increasing thickness of the crystal, that is when wave-fields of type 2 are highly absorbed.

IV-4 Relation between the solutions for incident spherical and plane waves

From (IV-3-2), we see that the amplitude of the reflected wave for an incident spherical wave is proportional to the Riemann function. The same result is obviously obtained if the incident wave is a plane wave limited by an infinitely thin slit; the incident amplitude $\mathfrak{D}_0^{(a)}$ in (IV-2-10) is then replaced by a delta function.

On the other hand, it is easy to see from (IV-2-7) and (IV-2-10) that the solution in the case of an incident plane wave can be written:

$$D_h^P \sim \mathfrak{D}_0^{(a)} \int_{-1}^{+1} e^{-2\pi i \Delta T y} J_0(G\sqrt{l^2-y^2})\,dy \qquad \text{(IV-4-1)}$$

where ΔT is the component of $(\mathbf{K}_0^{(a)} - \mathbf{k}_0)$ parallel to the entrance surface. If the couple of vectors $\mathbf{K}_0, \mathbf{k}_0$ is chosen such that $\beta_h = 0$, $\mathbf{K}_0$ is equal to $\mathbf{OL}_0$ (fig. 5) and ΔT is proportional to MM_0, that is to the parameter η which we have defined (equation (II-4-3)) to characterize the departure from Bragg' law of a plane wave.
Let us introduce a function $D_h'^S$ equal to $\mathfrak{D}_0^{(a)} J_0(G\sqrt{l^2-y^2})$ for $|y|<1$ and equal to zero for $|y|>1$. Equation (IV-4-1) shows that $D_h'^S$ and D_h^P are Fourier transforms. This result is very important since it shows as well that the solutions D_h^P

and D_h^S of the propagation equation for incident plane and spherical waves respectively are proportional to Fourier transforms. The reciprocal variables are ΔT or the departure from Bragg's law for D_h^P and the coordinate along the exit surface for D_h^S. This result can be applied to integrate the total reflected intensity over CB in the case of an incident spherical wave. This integral is also equal to the total intensity received in M if the crystal is traversed in the incident beam as is done in *traverse topographs*. Parceval's theorem shows that this intensity is equal to the integrated intensity (II-7-3) for the plane wave case. The intensity observed on a traverse topograph is therefore an oscillating function of thickness. An example is given in fig. 31.

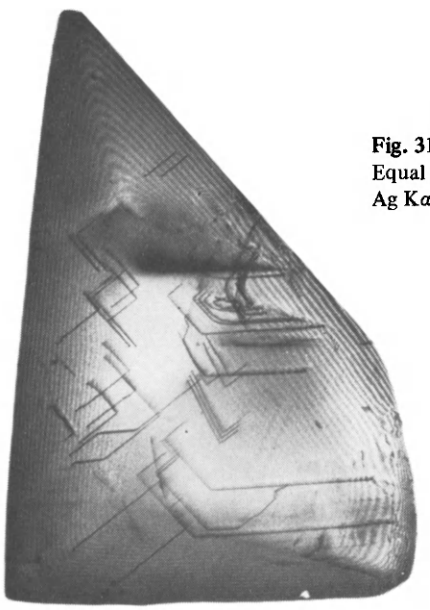

Fig. 31
Equal thickness fringes - pyramid shaped silicon crystal
Ag Kα - 111 reflection - After [84].

IV-5 Diffraction by a slit

When a beam is limited by a slit, diffraction effects occur and it is interesting to study their influence on the interference pattern inside a crystal. An example of such a situation is given by the experiment described in III-3.

Let us thus consider a beam limited by a slit of width e and falling on a crystal of thickness d where it excites wave-fields. At the exit surface of the crystal, these wave-fields decouple into their two wave components and we shall study the fine structure of their traces on a screen placed at a distance r from the slit (fig. 32).

There are two approaches to this problem. One is to extend the well known calculations of ordinary optics. The amplitude distribution on the screen is given in that case by a Fresnel integral:

$$\int_{v_1}^{v_2} (\exp - i\pi v^2/2)\,dv \qquad \text{(IV-5-1)}$$

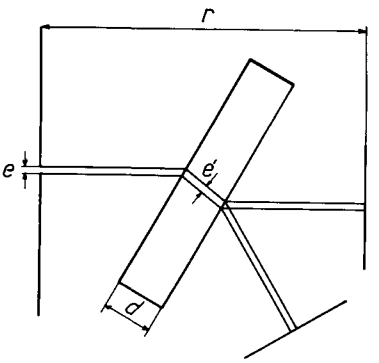

Fig. 32

and the shape of the diffraction pattern depends on the value of a parameter:

$$w = v_2 - v_1 = e\sqrt{2/r\lambda} \qquad \text{(IV-5-2)}$$

For instance, Fraunhofer diffraction corresponds to $w < 0.5$.

A similar calculation can be done when the beam crosses a crystal at or near the Bragg setting, but one has to take into account the angular amplification, or dispersion effect, described in III-1. If the region of the dispersion surface excited by the beam remains small, it can be shown [66] that the amplitude on the screen is also given by a Fresnel integral but that the parameter w is now equal to:

$$w = e' \sqrt{\frac{\cos\theta}{\cos\alpha}\,\frac{2}{A\,d\lambda}} = e' \sqrt{\frac{2\Re}{d}} \qquad \text{(IV-5-3)}$$

where e' is the width of the beam within the crystal (fig. 32), α the angle between the path of the X-rays and the reflecting planes, $\Re$ the radius of curvature of the dispersion surface.

One sees that the main effect is to obtain the same diffraction pattern as in air, but at a distance A times nearer. This effect has been confirmed by experiment [66]. It must be remembered that in the middle of the reflection range A is of the order of 10^4 or 10^5! Expression (IV-5-3) shows also that the diffraction pattern is the same it would be in air, but with a wave-length equal to $\Re^{-1}$.

Remembering that at the exact Bragg angle

$$A_{max} = \frac{2\sin^2\theta}{\cos\theta}\,\frac{\Lambda_0}{\lambda}$$

one notices also that the expression of w becomes similar to that taken in air if one replaces the wave-length λ by the Pendellösung fringe distance Λ_0 multiplied by a numerical factor; this quantity is of the order of the optical wave-lengths and the diffraction patterns are therefore of the same type as those observed in the same conditions (slit width e', distance d) with visible light!

The other approach to the problem is naturally to solve the fundamental equations (I-8-2) with appropriate boundary conditions. This has been done [42] and fig. 33 shows the variation of the diffraction pattern with the thickness d of the crystal. It is in good agreement with the pattern expected from the corresponding value of w.

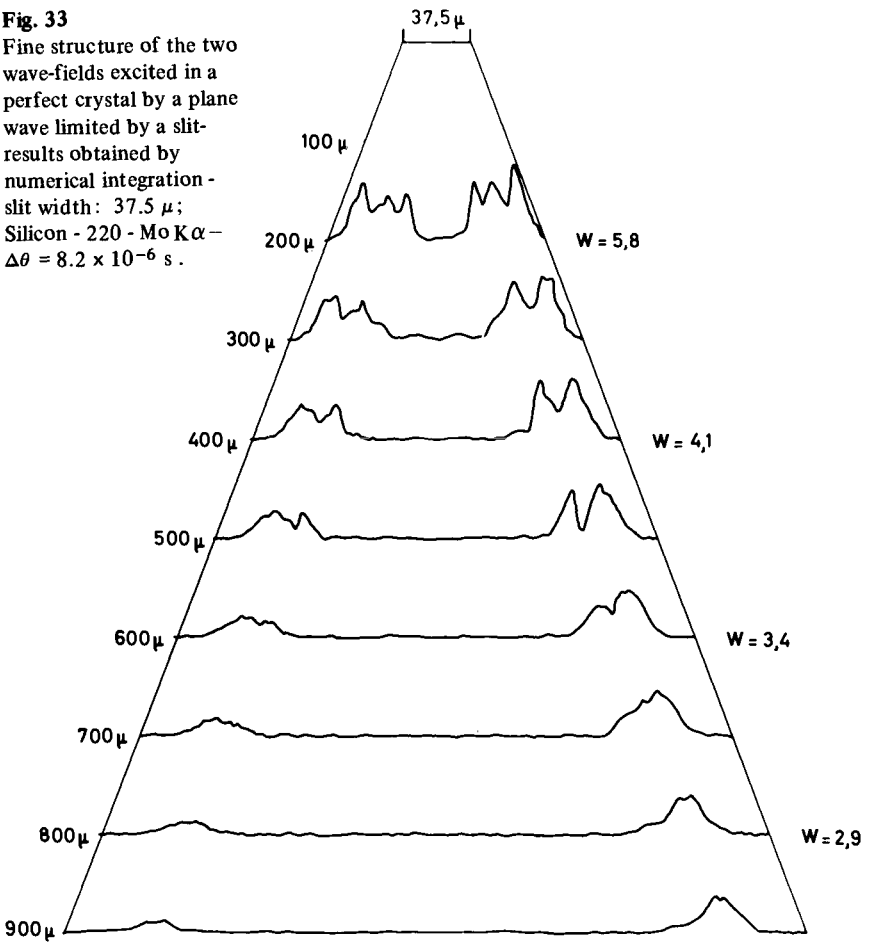

Fig. 33
Fine structure of the two wave-fields excited in a perfect crystal by a plane wave limited by a slit-results obtained by numerical integration - slit width: 37.5 μ; Silicon - 220 - Mo Kα - $\Delta\theta = 8.2 \times 10^{-6}$ s.

V Conclusion

The dynamical theory is quite remarquable in that its conclusions are always in very good agreement with experimental results. For example, the fundamental concept of wave-fields has been proved by several completely independant experiments. Although the theory originated fifty years ago, and is essentially based on the old electromagnetic theory, it is still very much alive and in constant progress. New chapters have been developped recently such as the anomalous absorption (1950), the direction of propagation of wave-fields (1952–1958), the extension to spherical waves (1961), the influence of diffraction effects (1966). At the same time, the improvement in the techniques has allowed old results to be observed experimentally, such as plane wave Pendellösung (1965) and Bragg case Pendellösung (1967) or the exact shape of the dispersion surface (1966). The angular resolution of the spectrographs has increased to the point that it is now possible to record rocking curves half a second wide!

What are the present day applications of the dynamical theory, independantly of the purely theoretical aspect? They lie mainly in two fields:

– *perfect crystals:* absolute and accurate structure factor measurements from Pendellösung fringes [67 to 71], accurate lattice parameter determinations, development of X-ray interferometers, [72, 73, 74].

– *imperfect crystals:* topographic techniques for the study of defects have developped considerably in recent years and are now in common use. They depend mainly on the dynamical theory for the interpretation of the contrast of images. The theory of the contrast due to long-range strains [75 to 78, 18, 43], dislocation lines [44, 45, 79, 80], stacking faults [81, 82] is now well understood and will have many applications.

References

[1] *Darwin, C.*, Phil.Mag. **27**, 315 and 675 (1914).
[2] *Ewald, P. P.*, Ann. Phys. Dtsch. **54**, 519 (1917).
[3] *von Laue, M., Friedrich, W., Knipping, P.*, München, Sitzungsbericht 383 (1912).
[4] *Borrmann, G.*, Physik. Z. **42**, 157 (1941).
[5] *Borrmann, G.*, Z. Physik. **127**, 297 (1950).
[6] *Campbell, H.*, Acta Cryst. **4**, 180 (1951).
[7] *von Laue M.*, Acta Cryst. **2**, 106 (1949).
[8] *Borrmann, G.*, Zeit. f. Krist., **106**, 109 (1954).
[9] *von Laue M.*, Acta Cryst., **5**, 619 (1952).
[10] *Borrmann, G.*, Naturwiss. **42**, 67 (1955).

[11] *Wagner, H.*, Z. Physik **146**, 127 (1956).
[12] *Kato, N.*, Acta Cryst. **11**, 885 (1958).
[13] *Ewald, P. P.*, Acta Cryst. **11**, 888 (1958).
[14] *Wagner, E. H.*, Z. Physik **154**, 352 (1959).
[15] *Borrmann, G.*, Beiträge zur Physik und Chemie des 20. Jahrhunderts. Vieweg & Sohn, 262 (1959).
[16] *Kato, N.*, Acta Cryst. **13**, 349 (1960).
[17] *Kato, N.*, Acta Cryst. **14**, 526, 627 (1961).
[18] *Takagi, S.*, Acta Cryst. **15**, 1311 (1962).
[19] *Kato, N.* and *Lang, A. R.*, Acta Cryst. **12**, 787 (1959).
[20] *Authier, A.*, C. R. Acad. Sci., Paris **251**, 2003 (1960).
[21] *Authier, A.*, Bull. Soc. Fr. Miner. **84**, 51 (1961).
[22] *von Laue, M.*, Röntgenstrahl-Interferenzen, **10**, 3rd ed. Frankfurt a. M. (1961).
[23] *Zachariasen, W.*, Theory of X-ray diffraction in Crystals. John Wiley, New York (1945).
[24] *James, R. W.*, The optical principles of the diffraction of X-rays, G. Bell and sons (1950).
[25] *James, R. W.*, Solid State Physics, **15**, 53 (1963).
[26] *Kohra, K.*, X-ray Crystallography (Maruzen Co Ltd.) II-9, 849 (1961).
[27] *Batterman, B. W.* and *Cole, H.*, Rev. Mod. Physics **36**, 681 (1964).
[28] *Borrmann, G.*, Zeit. f. Krist. **120**, 143 (1964).
[29] *Ewald, P. P.*, Rev. Mod. Phys. **37**, 46 (1965).
[30] *Borie, B.*, Acta Cryst. **23**, 210 (1967).
[31] *Warren, B. E.*, X-ray diffraction-under press.
[32] *von Laue, M.*, Ergebnisse exakt. Naturwiss. **10**, 133 (1931).
[33] *Parthasarathy, R.*, Acta Cryst. **13**, 802 (1960).
[34] *Laval, J.*, Lectures at the College de France (unpublished) (1960).
[35] *Ohtsuki, Y. H.*, J. Phys. Soc. Jap. **19**, 2285 (1964).
[36] *Kambe, K.*, Zeit. f. Naturforsch. **20a**, 1730 (1965).
[37] *Hildebrandt, G.* and *Wagenfeld, H.*, Acta Cryst. **16**, Supp. A 106 (1963).
[38] *Batterman, B. W.*, Phys. Rev. **134 A**, 1354 (1964).
[39] *Homma, S., Ando Y., Kato, N.*, J. Phys. Soc. Jap. **21**, 160 (1966).
[40] *Takagi, S.*, unpublished.
[41] *Authier, A., Simon, D.*, Acta Cryst. **A 24**, 517 (1968).
[42] *Authier, A., Malgrange C., Tournarie M.*, Acta Cryst. A **24**, 126 (1968).
[43] *Taupin, D.*, Bull. Soc. Fr. Miner. Crist. **87**, 469 (1964).
[44] *Taupin, D.*, Acta Cryst. **23**, 25 (1967).
[45] *Balibar, F.* and *Authier, A.*, Phys. Stat. Solidi, **21**, 413 (1967).
[46] *Wagenfeld, H.*, Phys. Rev. **144**, 216 (1966).
[47] *Borrmann, G.*, 7th Int. Congress of Crystallography, Moscow (1966).
[48] *Schwartz, G.* and *Rogosa, G. L.*, Phys. Rev. **95**, 951 (1954).
[49] *Brogren, G.* and *Addell, O.*, Ark. Fys., **9**, 1 (1954).
[50] *Kato, N.*, J. Phys. Soc. Jap. **10**, 46 (1955).

[51] *Battermann, B. W.* and *Hildebrandt, G.*, Phys. Statu Solidi. **23**, K 147 (1967).
[52] *Authier, A.*, J. Phys. Rad. **23**, 961 (1962).
[53] *Renninger, M.*, Zeit. für Naturforsch. **16a**, 1110 (1961).
[54] *Kohra, K.*, J. Phys. Soc. Japan **17**, 589 (1962).
[55] *Renninger, M.*, Acta Cryst. **8**, 597 (1955).
[56] *Bubakova, R., Drahokoupil, J., Fingerland, A.*, Czech. J. of Physics, **B 11**, 199 (1961).
[57] *Bubakova, R., Drahokoupil, J., Fingerland, A.*, Czech. J. of Physics, **B 12**, 538 (1962).
[58] *Bubakova, R., Drahokoupil, J., Fingerland, A.*, Czech. J. of Physics, **B 12**, 764 (1962).
[59] *Authier, A.*, C. R. Acad. Sci. Paris, **251**, 2502 (1960).
[60] *Authier, A., Malgrange, C., Velu, E.*, J. of Appl. Cryst. (1968), 1, 181.
[61] *Okkerse, B.*, Philips Research Rpts, **18**, 413 (1963).
[62] *Malgrange, C.* and *Authier, A.*, C. R. Acad. Sci. Paris, **261**, 3774 (1965).
[63] *Authier, A., Milne, D., Sauvage, M.*, Physica Statu Solidi, **26**, 469 (1968).
[64] *Sommerfeld*, Partial Differential equations. Academic Press, p. 52 (1949).
[65] *Hattori, H.* and *Kato, N.*, J. Phys. Soc. Japan, **21**, 1772 (1966).
[66] *Authier, A.* and *Malgrange, C.*, C. R. Acad. Sci. Paris, **262**, 429 (1966).
[67] *Hart, M.* and *Lang, A. R.*, Phys. Rev. Letters, **7**, 120 (1961).
[68] *Hattori, A., Kuriyama, H., Katagawa, T.* and *Kato, N.*, J. Phys. Soc. Japan, **20**, 988 (1965).
[69] *Hattori, H., Kuriyama, H., Kato, N.*, J. Phys. Soc. Japan, **20**, 1047 (1965).
[70] *Kato, N.* and *Tanemura, S.*, Phys. Rev. Letters, **19**, 22 (1967).
[71] *Hart, M.* and *Milne, D.*, Acta Cryst. **A 25**, 134 (1969).
[72] *Bonse, U.* and *Hart, M.*, Zeit. für Physik, **188**, 154 (1965).
[73] *Bonse, U.* and *Hart, M.*, Zeit. für Physik, **190**, 455 (1966).
[74] *Bonse, U.* and *Hart, M.*, Zeit. für Physik, **194**, 1 (1966).
[75] *Penning, P.* and *Polder, D.*, Philips Res. repts, **16**, 419 (1961).
[76] *Kato, N.*, J. Phys. Soc. Japan, **18**, 1785 (1963).
[77] *Kato, N.*, J. Phys. Soc. Japan, **19**, 67 (1963).
[78] *Kato, N.*, J. Phys. Soc. Japan, **19**, 971 (1964).
[79] *Kambe, K.*, Z. Naturforsch. **18a**, 1010 (1963).
[80] *Authier, A.*, Advances in X-ray analysis, Plenum Press, **10**, 9 (1967).
[81] *Kato, N., Usami, K., Katagawa, T.*, Advances in X-ray analysis, Plenum Press, **10**, 46 (1967).
[82] *Authier, A.*, Physica Statu Solidi, **27**, 77 (1968).
[83] *Malgrange, C.*, Thesis Paris (1967) (C.N.R.S. – A.O. 1895).
[84] *Authier, A.* and *Lang, A. R.*, J. of Appl. Phys., **35**, 1956 (1964).
[85] *Wagenfeld, H.*, Acta Cryst. **A 24**, 170 (1968).
[86] *Fues, E.*, Ann. Physik (5) **36**, 209 (1939).
[87] *Batterman, B. W.* and *Hildebrandt G.*, Acta Cryst. **A 24**, 150 (1968).
[88] *Borrmann, G., Hildebrandt G.* and *Wagner, H.*, Z. Physik Dtsch. **142**, 406 (1955).
[89] *Wagner, H.*, Z. Physik Dtsch. **146**, 127 (1956).
[90] *Kikuta, S.* and *Kohra, K.*, J. Phy. So. Japan **25**, 924 (1968).
[91] *Lefeld-Sosnowska, M.* and *Malgrange, C.*, Phys. Stat. Solidi **30**, K 23 (1968).

Dynamical Theory of Electron Diffraction

K. Kambe and K. Molière*)

With 6 figures

I. Introduction

The ratio of atomic scattering cross sections for electrons and X-ray photons is given by

$$\frac{\sigma_e}{\sigma_x} = \frac{1}{4}\left(\frac{\lambda}{\lambda_c \sin(\vartheta/2)}\right)^4 \cdot \left|\frac{Z-f}{f}\right|^2 .$$

Relativistic correction and polarization factor are neglected. ϑ is the scattering angle, λ the wave length, λ_c the Compton wave length, Z the atomic number, f the atomic scattering amplitude for X-rays which depends on the variable $s = (4\pi/\lambda) \cdot \sin(\vartheta/2)$. Within the range of s-values for which diffracted beams are observed in normal diffraction experiments the order of magnitude of this ratio (e. g. for Al) is $\approx 10^8$ (*Bragg* [1]). This illustrates the fact that, whereas in X-ray diffraction we are usually only concerned with single scattering, for electrons multiple scattering processes must be taken into account in almost every quantitative consideration. A single-scattering theory gives a good approximation only if the dimensions of the scattering subject are very small. In the wave-mechanical picture, the single-scattering theory is equivalent to the kinematical theory of diffraction.

The kinematical diffraction theory, which corresponds to the first approximation of Born's quantum-mechanical theory of scattering, assumes that every volume element of the scatterer is hit by the undisturbed incident wave and is excited to emit a spherical wave, the amplitude of which is proportional to the local, „scattering potential"; all the waves excited at different points of the scatterer are superimposed linearly at the point of observation without being disturbed by other volume elements of the scatterer.

Every experimental effect which cannot be described by this simple theory is called "dynamical". For nearly ideal crystals the dynamical X-ray effects are of considerable interest [2], especially in connection with anomalous absorption (Borrmann effect). In electron diffraction dynamical effects are discussed mainly for the following practical purposes:

*) Fritz-Haber-Institut der Max-Planck-Gesellschaft, Berlin-Dahlem

(i) In "conventional" structure analysis (i. e. evaluation of structure factors from measured integral intensities, e. g. of powder patterns) dynamical corrections can be introduced mainly for the low-index diffractions according to the so-called *Blackman* formula [3], based on the dynamical two-beam approximation for the transmission through plate-shaped crystals. A generalization for other crystal forms has been given recently by *Fujimoto* [4]. The applicability of these corrections has been tested extensively (mainly by *Raether* and his group [5]) and is discussed in various articles and books [6], [104]. These topics should be, therefore, not a subject of the present paper.

(ii) Dynamical effects have been proved to be important for evaluating finer details of the electron-microscope images of lattice faults (dislocations and stacking faults), obtained by transmission through thin foils. The theoretical and experimental aspects of these topics are also so extensively described elsewhere [7] that it is not necessary to treat them here.

(iii) Dynamical effects due to the interaction of more than two beams ("N-beam case") make it possible to determine relations between the phases of structure amplitudes. We thought that this is important enough to be included in our article because the relevant publications [8] do not seem to have received due attention in the literature.

(iv) In special experiments with single crystals dynamical N-beam effects can be utilized for the evaluation of structure factors (real and imaginary parts) from finer details of the diffraction patterns or electron micrographs. These are:

(a) The intensity distributions in diffraction patterns from thin plate-shaped crystals taken with convergent-beam or rotating-crystal techniques.

(b) The evaluation of equal-thickness fringes and extinction contours obtained in transmission micrographs of wedge-shaped crystals.

(c) The splitting and broadening of reflection spots in diffraction patterns obtained by transmission through wedge-shaped crystals.

These techniques may be summarized under the notation "unconventional structure analysis". This, especially in connection with the problems of absorption, will be the main subject of the present article.

It is felt that the dynamical theory is well developed at the present time for the case of electrons transmitted through thin crystals in the energy range of normal electron microscopy (30–150 keV); this is the field of "THEED" (= Transmission High-Energy Electron Diffraction). In this field, on the one hand, relativistic effects may be handled as corrections; on the other hand, the convergence of the dynamical approximations is relatively good.

The cases of "RHEED" (= Reflection High-Energy Electron Diffraction; that is, the case of grazing incidence) and "LEED" (= Low-Energy Electron Diffraction) and also the relativistic implications at very high energies have to be further developed theoretically and cannot be treated in detail in this article.

It was shown first by *Kamiya* and *Uyeda* (1961) [9] that the electrons scattered inelastically by the atoms of a crystal play an important part in the electron-microscopic diffraction contrast. In the last few years there have appeared various investigations concerning the interesting problem of diffraction of waves scattered with energy loss. We can here mention only the theoretical work of *Kainuma* (1955) [10], *Takagi* (1958) [11], *Howie* (1959) [12], *Fujimoto* and *Kainuma* (1963) [13], *Heidenreich* (1963) [14], *Fukuhara* (1963) [15], *Kainuma* (1965) [16], *Gjønnes* (1962, 66) [17] [18]. A discussion of this work is beyond the scope of this article.

II. Theory

II.1 Bethe's Theory

The dynamical theory of electron diffraction was developed by *Bethe* [19] in 1928. It was the aim of this theory to solve Schrödinger's equation inside a crystal plate, extended infinitely in two dimensions, adapting the solutions at the boundary faces to one incident plane wave and a set of diffracted plane waves leaving the surfaces into the vacuum.

We will briefly recapitulate here this theory. Neglecting for the moment the dynamics of the crystal particles (nuclei and electrons), we regard the potential energy in Schrödinger's equation as a static one, $V(\mathbf{r}) = -e \cdot \phi(\mathbf{r})$, acting on the scattered electron at the point $\mathbf{r}$. The energy of the incident electron is $e \cdot \phi_{acc}$, where ϕ_{acc} is the acceleration potential of the incident electrons. Then, if we put

$$K_0^2 = \frac{2me}{\hbar^2}\phi_{acc}, \quad U(\mathbf{r}) = \frac{2me}{\hbar^2}\phi(\mathbf{r}) , \tag{1.1a, b}$$

Schrödinger's stationary equation reads

$$\{\nabla^2 + K_0^2 + U(\mathbf{r})\}\,\psi(\mathbf{r}) = 0. \tag{1.2}$$

To derive Bethe's equations quickly it is convenient to make use of the wave-number ("momentum") representation. (1.2) is transformed then as follows:

$$(K_0^2 - k^2)\,\varphi(\mathbf{k}) + \int v(\mathbf{k}-\mathbf{k}')\,\varphi(\mathbf{k}')\,d^3k' = 0. \tag{1.3}$$

$\upsilon(\mathbf{k})$ is the Fourier transform of the potential $U(\mathbf{r})$, $\varphi(\mathbf{k})$ the momentum wave function depending on the coordinate $\mathbf{k}$ of reciprocal space. We take into account now the three-dimensional periodicity of the potential; that is, $\upsilon(\mathbf{k})$ is a lattice δ-function:

$$\upsilon(\mathbf{k}) = \sum_{\mathrm{g}} \upsilon_{\mathrm{g}}\, \delta\,(\mathbf{k} - 2\pi\,\mathrm{g}), \tag{1.4}$$

$\mathrm{g} = \mathrm{g}_1\,\mathbf{b}_1 + \mathrm{g}_2\,\mathbf{b}_2 + \mathrm{g}_3\,\mathbf{b}_3$ being a vector of the reciprocal lattice. (υ_{g} is called a "structure potential"; g is an abbreviation for the three indices $\mathrm{g}_1, \mathrm{g}_2, \mathrm{g}_3$.) We introduce now a constant vector $\mathbf{k}_0$ in reciprocal space, which will be specified later on. Instead of $\mathbf{k}$ in Eq. (1.3) we insert (with $\mathbf{h}$ being another reciprocal-lattice vector)

$$\mathbf{k}_{\mathrm{h}} = \mathbf{k}_0 + 2\pi\,\mathbf{h}. \tag{1.5}$$

The momentum function for this value of the wave vector is abbreviated

$$\varphi_{\mathrm{h}} = \varphi(\mathbf{k}_{\mathrm{h}}). \tag{1.6}$$

Inserting then (1.4) into (1.3) we arrive at once at Bethe's "Fundamental Equations of Electron Diffraction":

$$(K_0^2 + \upsilon_0 - k_{\mathrm{h}}^2)\,\varphi_{\mathrm{h}} + \sum_{\mathrm{g}}{}' \upsilon_{\mathrm{h-g}}\varphi_{\mathrm{g}} = 0 \tag{1.7}$$

(The term with $\mathrm{g} = \mathrm{h}$ is omitted in the summation and transferred to the "diagonal" term). This is an infinite system of linear homogeneous equations, which must be solved for a given value of $\mathbf{k}_0$ for the infinite set of unknown quantities φ_{h}.

$\varphi(\mathbf{k})$ is regarded as a lattice δ-function,

$$\varphi(\mathbf{k}) = \sum_{\mathrm{h}} \varphi_{\mathrm{h}}\, \delta\,(\mathbf{k} - \mathbf{k}_{\mathrm{h}}),$$

and if we go back to the coordinate representation, we find

$$\psi_{\mathbf{k}_0}(\mathbf{r}) = \sum_{\mathrm{h}} \varphi_{\mathrm{h}} \exp\{\mathrm{i}(\mathbf{k}_0 + 2\pi\,\mathbf{h}) \cdot \mathbf{r}\} \tag{1.8}$$

as a fundamental solution of Schrödinger's equation (1.1) in the periodic potential. This is called, according to *Ewald*, a "wave field" in the dynamical theory, and a "Bloch wave" in the electronic theory of solids. It has the character of a plane wave modulated with the translational symmetry of the crystal lattice.

Before considering the boundary conditions we anticipate that solutions of Eq. (1.7) can only exist for certain distinct values of the vector $\mathbf{k}_0$, which can be enumerated by an index j, the wave field index: $\mathbf{k}_0 \rightarrow \mathbf{k}_0^{(j)}$; accordingly the partial-wave amplitudes are indexed $\varphi_{\mathbf{h}}^{(j)}$, and the expression for the solution in the coordinate representation is written as a sum of Bloch waves (1.8):

$$\psi(\mathbf{r}) = \sum_j c_j \sum_{\mathbf{h}} \varphi_{\mathbf{h}}^{(j)} \exp\left\{ i \left(\mathbf{k}_0^{(j)} + 2\pi\mathbf{h} \right) \cdot \mathbf{r} \right\} . \tag{1.9}$$

This represents the solution in the space of the crystal, i.e., $0 < z < D$, the z-axis being taken perpendicular to the surface.

For formulating the solutions outside the crystal it is advantageous to choose the unit cell of the lattice such that the basis vectors $\mathbf{a}_1$, $\mathbf{a}_2$ are parallel to the entrance surface; $\mathbf{b}_3 = \dfrac{\mathbf{a}_1 \times \mathbf{a}_2}{(\mathbf{a}_1 \times \mathbf{a}_2) \cdot \mathbf{a}_3}$ is parallel to $\mathbf{n}$ (the inward normal of the entrance surface).

In the half-space $z < 0$ we assume an incident plane wave $\exp(i\mathbf{K}_0 \cdot \mathbf{r})$ with the z-component $K_{oz} > 0$. The propagation vectors $\mathbf{k}_0^{(j)}$ of the wave fields in the crystal are now connected with $\mathbf{K}_0$ by the definition that all their tangential projections must be equal to the tangential projection of $\mathbf{K}_0$. We write

$$\mathbf{k}_0^{(j)} = \mathbf{K}_0 + \tau_j \cdot \mathbf{n} \tag{1.10a}$$

and also, according to (1.5),

$$\mathbf{k}_{\mathbf{h}}^{(j)} = \mathbf{K}_{\mathbf{h}} + \tau_j \cdot \mathbf{n}, \qquad \text{with } \mathbf{K}_{\mathbf{h}} = \mathbf{K}_0 + 2\pi\mathbf{h}. \tag{1.10b}$$

τ_j is called the "Anpassung" (adaption) of the wave field j.

Obviously, for matching the waves on both sides of the entrance surface $z = 0$ we have to introduce on the vacuum side a set of reflected waves so that the wave function there is

$$\Psi^{\text{entr.}} = \exp(i\mathbf{K}_0 \cdot \mathbf{r}) + \sum_{g_1 g_2} R_{g_1 g_2} \exp\left(i\mathbf{K}_{g_1 g_2}^{(R)} \cdot \mathbf{r} \right), \quad z < 0.$$

$$\mathbf{K}_{g_1 g_2}^{(R)} \cdot \mathbf{n} < 0, \qquad \left| \mathbf{K}_{g_1 g_2}^{(R)} \right| = K_0 . \tag{1.11}$$

Similarly we assume in the vacuum below the exit surface z = D a set of transmitted waves

$$\Psi^{\text{exit}} = \sum_{g_1 g_2} T_{g_1 g_2} \exp\left(i\mathbf{K}^{(T)}_{g_1 g_2} \cdot \mathbf{r}\right), \qquad z > D.$$

$$\mathbf{K}^{(T)}_{g_1 g_2} \cdot \mathbf{n} > 0, \quad \left|\mathbf{K}^{(T)}_{g_1 g_2}\right| = K_0 \,. \tag{1.12}$$

The tangential projections of $\mathbf{K}^{(R)}_{g_1 g_2}$ and $\mathbf{K}^{(T)}_{g_1 g_2}$ on the surfaces of the crystal must, of course, coincide with the tangential projections of all the partial wave vectors $\mathbf{k}^{(j)}_g$ for which the index $g = (g_1 g_2 n)$, n arbitrary.

The boundary conditions are formulated in the well-known way by equating the function and its normal derivative on either side of the two surfaces respectively. (This has been considered most thoroughly by *Lamla* [20].) A pair of vacuum amplitudes, $R_{g_1 g_2}$ and $T_{g_1 g_2}$, with given g_1, g_2, is connected by the boundary conditions with all the partial-wave amplitudes of the wave fields in the crystal, $\varphi^{(j)}_{g_1 g_2 n}$, where n is any integral number (n = 0, ± 1, ± 2, ...), belonging to a row of reciprocal-lattice points perpendicular to the surfaces.

It is obviously impossible to handle the infinite system (1.7) for calculating the values of $\mathbf{k}^{(j)}_0$ (or τ_j) and $\varphi^{(j)}_g$. Following *Bethe,* we have to reduce the system to a finite one. If we take notice of the fact that all the structure potentials υ_g are very small compared to K_0^2 it is clear from Eq. (1.7) that φ_h can be strong only if the condition

$$|\mathbf{k}_0 + 2\pi\mathbf{h}| = K_0 \tag{1.13}$$

is nearly satisfied, a relation equivalent to Bragg's (or Laue's) kinematical condition for reflection from a set of net planes perpendicular to **h**. The procedure for reducing the system (1.7) is, accordingly, as follows: Cancel in the matrix of (1.7) all the rows and columns for which the diagonal elements (e. g. $K_0^2 + \upsilon_0 - k_f^2$), contained in these rows and columns, are large compared to υ_f. If N equations (with N unknown partial-wave amplitudes φ_g) are left then, the solution is called a N-beam approximation (case of N strong beams or case in which N − 1 strong Bragg reflections are excited). The weak beams, neglected in this first approximation, can be taken into account in Bethe's second approximation giving correction terms to be added to the structure potentials (see II. 2c, for the two-beam case).

In the case of nearly normal incidence of fast electrons which is considered here, we can assume that $K_{oz}^2 \gg \upsilon_g$ for any index g. Then it turns out that the amplitudes of back-scattered electron waves ($k^{(j)}_{gz} < 0$) are very small compared to the forward-scattered ones. In the reduction of the fundamental equations, consequently, only

the Bragg reflections giving rise to forward-scattered waves need to be taken into consideration. In the boundary conditions for the entrance surface the amplitudes $R_{g_1 g_2}$ (Eq. (1.11)) of the reflected vacuum waves can be, therefore, assumed to be zero. In this approximation the wave functions inside the crystal and on any exit surface of arbitrary position and orientation are completely defined by the conditions of incidence at the entrance surface.

It is convenient now to introduce a geometrical parameter describing the deviation of the conditions of incidence from the case in which Bragg's condition is exactly satisfied. The Bragg equation for the reciprocal-lattice vector $\mathbf{g}$ is $K_0 \sin \bar{\vartheta}_g = \pi|g|$, $\bar{\vartheta}_g$ being the Bragg angle. If ϑ_g is the actual angle between $\mathbf{K}_0$ and the reflecting set of net planes we define an "excitation error" ("Anregungsfehler") by the expression

$$\rho_g = 2 \frac{K_0^2}{K_g} \sin \bar{\vartheta}_g (\sin \vartheta_g - \sin \bar{\vartheta}_g) \tag{1.14a}$$

$$= \frac{1}{2K_g} \{ |\mathbf{K}_0|^2 - |\mathbf{K}_0 + 2\pi \mathbf{g}|^2 \} , \tag{1.14b}$$

where $K_g = |\mathbf{K}_0 + 2\pi \mathbf{g}|$. It is easily seen that ρ_g is, apart from a factor nearly equal to one, the distance of the reciprocal-lattice point g from the Ewald sphere, this distance being regarded as positive if the point is inside the sphere. For $g = 0$ we have, of course, $\rho_g = 0$. Inserting K_0^2 from (1.14b) and k_h^2 from (1.10b) into the diagonal elements $N_h = K_0^2 + v_0 - k_h^2$ of the matrix of the coefficients of the system (1.7), one obtains (regarding τ_j as negligible[1]) compared with K_{oz})

$$N_h = 2K_{hz} \left(\zeta_h + \frac{v_0}{2K_{hz}} - \tau \right). \tag{1.15}$$

$$\zeta_h = \frac{K_h}{K_{hz}} \rho_h = \frac{\rho_h}{\cos \Theta_h} \tag{1.14c}$$

is the distance of the reciprocal-lattice point from the Ewald sphere in the direction of the crystal normal $\mathbf{n}$ and Θ_h the angle between $\mathbf{K}_h$ and the normal of the entrance surface.

It is convenient now to rewrite the system (1.7) in an equivalent form, as follows: The matrix of the system is transformed by multiplying with the diagonal matrix $(2K_{hz})^{-1/2} \delta_{gh}$ from the left and from the right (the K_{hz} are assumed to be not zero). In this way one obtains

[1]) This simplification is convenient here, but of course not necessary, to allow a solution of the problem (cf. *Niehrs* and *Wagner* [21]).

$$\begin{pmatrix} \vdots & \vdots & \vdots & \\ \cdots \left(\frac{\upsilon_0}{2K_{oz}} - \tau\right) & \frac{\upsilon_{-g}}{2(K_{oz}K_{gz})^{1/2}} & \frac{\upsilon_{-h}}{2(K_{oz}K_{hz})^{1/2}} & \cdots \\ \cdots \frac{\upsilon_g}{2(K_{gz}K_{oz})^{1/2}} & \left(\zeta_g + \frac{\upsilon_0}{2K_{gz}} - \tau\right) & \frac{\upsilon_{g-h}}{2(K_{gz}K_{hz})^{1/2}} & \cdots \\ \cdots \frac{\upsilon_h}{2(K_{hz}K_{oz})^{1/2}} & \frac{\upsilon_{h-g}}{2(K_{hz}K_{gz})^{1/2}} & \left(\zeta_h + \frac{\upsilon_0}{2K_{hz}} - \tau\right) & \cdots \\ & \vdots & \vdots & \end{pmatrix} \begin{pmatrix} \vdots \\ K_{oz}^{1/2}\varphi_0 \\ K_{gz}^{1/2}\varphi_g \\ K_{hz}^{1/2}\varphi_h \\ \vdots \end{pmatrix} = 0. \tag{1.16}$$

This may be symbolized by $\sum_h (M_{gh} - \tau\delta_{gh})\, K_{hz}^{1/2}\varphi_h = 0$. The eigenvalue equation of the Hermitian matrix $\{M_{gh}\}$, called the "dispersion equation",

$$\det |M_{gh} - \tau\delta_{gh}| = 0, \tag{1.17}$$

gives generally N different real eigenvalues τ_j (or $\mathbf{k}_0^{(j)}$ according to Eq. (1.10a)) if N strong beams are considered. By solving this equation for different directions of the incident beam, keeping the energy constant, (i. e. for different compatible values of the excitation errors $\rho_g, \rho_h, \ldots$) one can construct the so-called "dispersion surface", that is, the locus of the endpoints of all possible progagation vectors $\mathbf{k}_0^{(j)}$ of the N wave fields[1]). This is an N-branch surface in reciprocal space, periodic with the reciprocal lattice.

Inserting the eigenvalues τ_j obtained from (1.17) into the system (1.16) one can calculate all the ratios of partial-wave amplitudes $\varphi_g^{(j)}/\varphi_0^{(j)}$, $\varphi_h^{(j)}/\varphi_0^{(j)}$, ... The amplitude of the h-th partial wave of the wave field j is then given by [21]

$$c_j\varphi_h^{(j)} = \frac{\varphi_h^{(j)}/\varphi_0^{(j)}}{\sum_g K_{gz}/K_{oz} \left|\varphi_g^{(j)}/\varphi_0^{(j)}\right|^2}. \tag{1.18}$$

If the exit surface is parallel to the entrance surface all the partial waves of the different wave fields j belonging to the same index h are superimposed and give rise to one transmitted beam $T_h \cdot \exp\{ iK_h^{(T)} \cdot \mathbf{r}\}$ in Eq. (1.12). In case of a wedge-shaped crystal every wave gives a separate transmitted vacuum beam (fine structure; interference multiple refraction).

---

[1]) Instead of this definition the dispersion surface is usually defined in the literature as the locus of the initial points of the vectors $\mathbf{k}_0^{(j)}$, the endpoints of all these vectors coinciding at the origin of the reciprocal lattice. Then the corresponding vectors $\mathbf{k}_h^{(j)}$ are directed from the same points of the dispersion surface ("tie-points") to the respective reciprocal-lattice points.

A discussion of the problems of Bethe's theory (reduction of the fundamental equations; elimination of back-scattering) and a method for calculation of intensities by use of matrix technique are given in a paper by *Niehrs* and *Wagner* [21]. It must be admitted, however, that neither these authors nor *Bethe* himself could give a rigorous mathematical proof for the procedure (or even for the possibility) of reducing the infinite system (1.7). The proof is still lacking. But, in connection with the applications enumerated in the introduction of this article various investigations have been performed in the meantime which can be regarded as attempts of experimental verification of Bethe's theory.

The aim of most of these experimental investigations was the confirmation of Bethe's approximation for two strong beams; the two-beam case is the only case for which the theoretical formula can be easily written down in closed form. This has been discussed in extenso in Bethe's paper.

In earlier years it appeared hopeless to evaluate an N-beam approximation with N greater than 3 or 4. Nowadays, however, with standard programs for matrix eigenvalues and eigenvectors, it is quite easy to manage a multi-beam case with large N by use of electronic computers in tolerable time. In the experimental part (see III.3) of this article some examples will be given which can be taken as proof of the applicability of Bethe's method.

With the aim of handling dynamical multi-beam cases other mathematical methods, different from Bethe's procedure, have been developed by various authors. The scattering-matrix theories of *Fujimoto* [22], *Niehrs* [23], and *Sturkey* [24] can be derived from, and are obviously in close connection to, Bethe's theory. Other methods make use of the general integral equations of scattering (1.19) (*Tournarie* [28], *Kambe* [29]), giving procedures of successive approximation by iteration solutions (*Fujiwara* [26], *Fengler* [27]). *Howie* and *Whelan* [30] found another form of the dynamical theory based on the concept of successive diffraction from a set of net planes, similar to *Darwin's* [31] early work on dynamical diffraction of X-rays. A so-called optical approach making use of the concept of phase-grating diffraction is due to *Cowley* and *Moodie* [32]. It can be shown (but this will not be a subject of this article) that all these methods are equivalent to Bethe's procedure and lead to the same results, if approximations inherent to the respective special theories are duly taken into account.

The theory of electron diffraction is formulated most generally as an integral equation ([25] p. 86)

$$\psi(\mathbf{r}) = \psi^{(0)}(\mathbf{r}) + \int G(\mathbf{r},\mathbf{r}')\, V(\mathbf{r}')\, \psi(\mathbf{r}')\, \mathrm{d}^3 \mathbf{r}' . \qquad (1.19)$$

$\psi^{(0)}$ is the incident wave and the Green function G has the usual form of an outgoing spherical wave. By writing (1.19) in different forms one can obtain all the special methods mentioned above (*Kambe*, unpublished). The first iterated solution gives, of course, the kinematical theory.

II. 2a Complex potential in Bethe's theory

In optics a complex index of refraction is commonly used for the description of waves attenuated by absorption. It was, therefore, an obvious idea to represent damped wave fields in crystals by replacing in Bethe's theory the real scattering potential $V(\mathbf{r})$ by a complex function

$$V^{(c)}(\mathbf{r}) = V^{(r)}(\mathbf{r}) + i V^{(i)}(\mathbf{r}). \tag{2.1}$$

This was first proposed by *Slater* (1937) [33](see also *Molière* [34]). In this way, of course, one obtains a non-Hermitian Hamiltonian. But if probability density $|\psi|^2$ and current $\mathbf{S}$ of the usual Schrödinger theory are used, one gets

$$\operatorname{div} \mathbf{S} = 2/\hbar \cdot V^{(i)}(\mathbf{r}) \cdot |\psi(\mathbf{r})|^2. \tag{2.2}$$

$-(2/\hbar)V^{(i)}$ may be interpreted as a spatial distribution of "absorption power". The complex potential was used first as a purely phenomenological aid. A foundation has been given in 1957 by *Yoshioka* [46], as described in II. 4.

The matrix of the dispersion equation (1.17) contains complex structure potentials if the theory with a complex potential is formally carried through as above in II.1:

$$\upsilon_0^{(c)} = \upsilon_0^{(r)} + i\upsilon_0^{(i)}; \quad \upsilon_g^{(c)} = \upsilon_g^{(r)} + i\upsilon_g^{(i)}\ ^{1}) . \tag{2.3}$$

The matrix M_{gh} is split, therefore, into a Hermitian and a skew-Hermitian part. The meaning of these two parts, and generally the background (experimental and theoretical) of the complex potential will be extensively discussed in the following parts of this article.

It has been emphasized by *von Laue* [162] that in a crystal each wave field $\psi_{k_0}(\mathbf{r})$ (1.8) which represents a fundamental solution of Schrödinger's equation must be affected by the absorption separately. The solutions of the dispersion equation become complex and, therefore, an imaginary part is added to the normal component $k_{oz}^{(j)}$ of the propagation vector of the wave field j. If we write this imaginary part $\mu_j/2$, the wave field is attenuated by a factor $\exp\left\{-\frac{\mu_j z}{2}\right\}$ and the intensity (mean current density) by a factor $\exp\{-\mu_j z\}$, where z is the depth of penetration into the crystal.

---

[1]) The second equation (2.3) cannot be understood, of course, in the general non-centrosymmetric case as an explicit decomposition of $\upsilon_g^{(c)}$ into a real and an imaginary part, because $\upsilon_g^{(r)}$ and $\upsilon_g^{(i)}$ are in general complex numbers.

II. 2b Formulae for the two-beam case

It may be useful to quote here some formulae of Bethe's two-beam case with complex potential (cf. e.g. [7]) mainly for the understanding of the experiments, although one has to expect many-beam effects in almost every practical application.

In the two-beam case we have the well-known "Pendellösung", that is, a periodic change of mean current density of the wave fields in the direction perpendicular to the entrance surface. In case of a reflection from a net plane g, the period of this oscillation ("extinction distance") is

$$\xi_g = 2\pi \frac{K_{oz}}{|v_g^{(r)}|}. \tag{2.4}$$

Further, the two wave fields are differently absorbed because the maxima and minima of the oscillations are differently distributed with respect to the crystal atoms. The anomalous absorption of electron wave fields (counterpart of Borrmann's effect with X-rays) is usually not so pronounced as in the X-ray case, where one of the wave fields is essentially totally absorbed. The absorption coefficents are

$$\mu_j = \mu_0 + (-1)^j \frac{\Delta\mu}{\sqrt{1+W^2}}, \qquad j = 1,2. \tag{2.5}$$

μ_0 is the "mean absorption coefficient", $\Delta\mu$ describes the anomalous absorption:

$$\mu_0 = \frac{v_0^{(i)}}{K_{oz}}, \qquad \Delta\mu = \frac{\mathrm{Re}\{v_g^{(i)}\}\ ^{1})}{K_{oz}}. \tag{2.6}$$

W in eq. (2.5) is Bethe's "selection error", proportional to the excitation error ζ_g (1.14c):

$$W = \frac{1}{2\pi}\zeta_g\xi_g = \frac{K_{oz}\zeta_g}{|v_g^{(r)}|}.$$

The amplitudes of the two wave fields are

$$\left.\begin{aligned} &A_0^{(1,2)} \exp\left\{ i\mathbf{k}_0^{(1,2)} \cdot \mathbf{r} \right\} + A_g^{(1,2)} \exp\left\{ i(\mathbf{k}_0^{(1,2)} + 2\pi\mathbf{g}) \cdot \mathbf{r} \right\} \\ &\text{with} \\ &A_0^{(1,2)} = \frac{\sqrt{1+W^2} \pm W}{2\sqrt{1+W^2}}, \quad -A_g^{(1)} = A_g^{(2)} = \frac{1}{2\sqrt{1+W^2}}, \end{aligned}\right\} \tag{2.7}$$

---

[1]) $\mathrm{Re}\{v_g^{(i)}\}$ represents the real part of $v_g^{(i)}$. We assume here that the origin of the coordinates is so chosen that $v_g^{(r)}$ is real and positive (cf. Footnote [1]) p. 10).

and

$$k_0^{(1,2)} = \mathbf{K}_0 + k_{oz}^{(1,2)} \cdot \mathbf{n},$$

where

$$k_{oz}^{(1,2)} = \frac{v_0^{(r)}}{2K_{oz}} + \frac{\pi}{\xi_g}\left(W \mp \sqrt{1+W^2}\right) + i\frac{1}{2}\left(\mu_0 \mp \frac{\Delta\mu}{\sqrt{1+W^2}}\right). \qquad (2.8)$$

The four plane waves of (2.7) are observable separately in the double-refraction experiments with wedge-shaped crystals (cf. III). In the case of parallel-sided plates the primary and reflected waves are superimposed at the exit surface giving rise to one primary and one reflected vacuum beam respectively.

The intensity of the diffracted transmitted wave as a function of the crystal thickness D and the selection error W (which changes with orientation of the crystal with respect to the incident beam) is proportional to

$$I_g = \frac{\exp\{-\mu_0 D\}}{2(1+W^2)}\left[\mathrm{Cosh}\left\{\frac{\Delta\mu \cdot D}{\sqrt{1+W^2}}\right\} - \cos\left\{2\pi \frac{\sqrt{1+W^2} \cdot D}{\xi_g}\right\}\right] \qquad (2.9)$$

(cf. *Hashimoto, Howie* and *Whelan* [36], *Watanabe, Fukuhara* and *Kohra* [163]). It is easily seen that this describes a damped oscillation.

For the undiffracted transmitted wave we have

$$I_0 = \frac{\exp\{-\mu_0 D\}}{2(1+W^2)}\left[(W-\sqrt{1+W^2})^2 \exp\left\{\frac{\Delta\mu \cdot D}{\sqrt{1+W^2}}\right\}\right.$$

$$+ (W+\sqrt{1+W^2})^2 \exp\left\{-\frac{\Delta\mu \cdot D}{\sqrt{1+W^2}}\right\}$$

$$\left. + \cos\left\{2\pi \frac{\sqrt{1+W^2} \cdot D}{\xi_g}\right\}\right]. \qquad (2.10)$$

This distribution is as a function of W asymmetric with respect to W = 0, where Bragg's condition is satisfied.

II. 2c Bethe's weak-beam approximation

In II. 1, the equations with large diagonal coefficients, $N_f = K_0^2 + \upsilon_0 - k_f^2$, were neglected in first approximation in the reduction of the infinite system (1.7). From these equations approximate values for the amplitudes φ_f may be obtained and inserted into the equations for the strong beams. This second approximation gives, after *Bethe*, additional "dynamical structure potentials". One has to replace

$$\upsilon_g \to \upsilon_g - \sum_{\substack{f \\ (\neq 0,g)}}{}'' \frac{\upsilon_{g-f}\upsilon_f}{N_f},$$
$$\upsilon_0 \to \upsilon_0 - \sum_{\substack{f \\ (\neq 0,g)}}{}'' \frac{\upsilon_{-f}\upsilon_f}{N_f}. \tag{2.11}$$

This procedure is, of course, only applicable if none of the terms in the summations is comparable in magnitude with υ_g or υ_0.

II. 3 Relation to the Band Theory

a) Bethe's dynamical theory is closely related to the energy-band concept in the electronic theory of solids, since both represent the electronic state in terms of Bloch functions. *Morse* (1930) [37] pointed out the close connection between the two problems and demonstrated that the Bragg peaks observed in LEED by *Davisson* and *Germer* (1927) [38] occur in the energy ranges which are forbidden in the band structure of the crystal. In HEED the connection with band theory is less obvious, but we consider here a few points which may be helpful for the understanding of Bethe's theory.

b) In band theory the Bloch functions are regarded as representing the stationary states of valence electrons in a crystal. The propagation vector $\mathbf{k}$ is given as a parameter and the eigenvalue of the energy $E(\mathbf{k})$ is calculated as a function of $\mathbf{k}$ from a secular equation corresponding to the dispersion equation (1.17). In Bethe's theory, on the other hand, the Bloch functions are used to construct the wave function of the scattered electron inside the crystal, given the energy of the electron. The two components of $\mathbf{k}$ parallel to the entrance surface are also given, and Eq. (1.17) determines the eigenvalues of the third component k_z of $\mathbf{k}$. In band theory $E(\mathbf{k}) = E$ represents a hypersurface in 4-dimensional $(E, \mathbf{k})$ space. The dispersion

surface of the dynamical theory is a cross section of this surface with the hyperplane E = const. The dispersion surface is an equienergy surface in reciprocal space like the Fermi surface in band theory (see Fig. 9.1., *Hirsch* et al. p. 211 [7]).

c) There is some difference between the two theories as to the physical interpretation of the periodic potential $V(\mathbf{r})$. In band theory the potential is, in the sense of Hartree's approximation, the average Coulomb potential due to the nuclei, the ion-core electrons, and all the valence electrons *minus* the one valence electron under consideration. This theory is usually concerned only with low-energy bands. In this case the exchange and correlation effects between the electron under consideration and the other electrons are not negligible and effect, actually, a considerable correction of the Hartree potential. The correct choice of the potential is in itself one of the main problems of band theory (*Sommerfeld-Bethe*, II. A. 14 [39]).

For electron diffraction, on the other hand, the potential is due to the nuclei and *all* the electrons belonging to the crystal. In HEED the energy E is usually so high in comparison with the energies of internal electrons that we may approximately neglect the exchange and correlation effects. The Hartree potential may be satisfactory; a somewhat more exact derivation of the potential is given in II.4.

d) For low-energy bands in band theory the plane-wave expansion (1.8) is mostly very badly convergent. To overcome this difficulty several methods have been developed [40], [41]. These expand the Bloch function in terms of modified plane waves, which have the form of a plane wave only in the region outside the ion cores. Inside the ion cores the modified plane waves have a form more proper for representing the rapid oscillation of the wave function. Hence, the expansion in terms of such modified plane waves converges much more rapidly than the simple plane-wave expansion. For the determination of the amplitudes $\varphi_{\mathbf{h}}$ of the modified plane waves we obtain an equation similar to (1.7):

$$(k^2 - k_{\mathbf{h}}^2)\,\varphi_{\mathbf{h}} + \frac{2m}{\hbar^2} \sum_{\mathbf{g}} \Gamma(\mathbf{k}, \mathbf{k}_{\mathbf{h}}, \mathbf{k}_{\mathbf{g}})\,\varphi_{\mathbf{g}} = 0. \tag{3.1}$$

Here the potential $v_{\mathbf{h}-\mathbf{g}}$ of (1.7) is replaced by the expression $(2m/\hbar^2)\,\Gamma(\mathbf{k}, \mathbf{k}_{\mathbf{h}}, \mathbf{k}_{\mathbf{g}})$. The actual form of this function depends on the special method chosen.

Formally, Eq. (3.1) can be obtained by the plane-wave expansion (1.8) from the Schrödinger equation

$$(\nabla^2 + k^2)\,\psi - \frac{2m}{\hbar^2} \int V_{ps}(\mathbf{k}, \mathbf{r}, \mathbf{r}')\,\psi(\mathbf{r}')\,d^3r' = 0, \tag{3.2}$$

where the potential energy term $U\psi$ of (1.2) is replaced by the expression

$$-\frac{2m}{\hbar^2}\int V_{ps}(\mathbf{k},\mathbf{r},\mathbf{r}')\,\psi(\mathbf{r}')\,d^3r'. \tag{3.3}$$

The "pseudopotential" $V_{ps}(\mathbf{k},\mathbf{r},\mathbf{r}')$ satisfies the periodicity condition

$$V_{ps}(\mathbf{k},\mathbf{r}+\mathbf{a}_m,\mathbf{r}'+\mathbf{a}_m)=V_{ps}(\mathbf{k},\mathbf{r},\mathbf{r}'), \tag{3.4}$$

where $\mathbf{a}_m$ is an arbitrary lattice-translation vector of the crystal. We can write

$$V_{ps}(\mathbf{k},\mathbf{r},\mathbf{r}')=-(2\pi)^{-3/2}\sum_{\mathbf{g}}\exp\{2\pi i\mathbf{g}\cdot\mathbf{r}\}\cdot$$
$$\cdot\int\exp\{i\mathbf{k}'\cdot(\mathbf{r}-\mathbf{r}')\}\cdot\Gamma(\mathbf{k},\mathbf{k}'+2\pi\mathbf{g},\mathbf{k}')\,d^3k'. \tag{3.5}$$

This relation can be proved directly by substitution into (3.2) and then verifying that Eq. (3.1) follows.

The Schrödinger equation (3.2) has the solution (1.8) for which $\varphi_{\mathbf{h}}$ and $E(\mathbf{k})$ are determined by (3.1). This solution is called the pseudo-wave function.

It is obvious that the use of one of the modified-plane-wave methods will bring much better approximation for LEED than the plane-wave expansion as pointed out by *Boudreaux* and *Heine* (1967) [42].

In HEED the convergence of the plane-wave expansion (1.8) is usually sufficiently rapid. Experience shows (cf. III.3.) that, as far as the intensities of strong diffracted waves are concerned, the numerical values calculated by the process of II. 1 converge reasonably with the increase of the number N of beams, so that we can restrict N to some limited number. *This does not mean, however, that the wave function inside the ion cores is sufficiently well reproduced by the superposition of the limited number of plane waves which are taken into account in the intensity calculation.* The same situation has been pointed out by *Slater* [40] (p. 245) in band theory. Since we take into account a limited number of Fourier coefficients $v_{\mathbf{h}-\mathbf{g}}$ in (1.16), the potential effectively used in the Schrödinger equation (1.2) is not $V(\mathbf{r})$ but a kind of pseudopotential in the above sense. Since all the higher-order terms are omitted, this pseudopotential has certainly a smoothed minimum at the centers of the ion cores, where the true potential has a sharp negative peak. Hence, the wave function which we obtain in the intensity calculation is not the true wave function but the pseudo-wave function belonging to this pseudopotential. The result of the intensity calculation is nevertheless correct because the waves emerging from the surfaces of the crystal are formed from the plane waves outside the ion cores, which are given equally well by the pseudo-wave function and by the true wave function.

II. 4 The "Inner Potential" of a Crystal

In Bethe's theory the periodic potential $V(\mathbf{r})$ is regarded as a static field. Usually it is assumed simply that $V(\mathbf{r})$ is a superposition of atomic potentials calculated from Thomas-Fermi-Dirac or Hartree-Fock atomic data[1]). At first sight this may be satisfactory, since the largest part of the potential is due to the nuclei and core-electrons of the crystal atoms. In particular cases the deviation from the free-atom data, due to chemical bonding, must be taken into account (*Harada* and *Kashiwase* (1962) [44]). A more accurate value of $V(\mathbf{r})$ is obtained, however, only if one further takes into account the dynamic behaviour of the crystal, that is, excitation of internal states of the crystal by the incident electron. In particular, this produces an imaginary part of $V(\mathbf{r})$.

The situation is just the same in the case of scattering of electrons by atoms (*Mott* and *Massey* [25]). One considers there also at first the scattering by the static central field of an atom. Then various corrections of the scattering amplitude are introduced considering the excited states of the atom. This type of corrections can be worked out in two different ways: either by correcting directly the scattering amplitude or by calculating some correction of the potential in order to obtain an "optical potential" in such a way that the solution of the Schrödinger equation with this optical potential results in the correct value of the scattering amplitude (*Mott* and *Massey* [25]). This type of optical potential is encountered also in the "optical model" in nuclear physics (*Goldberger* and *Watson* [45]).

Returning to our problem, we see at once that an "optical potential" should be the type of potential to be introduced into Bethe's theory and compared with experimental results (*Dederichs* [49]). *Yoshioka* (1957) [46] developed a general theory of potential for electron diffraction by crystals just in the same way as it is done for the problem of electron scattering by atoms[2]). His aim was to obtain the value of the imaginary part of the potential. We reproduce here only the basic part of his theory (in a slightly generalized form) to discuss the meaning of the "inner potential" more generally[3]).

The Schrödinger equation of the system consisting of the incident electron and the crystal is

$$\left(-\frac{\hbar^2}{2m} \nabla^2 + H_c + H' \right) \phi = E\phi \,, \tag{4.1}$$

---

[1]) The method of calculation is described in detail in the International Tables etc., Vol. 3. [43]

[2]) A similar theory was developed by *Molière* (1939) [47] for X-rays.

[3]) *Ohtsuki* and *Yanagawa* (1966) [48], *Dederichs* (1966) [49] have given more abstract but essentially equivalent theories.

where $-\hbar^2/2m \cdot \nabla^2$ is the kinetic energy of the incident electron; H_c is the Hamiltonian of all crystal particles, H' describes the interaction of the scattered electron with the crystal particles. E is the energy of the whole system, that is, the sum

$$E = E_e + E_c \ , \tag{4.2}$$

where E_e is the energy of the incident electron, and E_c is the *initial*[1]) energy of the crystal. The wave function ϕ depends upon $\mathbf{r}$ and $\mathbf{r}_1, \ldots, \mathbf{r}_N$, where $\mathbf{r}$ is the coordinate of the incident electron and the $\mathbf{r}_j$ are the coordinates of *all* the particles (nuclei and electrons) in the crystal. ϕ is expanded in the form

$$\phi(\mathbf{r}, \mathbf{r}_1, \ldots, \mathbf{r}_N) = \sum_n \psi_n(\mathbf{r}) \cdot a_n(\mathbf{r}_1, \ldots, \mathbf{r}_N), \tag{4.3}$$

where a_n is the normalized wave function representing the n-th stationary state of the crystal, satisfying the equation

$$H_c\, a_n = E_n\, a_n \ , \tag{4.4}$$

where E_n is the energy of the state a_n. One of the states a_n is regarded as the initial state and named a_0[1]). Then $\psi_0(\mathbf{r})$ in (4.3) describes the elastic scattering, and $\psi_n(\mathbf{r})$ the inelastic scattering by which the state of the crystal is changed from a_0 to a_n. We obtain then from (4.1)

$$\left(\nabla^2 + K_0^2 - \frac{2m}{\hbar^2} H'_{00}\right) \psi_0 = \frac{2m}{\hbar^2} {\sum_m}' H'_{0m}\, \psi_m \ , \tag{4.5}$$

$$\left(\nabla^2 + K_n^2 - \frac{2m}{\hbar^2} H'_{nn}\right) \psi_n = \frac{2m}{\hbar^2} {\sum_m}' H'_{nm}\, \psi_m \ , \tag{4.6}$$

where the primed sums run over $m \neq 0$ in (4.5) and over $m \neq n$ in (4.6),

$$K_n^2 = \frac{2m}{\hbar^2}(E - E_n) \tag{4.7}$$

and

$$H'_{nm} = \int a_n^*\, H' a_m \, d^3\mathbf{r}_1 \ldots d^3\mathbf{r}_N \ . \tag{4.8}$$

[1]) It is implied that we should take afterwards a statistical average of the intensities over the initial states. (cf. III.2.)

If we neglect the inelastic scattering completely we obtain from (4.5) the Schrödinger equation

$$\left(\nabla^2 + K_0^2 - \frac{2m}{\hbar^2} H'_{00}(\mathbf{r})\right) \psi_0 = 0. \tag{4.9}$$

H'_{00} can easily be shown to be a real and periodic function of $\mathbf{r}$. Thus, H'_{00} is the "true" static potential of the crystal for the elastic scattering of the incident electron. Since the wave function $a_n(\mathbf{r}_1 \ldots, \mathbf{r}_N)$ is written in a general form we can take into account, at least in principle, *all* the interactions among the particles in the crystal. We can, however, never specify the exact form of a_n so that we are compelled to be satisfied with various approximate forms of a_n. The most simple assumption is that a_n is the product of the free-atom wave functions, leading to the simple superposition of atomic potentials as mentioned above.

The right-hand side of (4.5) represents the effect of the inelastic scattering on the elastic scattering, and this gives the modification to the true potential H'_{00} leading to the optical potential. By applying to (4.5) and (4.6) a kind of iterative process, *Yoshioka* [46] shows that (4.5) can be written as

$$\left(\nabla^2 + K_0^2 - \frac{2m}{\hbar^2} H'_{00}(\mathbf{r})\right) \psi_0 - \frac{2m}{\hbar^2} \int A(\mathbf{r}, \mathbf{r}') \psi_0(\mathbf{r}') \, d^3\mathbf{r}' = 0, \tag{4.10}$$

where $A(\mathbf{r}, \mathbf{r}')$ is given approximately by

$$A(\mathbf{r}, \mathbf{r}') = -\frac{m}{2\pi\hbar^2} {\sum_{\substack{n \\ (\neq 0)}}}' H'_{on}(\mathbf{r}) H'_{no}(\mathbf{r}') \frac{\exp\{iK_n |\mathbf{r} - \mathbf{r}'|\}}{|\mathbf{r} - \mathbf{r}'|} . \tag{4.11}$$

More exact but more complicated forms may be obtained by further iteration (cf. *Ohtsuki* and *Yanagawa* [48], *Dederichs* [49]). $A(\mathbf{r}, \mathbf{r}')$ satisfies the periodicity condition

$$A(\mathbf{r} + \mathbf{a}_n, \mathbf{r}' + \mathbf{a}_n) = A(\mathbf{r}, \mathbf{r}') . \tag{4.12}$$

We note that $A(\mathbf{r}, \mathbf{r}')$ depends in general on K_0, that is, on the energy of the incident electron. It depends also on the choice of the initial state[1]) a_0 among the possible states a_n.

We find by inspection of (4.10) in comparison with (3.2) that the complex optical potential

$$V_{opt}(K_0, \mathbf{r}, \mathbf{r}') = \delta(\mathbf{r} - \mathbf{r}') H'_{00}(\mathbf{r}) + A(\mathbf{r}, \mathbf{r}') \tag{4.13}$$

---

[1]) see Footnote [1]) p. 17

has the same form as a pseudo-potential. V_{opt} is in general a *non-local* potential, that is, it is an integral operator connecting the action of distant volume elements $d^3\,\mathbf{r}'$ on some point $\mathbf{r}$ of the crystal. Furthermore it *depends on the energy* (i.e. on K_0) just as the pseudo-potential in band theory. $A(\mathbf{r}, \mathbf{r}')$, and accordingly $V_{opt}(K_0, \mathbf{r}, \mathbf{r}')$, is generally a non-Hermitian operator. Because of the periodicity of $H'_{00}(\mathbf{r})$ and $A(\mathbf{r}, \mathbf{r}')$, Eq. (4.10) has a Bloch-type solution (cf. (1.8)). Expanding H'_{00} in a Fourier series

$$\frac{2m}{\hbar^2} H'_{00}(\mathbf{r}) = -\sum_{\mathbf{h}} \upsilon_{\mathbf{h}} \exp\{2\pi i \mathbf{h} \cdot \mathbf{r}\} \,, \tag{4.14}$$

we obtain from (4.10)

$$(K_0^2 - k_{\mathbf{h}}^2)\varphi_{\mathbf{h}} + \sum_{\mathbf{g}} \left(\upsilon_{\mathbf{h}-\mathbf{g}} - \frac{2m}{\hbar^2} C_{\mathbf{hg}}\right)\varphi_{\mathbf{g}} = 0 \,, \tag{4.15}$$

where $C_{\mathbf{hg}}$ is given by

$$C_{\mathbf{hg}} = \frac{1}{\tau} \int_{\tau}\int_{\tau} A(\mathbf{r}, \mathbf{r}') \exp\{-i\mathbf{k}_{\mathbf{h}} \cdot \mathbf{r} + i\mathbf{k}_{\mathbf{g}} \cdot \mathbf{r}'\}\, d^3\mathbf{r}\, d^3\mathbf{r}', \tag{4.16}$$

where τ is the volume of the crystal. $C_{\mathbf{hg}}$ is in general a function of $\mathbf{k}_{\mathbf{h}}$ and $\mathbf{k}_{\mathbf{g}}$. From the fact that $A(\mathbf{r}, \mathbf{r}')$ is not Hermitian, the same property follows for $C_{\mathbf{hg}}$. That is, in general, we have

$$C_{\mathbf{hg}} \neq C^*_{\mathbf{gh}}. \tag{4.17}$$

Thus, if we write

$$\Gamma_{\mathbf{hg}} = \Gamma(K_0, \mathbf{k}_{\mathbf{g}}, \mathbf{k}_{\mathbf{h}}) = \frac{\hbar^2}{2m}\left(\upsilon_{\mathbf{h}-\mathbf{g}} - \frac{2m}{\hbar^2} C_{\mathbf{hg}}\right),$$

we obtain the relation (3.5) between this quantity and $V_{opt}(K_0, \mathbf{r}, \mathbf{r}')$ given by (4.13). $\upsilon_{\mathbf{h}-\mathbf{g}}$ is Hermitian since $H'_{00}(\mathbf{r})$ is real (see 4.8), but $C_{\mathbf{hg}}$, and consequently also $\Gamma_{\mathbf{hg}}$, is not Hermitian. If we write, after *Yoshioka* [46],

$$C_{\mathbf{hg}} = C^{(\mathrm{r})}_{\mathbf{hg}} + i\, C^{(\mathrm{i})}_{\mathbf{hg}}, \tag{4.19}$$

where $C^{(\mathrm{r})}_{\mathbf{hg}}$ and $C^{(\mathrm{i})}_{\mathbf{hg}}$ are both Hermitian, we can split $\Gamma_{\mathbf{hg}}$ into a sum of Hermitian and skew-Hermitian parts

$$\Gamma_{\mathbf{hg}} = \Gamma^{(\mathrm{H})}_{\mathbf{hg}} + i\,\Gamma^{(\mathrm{SH})}_{\mathbf{hg}}, \tag{4.20}$$

where

$$\Gamma_{hg}^{(H)} = \frac{\hbar^2}{2m} \upsilon_{h-g} - C_{hg}^{(r)} \tag{4.21}$$

and

$$\Gamma_{hg}^{(SH)} = - C_{hg}^{(i)}. \tag{4.22}$$

It was shown in II. 2 that the real part of $V^{(c)}(\mathbf{r})$ gives the Hermitian part of the element υ_{h-g}, and the imaginary part the skew-Hermitian part. We conclude, therefore, that the physically significant form of the "complex potential" assumed in II. 2 is actually the nonlocal optical potential (4.13). The "real part" of υ_{h-g} is the Hermitian part of Γ_{hg} given by (4.21), and the "imaginary part" is the skew-Hermitian part given by (4.22).

In II. 2 we have seen that the "imaginary part" $V^{(i)}(\mathbf{r})$ leads to the "absorption" of electrons by crystals. The quantum-mechanical interpretation of this phenomenological statement can be given according to Yoshioka's theory as follows.

From (4.5) and (4.6) we can construct the expressions $\psi_0^* \nabla^2 \psi_0 - \psi_0 \nabla^2 \psi_0^*$ and $\psi_n^* \nabla^2 \psi_n - \psi_n \nabla^2 \psi_n^*$. Integrating these expressions over the whole volume of the crystal, which is assumed for the moment to be limited, and applying Green's theorem, we obtain

$$\int \left(\psi_0^* \frac{\partial}{\partial \nu} \psi_0 - \psi_0 \frac{\partial}{\partial \nu} \psi_0^* \right) d^2 s = \frac{2m}{\hbar^2} \int \left(\psi_0^* \sum_{\substack{m \\ (\neq 0)}}{}' H'_{om} \psi_m - \psi_0 \sum_{\substack{m \\ (\neq 0)}}{}' H'^*_{om} \psi_m^* \right) d^3 r, \tag{4.23}$$

$$\int \left(\psi_n^* \frac{\partial}{\partial \nu} \psi_n - \psi_n \frac{\partial}{\partial \nu} \psi_n^* \right) d^2 s = \frac{2m}{\hbar^2} \int \left(\psi_n^* \sum_{\substack{m \\ (\neq n)}}{}' H'_{nm} \psi_m - \psi_n \sum_{\substack{m \\ (\neq n)}}{}' H'^*_{nm} \psi_m^* \right) d^3 r, \tag{4.24}$$

where the integrals on the left-hand sides are taken over the surface of the crystal, and $\partial/\partial\nu$ is the derivative in the direction normal to the surface. Summing the second equation over all n except n = 0, and comparing the right-hand side with (4.23), we obtain

$$\sum_{\substack{n \\ (\neq 0)}}{}' \int (j_n)_\nu \, d^2 s = - \int (j_0)_\nu \, d^2 s, \tag{4.25}$$

where $(j_m)_\nu$, m = 0,n, are the components of the electron current-density vector

$$\mathbf{j}_m = \frac{\hbar}{2im} (\psi_m^* \nabla \psi_m - \psi_m \nabla \psi_m^*) \tag{4.26}$$

normal to the surface.

The relation (4.25) is nothing but the law of conservation of the number of electrons, implying that the sum of the electron currents which flow out from the crystal by inelastic scattering is equal to the net flux of the electrons of the elastic-scattering part ψ_0 (including the incident wave) *into* the crystal. Thus, the electrons which contribute to the inelastic scattering are effectively "absorbed" in the crystal as far as the elastic-scattering part ψ_0 is concerned. From (4.10) we get

$$\int (j_0)_\nu \, d^2 s = \frac{1}{i\hbar} \iint \psi_0^* (\mathbf{r}) \left[A(\mathbf{r}, \mathbf{r}') - A^*(\mathbf{r}', \mathbf{r}) \right] \psi_0 (\mathbf{r}') \, d^3 r \, d^3 r'. \tag{4.27}$$

The quantity $-(1/i\hbar)[A(\mathbf{r},\mathbf{r}') - A^*(\mathbf{r}',\mathbf{r})]$ expresses the spatial distribution of the *non-local* "absorption power" (cf. II.2a), the amount of absorption depending on the values of ψ_0 at the two points $\mathbf{r}$ and $\mathbf{r}'$. From (4.16) and (4.19) it follows that

$$C_{hg}^{(i)} = \frac{1}{2i\tau} \iint [A(\mathbf{r}, \mathbf{r}') - A^*(\mathbf{r}', \mathbf{r})] \exp \{ - i\mathbf{k}_h \cdot \mathbf{r} + i\mathbf{k}_g \cdot \mathbf{r}' \} \, d^3 r \, d^3 r', \tag{4.28}$$

showing that $-C_{hg}^{(i)}$ is the Fourier transform of the spatial distribution of absorption power. If $A(\mathbf{r}, \mathbf{r}')$ would be local, then $C_{hg}^{(i)}$ would be the (h − g)-th Fourier coefficient.

Yoshioka does not refer to the physical interpretation of the real part $C_{hg}^{(r)}$, but a comparison with the corresponding theory for atoms (*Massey* and *Mohr* [50]) indicates that $C_{hg}^{(r)}$ is the term representing the "correlation", that is, the effect of the internal polarization of the crystal due to the Coulomb field of the incident electron. In the case of atoms the correlation effect is known to be negligible for high-energy electrons. In crystals the polarization may occur, for example, as the polarization of ion cores and, in the case of metals, as the screening effect of conduction electrons which leads to the "dielectric constant" of the metal. In any case, very little is known about $C_{hg}^{(r)}$ both theoretically and experimentally.

An interesting consequence of Yoshioka's theory is that, owing to the non-local character of the optical potential, the quantity C_{hg} depends not only on the energy of the incident electron, but also on its direction. This means that both the real and imaginary parts of $\upsilon_{h-g}^{(c)}$ in (II. 2) depend on the values of $\mathbf{k}_g$ and $\mathbf{k}_h$, that is, on the

values of excitation errors ρ_g and ρ_h. This is an additional reason for the dependence of the absorption constant μ_j on the energy and direction of the incident electron. (This dependence would also occur even if the quantities C_{hg} would be constant.) Up to this time, however, the interpretation of experiments has been mostly based on the assumption that there is no such angular dependence of C_{hg}.

We note that the present discussion is concerned only with the elastic scattering ψ_0, which can be obtained by solving (4.10). Experimentally the separation of the elastic scattering from the inelastic scattering by filtering is more or less incomplete. Therefore the comparison of the theoretical value resulting from (4.10) with experimental values is significant only if one can believe that one of the following conditions is realized:

1. The largest part of the measured intensity is due to elastic scattering.
2. The amount of inelastic scattering is comparable with that of elastic scattering, but the behaviour of the inelastic scattering is not much different from that of the elastic scattering so that the total scattering is practically proportional to the elastic scattering.

Whether these assumptions are true may depend on the particular kind of effect which is investigated.

In any case it may be desirable to have a theory with which one can calculate the total intensity from Eqs. (4.5) and (4.6). Then one should be able to compare the calculated and measured total intensity without bothering about filtering or about the validity of the assumptions mentioned above.

III. Comparison with Experiments

A large number of experiments have been done to determine the real and imaginary parts of structure potentials. We can mention here only a short list of experimental methods, referring only to papers which appear to be typical.

1. *Interference multiple refraction* (*Lehmpfuhl* and *Molière* [51, 52])

One observes the splitting of the diffraction spots in transmission through wedge-shaped crystals. Specimens are mostly a 90° wedge of a MgO crystal obtained by cleavage. In the two-beam case doublets are observed; the separation of the two spots of a doublet gives the real part $v_g^{(r)}$. The imaginary parts $v_0^{(i)}$ and $v_g^{(i)}$ are obtained from the half-widths of the distributions of the two spots. The crystal orientation is determined exactly by evaluating *Kikuchi* diagrams.

2. *Equal-thickness fringes* (*Kohra* and *Watanabe* [53], *Watanabe* [54], *Castaing* et al. [55], *Dupouy* et al. [56], *Uyeda* and *Nonoyama* [57])

Multiple refraction gives rise to Pendellösung fringes in electron-micrographs of MgO crystals. The spacing of the fringes gives the real part and the decrease of the fringe intensities with the thickness gives the imaginary part. The orientation can be determined from *Kikuchi* patterns taken by the "selected-area-diffraction method", and the thickness from the distance from the edge in the picture.

3. *Extinction-line contours* (*Hashimoto, Howie* and *Whelan* [58], *Hashimoto* [59])

The wedge-shaped regions near the edges of metal foils prepared by etching are often bent in such a way that one can observe, in electron-micrographs, extinction-line contours which show a variation of the intensity with the crystal thickness and orientation. The real part cannot be measured because the thickness change is unknown. The thickness is calculated, then, from an assumed value of the real part taken from theoretical considerations or from some other experiments. The imaginary part can be obtained from the intensity variation either along the lines of constant thickness or along the lines of constant orientation.

4. *Convergent-beam patterns* (*Kossel-Möllenstedt patterns*) (*Goodman* and *Lehmpfuhl* [60])

Plate-like crystals are used and, by making the beam focus on the crystal as small as possible (300 Å), a part of the crystal is selected where the plate is ideally flat. The intensity profile in the main diffraction spot determines the real part, and from the profile in the primary spot one obtains the imaginary part. The thickness of the crystal can be determined from the profiles in weakly excited reflections and the crystal orientation from *Kikuchi* lines (see [60]). The mean absorption constant can only be measured if one can make an "absolute measurement" of diffraction intensities, that is, a measurement of the ratios of the intensities of the diffracted beams to that of the incident beam.

5. *Crystal rotation method* (*Meyer* [61])

This is an alternative method to the convergent-beam technique to obtain the dependence of the intensity on the crystal orientation. *Meyer* carried out an absolute measurement to determine the mean absorption coefficient for Si and Ge.

We note that energy filters and analyzers are very important tools for the study of absorption (*Watanabe* [54], *Castaing* et al. [55], *Meyer* [61]). The experiments using polycrystals are also important sources of related data (*Horstmann* and *Meyer* [62], *Boersch* et al. [63], *Kuwabara* [64]).

III. 1 Effect of the inelastic scattering; Absorption

We have seen in II. 4 that the influence of the inelastic scattering on the elastic scattering gives rise to Yoshioka's terms C_{gh}. The imaginary part $C_{gh}^{(i)}$ represents the "absorption" of elastically scattered electrons by the inelastic scattering.

The inelastic scattering is accompanied by a change of the internal state of the crystal, for which mainly the following processes are responsible:

1. The excitation of the core electrons, sometimes called interband excitation,
2. the excitation of valence electrons, or conduction electrons in the case of metals, including the excitation of collective motion (plasma oscillation),
3. the excitation and deexcitation of lattice vibrations (creation and annihilation of phonons), giving rise to the thermal diffuse scattering (TDS).

Since these processes contribute to C_{gh} additively, we write

$$C_{gh} = C_{gh}^{CORE} + C_{gh}^{VAL} + C_{gh}^{TDS}. \tag{5.1}$$

III. 1.1 *Excitation of core electrons*

Yoshioka [46] calculated C_{gh} from the excitation of electron states in crystals assuming the tight-binding model. Since this model is good for the core electrons we may regard his values to be the terms C_{gh}^{CORE}. He applied, however, the Thomas-Fermi model for neutral atoms, so that C_{gh}^{VAL} is also included within the validity of the tight-binding model. In this model C_{gh} can be written as a sum of contributions from different atoms in an unit cell. He used for $A(\mathbf{r}, \mathbf{r}')$ the approximation (4.11), and, consequently, all elastic and inelastic-scattering processes following the first inelastic scattering are neglected. The salient results of *Yoshioka* are that

1. C_{gh} can be regarded practically as the product of the factor $\lambda_0 m/\tau_0$ and a constant, where τ_0 is the volume of the unit cell and λ_0 is the electron wavelength in the vacuum. The dependence on the direction of the incident wave can be neglected.

2. $C_{ho}^{(i)}$ has a character similar to V_h, that is, $C_{ho}^{(i)}$ is large when V_h is large, and it has the same sign as V_h if the crystal is centrosymmetric.
3. Just as V_0 (*Miyake* [65]), $C_{00}^{(r)}$ can be calculated from the experimental value of the diamagnetic susceptibility of the elements. The discrepancy found by *Miyake* [65] in the RHEED experiments between the calculated values of V_0 and the observed values may perhaps be explained by $C_{00}^{(r)}$.
4. $C_{00}^{(r)}$, $C_{00}^{(i)}$ and $C_{ho}^{(i)}$ for several reflections are calculated for MgO. The calculated values of $C_{ho}^{(i)}$ are about 1/100 of V_h and about ten times smaller than the observed values (*Honjo* and *Mihama* [66]).
5. $C_{ho}^{(r)}$ could not be evaluated because of the complexity of calculation.

Heidenreich [35] (cf. also *Heidenreich* [67], p. 157) derived the value of $C_{00}^{(i)CORE}$ from the formula

$$C_{00}^{(i)CORE} = \frac{\hbar^2 K_0}{2m} \sigma_0 N, \tag{5.2}$$

where N is the number of atoms/cm^3 and σ_0 is the total inelastic cross section per atom. He expressed σ_0 by a formula given by *Massey* [68] which leads to an expression of $C_{00}^{(i)CORE}$ somewhat different from that of *Yoshioka* [46]. The calculation was carried out for Na^+, Al^{3+}, Cu^+, Rb^+, and Ag^+ for 10 kV and 100 kV electrons. The value for $C_{00}^{(i)CORE}$ for MgO was also calculated, where the value of σ_0 is calculated for O^{--} from *Massey's* data [68],but only estimated for Mg^{++}.

Whelan [69] calculated the values of $C_{g0}^{(i)}$ by applying the Hartree-Fock model of atoms to Yoshioka's theory. For $C_{00}^{(i)}$ he used a formula of *Lenz* [70] which is, after *Whelan,* probably a better approximation than that of *Yoshioka* [46]. The contribution of the small-angle scattering to $C_{00}^{(i)}$ is omitted on the basis of Howie's theory [12], which shows that the small-angle inelastic scattering gives contrast effects similar to the elastic scattering. The values of $C_{00}^{(i)}$ and $C_{g0}^{(i)}$ for several reflections of Li, Be, Ne, Al, and Cu are calculated. It is concluded that the values of $C_{g0}^{(i)}$ are of the same order of magnitude as those of *Yoshioka* [46] and are too small to explain the experimental results.

Although it appears that the contribution of the core electrons is not important for absorption, we refer here to the interesting phenomenon of X-ray production accompanying the excitation of inner-core electrons, which shows a marked dependence on the Bragg reflection of the incident electron (*Duncumb* [71], *Hall* [72], *Miyake* et al. [73]).

III. 1.2 *Excitation of valence electrons; plasma oscillation*

1. $C_{00}^{(i)VAL}$

Since valence electrons are more strongly influenced by the interaction between the atoms than the core electrons they should be treated separately. Particularly the correlation effect between the valence electrons is so strong that it brings forth excitation of plasma oscillations by the incident electrons (*Pines* [74], *Raether* [75]). Energy analysis of inelastic scattering indicates that the plasma oscillations are excited not only in metals but also in semiconductors and insulators (e. g. MgO). Obviously this effect influences strongly the value of C_{gh}^{VAL}. To date, however, there is no general theory of C_{gh}^{VAL}.

Heidenreich [35, 67] calculated the value of $C_{00}^{(i)VAL}$ from the cross section for inelastic scattering by the excitation of plasma oscillation according to the homogenous-electron-gas model. He took Al as an example and obtained numerical values.

The excitation of plasma oscillations gives rise to small-angle inelastic scattering only, the intensity of which is, after *Howie* [12], approximately proportional to the elastic scattering, even if a Bragg reflection is taking place, so that it does not contribute to the "absorption" if it is not separated from the elastic scattering by an energy filter. *Watanabe* [76] observed, using his energy selecting microscope [54], that the mean absorption coefficient μ_0 of MgO, measured from the equal-thickness fringes, increased if the inelastic scattering by plasma oscillations etc. was filtered out. *Cundy* et al. [77] suggested that this increase is just the contribution of plasma excitations. *Meyer* [61] measured the values of μ_0 for Si and Ge also filtering out the inelastic scattering caused by the plasma excitations. He calculated by the method of *Heidenreich* [67] the contribution of the plasma excitations to μ_0 and added it to the contribution of TDS (see below). The measured values were about 50 % larger than the calculated values.

2. $C_{g0}^{(i)VAL}$

It is usually believed that the plasma excitations are not affected by the Bragg reflection of the incident wave (e. g. *Hirsch* et al. [7], p. 438). *Meyer* [61] observed that the intensity of the inelastic scattering of Si and Ge, accompanied by the plasma excitations, does not depend on the Bragg reflection (220). On the other hand, *Cundy* et al. [78] and *Ishida* et al. [79] observed in Al und Mg that the plasma excitations do depend on the Bragg reflection. *Watanabe* [76] found that the above mentioned increase of μ_0 by filtering depends apparently on the Bragg reflection of the incident wave. *Cundy* et al. [77] suggested that this verifies that the absorption by the plasma excitations depends on the Bragg reflection. This problem deserves a further investigation, especially since it implies that $C_{g0}^{(i)VAL}$ may not be as small as usually believed.

III. 1.3 *Excitation of lattice vibrations*

Yoshioka and *Kainuma* [80] calculated C_{gh}^{TDS} for MgO using Yoshioka's theory [46] and found that $C_{g0}^{(i)TDS}$ is about ten times larger than $C_{g0}^{(i)VAL}$, and gives the same order of magnitude as the experimental values. These authors took into account only one-phonon processes which are dominant only in the small-angle TDS. *Whelan* [81] calculated $C_{00}^{(i)\,TDS}$ and $C_{g0}^{(i)TDS}$ in a similar manner for several metals, as well as for C, Si, and Ge.

Hall and *Hirsch* [82] developed a theory which takes into account multiphonon processes, but only within the scope of the two-beam theory and the Einstein model of lattice vibration. The result gave the same order of magnitude of absorption coefficients as those of *Yoshioka* and *Kainuma* [80]. Values of mean and anomalous absorption coefficients were calculated for Al, Cu, Ag, Au, and Pb for a wide range of temperatures. *Hall* [83] showed that the Debye model leads to no essential difference.

Goringe [84] (Cu) and *Meyer* [61] (Si, Ge) compared the results of *Hall* and *Hirsch* [82] with experiments and found that the characteristics of temperature dependence agree well, but that the absolute values of the anomalous part $\Delta\mu_g$ were about two times larger than the calculated ones. The results of the many-beam calculation as shown in Fig. 3 indicate that this discrepancy may be explained, at least partly, by the many-beam effect according to which the effective value of $C_{g0}^{(i)}$ (to be introduced into the two-beam formula to fit the experimental values) depends considerably on the values of $C_{g0}^{(i)}$ of the weakly excited reflections.

III. 1.4 *"Absorption" by weak beams*

The weakly excited Bragg reflections which belong to the *elastic* scattering may act as a source of apparent absorption of the strongly excited reflections. *Gjønnes* [85] modified Bethe's corrections of structure potentials to be applied to crystals of limited size, and obtained an *imaginary* term in the corrections, which causes an apparent absorption for strong beams. He points out, however, that this is actually a "beating" of the strong beams, i. e., a long-period modulation of the intensity of strong beams and not a monotonic decrease.

Boersch, Jeschke, and *Raith* [86] developed a kind of multislice approach to the dynamical theory and applied to the scattering by a slice the "strong phase-grating" calculation which is effectively the pseudo-kinematical theory (*Hoerni* [87]). *Raith* [88] calculated for this purpose the complex atomic scattering amplitude by the multislice method of *Molière* [89]. Hence, the method of *Boersch* et al. is, in the many-beam form, equivalent to the phase-grating theory of *Cowley* and *Moodie* [32]. Applying the two-beam approximation to the scattering by a slice, *Boersch* et al. obtained an apparent absorption of strong beams which gives, in their case,

a monotonic decrease of intensity. They attributed this absorption to the transfer of intensity to weak beams. *Boersch* and his coworkers also developed theories of the absorption and its temperature dependence based on this assumption (*Glaeser* and *Niedrig* [90], *Albrecht* and *Niedrig* [91], *Jeschke, Raith,* and *Zorn* [92]).

Fukuhara [93] pointed out, however, that the two-beam approximation is not applicable to a slice since it does not guarantee the conservation of the sum of the intensities of various rays. Thus, the absorption calculated by *Boersch* et al. [86] in the two-beam approximation appears to be introduced by the violation of the intensity conservation, the intensity being lost from the whole system of beams and not transferred to weak beams [1]).

Hall and *Hirsch* [94], *Hall* [95] calculated the effect of weak beams on the absorption and concluded that under usual conditions it is small compared to the effect of the inelastic scattering.

Kainuma and *Yoshioka* [96] derived, applying the second Born approximation to *Fujiwara's* theory [26], Yoshioka's term C_{h0} for the strong beams which is found to be complex. The imaginary part $C_{h0}^{(i)}$ represents the absorption effect by the weak beams. This theory is obviously valid only for very thin crystals for which the second Born approximation is applicable.

III. 2. The Debye-Waller Factor

The thermal vibration of the crystal lattice influences the intensities of diffracted waves in two ways: 1. The incident electrons may excite or extinguish modes of lattice vibration. This gives rise to the thermal diffuse scattering (TDS) which gives a contribution to Yoshioka's term C_{gh}^{TDS}. This was discussed in III. 1.3.
2. Except at O °K the thermal excitation of lattice vibrations is always present in crystals so that the "initial state" of II. 4 may be any one of the *thermally* excited states of the crystal. The values $H'_{00}(\mathbf{r})$ and $A(\mathbf{r}, \mathbf{r}')$ depend in general on the initial state so that the resulting intensities of diffracted waves also vary with them. We should thus calculate the average of the intensity over the canonical ensemble of thermally excited states. We try to represent the difference between this average intensity $< I >$ and the intensity $I^{(id)}$ for the ideally rigid lattice by multiplying each of the Fourier potentials by an appropriate factor. With this modification we arrive again at a kind of "optical potential", which reproduces, when it is substituted into the Schrödinger equation, the correct value of the intensity (with respect to the ensemble average). This is the quantum-mechanical explanation of the origin of the Debye-Waller factor in the dynamical theory.

[1]) It should be noted that this statement remains a guess until an exact calculation of intensities is made.

Physically, the thermal excitation of the crystal occurs in two ways: one is the excitation of lattice vibrations, the other is the excitation of conduction electrons occuring in metals and semiconductors. To the authors' knowledge, however, the effect of the thermal excitation of conduction electrons has not been observed in electron diffraction. It may be caused by the fact that the contribution of conduction electrons to $H'_{00}(\mathbf{r})$ and $A(\mathbf{r}, \mathbf{r}')$ is relatively small; $H'_{00}(\mathbf{r})$ is mainly due to the contributions from atomic nuclei and ion-core electrons, $A(\mathbf{r}, \mathbf{r}')$ mainly from TDS. Hence we consider here only the thermal excitation of lattice vibrations.

We expand $H'^{(id)}_{00}(\mathbf{r})$, the value of $H'_{00}(\mathbf{r})$ for the ideally rigid lattice, in a Fourier series

$$H'^{(id)}_{00}(\mathbf{r}) = V^{(id)}(\mathbf{r}) = \sum_{\mathbf{g}} V_{\mathbf{g}}^{(id)} \exp\{2\pi i \mathbf{g} \cdot \mathbf{r}\} \quad . \tag{6.1}$$

Under the usual assumption regarding lattice vibration (Born-Oppenheimer approximation, harmonic character of vibration, Bloch or Nordheim model) the statistical average of $H'_{00}(\mathbf{r})$ can be written (*Takagi* [11]) as

$$\langle H'_{00}(\mathbf{r}) \rangle = \langle V(\mathbf{r}) \rangle = \sum_{\mathbf{g}} \langle V \rangle_{\mathbf{g}} \exp\{2\pi i \mathbf{g} \cdot \mathbf{r}\}, \tag{6.2}$$

where

$$\langle V \rangle_{\mathbf{g}} = V_{\mathbf{g}}^{(id)} \exp\{-M_{\mathbf{g}}\} . \tag{6.3}$$

The factor $\exp\{-M_{\mathbf{g}}\}$ is the Debye-Waller factor in the usual sense. That means that in the kinematical theory the integrated intensity of a reflection is given by

$$I_{\mathbf{g}} = I_{\mathbf{g}}^{(id)} \exp\{-2M_{\mathbf{g}}\}, \tag{6.4}$$

where $I_{\mathbf{g}}^{(id)}$ is the value for the ideally rigid lattice.

If we neglect the effect of the inelastic scattering completely, put $\langle H'_{00}(\mathbf{r}) \rangle$ into (4.9) in place of $H'_{00}(\mathbf{r})$, and calculate the intensities of diffracted waves, then a sort of averaged intensity results which we call here the "structure average" $I(\langle V \rangle)$. In the kinematical theory it can be shown (*Ott* [164]) that $I(\langle V \rangle)$ is equal to the true average $\langle I \rangle$:

$$I(\langle V \rangle) = \langle I \rangle. \tag{6.5}$$

In the dynamical theory it was shown by *Parthasarathy* (1960) [97] and, in a generalized form, by *Kambe* (1965) [98] that this equality also holds under the conditions usually realized in experiments. We note that the inelastic scattering is for the moment completely neglected.

It was verified by *Horstmann* (1965) [99] that the integrated intensities of Debye-Scherrer rings of Al, particularly their variation with temperature, agree satisfactorily with the values calculated essentially by the above procedure. This result appears to show that in his case (light atoms, thin crystal, *relative* integrated intensity) the effect of inelastic scattering was negligible.

If we want to take into account the effect of inelastic scattering, particularly the "absorption" of elastically scattered waves, we should investigate the dependence of $A(\mathbf{r}, \mathbf{r}')$ or C_{gh} on the thermal excitation of lattice vibrations. *Ohtsuki* (1966) [100] showed that the statistical average of C_{gh}^{CORE} (5.1) is given by

$$< C_{gh}^{CORE} > = C_{gh}^{CORE\ (id)} \exp \{ - M_{g-h} \} , \tag{6.6}$$

where $C_{gh}^{CORE\ (id)}$ is again the value for the ideal lattice. This expression is derived under the assumption that the electronic states of the atoms are not influenced by the thermal motion (Nordheim's rigid-ion model), so that it is valid only for the contributions from the ion-core electrons and not for valence (conduction) electrons.

If we calculate the intensities of elastic scattering by introducing $< V >_{g-h} + < C_{gh} >$ into Eq. (4.15) we obtain another kind of average intensity. Since this value is, according to the theory of *Dederichs* (1966) [49], obtained by taking the statistical average of the *amplitudes* of the diffracted waves we call it the "amplitude average" of intensity and write $I(< A >)$. It was pointed out by *Kambe* (1965) [98] that $I(< A >)$ is also equal to the *true* average $< I >$ if we can apply the rigid-ion model in the derivation of C_{gh}. Consequently, if C_{gh} would consist mainly of the contributions of ion-core electrons, C_{gh}^{CORE}, the intensity could be calculated by replacing in (4.15) V_{g-h} and C_{gh} by (6.3) and (6.6) respectively [1]. Unfortunately it is known that the main part of C_{gh} is usually C_{gh}^{TDS} and not C_{gh}^{CORE}.

For valence electrons Yoshioka's approximation by means of the tight-binding models is obviously not good. Particularly in the case of metals the excitation of plasma oscillations should decisively influence C_{gh}^{VAL} and its temperature dependence. It is also expected that C_{gh}^{VAL} is influenced by the *thermal* excitation of valence (conduction) electrons, which may occur, as mentioned above, in metals and semiconductors. To date very little is known about C_{gh}^{VAL} and its dependence on temperature. We may expect roughly that $< C_{gh}^{VAL} >$ is similar to $< C_{gh}^{CORE} >$ in ionic, covalent, and molecular crystals, and almost independent of the temperature in metals.

---

[1]) For the scattering of X-rays this procedure is completely satisfactory (*Kambe* [98], *Authier*, this volume) in virtue of the circumstances that 1) the imaginary part is due to excitation of ion-core electrons and that 2) the inelastic scattering is negligibly small compared to the elastic scattering.

The quantity C_{gh}^{TDS}, the contribution of TDS to C_{gh}, appears to be usually the main part of C_{gh} and it should certainly be influenced by the thermal excitation of lattice vibrations. The existing theories (cf. III.1.3) of C_{gh}^{TDS} are limited to the calculation of $< C_{gh}^{TDS} >$ so that they amount to the calculation of the "amplitude average" $I(< A >)$ and not the true average $< I >$. Anyway, the results of the calculations by *Hall* and *Hirsch* (1965) [82] and *Whelan* (1965) [81] reveal that C_{gh}^{TDS} depends on the temperature in a way very much different from $\exp\{-M_{g-h}\}$ so that it is almost certain that the true average $< I >$ may bring forth an effective "optical potential" value of C_{gh}^{TDS} which varies with temperature also quite differently from $\exp\{-M_{g-h}\}$. This has been proved by *Goringe* [84] and *Meyer* [61] (cf. III. 1.3).

Summarizing, we can use the Debye-Waller factor in the dynamical theory in the following cases:

1. We are concerned with an effect for which C_{gh} can be neglected. Then V is real and we use V_g in the form (6.3).
2. The physical conditions allow the assumption that the main part of C_{gh} is C_{gh}^{CORE} This may happen at very low temperatures where C_{gh}^{TDS} becomes small. Then (6.3) and (6.6) may be substituted in (4.15). If these conditions are not satisfied the effective value of C_{gh} may not change with temperature according to $\exp\{-M_{g-h}\}$. It is possible that V_h may show also a deviation from the form (6.3).

It should be noted that, as already pointed out in II. 4, almost all the theories of C_{gh} are concerned only with the intensity of elastic scattering. In ordinary experiments the elastic scattering is measured together with TDS superposed on it. Accordingly, this may result sometimes in a further deviation of the measured effective values of V_h and C_{gh} from (6.3) and (6.6).

III. 3 Many-beam Effects

An accurate determination of structure amplitudes requires a proper correction for the many-beam effect, that is, the influence of a great number of weakly excited reflections on the main strongly excited ones. Bethe's summation correction (II. 2c) is a powerful tool for estimating this effect. However, computor techniques yield a more accurate correction by the N-beam calculation of II. 1. We describe here the many-beam theory in connection with: (i) explicit many-beam cases in which more than one reflection are strongly excited simultaneously, giving rise to various anomalies, and (ii) implicit cases, in which the influence of weakly excited reflections on the strongly excited one is considered.

III. 3. 1 *Anomalies caused by simultaneous reflections;* Crystal symmetry

A large number of cases are reported in the literature (see *Laue* [101], *Bauer* [102], *Raether* [103], *Pinsker* [104], *Thomson* and *Cochrane* [105]) concerning special effects of the dynamical interaction between simultaneously excited reflections. Various anomalies were observed also in Kikuchi patterns. Theories, mainly based on Bethe's many-beam formulation (II. 1.), were developed for the explanation of these effects. We refer here only to the latest topics in this field.

a) Diffraction in transmission through wedge-shaped crystals: *Molière* and *Wagenfeld* (1958) [106], *Lehmpfuhl* and *Molière* (1961) [51] observed simultaneous reflections in multiple-refraction spots of MgO, thus confirming the validity of Bethe's many-beam formulation by analysing, effectively, the Bloch waves separately. *Lehmpfuhl* and *Reissland* (1968) [107] recorded photographically cross sections of the dispersion surface in many-beam cases by means of rotating the crystal and deflecting simultaneously the diffracted beams in proper directions. A few examples are shown in Fig. 1. A satisfactory agreement with Bethe's many-beam calculation was obtained. *Herzberg* (unpublished) calculated the anomalies by means of Bethe's summation corrections and obtained fairly good agreement with experiment. Similar anomalies were observed in electron microscope images of equal-thickness fringes (e. g. *Uyeda* and *Nonoyama* (1965) [57]) with corresponding anomalies in the absorption coefficient.

b) *Fujimoto* (1961) [108], *Fengler* (1961) [109], *Takagi* and *Morimoto* (1963) [110], *Fujime* et al. (1964) [111] investigated the intensity of forbidden reflections excited by Umweganregung.

c) *Cowley* and *Moodie* (1961) [32], *Miyake* et al. (1960) [112], *Cowley* et al. (1961) [113], *Gjønnes* and *Moodie* (1965) [114] discussed the effect that a forbidden reflection which could have a nonvanishing intensity by Umweganregung disappears again under certain conditions of symmetry. These symmetry conditions have been confirmed experimentally by *Goodman* and *Lehmpfuhl* (1964) [115] and *Fujime* et al. (1964) [111].

d) *Hirsch* et al. (1965) [7], *Blume* (1966) [116] and *Fukuhara* (1966) [117] developed Bethe's many-beam formulation in cases of high symmetry showing that one can factor the dispersion equation (1.17) into a product of lower-order determinants. Actually, this was already demonstrated in Bethe's classical paper [19].

e) *Pogany* and *Turner* (1968) [118] investigated symmetries of the diffraction patterns related to the "reciprocity" (*Kainuma* [10]), an inherent symmetry of Schrödinger's equation, and to the crystal symmetry.

f) The phase effect, which is discussed separately in 3.3, is closely related to c), d) and e), being concerned with *the symmetry of the crystal.*

g) The need for a many-beam treatment in the interpretation of "lattice images" in electron microscopy was pointed out by *Niehrs* (1962) [119], *Miyake* et al. (1964) [120] and is evidenced clearly in micrographs (e. g. *Labaw* (1964) [121], *Komoda* (1966) [122], *Yada* (1967) [123]).

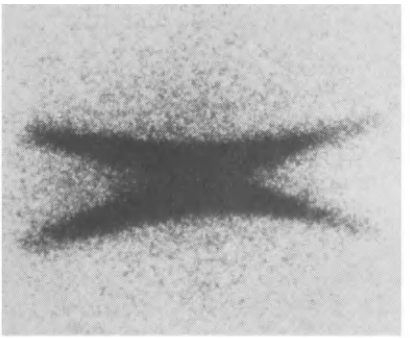

(a)

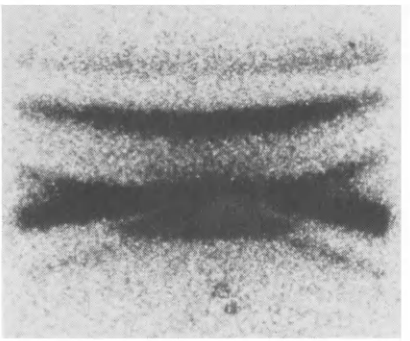

(b)

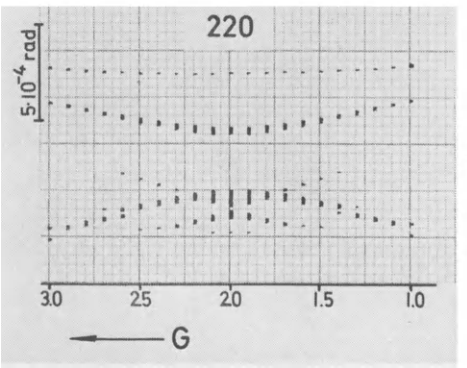

(c)

Fig. 1
Sections of the dispersion surface obtained by the multiple refraction method using a 90° wedge of a MgO crystal.
(a) The two-beam case of the (220) reflection showing the typical hyperbola.
(b) The many-beam case in which the incident beam is nearly parallel to the $[\bar{1}10]$ zone axis; the (220) reflection is strongly disturbed by the (002) and other reflections.
In both cases a) and b) the Bragg condition is satisfied at the center of the pictures where

$$G = -\frac{4(\vec{k}_0^{(r)} \cdot \vec{b}_{220})}{2\pi \left|\vec{b}_{220}\right|^2} = 2$$

(c) Calculated intensities of the (220) reflection on the branches of the dispersion surface. 17 beams belonging to the zeroth Laue zone of the $[\bar{1}10]$ zone axis are taken into account. (*Lehmpfuhl* and *Reissland* [107]). (Electron energy 60 keV)

III. 3.2 *Weak-beam Corrections of Structure Potentials*

a) Systematic and accidental interactions

According to *Hoerni* (1956) [87] there are two categories of interaction of weak beams with strong beams, namely, systematic and accidental interactions. The systematic interactions are those between the different orders of reflections on the same set of net planes. In other words, the reciprocal-lattice points corresponding to these reflections lie on the same reciprocal-lattice rod. All other weak reflections produce accidental interactions. The systematic interactions are always present independent of the azimuth angle of the strongly excited reflections, giving rise to a "systematic failure" of the measured value of structure amplitudes, whereas the accidental interactions change rapidly with the azimuth and can often be reduced to a negligibly small amount by a proper choice of the azimuth.

b) Corrections for systematic interactions

A pronounced effect of systematic interactions is the anomalously small intensity of a second-order reflection of some low-index netplane (e. g. *Lehmpfuhl* and *Molière* (1961) [51], *Horstmann* and *Meyer* (1962) [62], *Nagata* and *Fukuhara* (1967) [124], *Kimoto* and *Nishida* (1967) [125], *Watanabe* et al. (1968) [126] [165]). This is due to the diminishing influence of the weakly excited first-order reflection, as can be easily seen from the form of Bethe's summation corrections (II. 2 c). Since this effect has to do with the difference between structure amplitudes it is sensitively influenced by the electron energy because of the relativistic effect (III.4.) and by the temperature because of the Debye-Waller factor (see III. 2.) (cf. also *Howie* and *Valdré* (1967) [127]).

The weak beams influence also C_{gh}, leading to a correction of the absorption coefficient (*Goringe* et al. (1966) [128], *Goodman* and *Lehmpfuhl* (1967) [60], *Metherell* and *Whelan* (1967) [129], *Metherell* (1967) [130].

Howie and *Whelan* (1960) [131] (cf. *Hirsch* et al. (1965) [7], p. 281) carried out a model calculation, by use of Bethe's many-beam method (II.1.), for Al (111) considering systematic interactions. They considered two models of the "imaginary part" of the structure potential. One of them is given by the relation $V^{(i)}(\mathbf{r}) = \text{const.} \times V^{(r)}(\mathbf{r})$ (const. = 0.1), the other represents $V^{(i)}(\mathbf{r})$ as a lattice δ-function. They concluded that the former model shows better agreement with the observations of extinction contours.

Heidenreich (1964) [67] suggested that the "dark band" between the $(\bar{h}\bar{k}\bar{l})$ and (hkl) extinction contours[1]) might be satisfactorily explained by systematic interactions and that there would be no need for an imaginary part $V^{(i)}(\mathbf{r})$. *Howie* and

[1]) *Hashimoto, Howie* and *Whelan* (1962) [36]

Whelan (cf. *Hirsch* et al. (1965) [7]) found, however, that the asymmetry calculated without an imaginary part turned out to be too small to give an agreement with the observations.

Goodman and *Lehmpfuhl* (1967) [60] investigated MgO (200) with systematic interactions by use of Kossel-Möllenstedt patterns. They found that one can proceed in the following way:

1. The thickness of the crystal is determined first very accurately (up to one atomic layer) by observing the profiles of weak beams, which are fairly insensitive to the values of structure potentials.
2. The real part of the structure potential of the main reflection can then be determined fairly accurately by comparing the intensity profile of the main reflected beam with the calculated curve, which is fairly insensitive to the value of the imaginary part of the main structure potential and of the real and imaginary parts of other structure potentials belonging to weak beams.
3. The asymmetry in the profile of the (000) beam can then be well reproduced by the calculation if a proper combination of imaginary parts is chosen. Again, the two models for $V^{(i)}(\mathbf{r})$ according to *Howie* and *Whelan* (1960) [131] were introduced into the calculation and a better agreement was obtained by the δ-function model, in contradiction to *Howie* and *Whelan*.
4. The relativistic correction (see III. 4) and a proper choice of the ionic potential of O^{--} were essential for a good agreement between theory and experiment.

Table 1 demonstrates the effectiveness of the corrections applied to the experimental value in the case of MgO (200). The calculation for neutral atoms gives 7.4 volts, for ions 7.01 volts, to be compared to the experimental value 7.02 volts.

Table 1. Successive corrections applied to the experimental value of $V_{200}^{(r)}$ of MgO (electron energy 80 keV) determined by the convergent-beam method (*Goodman* and *Lehmpfuhl* [60]). The first value 8.8 V is obtained if the observed intensities are interpreted by the two-beam approximation without any correction, the second value 7.61 V by the two-beam formula corrected for relativity, and so on.

corrections[1])			$V_{200}^{(r)}$ (Volt)
relativistic	many-beam	Debye-Waller	
−	−	−	8.8
+	−	−	7.61
+	+	−	6.92
+	+	+	7.02
		Theory:	7.01

[1]) +: applied, −: not applied

Goodman and *Lehmpfuhl* (1967) [60] used the multiple-slice phase-grating method so that the dispersion surface and the absorption coefficients for Bloch waves did not appear explicitly in the calculation. *Lehmpfuhl* (unpublished) confirmed that Bethe's many-beam method (II.1.) produces exactly the same intensity profiles.

Fig. 2 shows the dispersion surface for the MgO (200) system obtained by a 7-beam calculation after Bethe's method (*Kambe*, unpublished). The reflections taken into account were ($\bar{4}00$), ($\bar{2}00$), (000), (200), (400), (600), (800). Fig. 3 shows the absorption coefficients calculated by the standard perturbation method (1st order) for the Bloch functions belonging to each branch of the dispersion surface. Three models were taken for the imaginary part $V^{(i)}(\mathbf{r})$:

1. $V^{(i)}(\mathbf{r})$ proportional to the real part $V^{(r)}(\mathbf{r})$.
2. Lattice δ-function.
3. $V^{(i)}_{200}$ and $V^{(i)}_{400}$ are given the same value (0.14 volts) as in the case of the δ-function, $V^{(i)}_{h00}$ for higher orders being set equal to zero.

The lower part of Fig. 3 shows the intensity profiles of the (000)-beam corresponding to the three models. The profiles of the (000)-beam and the other beams (not

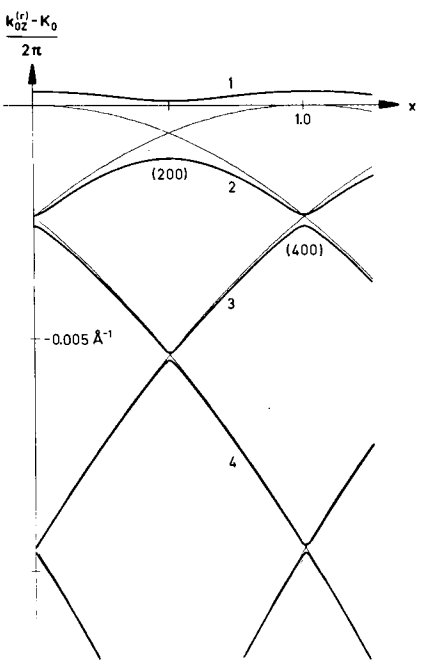

Fig. 2
Dispersion surface of the MgO (200) system. Result of a 7-beam calculation (see text). The horizontal axis is

$$x = -(\vec{k}_0^{(r)} \cdot \vec{b}_{200})/2\pi \left| \vec{b}_{200} \right|^2 .$$

The large hyperbola on the top at the position x = 0.5 represents approximately the two-beam case of (200). The second lower hyperbola at x = 1.0 is the (400). In both cases the hyperbola is strongly deformed from the pure two-beam form by the many-beam effect.
(Electron energy 79.5 keV)
The curves not labelled correspond to the diagonal terms of Mgh, Eq. (1.17).

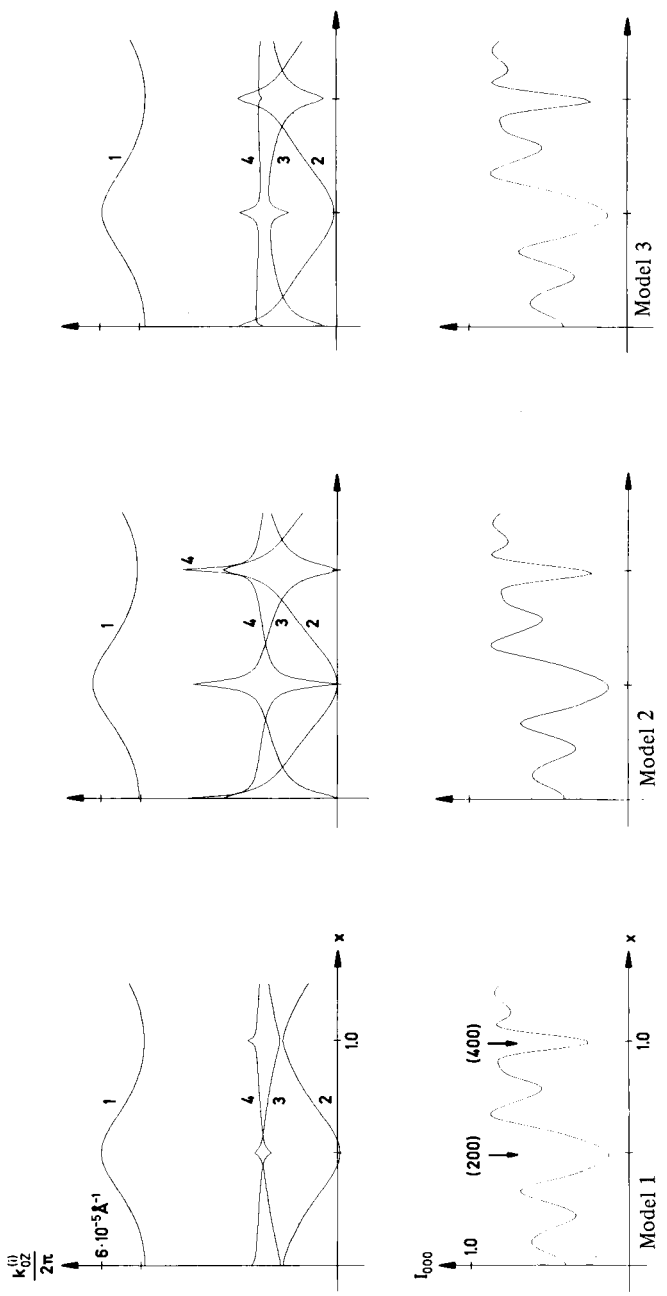

Fig. 3 Absorption coefficients of Bloch waves represent by the imaginary parts of the wave vector $\mathbf{k}_0^{(i)}$ (the numbers labelling the curves correspond to the numbers labelling the branches in Fig. 2), and the intensity of the profiles of the (000)-beam I_{000} in the convergent-beam patterns calculated for the 7-beam case of Fig. 2 (see text). $x = -(\vec{k}_0^{(i)} \cdot \vec{b}_{200})/2\pi \left|\vec{b}_{200}\right|^2$. (Electron energy 79.5 keV. Chrystal thickness 670 Å).

shown) for model 1 and model 2 are almost exactly the same as those of *Goodman* and *Lehmpfuhl* (1967) [60]. The profile for model 3 is practically equal to that of model 2, indicating that the profile of the (000)-beam in the observed region is insensitive to the values of $V_g^{(i)}$ for higher orders than (400). We may conclude therefore that the values of $V_{200}^{(i)}$ and $V_{400}^{(i)}$ *are* determined to be both equal to 0.14 volts irrespective of the values of the higher-order $V_g^{(i)}$'s.

III. 3.3 *Effect of the Phases of Structure Amplitudes*

Observation of diffraction intensities in the many-beam case makes it possible to determine the phases of structure amplitudes. This is a method additional to the various procedures (see Karle, Vol. 1 [132]) usually applied in structure analysis. Hitherto, no practical application has been possible because of the severe requirements with respect to the preparation of the crystals [1]). In favourable cases, however, this method may serve in the course of structure analysis as a short cut or an auxiliary proof of some assumption on phases. There are two possibilities of practical application:

1. Determination of the values of linear combinations of phases (*Fues* [133], *Kambe* [8]), which are called the "invariants" of the crystal structure (see *Karle*, Vol. 1 [132]).
2. Determination of the direction of a polar axis by virtue of the failure of Friedel's law (*Miyake* and *Uyeda* [134], *Niehrs* [135], *Fujimoto* [22], *Fengler* [109]).

Generally, the intensities of diffracted waves depend on the relative phases of structure potentials U_g if more than two beams take part in the diffraction. For example, in the three-beam case one finds, by means of Bethe's theory (*Kambe* [8]), that the invariant $\phi_{hh'} = \alpha_h + \alpha_{-h'} + \alpha_{h'-h}$, where α_h etc. are the phase angles, influences the intensities. It is therefore possible, at least in principle, to determine the value of $\phi_{hh'}$ from observation. Thus,

1. if any one of the $\phi_{hh'}$'s is not equal to 0 or π we can decide at once that the crystal has no center of symmetry,
2. if we know the values of α_h and $\alpha_{-h'}$ we can obtain the value of $\alpha_{h'-h}$, and
3. if we know already the structure of a non-centrosymmetric crystal we can differentiate between the enantiomorphic alternatives from the sign of $\phi_{hh'}$.

A quantitative determination of $\phi_{hh'}$ requires usually a relatively accurate measurement of intensities. There are, however, a few simplified procedures which may be more useful in practice.

[1]) For observing dynamical effects one has to investigate the diffraction at an ideally perfect region of a crystal. To get a better chance for meeting such conditions it is desirable to use a beam with an extremely fine focus. A further development of the convergent-beam technique in this direction (cf. *Goodman* and *Lehmpfuhl* [60]) seems to be promising for an extended application of many-beam effects to the problem of phase determination.

It has been shown by *Kambe* [8] that one can frequently determine the sign of $\cos \phi_{hh'}$ by observing only qualitatively the intensity distribution in a Kossel-Möllenstedt pattern. Fig. 4 shows schematically the calculated distributions in the diffraction spots in a three-beam case where the two reflections h and h′ are simultaneously excited. The dotted lines indicate the three pairs of Kikuchi lines. The curves in

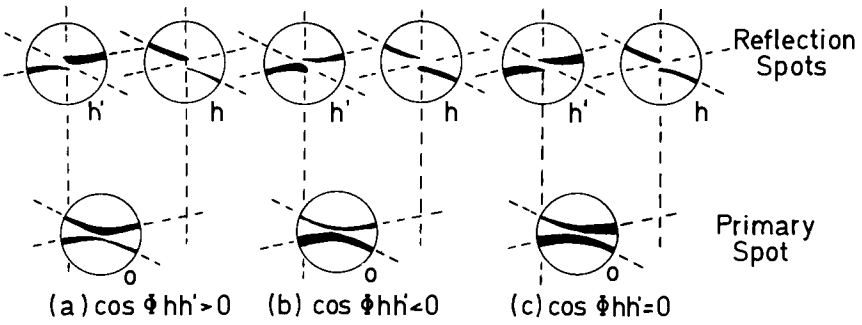

Fig. 4
Calculated intensity distributions in diffraction spots of convergent-beam patterns showing the characteristic dependence on the value of $\cos \phi_{hh'}$ (see text). (*Kambe* [8])

the circular spots appear dark in the primary and bright in the reflected beam. The structure resembling a hyperbola in the primary spot indicates the anomalous bending of the Kossel-Möllenstedt lines due to the coupling between the two reflections. In the reflection spots the curves are split up into two parts in each spot. If $\cos \phi_{hh'} > 0$, then the parts *inside* the Kikuchi band h-h′ (the region between the vertical Kikuchi lines h-h′ and h′-h) are stronger than the parts outside the band. If $\cos \phi_{hh'} < 0$ the opposite is true. If $\cos \phi_{hh'} = 0$ there is no difference between the two parts. Correspondingly, the branches of the hyperbola in the primary spot appear different depending on the sign of $\cos \phi_{hh'}$. Fig. 5 demonstrates the situation in the case of graphite. In the centro-symmetrical case $\phi_{hh'}$ is either 0 or π, so that this procedure is completely sufficient for the determination of $\phi_{hh'}$.

The intensities of diffracted waves in a many-beam case show sometimes a marked asymmetry even when we can assume that the external geometry (crystal form, direction of incidence with respect to the lattice) and the geometry of the Bravais lattice is completely symmetric (see Fig. 6). If the crystal has no center of inversion this asymmetry can often be regarded as a failure of Friedel's law (*Miyake* and *Uyeda* [136], *Goodman* and *Lehmpfuhl* [137]). This is a peculiar property of the many-beam interaction in the dynamical theory. *Miyake* and *Uyeda* [134] and *Niehrs* [135] proved that a failure of Friedel's law does not appear in two-beam cases.

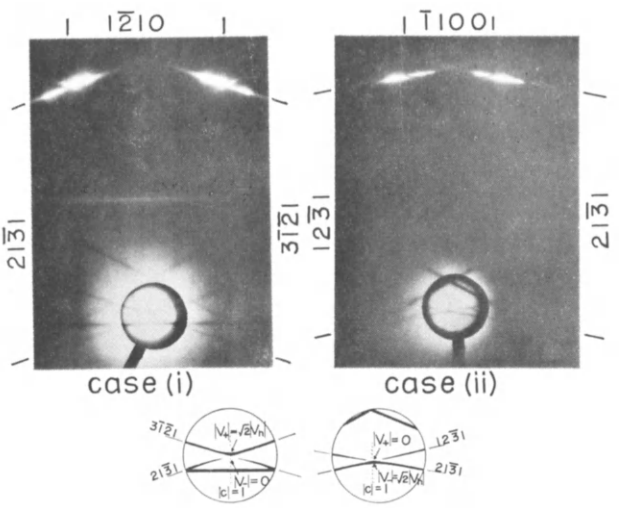

Fig. 5
Convergent-beam patterns of graphite showing the phase effect predicted by the calculation shown in Fig. 4. Sketches illustrate the intensity distribution in the primary spot.
Case (i) $\cos\phi_{hh'} = 1$.
Case (ii) $\cos\phi_{hh'} = -1$.
The indices at the sides of pictures indicate the Kikuchi-line pairs. (For detail see *Kambe* [8].)
(Electron energy 41 keV, Chrystal thickness 1,000 Å.)

If we know partly the symmetry of the structure, then we may prove quickly, by observing the above kind of asymmetry, that an inversion center does not exist. Thus, if we have already a two-fold axis we may prove the existence of a mirror plane perpendicular to this axis by the above method. If there is no mirror symmetry in the pattern, then the structure has no inversion center[1]). The opposite is not always true because we may have a symmetric projection of an asymmetric structure on the plane nearly perpendicular to the incident beam (zero-order Laue zone, *Thomson-Cochrane*, p. 80 [105], *Hirsch* et al. p. [7]). In any event this kind of proof requires exclusively qualitative observations of diffracted beams.

If we know already the structure we can determine the direction of a polar axis of the crystal by applying the above mentioned criteria of symmetry (*Goodman* and *Lehmpfuhl* [137]). This may require also only qualitative or semiquantitative observation of intensity distributions of diffracted beams.

Kainuma and *Lipscomb* [138] have suggested that the asymmetry of diffraction intensities may be applied directly to structure analysis by means of Ps (Patterson sine) functions. However, since Ps functions are concerned with the magnitude of differences of intensities a high accuracy of the intensity measurement may be necessary.

---

[1]) In the case of reflection experiments it can happen that an asymmetry appears although the crystal has an inversion center (*Uyeda* and *Miyake* [140]). This is due to the fact that in the case of reflection only a few atomic layers, which may have no inversion symmetry, take part in diffraction. A change of symmetry with the penetration of the incident electrons was observed in LEED by *Deville, Eberhart,* and *Goldsztaub* [141].

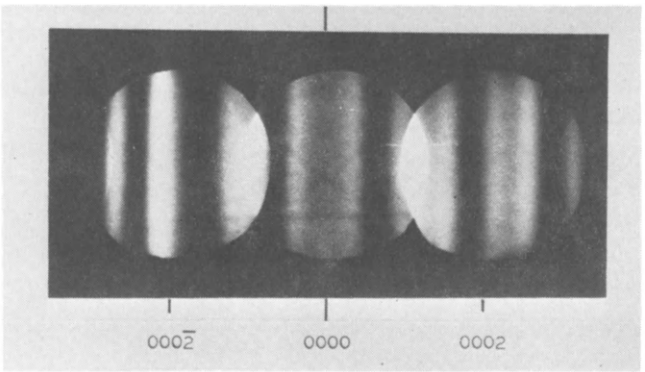

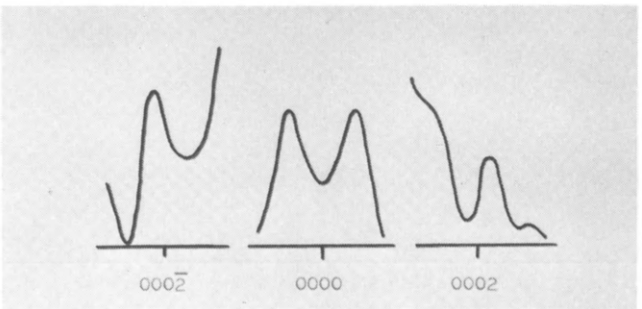

Fig. 6
(a) Convergent-beam pattern of CdS (0002) system showing the failure of Friedel's law.
(b) Calculated values by considering 13 reflections in the (0002) system. The deviation from the observation is probably caused by neglecting accidental interactions. (Courtesy *Goodman* and *Lehmpfuhl* (cf. [137]).) (Electron energy 79.5 keV, thickness 650 Å)

There are a few suggestions (*Hoerni* [87], *Parthasarathy* [139], *Kainuma* and *Lipscomb* [138]) to interpret the failure of Friedel's law in the dynamical theory in terms of the "complex atomic scattering amplitude" which appears in the pseudo-kinematical theory (*Hoerni* [87]). The origin of this idea is obviously the analogy with the anomalous-dispersion method in X ray diffraction (see *Karle*, Vol. 1 [132]). We know indeed that a failure of Friedel's law can be predicted in many-beam cases even if there is no absorption and the atomic scattering amplitude is

real, for example, in the case of X-rays (*Miyake* and *Uyeda* [134], *Niehrs* [135]). Nevertheless the "complex atomic scattering amplitude" may be at least partly a cause of the failure of Friedel's law. In fact, *Hoerni* has demonstrated an example ((111) of CdS) where this statement appears to hold, by comparing the results of the pseudo-kinematical theory and the dynamical theory. However, since we know (*Hayashi* [142]) that the pseudo-kinematical theory can be applied only to extremely thin crystals, the idea of the "complex atomic scattering amplitude" seems to be not applicable to practical problems of phase determination.

The above discussion is concerned with nonabsorbing crystals. There exists always, however, an absorption by atoms, and different kinds of atoms absorb more or less differently. This gives rise to a failure of Friedel's law in crystals containing different kinds of atoms (e. g. ZnS). As pointed out by *Kainuma* and *Lipscomb* [138], this is the true counterpart to the anomalous-absorption effect in the X-ray case. This absorption effect may be more suitable for practical applications than the asymmetry caused by the many-beam effect because it appears also in the integrated intensities of weak reflections, for which the kinematical theory is applicable.

III. 4. Relativistic Corrections

The relativistic dynamical theory of electron diffraction by crystals has been developed (*Weisskopf* [143]), at first, in connection with the problem of spin-polarization of scattered electrons. Very interesting historical accounts of this subject may be found in the books of *Thomson-Cochrane* [105] and *Pinsker* [104]. The problem of the energy dependence of υ_g and C_{gh} led to a renewal of interest in the relativistic theory. Developing the dynamical theory from Dirac's equation *Fujiwara* (1961) [144] and *Howie* (1962) [145] showed that the relativistic effect practically requires two corrections:

(i) Correction of de Broglie wavelength

$$\lambda = \lambda_0 \left(1 + \frac{e\phi_{acc}}{2m_0c^2}\right)^{-\frac{1}{2}} = \lambda_0 \left(\frac{2\sqrt{1-\beta^2}}{1+\sqrt{1-\beta^2}}\right)^{\frac{1}{2}} = \lambda_c \frac{\sqrt{1-\beta^2}}{\beta}\,, \qquad (8.1)$$

where $m_0c^2 = 5.11 \cdot 10^5$ eV is the rest energy of an electron, $\lambda_0 = h(2m_0e\phi_{acc})^{-1/2}$ is the nonrelavistic wavelength, and $\lambda_c = h/m_0c = 0{,}0246$ Å is the Compton wavelength.

(ii) Correction of the electron mass

$$m = m_0(1-\beta^2)^{-\frac{1}{2}} = m_0\left[1+\left(\frac{\lambda_c}{\lambda}\right)^2\right]^{\frac{1}{2}} = m_0\left[1+\frac{e\phi_{acc}}{m_0c^2}\right] \qquad (8.2)$$

in the Schrödinger Eq. (1.2) [1]). Since the electron mass m appears always combined with Fourier potentials υ_g (see II.1), the correction of m can be regarded as a correction of υ_g of the form

$$\upsilon_g^{(rel)} = \upsilon_g \cdot \frac{m}{m_0} \quad , \tag{8.3}$$

where υ_g is the "static" potential defined by (4.14), which is independent of the energy of the incident electrons. *Miyake* et al. (1963) [146] confirmed this dependence of $\upsilon_g^{(rel)}$ on energy ϕ_{acc} by means of the multiple-refraction method (see p. 23).

Applying the Green's function method of quantum field theory to the relativistic dynamical theory, *Terakura* et al. (1966) [148] confirmed the anticipation of *Miyake* et al. (1962) [149] and *Howie* (1962) [145] that the relativistic expression for $2m/\hbar^2\ C_{gh}$ is just the same as Yoshioka's nonrelativistic expression if the above corrections are applied to m and to the product λm which is contained in C_{gh} as a factor (cf. III. 1.1). This leads to a correction to C_{gh} of the form

$$C_{gh}^{(rel)} = C_{gh} \left(\frac{\lambda}{\lambda_0}\right) \left(\frac{m}{m_0}\right)^2 \quad . \tag{8.4}$$

We note that the "imaginary part" $\upsilon_g^{(i)}$ should have a correction different from the real part, and that, unlike the real part, the imaginary part is itself a function of λ_0 even before the relativistic correction is applied. It is proportional to λ_0 (III. 1.1).

The extinction distance ξ_g, Eq. (2.4), and the mean absorption distance $\xi_0' = 2\pi/\mu_0$, where μ_0 is the mean absorption coefficient (2.6), should change correspondingly with the electron energy in the form

$$\xi_g^{(rel)} = \beta\, \xi_{g(\lambda \to 0)}$$

and

$$\xi_0'^{(rel)} = \beta^2\, \xi_{0(\lambda \to 0)}' \quad ,$$

where $\xi_{g(\lambda \to 0)}$ and $\xi_{0(\lambda \to 0)}'$ are the limiting values at $\lambda \to 0$ (*Hirsch* (1962) [150]). These changes of ξ_g and ξ_0' have been verified experimentally by observing equal-thickness fringes by *Hashimoto* et al. (1962) [151], *Hashimoto* (1964) [59], *Dupouy* et al. (1965) [56], *Ayroles* and *Mazel* (1967) [159], *Metherell* and *Whelan* (1967) [129], *Fujita* et al. (1967) [153]. Actually, *Dupouy* et al. observed deviations from the above correction formulae. These deviations have been explained theoretically by *Goringe* et al. (1966) [128] in terms of the many-beam effect (cf. also *Howie* (1966) [154], *Metherell* and *Whelan* (1967) [129]) and by *Ohtsuki* and *Yanagawa* [155], *Terakura* et al. (1966) [148] in terms of the retardation effect.

[1]) A convenient table for these correction factors is given by *Marton* et al. (1956) [147].

Ohtaka et al. (1967) [156] investigated the effect of Bremsstrahlung and the vector potential at high energies and came to the conclusion that the contributions of these effects to C_{gh} are one or two orders of magnitude smaller than that of electron excitation.

Various consequences of the relativistic change of v_g and C_{gh} have been discussed by *Fujiwara* (1961) [144], *Miyake* et al. (1962) [149] and *Uyeda* (1968) [157]. The following items may be most important:

(i) The intensities of scattered waves do not always approach the kinematical values with an increase of electron energy (*Fujiwara* (1961) [144]).

(ii) The intensities of weakly excited beams, which for particular conditions should not change with λ according to the nonrelativistic theory, *increase* with the decrease of λ. (*Dupouy* et al. (1965) [56], *Ayroles* and *Mazel* (1967) [152], *Uyeda* (1968) [157]).

Accordingly, Bethe's summation corrections (sec II. 2c), which also should not, for particular conditions, change with λ after the nonrelativistic theory (*Miyake* (1959) [158]), become *larger* with the decrease of λ. This means that an *increase of the many-beam effect takes place with increasing electron energy* (*Goringe* et al. (1966) [128], *Ayrole* and *Mazel* (1967) [152], *Uyeda* (1968) [157]).

Uyeda [157] pointed out that the increase of the many-beam effect can be observed most distinctly at anomalously low values of the effective structure amplitude of a second-order reflection (III. 3.2.b)). In favourable cases it happens that the effective value of the second-order structure potential goes through zero as a function of λ (*Uyeda* (1968) [157], *Watanabe* et al. (1968) [126], [165], *Nagata* and *Fukuhara* (1967) [124]). This effect has proved to be very helpful for an exact determination of structure amplitudes (*Watanabe* et al. [165]). *Watanabe* observed Kikuchi lines since they are relatively insensitive to the crystal thickness and the direction of the incident electron.

Honjo and *Kitamura* (1961) [159] proposed that relative values of structure potentials should be measurable by extrapolation to the limit $\lambda \to 0$ in a set of experiments performed with stepwise increased energy. It is a very important consequence of the relativistic theory that it is impossible to arrive, in this way, at the value $\lambda = 0$. *Miyake* et al. (1961) [160] showed in an example that the difference between the virtual limit and the true limit can be 5%, which is by no means immaterial. (Cf. also *Kitamura* (1961) [166])

Another interesting application of the relativistic effect to the integrated intensity is given in the paper of *Fujime* et al. (1964) [161] on the study of the origin of satellites in the diffraction patterns of alloys having anti-phase domains.

References

[1] *Bragg, W. H.* and *Bragg, W. L.*, The Crystalline State, Vol. I, London 1933, p. 256.
[2] *Authier*, this volume.
[3] *Blackman, M.*, Proc. Roy. Soc. London A **173**,68 (1939).
[4] *Fujimoto, F.*, Z. Naturforsch. **20a**, 367 (1965).
[5] e. g. *Horstmann, M.*, Z. Phys. **188**, 124 (1965).
[6] e. g. *Vainshtein, B. K.*, Adv. Struct. Res. Diff. Meth., Vol. I, p. 24 (1964).
[7] *Hirsch, P. B.* et al., Electron Microscopy of Thin Crystals, London 1965.
[8] *Kambe, K.*, J. Phys. Soc. Japan **12**, 13, 25 (1957).
[9] *Kamiya, Y.* and *Uyeda, R.*, J. Phys. Soc. Japan **16**, 1361 (1961).
[10] *Kainuma, Y.*, Acta Cryst. **8**, 247 (1955).
[11] *Takagi, S.*, J. Phys. Soc. Japan **13**, 278, 287 (1958).
[12] *Howie, A.*, Proc. Roy. Soc. London **A 271**, 268 (1963).
[13] *Fujimoto, F.* and *Kainuma, Y.*, J. Phys. Soc. Japan **17**, Suppl. B-II 140 (1962), **18**, 1792 (1963).
[14] *Heidenreich, R. D.*, J. Appl. Phys. **34**, 964 (1963).
[15] *Fukuhara, A.*, J. Phys. Soc. Japan **18**, 496 (1963).
[16] *Kainuma, Y.*, J. Phys. Soc. Japan **20**, 2263 (1965).
[17] *Gjønnes, J.*, J. Phys. Soc. Japan **17**, Suppl. B-II 137 (1962).
[18] *Gjønnes, J.*, Acta Cryst. **20**, 240 (1966).
[19] *Bethe, H.*, Ann. Phys. (4) **87**, 55 (1928).
[20] *Lamla, E.*, Ann. Phys. (5) **32**, 178, 225 (1938).
[21] *Niehrs, H.* and *Wagner, E. H.*, Z. Phys. **143**, 285 (1955).
[22] *Fujimoto, F.*, J. Phys. Soc. Japan **14**, 1558 (1959), **15**, 859, 1022 (1960), **17** Suppl. B-II 101 (1962).
[23] *Niehrs, H.*, Z. Naturforsch. **14a**, 504 (1959).
[24] *Sturkey, L.*, Proc. Phys. Soc. **80**, 321 (1962).
[25] *Mott, N. F.* and *Massey, H. S. W.*, The Theory of Atomic Collisions, 3rd ed., Oxford 1965.
[26] *Fujiwara, K.*, J. Phys. Soc. Japan **14**, 1513 (1959).
[27] *Fengler, H.*, Z. Naturforsch. **16a**, 1205 (1961).
[28] *Tournarie, M.*, Bull. Soc. franc. Min. Crist. **83**, 179 (1960), C. R. Acad. Sci. **252**, 2862 (1961), J. Phys. Soc. Japan **17** Suppl. B-II 98 (1962).
[29] *Kambe, K.*, Z. Naturforsch. **22a**, 422 (1967).
[30] *Howie, A.* and *Whelan, M. J.*, Proc. Roy. Soc. London A **263**, 217 (1961).
[31] *Darwin, C. G.*, Phil. Mag. **27**, 315, 675 (1914).
[32] *Cowley, J. M.* and *Moodie, A. F.*, Acta Cryst. **10**, 609 (1957), **12**, 353, 360 (1959), J. Phys. Soc. Japan **17** Suppl. B-II 86 (1962).
[33] *Slater, J. C.*, Phys. Rev. **51**, 840 (1937).
[34] *Molière, K.*, Ann. Phys. (5) **34**, 461 (1939).
[35] *Heidenreich, R. D.*, J. Appl. Phys. **33**, 2321 (1962).
[36] *Hashimoto, H., Howie, A.* and *Whelan, M. J.*, Proc. Roy. Soc. London A **269**, 80 (1962).
[37] *Morse, P. M.*, Phys. Rev. **35**, 1310 (1930).
[38] *Davisson, C. J.* and *Germer, L. H.*, Phys. Rev. **30**, 705 (1927), Proc. Nat. Acad. Amer. **14**, 317 (1928).
[39] *Sommerfeld, A.* and *Bethe, H.*, Handbuch der Physik (Geiger/Scheel) Vol. 24/2.
[40] *Slater, J. C.*, Quantum Theory of Molecules and Solids, Vol. 2, New York 1965.

[41] *Ziman, J. M.*, Principles of the Theory of Solids, Cambridge 1964.
[42] *Boudreau, D. S.* and *Heine, V.*, Surface Science **8**, 426 (1967).
[43] International Tables for Xray Crystallography, Vol. 3, Birmingham 1962.
[44] *Harada, J.* and *Kashiwase, Y.*, J. Phys. Soc. Japan **17**, 829 (1962).
[45] *Goldberger, M. L.* and *Watson, K. M.*, Collision Theory, New York 1964.
[46] *Yoshioka, H.*, J. Phys. Soc. Japan **12**, 618 (1957).
[47] *Molière, G.*, Ann. Phys. (5) **35**, 272 (1939).
[48] *Ohtsuki, Y. H.* and *Yanagawa, S.*, J. Phys. Soc. Japan **21**, 326 (1966).
[49] *Dederichs, P. H.*, Phys. kondens. Mat. **5**, 347 (1966).
[50] *Massey, H. S. W.* and *Mohr, C. B. O.*, Proc. Roy. Soc. London **A 140**, 613 (1933), **A 146**, 880 (1934).
[51] *Lehmpfuhl, G.* and *Molière, K.*, Z. Phys. **164**, 389 (1961).
[52] *Lehmpfuhl, G.* and *Molière, K.*, J. Phys. Soc. Japan 17 Suppl. B-II 130 (1962).
[53] *Kohra, K.* and *Watanabe, H.*, J. Phys. Soc. Japan **16**, 580 (1961).
[54] *Watanabe, H.*, Japan. J. Appl. Phys. **3**, 480 (1964).
[55] *Castaing, R., El Hili. A.* and *Henry, L.*, C. R. Acad. Sci. **262 B**, 169, 1051 (1966).
[56] *Dupouy, G., Perrier, F., Uyeda, R., Ayroles, R.* and *Mazel, A.*, J. Microscopie **4**, 429 (1965).
[57] *Uyeda, R.* and *Nonoyama, M.*, Japan, J. Appl. Phys. **4**, 498 (1965).
[58] *Hashimoto, M., Howie, A.* and *Whelan, M. J.*, Proc. Roy. Soc. London **A 269**, 80 (1962).
[59] *Hashimoto, H.*, J. Appl. Phys. **35**, 277 (1964).
[60] *Goodman, P.* and *Lehmpfuhl, G.*, Acta Cryst. **22**, 14 (1967).
[61] *Meyer, G.*, Phys. Letters **20**, 240 (1966), Z. Naturforsch. **21a**, 1524 (1966).
[62] *Horstmann, M.* and *Meyer, G.*, Acta Cryst. **15**, 271 (1962).
[63] *Boersch, H., Bostanjoglo, O.* and *Niedrig, H.*, Z. Phys. **180**, 407 (1964).
[64] *Kuwabara, S.*, J. Phys. Soc. Japan **22**, 1245 (1967).
[65] *Miyake, S.*, Proc. Phys.-Math. Soc. Japan **22**, 666 (1940).
[66] *Honjo, G.* and *Mihama, K.*, J. Phys. Soc. Japan **9**, 184 (1954).
[67] *Heidenreich, R. D.*, Fundamentals of Transmission Electron Microscopy, New York 1964.
[68] *Massey, H. S. W.*, Advances in Electronics, Vol. 4, p. 1, New York 1952.
[69] *Whelan, M. J.*, J. Appl. Phys. **36**, 2099 (1965).
[70] *Lenz, F.*, Z. Naturforsch. **9a**, 185 (1954).
[71] *Duncumb, P.*, Phil. Mag. **7**, 2101 (1962).
[72] *Hall, C. R.*, Proc. Roy. Soc. London **A 295**, 140 (1966).
[73] *Miyake, S., Hayakawa, K.* and *Miida, R.*, Acta Cryst. **A24**, *182 (1968).*
[74] *Pines, D.*, Elementary Excitations in Solids, New York 1963.
[75] *Raether, H.*, Springer Tracts in Mod. Phys. **38**, 84 (1965).
[76] *Watanabe, H.*, 6th Int. Congr. El. Micr. Kyoto, Vol. 1, p. 63, 1966.
[77] *Cundy, S. L., Metherell, A. J. F.* and *Whelan, M. J.*, Phys. Letters **A24**, 120 (1967).
[78] *Cundy, S. L., Metherell, A. J. F.* and *Whelan, M. J.*, 6th Int. Conf. El. Micr. Kyoto, Vol. 1, p. 87, Tokyo 1966.
[79] *Ishida, K., Mannami, M.* and *Tanaka, K.*, J. Phys. Soc. Japan **23**, 1362 (1967).
[80] *Yoshioka, H.* and *Kainuma, Y.*, J. Phys. Soc. Japan **17** Suppl. B-II 134 (1962).
[81] *Whelan, M. J.*, J. Appl. Phys. **36**, 2103 (1965).
[82] *Hall, C. R.* and *Hirsch, P. B.*, Proc. Roy. Soc. London **A 286**, 158 (1965).
[83] *Hall, C. R.*, Phil. Mag. **12**, 815 (1965).
[84] *Goringe, M. J.*, Phil. Mag. **14**, 93 (1966).
[85] *Gjønnes, J.*, Acta Cryst. **15**, 703 (1962).

[86] *Boersch, H., Jeschke, G.* and *Raith, H.*, Z. Phys. **181**, 436 (1964).
[87] *Hoerni, J. A.*, Phys. Rev. **102**, 1534 (1956).
[88] *Raith, H.*, Acta Cryst. **A24**, 85 (1968).
[89] *Molière, G.*, Z. Naturforsch. **2a**, 133 (1947).
[90] *Glaeser, W.* and *Niedrig, H.*, J. Appl. Phys. **37**, 4303 (1966).
[91] *Albrecht, W. W.* and *Niedrig, H.*, 6th Int. Congr. El. Micr. Kyoto, Vol. 1, p. 51, 1966.
[92] *Jeschke, G., Raith, H.* and *Zorn, K.-L.*, 6th Int. Congr. El. Micr. Kyoto, Vol. 1, p. 97, 1966.
[93] *Fukuhara, A.*, Proc. Phys. Soc. **86**, 1031 (1965).
[94] *Hall, C. R.* and *Hirsch, B.*, Phil. Mag. **12**, 539 (1965).
[95] *Hall, C. R.*, Phil. Mag. **14**, 155 (1966).
[96] *Kainuma, Y.* and *Yoshioka, H.*, J. Phys. Soc. Japan **21**, 1352 (1966).
[97] *Parthasarathy, R.*, Acta Cryst. **13**, 802 (1960).
[98] *Kambe, K.*, Z. Naturforsch. **20a**, 1730 (1965).
[99] *Horstmann, M.*, Z. Phys. **183**, 375 (1965).
[100] *Ohtsuki, Y. H.*, J. Phys. Soc. Japan **21**, 2300 (1966).
[101] *von Laue, M.*, Materiewellen und ihre Interferenzen, Leipzig 1948.
[102] *Bauer, E.*, Electronenbeugung, München 1958.
[103] *Raether, H.*, Handbuch der Physik (Flügge), Vol. 32, p. 443, Berlin 1957.
[104] *Pinsker, Z. G.*, Electron Diffraction, London 1953.
[105] *Thomson, G. P.* and *Cochrane, W.*, Theory and Practice of Electron Diffraction, London 1939.
[106] *Molière, K.* and *Wagenfeld, H.*, Z. Krist. **110**, 175 (1958).
[107] *Lehmpfuhl, G.* and *Reissland, A.*, Z. Naturforsch., **23a** 544 (1968).
[108] *Fujimoto, F.*, J. Phys. Soc. Japan **16**, 936 (1961).
[109] *Fengler, H.*, Z. Naturforsch. **16a**, 1214 (1961).
[110] *Takagi, M.* and *Morimoto, S.*, J. Phys. Soc. Japan **18**, 819 (1963).
[111] *Fujime, S., Watanabe, D.* and *Ogawa, S.*, J. Phys. Soc. Japan **19**, 711, 2292 (1964).
[112] *Miyake, S., Takagi, S.* and *Fujimoto, F.*, Acta Cryst. **13**, 360 (1960).
[113] *Cowley, J. M.* et al., Acta Cryst. **14**, 87 (1961).
[114] *Gjønnes, J.* and *Moodie, A. F.*, Acta Cryst. **19**, 65 (1965).
[115] *Goodman, P.* and *Lehmpfuhl, G.*, Z. Naturforsch. **19a**, 818 (1964).
[116] *Blume, J.*, Z. Phys. **191**, 248 (1966).
[117] *Fukuhara, A.*, J. Phys. Soc. Japan **21**, 2645 (1966).
[118] *Pogany, A. P.* and *Turner, P. S.*, Acta cryst. **A24**, 103 (1968).
[119] *Niehrs, H.*, J. Phys. Soc. Japan **17** Suppl. B-II 104 (1962).
[120] *Miyake, S., Fujiwara, K., Tokonami, M.* and *Fujimoto, F.*, Japan. J. Appl. Phys. **3**, 276 (1964).
[121] *Labaw, L. W.*, Acta Cryst. 17, 46 (1964).
[122] *Komoda, T.*, Japan, J. Appl. Phys. **5**, 1120 (1966).
[123] *Yada, K.*, Acta Cryst. **23**, 704 (1967).
[124] *Nagata, F.* and *Fukuhara, A.*, Japan. J. Appl. Phys. **6**, 1233 (1967).
[125] *Kimoto, K.* and *Nishida, I.*, J. Phys. Soc. Japan **22**, 744 (1967).
[126] *Watanabe, D., Uyeda, R.* and *Kogiso, M.*, Acta Cryst. **A24**, 249 (1968).
[127] *Howie, A.* and *Valdré, U.*, Phil. Mag. **15**, 777 (1967).
[128] *Goringe, M. J., Howie, A.* and *Whelan, M. J.*, Phil. Mag. **14**, 217 (1966).
[129] *Metherell, A. J. F.* and *Whelan, M. J.*, Phil. Mag. **15**, 755 (1967).
[130] *Metherell, A. J. F.*, Phil. Mag. **15**, 763 (1967).
[131] *Howie, A.* and *Whelan, M. J.*, Proc. Europ. Reg. Conf. El. Micr. (Delft) **1**, 181 (1960).

[132] *Karle, J.*, Adv. in Str. Res. by Diff. Meth., Vol. **1**, p. 55, 1964.
[133] *Fues, E.*, Z. Phys. **125,** 531 (1949).
[134] *Miyake, S.* and *Uyeda, R.*, Acta Cryst. **8,** 335 (1955).
[135] *Niehrs, H.*, Z. Phys. **140,** 106 (1955).
[136] *Miyake, S.* and *Uyeda, R.*, Acta Cryst. **3,** 314 (1950).
[137] *Goodman, P.* and *Lehmpfuhl, G.*, Acta Cryst., A **24** 339 (1968).
[138] *Kainuma, Y.* and *Lipscomb, W. N.*, J. Phys. Soc. Japan **16**, 495 (1961).
[139] *Parthasarathy, R.*, Acta Cryst. **14,** 690 (1961).
[140] *Uyeda, R.* and *Miyake, S.*, Acta Cryst. **10,** 53 (1957).
[141] *Deville, J.-P., Eberhart, J.-P.* and *Goldsztaub, S.*, C. R. Acad. Soc. Paris **264 B,** 124, 289 (1967).
[142] *Hayashi, M.*, J. Phys. Soc. Japan **15**, 2054 (1960).
[143] *Weisskopf, H.*, Z. Phys. **93,** 561 (1935).
[144] *Fujiwara, K.*, J. Phys. Soc. Japan **16,** 2226 (1961), **17** Suppl. B-II 118 (1962).
[145] *Howie, A.*, Discussion by Whelan to Fujiwara (1962) [144].
[146] *Miyake, S., Fujiwara, K.* and *Suzuki, K.*, J. Phys. Soc. Japan **18,** 1306 (1963).
[147] *Marton, L., Marton, C.* and *Hall, W. G.*, Nat. Bur. Stand. Circular **571,** Washington 1956.
[148] *Terakura, K., Ohtsuki, Y. H.*,and *Yanagawa, S.*, J. Phys. Soc. Japan **21,** 1973 (1966).
[149] *Miyake, S., Fujiwara, K.* and *Suzuki, K.*, J. Phys. Soc. Japan **17** Suppl. B-II 124 (1962).
[150] *Hirsch, P. B.*, J. Phys. Soc. Japan **17** Suppl. B-II 143 (1962).
[151] *Hashimoto, H.* et al., J. Phys. Soc. Japan **17** Suppl. B-II 170 (1962).
[152] *Ayroles, R.* and *Mazel, A.*, J. Microscopie **6,** 135 (1967).
[153] *Fujita, H.*, et al., Japan. J. Appl. Phys. **6,** 214 (1967).
[154] *Howie, A.*, Phil. Mag. **14,** 223 (1966).
[155] *Ohtsuki, Y. H.* and *Yanagawa, S.*, J. Phys. Soc. Japan **20,** 2295 (1965).
[156] *Ohtaka, K., Ohtsuki, Y. H.* and *Yanagawa, S.*, J. Phys. Soc. Japan **23,** 566 (1967).
[157] *Uyeda, R.*, Acta Cryst. **A24,** 175 (1968).
[158] *Miyake, S.*, J. Phys. Soc. Japan **14,** 1347 (1959).
[159] *Honjo, G.* and *Kitamura, N.*, Acta Cryst. **10,** 533 (1957).
[160] *Miyake, S.* et al., J. Phys. Soc. Japan **16,** 2336 (1961).
[161] *Fujime, S.* et al., J. Phys. Soc. Japan **19,** 1881 (1964).
[162] *von Laue, M.*, Acta Cryst. **6,** 217 (1953).
[163] *Watanabe, H.* et al., J. Phys. Soc. Japan **17** Suppl. B-II, 195 (1962).
[164] *Ott, H.*, Ann. Physik (5) **23,** 169 (1935).
[165] *Watanabe, D.* et al., Acta Cryst **A 24** 580 (1968).
[166] *Kitamura, N.*, J. Phys. Soc. Japan **16** 2254 (1961).

Small Angle Scattering

R. Hosemann, A. Schönfeld, W. Wilke*)

With 16 figures

1. Introduction

There exist several detailed publications on small angle scattering [4, 11a, 17, 21, 26, 28, 30b, 36, 42, 44, 53, 56, 58, 60]. It is the aim of this article to summarize those most important features of the background of small angle analysis (section II) which are of interest because they might lead to further development in the subject and also to provide some examples showing how successful is the direct analysis of small angle scattering (sometimes in combination with wide angle scattering). Small angle diffraction is concerned with the diffraction phenomena at scattering angles not larger than some angledegrees, hence gives data of dimensions 10–1000 times larger than those obtained from wide angle scattering. In most cases wavelength of the order of 1 Å are used, hence small angle scattering depends on and gives information about colloidal, super- or macromolecular structures, superstructures, microdomains etc. of 10–1000 Å size. These structures generally are not so regularly arranged as many atomistic structures, since each brick (motif) consists of many atoms. Superlattices with a undistorted periodicity as in crystals only exist in special cases (protein crystals). Most structures under consideration are of the paracrystalline or „amorphous" type (section IV).

The more irregular the arrangement of the bricks (particles), the more interparticular interferences are cancelled. Finally we meet a type of scattering, first described in principle by *Lord Rayleigh,* the „continuous" small angle scattering (section III). This phenomenon exists only if the polydispersity of the scattering units is not smaller than their packing density. In fibers, plastics, etc. on the other hand the bricks are ultrafibrils, and build up nematic or smecticlike structures of sometimes higher regularity. They give rise to a discontinuous small angle scattering (section IV). In many cases the analysis of the Q-function is quite helpful both for statistical consideration and for obtaining electron density maps of micro crystals (section VI). Combination of continuous and discontinuous diffraction phenomena of small and wide angle scattering often gives unique informations (section V). A short review on further applications gives evidence of the wide field, where the information of small angle scattering is successful (section VII). A bibliography from 1955–1967 is added as complete as possible. It is the continuation of the work of *Yudowitch* in the book of *Guinier* and *Fournet* [28].

*) Fritz-Haber-Institut der Max-Planck-Gesellschaft, Berlin-Dahlem

2. Background of small angle analysis

$\rho(\mathbf{x})\ [A]^{-3}$ *density distribution* of the sample under consideration; for X-rays, electrons, neutrons density of the electrons, electrons and protons, nuclei and spin density.

$\mathbf{x}$ [Å] *vector* with the orthogonal coordinates $x_1\ x_2\ x_3$ expanding the physical space.

λ [Å] *wave length* of the primary radiation.

s_0, s *unit vectors* in the direction of the primary and diffracted beam.

$\mathbf{b}$ [$Å^{-1}$] *reciprocal vector* with the orthogonal coordinates $b_1\ b_2\ b_3$ expanding the reciprocal (Fourier)space.

Fouriertransformation

$$\mathcal{F} = \int dv_x\, e^{-2\pi i \mathbf{b}\mathbf{x}} \quad ; \quad \mathcal{F}^{-1} = \int dv_b\, e^{2\pi i \mathbf{b}\mathbf{x}}$$

symbol of Fouriertransformation, Inverstransformation

dv_x, dv_b *volume element* in the $\mathbf{x}$-, $\mathbf{b}$-space

$\mathbf{bx} = b_1x_1 + b_2x_2 + b_3x_3$ scalar product of $\mathbf{x}$ and $\mathbf{b}$.

Ewald construction

$$\mathbf{b} = \frac{\mathbf{s} - \mathbf{s}_0}{\lambda} \quad ; \quad b = \frac{2 \sin \vartheta}{\lambda} \tag{1}$$

2ϑ scattering angle

The scattered intensity is proportional to

$I(\mathbf{b})$ *intensity function.* The proportional factors (Lorentz, Polarisation etc) here are not discussed. See for detail [4, 28, 42, 60].

$$I(\mathbf{b}) = \overline{R(\mathbf{b})\,R(\mathbf{b})^*} \quad ; \quad R(\mathbf{b}) = \mathcal{F}\rho(\mathbf{x}) \tag{2}$$

$R(\mathbf{b})$ the scattering amplitude is dimensionless. As a consequence of collimation errors, exposure time etc. only an average $\overline{RR^*}$ is observable (see eq. 19)

$\widehat{g_1 g_2}$, $\widehat{G_1 G_2}$ folding (convolution) products:

$$\widehat{g_1 g_2} = \int g_1(\mathbf{y})\ g_2(\mathbf{x}-\mathbf{y})\, dv_y \quad ; \quad \widehat{G_1 G_2} = \int G_1(\mathbf{c})\, G_2(\mathbf{b}-\mathbf{c})\, dv_c \tag{3}$$

Folding theorem of Fourier transform:

$$\mathcal{F}\widehat{g_1 g_2} = G_1 G_2 \; ; \quad \mathcal{F} g_1 g_2 = \widehat{G_1 G_2} \tag{4}$$

$$G_1(0) = \int g_1(x)\, dv_x \; ; \; \lim_{b \to 0} \widehat{G_1 G_2} = \int G_1(c)\, G_2(-c)\, dv_c = \int g_1(x)\, g_2(x)\, dv_x$$
(Parseval's theorem)

Q-function: expectation value of the folding square of $\rho(x)$ defined by:

$$g_1(x) = \rho(x) \; ; \quad g_2(x) = \rho(-x), \text{ hence}$$

$$\mathcal{F}^{-1} I(b) = Q(x) = \overline{\tilde{\rho}}^{\,2}(x) = \int \rho(y)\, \rho(y+x)\, dv_y \tag{5}$$

For an unbounded ideal crystal $Q(x)$ is the Patterson-function, for statistically distorted structures $Q(x)$ with respect to the position of the scattering centers is nothing else than the

Q correlationfunction. If x_k is the position of the centre of particle k, $\rho_k(x)$ its structure if $x_k = 0$ and $N_k = \int \rho_k(x)\, dv_x$ its number of electrons, and $P(x-0)$ a point function in the ϵ-neighbourhood of $x = 0$:

$$P(x-0) = 0 \text{ if } |x| > \epsilon; \int P(x)\, dv_x = 1$$

then the electron density distribution is given by

$$\rho(x) = \sum_{k=1}^{M} \rho_k(x - x_k) = \sum_{k=1}^{M} \widehat{\rho_k(x)\, P(x - x_k)} \tag{6}$$

and the correlation function by

$$Q(x) = \sum_{i=1}^{M} \sum_{k=1}^{M} \widehat{P(x - x_i + x_k)\, \rho_i(x)\, \rho_k(-x)} \tag{7}$$

M number of particles.

The a priori distance statistics $W(x)$ of Debye (1930) corresponds to the correlation function

$$\frac{v}{M^2} Q_W(x) = W(x) = \frac{v}{M^2} \sum_{i \neq k}^{M} \sum^{M} \overline{P(x - x_i + x_k)} \tag{7a}$$

v volume of the sample. In powder diagrams and isotropic liquids W within the error of experiment is rotational symmetric: $W(\mathbf{x}) = W(x)$.

For not overlapping particle densities one immediately finds that

$$Q(0) = \sum_{k=1}^{M} \overset{2}{\widetilde{\rho}}_k(0) \; ; \quad \int Q(\mathbf{x})\, dv_x = M^2 \overline{N^2}_k = \left[\sum_{k=1}^{M} N_k\right]^2 \tag{8}$$

$G_i(\mathbf{b})$ precision function. Because of collimation errors in all physical experiments many details of Q are lost. Taking into account the angular divergency of the two unit vectors s_0 and s one can define a function $G_i(\mathbf{b})$ normalized to unity, whose shape is given by the angular distribution of s_0, s in the primary (scattered to the point of observation) beam. Then the intensity function $I(\mathbf{b})$ is given by

$$I(\mathbf{b}) = \widehat{(RR^*)} G_i \; ; \quad \int G_i(\mathbf{b})\, dv_b = 1 \tag{9}$$

The larger the precision of the experiment, the more $G_i(\mathbf{b})$ is similar to a point function in $\mathbf{b}$ – space. By the folding process (9) many details of Q are lost. To understand this, we introduce

$g_a(\mathbf{x})$ *shape function* of the domain of information in $\mathbf{x}$ space.

Its volume v_a is

$$v_a = \int g_a(\mathbf{x})\, dv_x = G_i(0). \tag{10}$$

$g_a(\mathbf{x})$ is defined by

$$\mathcal{F}^{-1} G_i(\mathbf{b}) = g_a(\mathbf{x}) = \begin{cases} 1 \text{ for all } \mathbf{x} \text{ within the domain of information} \\ 0 \text{ for all } \mathbf{x} \text{ outside the domain of information} \end{cases} \tag{11}$$

From (9) one obtains by inverse transformation the observable details of $Q(\mathbf{x})$:

$$Q_{obs}(\mathbf{x}) = \overset{2}{\widetilde{\rho}}(\mathbf{x})\, g_a(\mathbf{x}) \tag{12}$$

All details of the structure $\rho(\mathbf{x})$ concerning distances and dimensions larger than those of v_a are cut off in $Q_{obs}(\mathbf{x})$, hence are not observable. The convenient small angle cameras [see eg. [28, 455, 475]] have collimation errors of the order of at least 10^{-3} radians, hence v_a has a diameter of at most 1000 Å. Details of $\rho(\mathbf{x})$ observable can be defined by

$$\rho(\mathbf{x})\, g_a(\mathbf{x} - \xi) = \rho(\mathbf{x}, \xi) \tag{13}$$

In most experiments v_a is much smaller than the volume v of the sample. Since the intensity depends on the density distribution $\rho(\mathbf{x})$ of all parts of the sample, the position of $g_a(\mathbf{x}, \xi)$ must be taken by varying ξ so that all electrons, protons etc. give the same contribution (absorption effects are not discussed here, see [30b, 42]).

Now one understands the meaning of the cross-bars in (2) and (5). It is not a time-average, but a space average (see Fig. 1), called

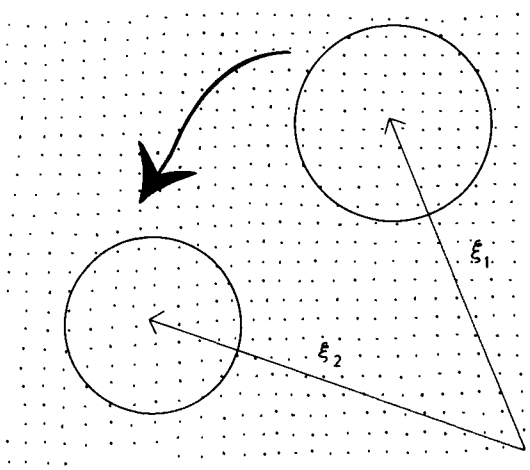

Fig. 1
ξ-average of a point structure. The circle represents schematically the volume v_a of information, which according to eqs. (13) and (14) must be shifted over the whole point structure to collect all information available in the functions Q_{obs} and I_{obs} (eqs. (19) and (20a))

ξ-average: The cross-bar in (5) indicates, that the average of $\overset{2}{\widetilde{\rho}}(\mathbf{x})$ is defined by taking all possible positions of ξ and dividing by their number:

$$\frac{v_a}{v} \cdot Q(\mathbf{x}) = \frac{1}{v_a} \int_{v_a} \overset{2}{\widetilde{\rho(\mathbf{x}, \xi)}}\, dv_\xi = \overline{\overset{2}{\widetilde{\rho(\mathbf{x}, \xi)}}}_a \qquad (14)$$

The factor v_a/v must be taken into account, since the function (13) only contains $v_a/v \cdot 100\,\%$ of the scattering centers. Strictly spoken, G_i in (9) must be replaced by $|G_i|^2/v_a$ and g_a in (12) by $\overset{2}{\widetilde{g}}_a/v_a$. Since $g_a(\mathbf{x})$ is the shape function of the domain of information, one obtains

$$\overset{2}{\widetilde{g}}_a(0) = \int g_a^2(\mathbf{x})\, dv_x = v_a$$

and hence G_i^2/v_a again is normalized to unity and similar to (10) (see eq. 4) the relations hold:

$$\int \underset{\sim}{2} g_a(\mathbf{x})/v_a \cdot dv_x = v_a = \frac{1}{v_a} |G_i(0)|^2 \qquad (15)$$

$$\frac{1}{v_a}\int |G_i(\mathbf{b})|^2 \, dv_b = \frac{\underset{\sim}{2} g_a(0)}{v_a} = 1$$

$S(\mathbf{b})$: *shape amplitude* of the sample

$$S(\mathbf{b}) = \mathcal{F}\, s(\mathbf{x}) \; ; \; \int s(\mathbf{x})\, dv_x = v$$

$$\underset{\sim}{2} s(0) = \int s(\mathbf{y})\, s(\mathbf{y})\, dv_y = v \qquad (16)$$

$s(\mathbf{x})$ similar to (11) is the shape function which has the value 1 inside, and zero outside of the volume v of the sample.

ρ *mean density* of the sample:

$$\bar{\rho} = \frac{1}{v}\int \rho(\mathbf{x})\, dv_x \qquad (17)$$

I_s volume scattering. Mostly within the primary beam, hence not observable is the volume scattering I_s (Debye 1930):

$$I_s(\mathbf{b}) = \bar{\rho}^2 S^2(\mathbf{b}) \; ; \quad S^2(0) = v^2, \int S^2(\mathbf{b})\, dv_b = v \qquad (18)$$

I_{obs} the observable small angle scattering. It is given by ($S^2(\mathbf{b})$ pointlike compared with $G_i(\mathbf{b})$)

$$\mathcal{F}\, Q_{obs}(\mathbf{x}) = I_{obs}(\mathbf{b}) = (RR^* - \widehat{I_s})\, \widehat{G_i} = \overline{RR^*}(\mathbf{b}) - \bar{\rho}^2 v G_i(\mathbf{b}) \qquad (19)$$

The small angle scattering just outside of the primary beam is obtained by extrapolating I_{obs} to zero angle

$$\lim_{\mathbf{b}\to 0} I_{obs}(\mathbf{b}) = \int Q_{obs}(\mathbf{x})\, dv_x = \overline{\left[\int (\rho(\mathbf{x}) - \bar{\rho})\, dv_x\right]^2} \qquad (20)$$

and

$$\int I_{obs}(\mathbf{b})\, dv_b = Q_{obs}(0) = \int (\rho - \bar{\rho})^2\, dv_x = v(\overline{\rho^2} - \bar{\rho}^2) \,. \tag{20a}$$

From (13), (14), (19) one obtains

$$Q_{obs}(\mathbf{x}) = \frac{v}{v_a} \overline{\widetilde{\rho(\mathbf{x}, \xi)_a}^2} - \bar{\rho}^2 v\, g_a(\mathbf{x})$$

Hence

$$\lim_{b \to 0} I_{obs}(\mathbf{b}) = \int Q_{obs}(\mathbf{x})\, dv_x = \frac{v}{v_a} \int \left[\overline{\widetilde{\rho(\mathbf{x}, \xi)_a}^2} - \bar{\rho}^2 v_a g_a(\mathbf{x}) \right] dv_x \tag{21}$$

$$= N(v) \cdot \frac{\overline{N^2}(v_a) - \overline{N}^2(v_a)}{\overline{N}(v_a)} = \frac{N(v)}{\overline{N}(v_a)}\, \Delta^2 N(v_a)$$

The more $\rho(\mathbf{x})$ fluctuates around the mean density $\bar{\rho}$, the more intensity is scattered. But this fluctuation must be irregular. $\overline{N}(v_a)$, $N^2(v_a)$ is nothing else than the number average, squared number average of electrons, protons, electron spins, nuclei in the domain v_a of measurement. Since this number depends on $g_a(\mathbf{x}, \boldsymbol{\xi})$, it depends on the vector $\boldsymbol{\xi}$, which is varied over all positions (eq. 13, 14). For ideal periodic ρ-functions as in ideal crystals $\Delta^2 N(v_a)$ is zero, if g_a has the shape of n lattice cells [42].

If a small angle scattering exists, it mostly depends on the volume v_a of information. The larger v_a, the more point like the precision function $G_i(\mathbf{b})$, the smaller the scattering angles under observation. If for instance the colloidal inhomogeneities have an averaged diameter of 500 Å and the precision only corresponds to a volume v_a with 200 Å diameter, the small angle scattering of these inhomogeneities lies outside the domain of observation (inside the primary beam). Then with increasing v_a, $I_{obs}(0)$ increases. In mixed crystals (for instance Al-Ag or Zn-Ag annealed or age hardened) the Ag atoms migrate from outer zones, forming clusters of higher electron density, whilst the boundary has a lower density than $\bar{\rho}$. These „particles", hence have an observable density $\rho(\mathbf{x}) - \bar{\rho}$ with the volume integral $\int (\rho(\mathbf{x}) - \bar{\rho})\, dv_x = 0$ (Guinier-Preston zones). Starting with low precision (diameter $v_a \sim 100$ Å) $\lim_{b \to 0} I_{obs}(\mathbf{b})$ begins to increase, since the Ag-site centres have diameters of this order. With increasing diameter to 1000 Å the $\lim_{b \to 0} I_{obs}(\mathbf{b})$ again goes

to zero. Now the fluctuation $\Delta^2 N(v_a)$ decreases with increasing diameter, since the particles have the integralvalue $\int(\rho-\bar{\rho})\,dv_x = 0$ and hence no longer can contribute to $\Delta^2 N(v_a)$, if v_a is large enough. Such inhomogeneities produce a diffuse small angle ring, inside a small intensity [27, 28]. Another interesting case, $I_{obs}(\mathbf{b} \to 0)$ independent of v_a, is realized, if

$$\frac{\Delta^2 N(v_a)}{N(v_a)} = \text{const. indep. of } v_a \tag{21a}$$

Such distortions one meets in paracrystalline lattices. The most extreme case const. = 1 is realized for ideal gases and distance statistics of the Boltzmann-Type. Now the small angle scattering for pointlike particles within a certain **b**-domain is a constant.

3. Continuous small angle scattering. Particle scattering

The structure (6) with M particles of the density $\rho_k(x)$ and

particle amplitudes $f_k(\mathbf{b}) = \mathcal{F}\rho_k(x)$, $f_k(0) = \int \rho_k(x)dv_x = N_k$ (22)

has in the case of statistical arrangements for N and N^2 according to (7) a value

$$\bar{N} = \bar{M}\,\bar{N}_k; \quad \overline{N^2} = \bar{M}\,\overline{N_k^2} + \overline{M(M-1)}\,\bar{N}_k^2 \tag{23}$$

Hence from (21) one obtains

$$\lim_{\mathbf{b}\to 0} I_{obs} = \bar{M}\left[\overline{N_k^2} + \bar{N}_k^2\left(\frac{\Delta^2 M(v_a)}{\bar{M}(v_a)} - 1\right)\right] \tag{24}$$

From (7) one obtains (cf. eq. 7,7a, 8)

$$I_{obs} = I_P + I_W$$

$$I_p = \sum_{k=1}^{M} f_k^2 = M\,\overline{f_k^2} \tag{25}$$

$$I_W = M\,\tilde{f}_k^2\,(w(\mathbf{b})-1)$$

$$(w(\mathbf{b})-1) = \frac{M}{V}\,\mathcal{F}(W(\mathbf{x})-1) \tag{26}$$

$W(\mathbf{x})$ is defined in (7a). The

interparticle interferences I_w can be neglected, if

$$w(\mathbf{b}) \sim W(\mathbf{x}) \sim \frac{\Delta^2 M(v_a)}{M(v_a)} \sim 1 \quad \text{for all } \mathbf{x}, \mathbf{b}, \text{ in the domain } v_a \text{ of information} \tag{27}$$

Particle scattering factor I_P: Then

$$I_{obs}(\mathbf{b}) \sim I_P(\mathbf{b})$$

Strictly this phenomenon, first discussed quantitatively by *Lord Rayleigh*, only takes place if the distance distribution of the centers of the particles k is a Boltzmann-statistics. For highly diluted systems I_{obs} practically equals I_p. There exists then a small angle scattering, continuously decreasing with increasing **b**. But near its maximum care has to be taken, since here w (**b**) begins to differ from unity [28, 42, 58].

In many cases $W(\mathbf{x})$ and $w(\mathbf{b})$ show

rotational symmetry. Then in (26)

$$\mathcal{F} = \frac{2}{b}\int_0^\infty r \sin(2\pi br)\,dr\,; \quad \mathcal{F}^{-1} = \frac{2}{r}\int_0^\infty b \sin(2\pi rb)db \tag{28}$$

Within the domain of small angle scattering I_{obs} is practically independent of the atomic structure of the particles. If the electron density $\rho(\mathbf{x})$ even in 10 Å dimensions is almost constant (ρ_0), one can introduce a

particle shape function $s_k(\mathbf{x})$ similar to the shape functions s and g_a (eq. 16 and 17). Then

$$\rho_k(\mathbf{x}) \sim \rho_0\, s_k(\mathbf{x}); \; \mathcal{F} S_k(b) = s_k(\mathbf{x}); \; v_k = \int s_k(\mathbf{x})\,dv_x = S_k(0) \tag{29}$$

Gauss approximation of the particle factor $|f_k|^2$. Expanding $e^{-2\pi i \mathbf{b}\mathbf{x}}$ in a Fourier series, one obtains from eq. (22)

$$f_k(\mathbf{b}) = \int \rho_k(\mathbf{x}) \sum_{n=0}^{\infty} \frac{1}{n!} (-2\pi i \mathbf{b}\mathbf{x})^n dv_x = N_k \sum_{n=0}^{\infty} \frac{(-2\pi i)^n}{n!} b^n (\Delta_n x_b)^n$$

$$\text{where} \quad \Delta_n x_b = \frac{1}{N_k}\left[\int \rho_k(\mathbf{x})\,(\mathbf{b}\mathbf{x}/b)^n dv_x\right]^{1/n} \tag{30}$$

Standard deviation of the shape $\Delta_2 x_b$

Of most interest is the exponent $n = 2$, which gives the standard deviation of the vector $\mathbf{x}$, weighted with $\rho(\mathbf{x})$, in the direction of $\mathbf{b}$. Since the centre of $\rho_k(\mathbf{x})$ lies at $\mathbf{x} = 0$, $\Delta_1 = 0$ and one obtains from (30) correct for $n = 2$, approximately for $n = 3, 4, 5 \ldots$

$$f_k(\mathbf{b}) \sim N_k \, e^{-2\pi^2 \Delta_2^2 x_b \cdot b^2} \tag{31}$$

Introducing orthogonal principal axes one obtains for the

particle factor

$$f_k^2(\mathbf{b}) = N_k^2 \, e^{-4\pi^2 (\Delta_2^2 x_1 b_1^2 + \Delta_2^2 x_2 b_2^2 + \Delta_2^2 x_3 b_3^2)} \tag{32}$$

Guinier approximation for globular particles

For globular particles $\Delta_2 x_b$ is practically independent of the direction of b. From (32) one obtains

$$f_k^2(b) = N_k^2 \, e^{\frac{-4\pi^2}{3} (\Delta_2 x)^2 b^2} \tag{32a}$$

In the two dimensional case of circles (one dimensional case of rods) the denominator 3 must be replaced by 2 (1)

Radius of gyration $\Delta_2 x$

$$(\Delta_2 x)^2 = \int \rho_k(\mathbf{x}) \, \mathbf{x}^2 \, dv_x \tag{33}$$

If $\rho_k(\mathbf{x})$ is of the type (29) one obtains:

sphere with the radius R : $\Delta_2 x = \sqrt{\frac{3}{5}} R$

circle, disc: $\Delta_2 x = \frac{1}{\sqrt{2}} R$ (33a)

rod with length 2R: $\Delta_2 x = \frac{1}{\sqrt{3}} R$

See for further details table I.

Table I. Radii of gyration $\Delta_2 x$ for different shapes of particles. 2R, 2R, 2Rc their lengths in the three principal directions x_1, x_2, x_3. v_k is the a particle volume, $3a/R$ a relation between surface and volume of the particle

	sphere	Rot. ellipsoid	cylinder	prism
$\Delta_2 x$	$R\sqrt{3/5}$	$R\sqrt{(2+c^2)/5}$	$R\sqrt{(1{,}5+c^2)/3}$	$R\sqrt{(2+c^2)/3}$
v_k	$\frac{4}{3}\pi R^3$	$\frac{4}{3}\pi R^3 c$	$2\pi R^3 c$	$8R^3 c$
a	1	$\frac{1}{2c} + \frac{1}{2}\frac{\arcsin\sqrt{1-c^{-2}}}{\sqrt{1-c^{-2}}}$	$\frac{1}{3}(1+2c)/c$	$\frac{1}{3}(1+2c)/c$

The circle, disc, rod of eq. 33a is a special case of Table I with $c = 1$, $c \ll 1$ and $c \gg 1$

Guinier-Warren-plot ln I - b^2

For globular particles: $\Delta_2 x_1 \sim \Delta_2 x_2 \sim \Delta_2 x_3 = \frac{\Delta_2 x}{3}$; $c \sim 1$

lamellae (disc like) particles: $\Delta_2 x_1 \sim \Delta_2 x_2 \gg \Delta_2 x_3$; $c \ll 1$

rod like particles $\Delta_2 x_1 \sim \Delta_2 x_2 \ll \Delta_2 x_3$; $c \gg 1$

x_3 again the axis of elongation c.

The particle factor according to equ. (32) in **b**-space is globular, rod like, disc like.

If the particles are totally unoriented in the sample $I_{obs}(b)$ is spherically symmetric and proportional to

$$I_{obs}(b) \sim \int \overline{f_k^2}(b)\, d\Omega \tag{34}$$

$d\Omega$ element of the surface of a sphere with radius b in the **b**-space. Now plotting ln I_{obs} (sphere), ln $b^2 I_{obs}$ (disc), ln $b\, I_{obs}$ (rods) against b^2, one obtains in a certain b-interval a straight line

$$\begin{aligned}
&\text{spheres:} && (\ln I)/b^2 \sim \frac{-4\pi^2}{3}(\Delta_2 x)^2 && 0 \lesssim b \lesssim 0.3/\Delta_2 x \\
&\text{lamellae:} && \ln(b^2 I)/b^2 \sim -4\pi^2(\Delta_2 x_3)^2 && \frac{1}{\Delta_2 x_1} < b \lesssim 0.3/\Delta_2 x_3 \\
&\text{rods:} && \ln(bI)/b^2 \sim -4\pi^2\ (\Delta_2 x_1)^2 && \frac{1}{\Delta_2 x_3} \lesssim b \lesssim 0.3/\Delta_2 x_1
\end{aligned} \tag{35}$$

To get information about the lateral dimension $\Delta_2 x_1 \sim \Delta_2 x_2$ of the lamellae and of the length $\Delta_2 x_3$ of the rod, one must study the small angle scattering at smaller angles

$$\begin{aligned}
&\text{lamellae:} && \ln I/b^2 \sim -(\Delta_2 x_1)^2 && b < \frac{1}{\Delta_2 x_1} \\
&\text{rods:} && \ln I/b^2 \sim -(\Delta_2 x_3)^2 && b < \frac{1}{\Delta_2 x_3}
\end{aligned} \tag{36}$$

Porods formulae

For globular particles with constant electron density ρ_0, following eq. (29), the intensity in certain b-intervals sometimes is given by

$$I_{obs} = (\Delta\rho_0)^2 \frac{0}{8\pi^3 b^4} \quad b > \frac{2}{R} \tag{37}$$

$\Delta\rho_0$ is the difference of ρ_0 and the mean density of the sample $\bar{\rho}$ (cf. 21), 0 [Å^2] is the surface of the particles. According to *Luzzati, Witz* and *Nicolaieff* [169] often at such large b-values interference effects of the atomistic structure of $\rho_k(x)$ occur, which disturb a b^{-4}-dependence. Another formula is quite sensitive on interparticle interferences I_w. From (8) and (25) one obtains

$$\int I\, dv_b = Q(0) = (\Delta\rho_0)^2 M \bar{v}_k; \quad I_P(0) = (\Delta\rho_0)^2 M \overline{v_k^2}$$

hence

$$4\pi \int b^2 I(b)\, db = \frac{I_P(0)}{\bar{v}_k} = \frac{\overline{v_k^2}}{\bar{v}_k} = \bar{v}_k(1+\Delta^2 v_k) \tag{38}$$

Since according to (26) I(b) near b = 0 is mostly affected by I_W, $I_P(0)$ is often not observable, hence (38) not successful.

Absolute intensity measurement

There exist some papers concerned with absolute intensity measurements giving information about the mean volume $\bar{v}_k$ and number M of particles of a different electron density etc [57, 488]. From (21) one directly obtains $\Delta^2 N(v_a)$, from (38):

$$\int I_{obs}\, dv_b = Q_{obs}(0) \cong (\Delta\rho_0)^2 M \bar{v}_k$$

which depends on three unknown parameters. To obtain information about $M, \bar{v}_k$ $\Delta\rho_0$ in detail, a model of the sample under investigation has to be introduced or some of the parameters have to be known from other research technics (relative course of I_{obs} (b), wide angle scattering (cf. section VI), electron microscopy etc.) The additional conditions reduce the ability of this method. Examples of absolute intensity measurements: [58–61, 150, 168, 169]; cold worked metals [380–382, 390, 394, 396, 397, 399] binary and ternary alloys [408, 409, 422–424, 427, 433, 434].

Polydisperse systems

According to *Hosemann, Bagchi* [42] for globular particles using the Guinier approximation (32) and a weight distribution function H(R) of radii R:

$$H(R) = \frac{K(n)}{R_0}\left(\frac{R}{R_0}\right)^n e^{-(R/R_0)^2}; \quad \frac{1}{K(n)} = \frac{1}{2}\left(\frac{n-1}{2}\right)! = \frac{1}{2}\Gamma\left(\frac{n+1}{2}\right) \tag{39}$$

one obtains

$$I_P = \frac{M(\Delta\rho_0)^2 \bar{v}_k^2}{\left[1+\frac{1}{5}(2\pi b R_0)^2\right]^{\frac{n+4}{2}}} \tag{40}$$

The weight averaged $<R>$ and its standard deviation (polydispersity) g_R are given by

$$<R> = R_0 \frac{K(n)}{K(n+1)} \sim R_0 \frac{n+1}{\sqrt{2n+3}}$$

$$g_R = \left[\frac{<R^2>}{<R>^2} - 1\right]^{1/2} = \left[\frac{K^2(n+1)}{K(n+2)\,K(n)} - 1\right]^{1/2} \sim \frac{1}{\sqrt{2n+2}} \tag{41}$$

For $g_R \lesssim 0.2$ (40)within the errors of experiment equals (32a) and (33a),otherwise the slope $d \ln I_{obs}(b)/db^2$ decreases with increasing b. One obtains (c is defined in Table 1):

$$\lim_{b \to 0} \frac{d \ln I_P(b)}{d\, b^2} = - \frac{4\pi^2}{5} <R>^2 \frac{2+c^2}{3}(1 + 6g_R^2)(1 + g_R^2) \ . \qquad (42)$$

In many cases the interparticle interference from I_W (eq. 26) at small angles cannot be neglected.

Systems with high packing density ϵ^3

ϵ^3 is defined by the total volume of the particles divided through v

$$\epsilon^3 = \frac{1}{v} \sum_{k=1}^{M} v_k \qquad (43)$$

It can be proved [42] that in a b^2I-b-plot I_W is practically of no influence if

$$\epsilon^3 \lesssim g_R \qquad (44)$$

The $b^2 I_{obs}$-b-analysis

According to Fig. 2 in the b^2I-b-plot the b-values b_m and b_0 are evident, the position of the maximum and the intersection between tangent through the inflection point and the abscissa. One obtains:

$$g_R = \sqrt{\frac{M-2{,}1}{9{,}6-2M}} \ ; \ <R> = \frac{0{,}96}{2\pi b_m} \frac{9{,}6-2M}{\sqrt{7{,}5-M}} \ ; \ M = \frac{b_0}{b_m} \qquad (45)$$

The advantage of this method is, that contrary to the above mentioned methods here I_W does not disturb so much the results, since $I_{obs}(b)$ is not used for $b < b_m$. For systems with higher packing density the results can be corrected [42]. From table 2 we can see, that ELF 5 with g_R = 45 % up to packing densities ϵ^3 = 35 % shows essentially particle scattering I_P in the $b^2 I_P$-b-plot:

Table 2. Analysis of continuous small angle scattering of carbon black ELF 5 (Cabot Inc., Boston) with the b^2I-b-Method [41, 42]

Nr.	ϵ^3	m ±8% (g/cm^2)	b_m ±5% ($Å^{-1} \times 10^{-4}$)	b_0 ±5% ($Å^{-1} \times 10^{-4}$)	M_{obs} ±7%	g_R ±17%	$<R>$ ±11% (Å)
1	0,08	0,017	14,6	45	3,06	0,43	212
2	0,17	0,011	15,5	46	2,96	0,40	198
3	0,44	0,012	21,0	56	2,65	0,32	153
4	0,08	0,066	16,0	51	3,20	0,45	187
5	0,18	0,065	16,3	53	3,24	0,46	187
6	0,25	0,071	16,6	54	3,23	0,46	182
7	0,28	0,067	16,6	54	3,23	0,47	182
8	0,33	0,067	19,2	61	3,17	0,44	159
9	0,35	0,067	19,5	62	3,20	0,45	156
10	0,46	0,055	22,0	65	2,96	0,40	140
11	0,08	0,10	16,8	56	3,32	0,47	175
12	0,25	0,10	18,2	62	3,39	0,49	162
13	0,32	0,106	19,8	65	3,31	0,47	151
14	0,34	0,11	20,6	66	3,23	0,46	147
15	0,44	0,10	22,3	69	3,07	0,42	138
16	0,08	0,13	18,2	62	3,42	0,49	160
17	0,17	0,12	18,2	62	3,42	0,49	161
18	0,42	0,13	23,5	75	3,19	0,45	128
19	0,43	0,12	22,6	72	3,17	0,44	134

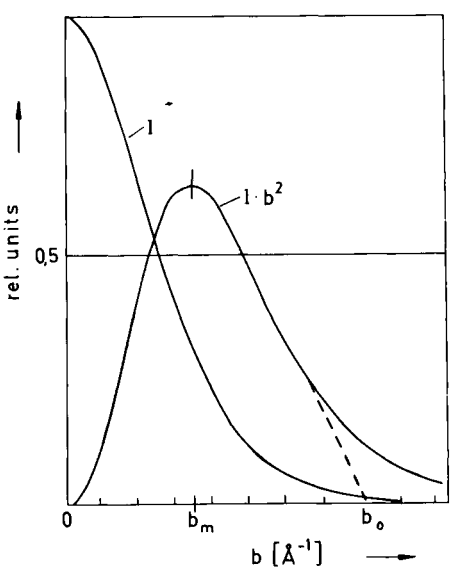

Fig. 2
The b^2 I-b-plot for densily packed polydisperse globular particles (eq. (45)).

The inner surface of a colloidal system

The inner surface 0 is given by (γ a constant):

$$0 = \bar{M}\,\gamma \int 4\pi R^2 c\, h(R)\, dR$$

γ depends on the shapes of the particle. h(R) is the number frequency of particles with dimension 2 R and is connected with the weight distribution H(R) by (see eq. (39)):

$$v_k(R)\, h(R) = \bar{v}_k H(R)$$

$v_k(R)$ is the volume of a particle k with the dimension 2 R; Substituting this and (43) one obtains

$$0 = \bar{v}_k \bar{M}\,\gamma \int \frac{4\pi R^2 c}{v_k(R)}\, H(R)\, dR = 3\alpha \left\langle \frac{1}{R} \right\rangle \epsilon^3 v \qquad (46)$$

α is calculated in table 1 for some shape functions.
ϵ^3 is known from macroscopic data and

$$\left\langle \frac{1}{R} \right\rangle \cong \frac{1}{\langle R \rangle} \cdot \frac{1 - g_R^2}{1 - 2g_R^2}$$

is known from the b^2I-b-plot and eq. (41). See for details [42].

Multiple small angle scattering

If the sample is not thin enough, the small angle scattering produced in the first part of the sample again produces small angle scattering. Hence I_{obs} is smeared out and $\langle R \rangle_{calc}$ is too small. This clearly can be seen from table 2 for samples with m = 0.06 g/cm^2 substance or more. The polydispersity is practically not effected.

Lamellae with an inner structure

If the lamellae like particles k have an electron density $\rho(x_3)$ which varies with the axis x_3 and is practically independent of x_1 and x_2 one obtains instead of (32)

$$f_k^2 = |R(b_3)|^2\, e^{-4\pi^2(\Delta_2^2 x_1 b_1^2 + \Delta_2^2 x_2 b_2^2)}; \quad R(b_3) = \mathcal{F} \int\int \rho(\mathbf{x})\, dx_1\, dx_2 \qquad (47)$$

Hence contrary to (35) in a b^2I-b-plot in the b-domain defined on the righthand side of (35) one obtains information on the macrostructure $\rho(x_3)$ parallel to the normal of the lamellae.

$$b^2 I(b) \sim |R(b_3)|^2 \quad \text{for} \quad \frac{1}{\Delta_2 x_1} \lesssim b$$

Trial and error methods for shapes of particles

To obtain more information on the shape function $s_k(x)$ of the particles (eq. 29), shape amplitudes $S_k(b)$ were calculated and tabulated [4, 28, 60]. *Miller* and *Schmidt* [73] calculated cylinders with different cross sections, *Mittelbach* and *Porod* [74–77] three-axial rotational ellipsoids and cylinders. *Kirste* [46, 47, 48], *Fedorow* [20], *Heine* et al. [32–34], *Stokes* [99] and *Peterlin* [82] calculated the scattering curves for chain molecules, *Kratky* and coworkers studied linear molecules highly diluted. Here a $bI(b)$-b-plot is helpful, in providing information about the structure $\rho(x_3)$ along the fiber axis (see „rods" in eq. (35)).

Scattering functions of rotational ellipsoids are also given in [5, 35, 51, 71, 88], for rods and discs in [15] and [90]. Polydisperse systems were explicitly calculated for different shapes and distribution functions [86]. *Kreutz* [162] could prove directly, that the lamellae of chloroplasts have centres with negative density (compared with the electron density of the solvent).

4. Discontinuous small angle scattering

For colloidal systems with distance statistics different from ideal gases (27) no longer holds. Interparticle interferences, given by I_W (eq. 26) must be taken into account. If the particles, clusters, and domains do not overlap one obtains from (7) and (8) an important formula:

$$\int I_W(b)\, dv_b = Q_w(0) = 0 \tag{48}$$

$I_W(b)$ modulates I_{obs} without changing its integral value!

Amorphous macrostructures

There exist many structures, where inequality (44) does not hold, but only one or perhaps two quite diffuse halos appear. Fraunhofer patterns of such quite irregular structures of polydisperse particles are shown in Fig. 3. The microphotometercurves of Fig. 4 illustrate the phenomenon (*Joerchel* [57]). The function w(b) defined in (26) has some important features:

$$\text{From (48)} \quad \int (w(\mathbf{b}) - 1)\, dv_b = 0$$

$$\text{From (21)} \quad \lim_{b \to 0} w(\mathbf{b}) = \frac{\Delta^2 M}{\overline{M}} \tag{49}$$

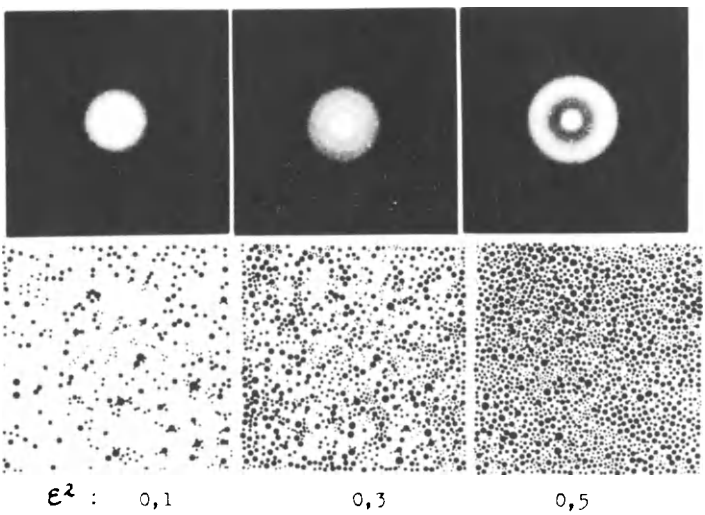

Fig. 3. Three models with the same polydispersity $g_R = 0.3$ but varying two dimensional packing density $\epsilon^2 = 0.5, 0.3, 0.1$. The Fraunhofer patterns according to eq. (44) show a diffuse interference ring only for $\epsilon^2 = 0.5$.

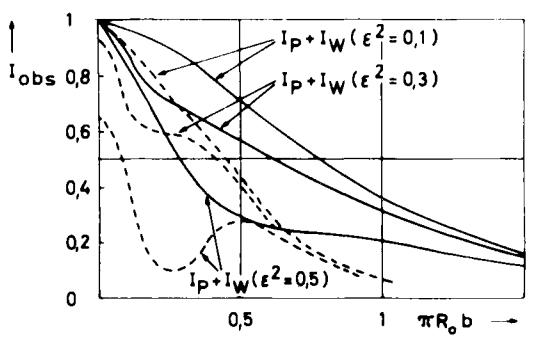

Fig. 4
Microphotometer curves of fig. 5 ($g_R = 0.3 \ldots$) and for $g_R = 0.75$. (–) Only for $g_R = 0.75$, $\epsilon^2 = 0.1$ I_W can be neglected and a pure particle scattering I_P exists (eqs. (25) and (26)).

Two further conditions can be found from ϵ^3 and g_R. Herewith a four parametric w-function (sum of two centro symmetric Gaussian functions) is defined. It agrees with the observed functions of Fig. 4 [42].

Non spherically symmetric structures

The small angle scattering of synthetic and natural fibers, stretched plastics, biological and synthetic single crystals of macromolecules often show a non spherical symmetric small angle scattering. Now the correlation function (7) is no longer spherically symmetric and eq. (28) can no longer be used.

Even in glasses, meltcrystallized high polymers, liquids with spherically symmetric intensity-functions $I_{obs}(\mathbf{b})$ one has to take into account, that in microdomains three dimensional lattices can exist. If these microlattices are disoriented against each other, the summation in (7) gives an observable spherically symmetric function similar to that for powders of metals, which produce Debye-Scherrer-diagrams. It is impossible to transform $I_{obs}(\mathbf{b})$ of crystalline powder diagrams with (28). The mathematical difficulties are much too great because of the large number of Debye-scherrer lines.

On the other hand in noncrystalline material there exist only a few more or less diffuse spherically symmetric maxima.

The Concept of the theory of paracrystals

This theory [30b, 42, 107b] takes over from the crystallography the concept of lattices, but in a more generalized form-(second line of table 3). From the conventional theory of liquids it takes over the concept of the same a priori distance statistics for all particles k (third line of table 3). In the crystalline lattice with thermal motions the quotient $\Delta^2 N(v_a)/\overline{N}(v_a)$ of eq (21) approaches zero with increasing v_a (see the – sign in line 3 of table 3).

In an ideal gas (conventional liquid) this quotient is 1 (constant between zero and one). In a paracrystalline lattice the quotient has a constant limiting value different from zero too.

The concepts of line 2 and 3 have been taken over from the conventional theories to the paracrystals (+ signs). It is therefore a unified theory of the crystalline and noncrystalline states.

The +-sign in line 1 of table 3 makes clear, that a three dimensional long range order may or may not exist in a paracrystal. Only for point-like coordination statistics $H_k(\mathbf{x})$ is it established (see below). The ±-sign in line 4 emphasizes that for single paracrystals $Q(x)$ is not spherical symmetric.

Table 3. Fundamentals of the structure theories

concept	Paracrystals			gaseous, amorphous
	crystal convent.		liquid convent.	
long range order	+	+···	–	–
lattice	+	+	–	–
$\lim \Delta^2 N(v_a)/\bar{N}(v_a)$ = const. $\neq 0$ for all v_a	–	–+	+	+
Q(x) spherically symmetric	–	–+	+	+

The convolution polynom z(x)

If the M particles k build up a paracrystalline single lattice, the correlation function in (7) in the simplest case is defined by a convolution polynom of three coordination statistics $H_1(x), H_2(x), H_3(x)$.

$$z(x) = \frac{1}{M} \sum_{i=1}^{M} \sum_{k=1}^{M} \overline{P(x - x_i + x_k)} = \sum_{P_1} \sum_{P_2} \sum_{P_3} H_{P_1 P_2 P_3}(x)$$

$$H_{P_1 P_2 P_3}(x) = P(x-0) \overbrace{H_1 H_1 H_1 \ldots H_1}^{P_1 \text{ times}} \overbrace{H_2 H_2 \ldots H_2}^{P_2 \text{ times}} \overbrace{H_3 H_3 \ldots H_3}^{P_3 \text{ times}}$$

Each coordination statistic $H_r(x)$ is a three dimensional function and gives the distance statistics of the centers of two neighbouring particles in the direction r (r = 1, 2, 3)

The paracrystalline lattice factor Z(b)

$$Z(b) = \mathfrak{F} z(x) = \frac{1}{v_r} P(b-0) + \prod_{r=1}^{3} \mathrm{Re} \frac{1 + F_r(b)}{1 - F_r(b)} ; \quad F_r(b) = \mathfrak{F} H_r(x) \qquad (51)$$

v_r is the averaged volume of a lattice cell. Each lattice cell contains a certain number of particles (molecules, monomers, macromolecules, microdomains etc.) with the electron density $\rho_r(\mathbf{x})$. In the simplest case of no further correlations existing between them,one obtains

$$Q(\mathbf{x}) = M(\overline{\tilde{\rho}^2} - \overline{\tilde{\rho}}^2) + \overline{\tilde{\rho}}_r^2 \frac{1}{v_r} \widehat{(z\tilde{s})^2} \tag{52}$$

$s(\mathbf{x})$ is the shape function of the paracrystal (eq. 16).

The intensity function $I(\mathbf{b})$ is given by $\mathcal{F}\, Q(\mathbf{x})$ from (52):

$$I(\mathbf{b}) = M(\overline{f_r^2} - \bar{f}_r^2) + \frac{\bar{f}_r^2}{v_r} \widehat{(Z|S|^2)} \tag{53}$$

In the discontinuous small angle scattering such intensity functions are often of interest. In fibrous proteins such as α and β-keratin [213a, 298] or collagen [215, 250, 257, 365] there exists a long period of some 100 Å parallel to the chains. In the lateral direction more or less diffuse paracrystalline reflexions with lattice constants from 5–80 Å or more are observable. The situation is similar in synthetic high polymers (see below).

The interference function w(b)

$w(\mathbf{b})$ contrary to (26) is now not spherically symmetric:

$$w(\mathbf{b}) = \prod_{r=1}^{3} \mathrm{Re}\, \frac{1+F_r}{1-F_r} \tag{54}$$

It automatically fulfils the conditions of eq. (49).

The cell edge fluctuation

The averaged cell edge vector $\bar{x}_r$ and its standard deviation $\Delta_2 x_r$ in the direction of the unit vector s_b is analogous to (30) defined by:

$$\bar{x}_r = \int x\, H_r(\mathbf{x})\, dv_x \;;\; (\Delta_2 x_r)_s^2 = \int (\mathbf{x} - \bar{x}_r, s_b)^2\, H_r(\mathbf{x})\, dv_x \tag{55}$$

The relative fluctuations g_{rs}

$$g_{rs} = \frac{(\Delta_2 x_r)_s}{|\bar{x}_s|} \tag{56}$$

of all three cell edges (3 x 6 = 18 statistical parameters) define the structure and the character of its intensity function.

The number of discontinuous reflections

If n_{sr} is the number of higher orders of a basic reflection in the direction s not merging into the adjacent reflection, which is neighboured in the direction r, then the following relation holds

$$n_{sr} \sim \frac{0{,}3}{g_{rs}} \tag{57}$$

Fluctuations of 20 % or more produce a nearly continuous small angle scattering. Calling the fiber axis by the index 3 (cf. eq. (35)) the following $\bar{x}_r$ and g_{rs} values are observed:

Table 4. Superstructures in natural and synthetic high polymers Index 1, 2, 3: Direction of back bond linkage (= hydrogen bonds), fiber axis (= covalent bond), secondary (= van der Waals) bond.

	a_1^m	a_3^m (Å)	a_2^m	g_{11}^m	g_{13}^m (%)	g_{31}^m	g_{33}^m	g_{12}^m
1 Chymotrypsin-(moist)	68	50	66	2,2	2,0	2,2	2,0	2,0
2 β-keratin (dry)	34	95	?	7,4	3,9	5,4	1,5	20
3 collagen (untreated)	110	655	?	2,3	4,6	2,0	0,9	>20
4 keratin	83	198	?	6,0	2,6	35	0,9	>20
5 polyurethan (stretched)	20	70	?	>30	>25	>30	>25	>20
6 polyethylene (hot stretched)	100	120	100	>30	~ 5	< 4	~ 8	~ 4

Calculation of the g_{sr}-values

The integral width δb_{rs} in the direction s of a reflection by a family of N_r netplanes is given by

$$\delta b_{rs} = \frac{1}{\bar{a}_s}\left(\frac{1}{N_s^2} + (\pi g_{sr} h_r)^4\right)^{+1/2} \tag{58}$$

$a_s \cdot N_s$ is the size of the lattice in the direction s

$h_r = 1, 2, 3, 4 \ldots$ is the order of the reflection lying on an axis b_r with netplane distance $\bar{a}_r$. Let 1, 3 be the horizontal (vertical) direction. In the model of Fig. 5 $g_{13} \sim 0.3$ (horizontal rows with large statistical curvature). According to (57) $n_{31} < 1$, hence all reflections adjacent in the horizontal direction merge into each other with exception of $h_3 = 0$, which are the reflections on the equator. The paracrystalline lattice of Fig. 6 on the contrary has straight horizontal lines, whereas all other distances are disturbed. Hence $g_{13} = 0$, $\delta b_{31} = 0$, only the reflections (Oh_3) have nonparacrystalline shapes in the direction 1. In direction 3 they are broadened.

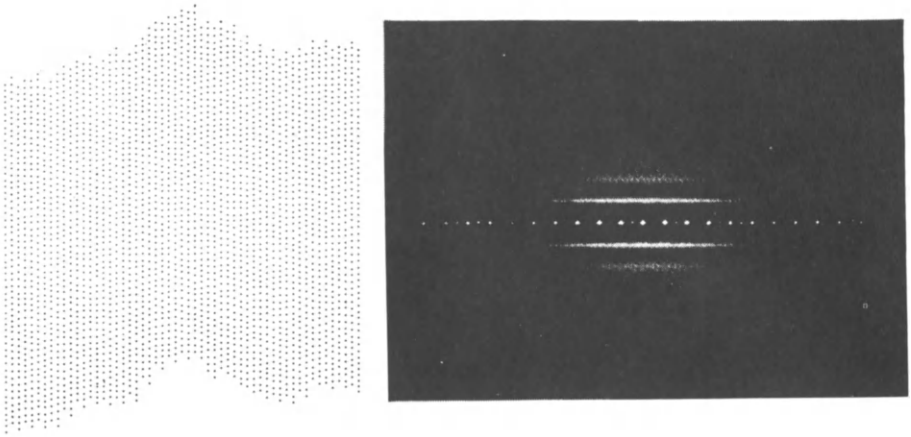

Fig. 5. Fraunhofer diffraction of a twodimensional paracrystalline lattice with $g_{13} = 0.3$; $g_{11} = g_{31} = 0$; $g_{33} = 0.1$ According to eq. (58) the integral widths of the reflections are unlike zero for δb_{33} and δb_{31} and smear together with their horizontal neighbours even for the first layer lines (eq. 57).

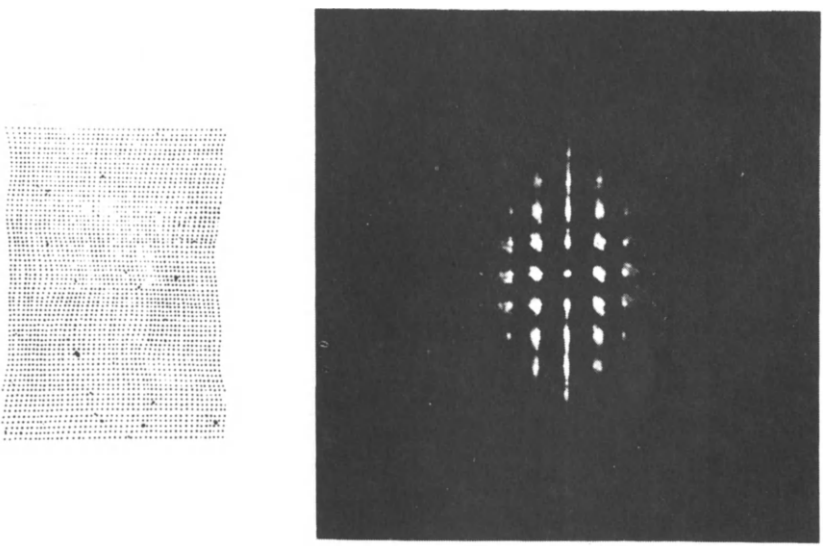

Fig. 6. Fraunhofer diffraction of a twodimensional paracrystalline lattice with $g_{13} = 0$; g_{11}, g_{33} and g_{31} different from zero. According to eq. (58) only the integral widths δb_{31} are zero, hence only the reflections (Oh_3) along the meridian are crystalline like in the horizontal direction.

Lamellar systems

Bundles of parallel oriented lamellae give rise to a series of meridional reflections (ooh_3), whose number n_3 depends on the g_{33}-value of the bundle structure. For example bundles of polyethylene (P.E.) single crystals, isothermally crystallized from 0,05 % xylene solution or meltcrystallized P.E., stretched and annealed show g_{33} down to 10 % (3 orders of meridional reflections) cf. Fig. 7.

In lamellar systems of chloroplasts, depending on their preparation, g_{33} values between 20 and 5 % are obtainable [157, 158, 161, 162].

Practically all natural and synthetic fibers and plastics of linear high polymers offer paracrystalline lamellar structures [14, 56, 58, 260, 334] (see below). More detailed calculations are given by *Tsvankin* [103, 104], and one of us [42].

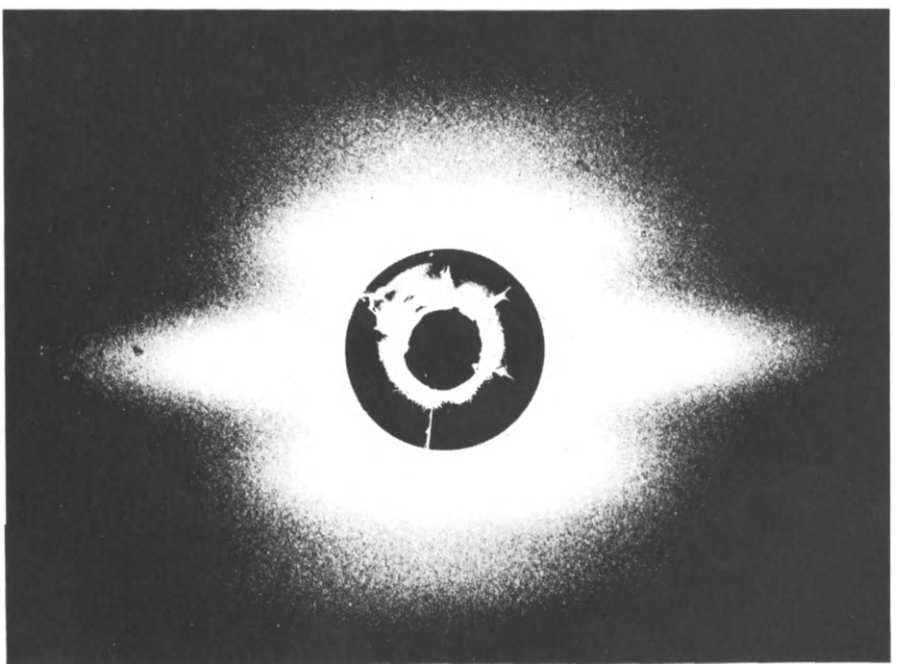

Fig. 7. Small angle X-ray pattern of linear P.E., annealed for 3 hours at 90 °C, then stretched at 20 °C six times and again anneaded at 90 °C for 18 h and 3 h at 128 °C, then again stretched at 20 °C ten times.

Densily packed ultrafibrils

In Fig. 8 600 steelballs with a polydispersity $g_R \sim 10\,\%$ (cf. eq. (41)),randomly mixed in the highest possible density,are photographed. In the *Fraunhofer* pattern of Fig. 9 about 4 diffuse rings with a spurious hexagonal symmetry indicate the existence of small paracrystalline domains. With increasing volume v_a (cf. eq. 10) the rings become absolutely homogenous. Figs. 8 and 9 represent the equatorial scattering of linear high polymers with ultrafibrils as paracrystalline clusters. (see below).

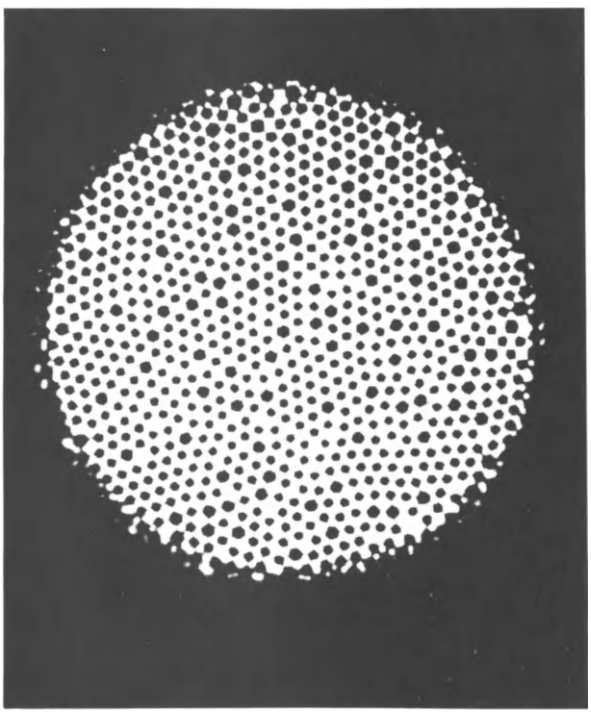

Fig. 8. Shadow photograph of 600 densily packed steelballs of different sizes (polydispersity $g_R \sim 10\,\%$, see eq. (41) and (45)), model for a cross section of stretched linear polyethylene. The balls represent the chain molecules, the paracrystalline clusters the ultrafibrils.

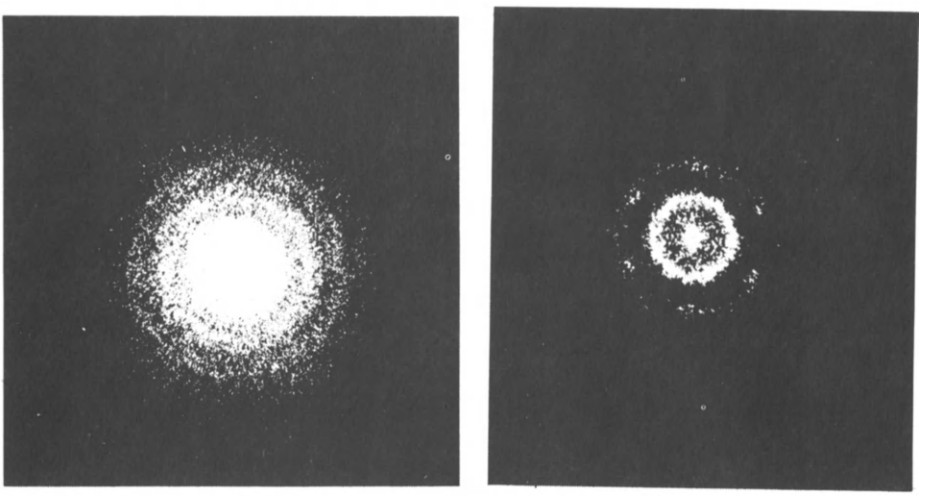

Fig. 9. Fraunhofer pattern of fig. 8 is a model for the intensity of a noncrystalline solid. As with 600 particles the intensity function differs from the expectation value I_{obs}, the diffuse interference rings have a slight suggestion of a hexagonal structure in them, produced by the few paracrystalline domains in fig. 8. left side long, right side shorter exposure time.

6. Combination of continuous and discontinuous diffraction phenomena

In the conventional crystallography the intensities of Bragg reflections $(h_1 h_2 h_3)$ are measured, which are proportional to the structure factor $f_r(b)^2$ (eq. (53)). The reflection 000 is not discussed, since crystallographers mostly know the number N_r of electrons in a lattice cell

$$N_r = f_r(0) = \int \rho_r(x)\, dv_x \qquad (59)$$

As we have seen above, the small angle scattering has not only an integral value proportional to N_r but also a line profile. Some examples may illustrate how useful information from the (000) and $(h_1 h_2 h_3)$ line profiles can be. In chapt. VI some structural factors observed in small angle scattering are discussed.

Ultrafibrils in polyethylene (P.E.)

Measuring carefully the line profiles of the wide angle (hhO) reflections of hot stretched linear P.E. in the direction 1 orthogonal to the fiber axis, one obtains in a Guinier - Warren plot line profiles, which can be synthesized by two gaussian functions (Fig. 10). Plotting the integral width δb_{11} of each of them squared against h^4 (Fig. 11) one obtains according to (58) linear lines which give information about the diameter L of the particles and the g_{11}-values of their paracrystalline chain-molecule-lattice.

From their slope the g_{11}-values of the paracrystalline distortions can be calculated between adjacent chain molecules. From the intersection of the straight lines with the ordinate one obtains the averaged particle size L in the lateral direction (see. Fig. 8 and 9).

Table 5. Ultrafibrils in cold [200] and hot [266] stretched P.E.

	From wide angle reflections hhO		From 000	
	L [Å] hot stretched	g_{11} [%]	L [Å] hot stretched	L [Å] cold stretched
component 1	83	3,2	91	104
component 2	175	2,2	186	211
component 3	?	?	309	437

One obtains three sizes from the small angle scattering on the equator in the same way. Two of them are equivalent with wide angle results. Hence in the P.E. coherently scattering paracrystalline domains exist which produce the slope of the 000-reflection, one size L = 300 Å resp. 400 Å (Component 3 in table 5) is produced by clusters of 100 Å and 200 Å thick ultrafibrils, which together do not scatter coherent Bragg-reflections. This size hence cannot be observed in the (hk0) reflections, only at (000). Its existence at (000) proves, that the grain boundaries between mosaic-blocks have a lower electron density.

Small angle scattering of holes

In the literature one often meets with the statement, that the small angle scattering is produced by holes, [239, 245, 246, 308, 313], cracks etc. in the material and that the slope of small angle scattering depends on the size of these domains of low electron density [332, 339, 348]. This is true only, if the holes have convex shapes as

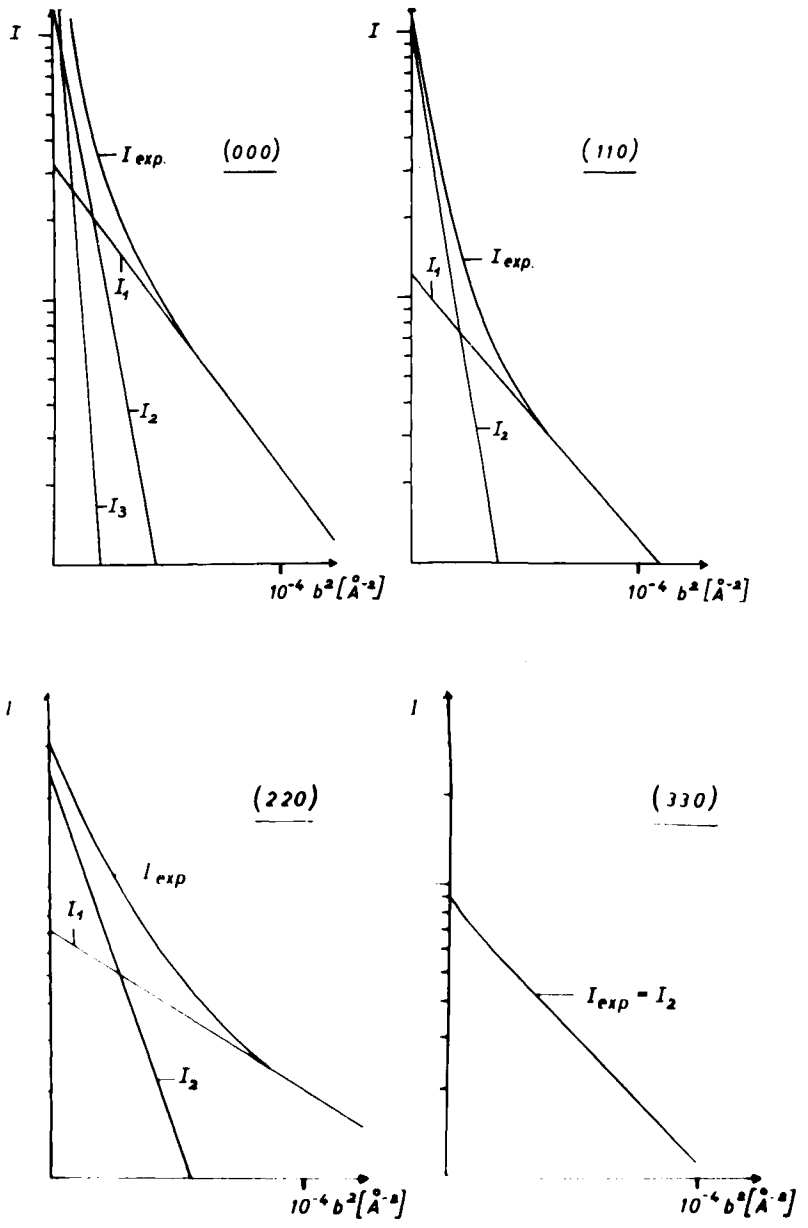

Fig. 10. Gaußian analysis of the reflections 000, 110, 220, 330 of hot stretched linear polyethylene, 000 alone has three components (see table 5).

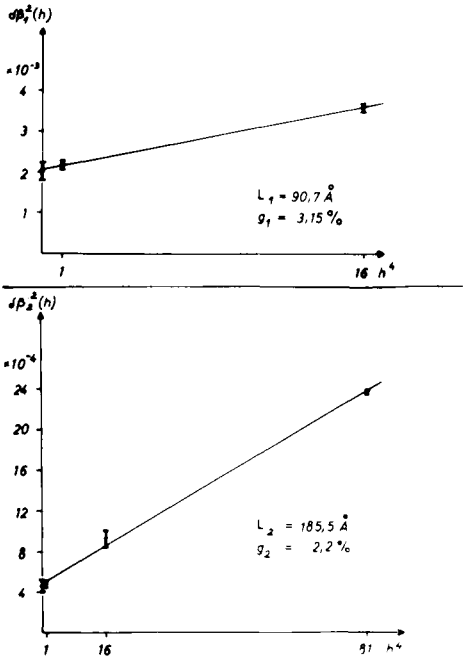

Fig. 11
$\delta b^2 - h^4$ -plot of the components 1 and 2 of fig. 8. The intersection with the ordinate gives the diameters L of the ultrafibrils, the slope the paracrystalline interatomic distortions.

the holes in cheese of Switzerland. It can be proved [42] that the slope of small angle scattering depends on those domains, which have convex surfaces, regardless whether the electron density of these domains is larger or smaller than their environment. In the model of Fig. 8 for instance, used for the Fraunhofer pattern of Fig. 9, the transparent parts for light are the holes between the spheres. They have concave surfaces. The intensity depends not on their sizes and shapes, but on the paracrystalline microlattices and the shapefactor of the spheres which have a convex surface. Obviously between the more or less spherical cross sections of the ultrafibrils in P.E. grain boundaries of lower electron density exist. Otherwise a small angle scattering (000 reflection in Fig. 10) would not exist. These „holes" never affect the relative course of the small angle scattering, since they depend on the shape and positions of the ultrafibrils. These interspatial „particles" have quite irregular shapes and their positions are strongly correlated by the shapes and positions of the ultrafibrils. Their interference term $w(\mathbf{b})$ (eq. 26) and particle factor $f_K^2(\mathbf{b})$ (eq. 25) is practically uncalculable. Particle scattering of holes was observed e. g. in cold stretched polystyrene or in cleavages enforced in polystyrene [272a] Fig. 12 shows the electron microscopic picture, Fig. 13 the small angle scattering of such cold worked domains. It has the same slope along the equator and meridian, but is weaker along the equator. From this slope one obtains spherical holes with an averaged diameter of $2 <R> \sim 200$ Å in accordance with the electron microscopic picture (Fig. 12).

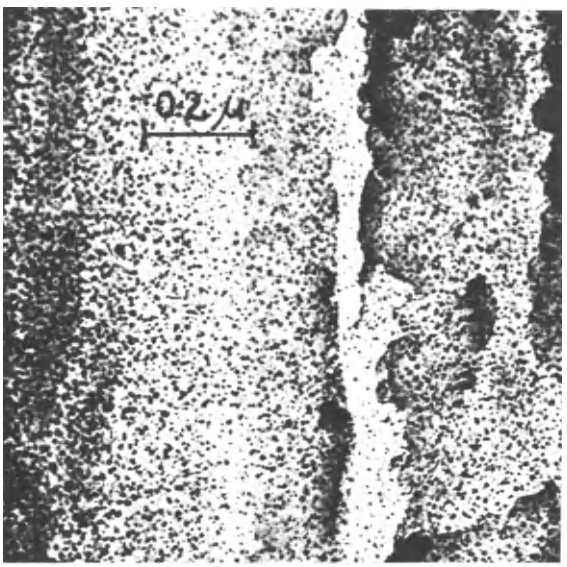

Fig. 12
Electron microscopic picture of the globular holes in cold worked polystyrene.

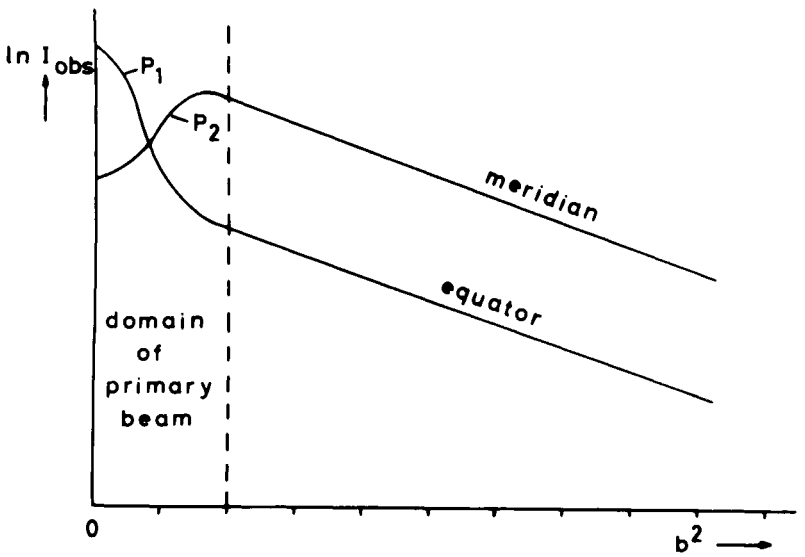

Fig. 13. Schematic diagram of the small angle scattering of cold worked polystyrene. P_1 the unobserved component I_2 (eq. 60) for holes in amorphous layers, P_2 for holes along the ultrafibrils.

Backfolding of chain molecules

Most of the linear high polymers show along the fiber axis a meridional reflection (Fig. 7) indicating a periodicity of 100–600 Å (depending on heat treatment, stretching etc.) Hence the projection of $\rho(x)$ on the fiber axis x_3 must have such a periodicity too.

Obviously paracrystalline domains of higher electron density are alternating with lower ρ-domains. The fringe micelle model often can not explain quantitatively the large intensity of this meridional small angle scattering for high molecular weight compounds since the number of ends of chain molecules is too small. The model of Fig. 14 gives a schematic representation of the variety of chain conformations and supermolecular correlations, which covers long chain compounds from bundles of single crystals (bottom right) over hot stretched and annealed material (centre) to cold drawn samples (left), and can explain most of the small angle patterns. Here in cold worked material the „amorphous" domains can sometimes show globular holes which are concentrated orthogonal to x_3 along amorphous layers which are domains of higher distorted chains. The I_{obs}-function of such structures is described above (Fig. 11).

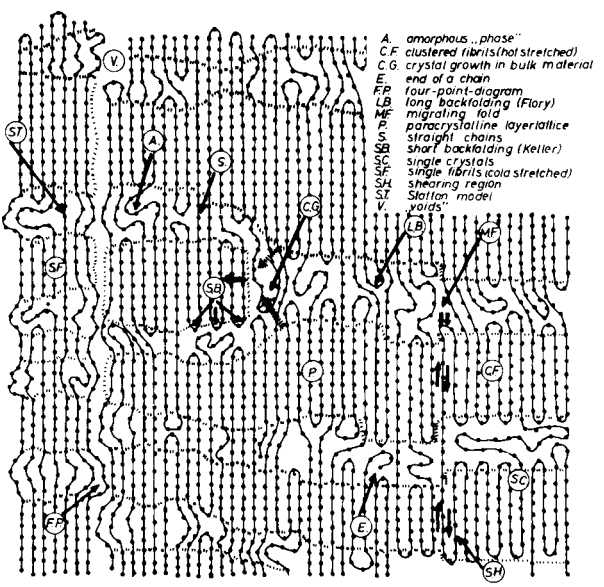

Fig. 14
Model of linear high polymers with backfolding chains of three types α, β, γ and smectic and nematic superstructures depending on heat – and mechanical treatment.

Smectic and nematic superstructures

According to table 4 superstructures with different g_{ik}-values exist. In the conventional classification two play a predominant role

nematic: $g_{13} \sim g_{23}$ large all other g_{ik} smaller

smectic: $g_{13} \sim g_{23}$ small all other g_{ik} larger

According to Fig. 7 in many long chain compounds ultrafibrils with diameters of 100–300 Å exist, which have a kind of periodicity along their fiber axis. The more (for instance by annealing) the positions of the domains of higher electron density of adjacent ultrafibrils are correlated to each other, the more a less statistically curvated paracrystalline layer structure is formed (g_{13} and g_{23} smaller). The structure gets more and more smectic features though consisting of more or less latent ultrafibrils [10, 11].

Explanation of Fig. 13

Since $I_{obs}(\mathbf{b})$ is an analytic function, the equatorial and meridional scattering of Fig. 13 must have the same value at $\mathbf{b} = 0$. The peaks P_1 resp. P_2 are not observable since by folding with the precision function $G_i(b)$ (see. eqs. (9) and (19)) they lie inside of the primary beam. To understand Fig. 13 one has to add to the particle scattering I_P of the holes with radius R a component I_2, depending on a dimension L larger than the diameter of the domain v_a of information, hence not measurable:

$$I_P \sim \exp\left\{-\frac{4\pi^2}{5} R^2 b^2\right\} \quad I_2 \cong \beta \exp\left\{-2\pi^2\left[C^2(b_1^2 + b_2^2) + D^2 b_3^2\right]\right\} \tag{60}$$

First possibility: The holes lie in the amorphous layers, which have a thickness ~ 2 R and a large lateral dimension $L \gg R$. Then

$$C = L \gg R \quad D \sim R$$

I_2 along the equator is unobservably small, along the meridian proportional to I_p. After folding with G_i one obtains an I_{obs} (cf. (19)) which has the same slope in both directions, but is proportional to

$$\text{equator:} \quad I_{obs} \sim 1 \quad \text{meridian:} \quad I_{obs} \sim 1 + \beta \tag{61}$$

Second possibility:

The holes lie at interspatial lateral sites between ultrafibrils

$$C \sim R \quad D = L \gg R$$

$$\text{equator:} \quad I_{obs} \sim 1 + \beta \quad \text{meridian:} \quad I_{obs} \sim 1 \tag{62}$$

Since the observed equatorial scattering is weaker than the meridional, one has now two possibilities:

Case		holes lie along	mean density of amorphous regions
1	$C = L;\ D \sim R;\ \beta > 0$	layers	between that of holes and crystallites
2	$C = R;\ D \sim L;\ \beta < 0$	ultrafibrils	larger than that of crystallites

Case 2 means, that the Fouriertransform of I_2 gives a function Q_2, which has a long tail of the opposite sign as Q_p along the fiber axis. Since $\overline{\rho_k}$ in the holes is smaller than $\overline{\rho}$ of the sample, $\overline{\rho_u}$ in the ultrafibrillar domain of this tail must be larger than $\overline{\rho}$ of the sample. This is possible only, if the holes lie directly in the amorphous regions of the ultrafibrils and not along their lateral grain boundaries. Then $C \gg D$ in contradiction to (62).

Case 2 hence can be discarded. P_1 in Fig. 13, though not directly observable, is the reasonable solution: The holes lie in the amorphous regions of the smectic layer structure. The mean electron density ρ_L of the amorphous layers has a value between ρ_k and ρ.

This is one of the first cases, where directly can be proved, that the course of the intensity function I(b) depends on the shape of holes, which therefore must have a convex surface. In many other examples in literature they have a concave shape (fig. 3 and 8) and the slope of I(b) depends on the shape of the clusters of higher electron density

7. Colloidal structure factors f_r^2

Many small angle scattering studies yield no further information of the structure inside a colloidal particle or microdomain. Introducing the shape function $G_a(\mathbf{b})$ of the domain of small angle scattering, the information of small angle scattering is defined by

$$I_{sa}(\mathbf{b}) = I_{obs}(\mathbf{b})\, G_a(\mathbf{b});\quad Q_{sa}(x) = Q_{obs}(x)\, \widehat{g_i(x)} \qquad (63)$$

$g_i(x) = \mathfrak{F}^{-1} G_a(\mathbf{b})$ is a function normalized to unity, which smears out all atomistic details. If the particle has different mean electron densities at different parts, eq. (29) no longer is sufficient and the folding with $g_i(x)$ no longer smears out fine details, since they are structures in superatomistic dimensions (> 7 Å). The trial and

error methods of the particle component I_P for instance deal with scattering factors of caved cylinders and spheres which sometimes fit better with the I_{obs} than those of particles with constant ρ_0. The Guinier Preston zones in Al-Zn have spherical kernels with higher electron density than $\bar{\rho}$ surrounded by shells of lower density than $\bar{\rho}$ (see below).

Lamellae systems in chloroplasts

The small angle scattering of chloroplasts after extraction of lipids sometimes gives a pure particle scattering I_P, which in a ln $b^2 I_P$-b^2-diagram shows in a certain b-region a linear slope [157]. According to (35) lamellae exist with $\Delta_2 x_3 = 13{,}5$ Å.

If the lamellae have a constant electron density, their thickness 2 R is according to (33)

$$2R = 2\sqrt{3}\ \Delta_2 x_3 = 45 \pm 2\text{Å}$$

In other preparations the lamellae are packed together in bundles with small g_{33}-values and, hence, give rise to interlamellae interferences, corresponding to a long mean Bragg distance $D = 36 \pm 1$ Å. This value is much smaller than 45 Å. Hence the electron density in the lamellae along x_3 cannot be a constant ρ_0, but must be concentrated on the top and bottom of the lamellae. One obtains an integral relation for the density distribution $\rho_r(x_3)$ and hence for the colloidal structure factor f_k^2:

$$\Delta_2^2 x_3 = \frac{1}{\rho_0 D} \int_{-D/2}^{+D/2} x_3^2 \rho_r(x_3) \begin{cases} = \dfrac{D^2}{7} & \text{from experiment} \\ = \dfrac{D^2}{12} & \text{if } \rho_r = \rho_0 \text{ would be a constant} \end{cases} \tag{64}$$

Shape of microcrystallites in chloroplasts

In anhydrous formic acid the lamellae desintegrate into microcrystallites. In Webers solvent the 000 reflexions in a Guinierplot give near b = 0 straight lines. Their slope corresponds to a rayon of gyration of $\Delta_2 x = 70$Å (eq. 33). The outer profile of the 000 reflections analyzed by trial and error methods (see above) corresponds to a quotient of the principal axis (cf. 32) of

$$\Delta_2 x_1 : \Delta_2 x_2 : \Delta_2 x_3 = 5 : 5 : 1$$

Since $\Delta_2 x_3 = 13.5$ Å, small platelets exist with dimensions of about

$$170\text{ Å} : 170\text{ Å} : 36\text{ Å} \tag{65}$$

Lattice of the microcrystallites

The above mentioned small angle scattering, only observable in high diluted preparations, is so weak, that it is only observable in slit cameras (for instance in a *Kratky* camera [464–468] with exposure times of 50–100 hours. After elimination of slit smearing [28, 494, 499, 507, 508] in a $b^2 I$-b-plot five interference maxima can be observed outside of the 000 reflection (Fig. 15). They can be analyzed by addition of 5 Gaussian like humps with a lattice constant d = 41,7 Å [161, 162, 157, 158]. Their Miller indices (hko) and (hkl) are plotted in Fig. 15. From the integral widths of the humps one obtains according to (58) $N_1 = N_2 = 4$ lattice cells. Hence 4 x 41,7 ~ 170 Å is the averaged lateral size of the microcrystallites in accordance with (65).

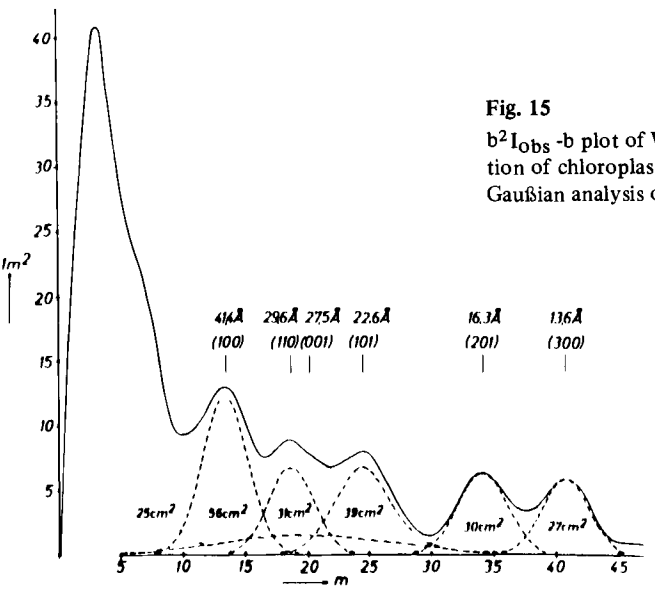

Fig. 15
$b^2 I_{obs}$ -b plot of Weber's protein preparation of chloroplast microcrystals and the Gaußian analysis of their reciprocal lattice.

The centrosymmetric colloidal structure factor f_r^2 of the micro crystallites

According to (53) $f_r^2(\mathbf{b})$ is only observable in the „Braggwindows" of $\widehat{Z|S|^2}$ since outside the windows $\widehat{Z|S|^2}$ is unobservably small, hence $f_r^2(\mathbf{b})$ there is without influence on I. Nevertheless the continuous functions $f_r^2(\mathbf{b})$ can be constructed by using threeaxial Gaussian approximations (32). See for details [42].

Its Fourierinverstransform unequivocally leads to the colloidal density distribution $\rho_r(x)$, if a center of symmetry exists. In Fig. 16 the three dimensional $\rho_r(x_1 x_2 0)$ distribution (centre of symmetry at 000) is plotted in relative density units. At the centre a „negative" hole (its density is smaller than that of the solvent) arises, outside four positive humps. The shape of this hole corresponds to the shape of a porphyrinring. Obviously in extracting the lipids from the chloroplasts it was removed too [134, 164].

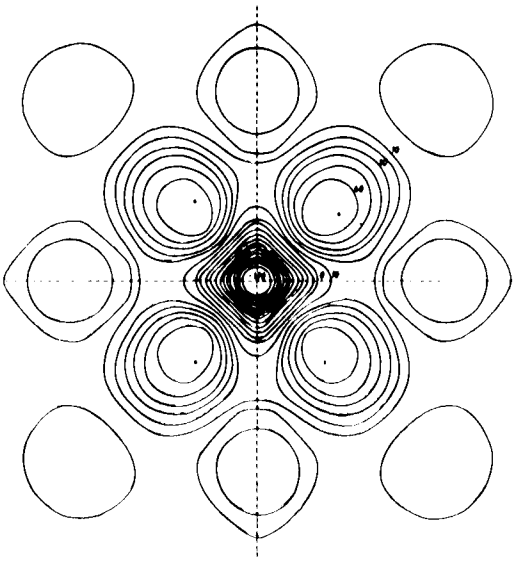

Fig. 16
Three dimensional electron density (arbitrary units) along $(x_1, x_2, 0)$ for the centrosymmetric solution of a lattice cell of chloroplast protein structure. The quadratic centre has the shape and size of a porphyrinring and is negative, since the porphyrinring of a chlorophylmolecule was removed by preparation from the proteinlayers.

Noncentrosymmetric solutions

In all the literature on small angle scattering only centrosymmetric shapes of particles are discussed, since direct informations about deviation from this symmetry are not available. If for instance the electron density $\rho_k(x)$ of a particle k has no centre of symmetry, it can always be synthetisized by an even density ρ_1, and an odd density ρ_2

$$\rho_1(x) = +\rho_1(-x);\ \rho_2(x) = -\rho_2(-x);\ \rho_k = \rho_1 + \rho_2$$

Then the Fouriertransform $R_1(R_2)$ of $\rho_1(\rho_2)$ is a real (imaginary) function and hence the particle factor $f_k^2(b)$ is defined by

$$|f_k^2(b)| = |R_1^2(b)| + |R_2^2(b)| \qquad (66)$$

$$R_1(b) = R_1(-b);\quad R_2(b) = -R_2(-b)$$

Observable is solely the sum $f_k^2(\mathbf{b})$. It represents a manyfold of solutions

$$|R_1^2(\mathbf{b})| \leqslant |f_k^2(\mathbf{b})|$$
$$|R_2^2(\mathbf{b})| = |f_k^2(\mathbf{b})| - |R_1^2(\mathbf{b})| \tag{67}$$

Though the conventional analysis of small angle scattering only discusses the special case $R_2(\mathbf{b}) = 0$, its importance for research in colloidal dimensions is obvious.

8. Further applications

High diluted systems

According to (38) an absolute measurement of the total small angle scattering gives direct information on the total number of electrons N_k in a particle k, if the interference term I_w (eq. (35)) can be neglected. Knowing the chemical composition of the particle, one obtains its molecular weight. For details see *Luzzati* [69. 168, 169] and *Kratky* [60, 61]. Taking moreover into account the relative course of $I_P(b)$ one obtains some more information: Solvents of cellulose nitrate for instance proved, that according to *Staudinger* the single chain molecules more or less are stretched [143]. Their mean lengths depend on the solvent, indicating that the chains are composed of statistical fibre elements with a length of ~ 200 A.

Similar investigations on tobacco mosaic virus prove, that in some solvents single monomers, in others small clusters of rodlike monomers exist [108].

Liquids near the critical point have an increasing $\Delta^2 N$ (eq. 21) indicating clustering effects and statistical droplets (In Argon see [181], Neon [180], paraffins [120]).

Similar cluster effects produce a typical small angle scattering in solvents near the critical temperature of solution. An example is given for C_7F_{16} in C_8H_{18}. In mixtures 1 : 1 maximal clusters of C_7F_{16} consisting of 140 molecules were observed [115, 116, 117].

Colloidal particle sizes and size distributions were investigated on gels [110, 111, 135], especially silicagel,and carbon black [117, 165, 172, 184]. Some investigations critically discussed the influence of polydispersity g_R and packing density ϵ^3 [115, 421] according to eq. [41, 44, 49]. Small angle scattering of graphite and carbon is sometimes explained by holes and dislocations [109, 119. 125, 126, 129, 170, 175].

Bulk polymers, glasses

In solid high polymers the intensity distribution along the equator and meridian (see Fig. 13) depends on heat treatment, stretching, pressing etc. The long period above a critical temperature increases with annealing time, if the sample afterwards is measured at room temperature (see e.g. [228a])

Measurements directly at the annealing temperature prove the existence of a reversible change of the long period and the total intensity [315, 326, 379].

An attempt was made to understand the complex phenomenon of supramolecular structures by introducing three mean types of chain conformation (see Fig. 14): α-type, crystalline like with backfolding within 3–5 monomers, β-type, mostly on the lateral grain boundaries of the ultrafibrils with a high percentage of kinks, caterpillars etc, and γ-type, mostly in the „amorphous" regions in the fiber direction between adjacent „crystalline" domains. At this moment only a few g_{ik}-values of the respective paracrystalline distortions are available, since the quantitative evaluation of the discontinuous small angle scattering is in the very beginning [370b].

This in combination with measurements of the macroscopic density, diamagnetic susceptibility, NMR as a function of annealing time and temperature, stretching etc. will give many new informations in future.

Since according to Fig. 15 there are many features in common between melt crystallized material and material crystallized from high diluted solution, small angle scattering seems to be a useful way of deciphering the supramolecular structure and its connection with the physico-chemical behaviour of high polymers [192, 267].

The similarity of the superstructure of synthetic high polymers and biological fibers is obvious. Aging and desease changes the superstructure of collagen [201, 157, 304]. The small angle scattering of glasses sometimes comes from micropores, produced by spinning [353] (cf. Fig. 12), sometimes by other heterogeneities [203, 234, 316, 330]. Sometimes reflexions on the surface play a role [368].

Metals

An intensive X-ray small angle intensity of deformed metals often is produced by twofold *Bragg* reflexions [382a, 389a, 401a, 402]. This could be proved directly by neutron scattering where a twofold scattering can be discarded [380, 382, 396]. Absolute intensity measurements, carefully corrected, are explained by clusters of vacancies and dislocation rings [384a], inhomogeneous strain distributions [1, 2] non linear dilatations [91, 92] or linear strain fields around step dislocations [9a].

Here reflections on the surfaces can also disturb the analysis [395, 404a]. The double Bragg reflections do not occur in plastically deformed single crystals, if not in reflection position [24, 385]. To get more detailed direct information, not only the total scattered intensity but its function $\mathbf{I(b)}$ should be measured.

Quenched or neutron irradiated metals produce a remarkable small angle scattering because of point defects [382, 398] or clusters of *Smekal* defects [396]. After annealing Cu at 570 °C the small angle scattering disappears. On annealing at lower temperatures clustering of the defects to holes with 20–40 Å diameter occurs if the samples before this were quenched with high velocity (~ 30000 °C/sek) [397].

Neutron small angle scattering of ferromagnetic metals gives small angle scattering effects of point defects and clusters about 100 times larger because of the magnetic inhomogeneities [62]. Thus better data were obtained on dislocation density and on average distances of families of dislocations in cold deformed Ni [399].

In metallic alloys as Al-Zn, Al-Cu, Au-Ni, Al-Ag, Al-Mg-Zn Guinier Preston zones give rise to small angle scattering. The shape and size of these zones,which can be analyzed directly [408], affect the electric conductivity, Young's modulus, hardness, Hall constant, thermo-potential etc. An example is given by Al-Zn alloys with 4–40 at % Zn [409]. Clusters with 69 at % Zn surrounded by a phase with 1,8 at % Zn are formed within one minute of annealing. By further annealing the clusters grow up to diameters of 2 R = 100 Å without changing their total volume. At 2 R ~ 35 Å the spherical zones become disc like and the Young's modulus and conductivity change in a characteristic way [414, 419, 420, 434, 435, 436, 437].

In Al-Ag-alloys on the other hand the Guinier Preston zones have an integral density equal $\bar{\rho}$, hence $\lim_{b \to 0} I_{obs} = 0$ (eq. 20): The Ag-atoms in certain domains migrate into clusters forming spherical clusters of higher Ag-concentration (90 at %) with an outer shell of low concentration and around this a phase unchanged in composition [433]. Some minutes afterwards at room temperature this phase has totally disappeared and the radii of the clusters increase from 10 to 70 Å [427]. The small angle scattering of Al-Cu-alloys is similar. However, on annealing at 200 °C a new phenomenon can be observed: In single crystals the small angle scattering no longer is spherically symmetric but shows the existence of platelets orthogonal to (100). Discussing the wide angle reflections one can prove that (100)-netplanes of Cu-atoms change with those of 25 at-% Cu, then pure Al, again 25 at-% Cu, etc. These atomistic lamellar like superstructures are called Guinier Preston II Zones [433] A small angle scattering in Au-Ni-alloys is disturbed by double Bragg-reflexions, hence could not be analyzed satisfactorily [439].

Small angle scattering on surfaces

If the waves touch a surface nearly tangentially, total reflection occurs since the refraction index of matter is smaller than unity, *Yoneda* [444] observed in addition to this a small angle scattering, which was explained by *Warren* and coworkers [433] as due to a nonplanar surface with roughnesses in colloidal dimensions. Objections that this phenomenon is produced by collimation errors [442] were refuted by *Guentert* [441]. Such surface studies open a new possibility of investigating the colloidal structure of surfaces.

This work was supported by the European Recovery Program in Berlin and the Deutsche Forschungsgemeinschaft. Dr. Kreutz from the Technical University Berlin-Charlottenburg kindly has given us recent results of his work. We are grateful for the help of *Dr. Ruscher* (Berlin, Teltow-Seehof), *Dr. Tsvankin* (Moscow) and *Dr. Damaschun* (Jena), who kindly supported us with literature references. *Professor Baily* (London) kindly has examined the English translation.

References

General references, mainly theoretical and comprehensive

[1] *Atkinson, H.H., Hirsch, P.B.,* Phil. Mag. **3**, 213 (1958), The Theory of Small Angle Scattering from Dislocations.

[2] *Atkinson, H.H., Hirsch, P.B.,* Phil. Mag. **3**, 862 (1958), The Theory of Small Angle Scattering from Extended Dislocations.

[2a] *Atkinson, H.H.,* J. appl. Phys. **30**, 637 (1959), Small Angle Scattering of X-rays and Neutrons from Deformed Metals.

[3] *Baro, R., Luzzati, V.,* Acta Cryst. **12**, 144-148 (1959), Diffusion Centrale Multiple des Rayons X par la Matiere Heterogne. II. Quelques Verifications Experimentales.

[4] *Beeman, W.W., Kaesberg, P., Anderegg, Y.M., Webb, M.B.,* Handbuch der Physik, **32**, 321-389 (1957), (Flügge), Size of Particles and Lattice Defects. A. Size and shape of particles from small angle x-ray scattering.

[5] *Beidl, G., Bischof, M., Glatz, G., Porod, G., v. Sacken, J.Ch., Wawra, H.,* Zs. f. Elektr.Chem. **61**, 1311-1318 (1957), Zur Röntgenkleinwinkelstreuung und Lichtstreuung verdünnter kolloider Systeme, Streukurven regelmäßiger Körper.

[6] *Betekhtin, V.I., Slutsker, A.I.,* Fis. Metall. I. Metalloved., **21**, 358 (1966), Das Verhältnis der doppelten Röntgenreflexionen im Innern und zwischen den Körnern in polykristallinen Metallen.

[7] *Betekhtin, V.I., Slutsker, A.I.,* Fiz. Tverdogo Tela (USSR), **8**, 767-73 (1966), Small Angle X-Ray Scattering by Mosaic Structure in Metals.

[8] *Bezirganyan,* Soviet Phys.-Technical Phys. **7**, 549-53 (1962), X-Ray Scattering in Gases, Liquids and Amorphous Bodies.

[9] *Bienenstock, A., Bagley, B.G.,* J. Appl. Phys. **37**, 4840-47 (1966), Calculations of upper bounds to the small angle scattering from crystallite models of amorphous materials.

[9a] *Blin, J.,* Acta Met. **5**, 528 (1957), Diffusion Centrale des Rayons X par les Dislocations.

[10] *Bonart, R.,* Kolloid-Z. **194**, 97 (1964), Parakristalline Schichtgitter in verstreckten Linearpolymeren. I. Die Querstruktur.

[11] *Bonart, R.,* Kolloid-Z. u. Z. f. Polymere, **211**, 14-33 (1966), Kolloidstrukturen in verstreckten Hochpolymeren. Streutheorie des parakristallinen Schichtgitters.

[11a] *Brumberger, H.,* (Ed.) Small Angle X-Ray Scattering, Proceedings of the conference held at Syracuse University, June 1965, Gordon & Breach, New York, (1967).

[12] *Brusset, H., Donati, J.R.,* C.R. Acad.Sci., (France), **261**, 1823-1826 (1965), Structure Scale of a Heterogeneous Substance by Multiple Scattering of X-Rays at Small Angles.

[13] *Brümmer, O., Klimanek, P.,* Z. Naturf. **161**, 1098-1100 (1961), Ein Beitrag zur Auswertung der Kontinuierlichen Röntgenkleinwinkelstreuung monodisperser verdünnter Systeme.

[14] *Bonart, R., Hosemann, R.,* Z.f. Elektrochem., Ber. d. Bunsenges. f. phys. Chem. **64**, 314-321 (1960), Zur Analyse der Langperiodeninterferenzen.

[15] *Burge, R.E., Draper, J.C.,* Acta Cryst. **22**, 6-13 (1967), Small Angle X-Ray Scattering by Rods and Sheets: The Interpretation of Line Collimation Results.

[16] *Caulfield, D., Ullman, R.,* J. appl. Phys. **33**, 1737 (1962), High-Angle Limit in Low-Angle Scattering and its Effect on the Determination of Surface Area.

[17] *Coll, H.*, Angew. Chem. **73**, 232–239 (1961), Strukturbestimmungen regelloser Strukturen mittels Streustrahlung.
[17a] *Croft, W.J.*, Encycl. Ind. Chem. Anal. **3**, 796-817 (1966), X-ray methods of analysis.
[18] *Debye, P., Anderson, H.R., Brumberger, H.*, J. appl. Phys. **28**, 679 (1957), Scattering by an Inhomogenous Solid. II. The Correlation Function and its application.
[19] *Debye, P.*, Z. Phys. **156**, 256-264 (1959), Röntgenstreuung in Körpern mit regelloser Struktur.
[20] *Fedorov, B.A.*, Vysokomol. Soedin. **8**, 1506 (1966), Theory of small angle x-ray scattering by long rigid macromolecules in solution.
[20a] *Feigin, L.A.*, Kristallografiya **12**, (2), 274-80 (1967), Absolute intensity of small-angle x-ray scattering with slit systems and calculation of molecular weight of macromolecules.
[21] *Filipovich, V.N.*, Zh. Tekh. Fiz. **26**, 398-416 (1956), and Soviet Phys.-Technical Physics **1**, 391-408 (1956), The Theory of Small-Angle Scattering of X-Rays.
[22] *Fournet, G.*, J. Phys. Radium, **17**, 940-3 (1956), The limiting value, for very Small-Angles, of the observable Intensity of X-Rays scattered by fluids.
[23] *Fournet, G.*, Hdb. der Physik, **32**, 238 (1957), (Flügge) Study of the Structure of Fluids and amorphous Substances by means of X-Ray Diffraction.
[24] *Fricke, H., Gerold, V.*, Z. f. Metallkunde, **50**, 136 (1959), Sekundäre Beugungserscheinungen von Röntgenstrahlen an verformten Metallen.
[25] *Gerold, V.*, Z. f. Elektrochem. **60**, 405–411 (1956), Zur Auswertung der Röntgen-Kleinwinkelstreuung mittels Fourieranalyse.
[26] *Gerold, V.*, Z. f. angew. Physik, **9**, 43 (1957), Die Kleinwinkelstreuung der Röntgenstrahlen und ihre Anwendung.
[27] *Gerold, V.*, Erg. exakt. Naturwiss. **33**, 105 (1961), Röntgenographische Untersuchungen von Gitterstörungen in Mischkristallen.
[27a] *Gerold, V.*, J. Phys. Rad. **23**, 812-16 (1962), Physical Properties of Solid Solutions containing Spherical Guinier-Preston Zones.
[28] *Guinier, A., Fournet, G., John Wiley & Sons*, Inc. New York (1955), Small-Angle Scattering of X-Rays.
[29] *Guinier, A.*, Solid State Physics, **9**, 293-398 (1959), Heterogenities in Solid Solutions.
[30] *Guinier, A., Gyon, E.*, J. appl. Phys. **30**, 622 (1959), Internal Double Reflection in a Perfect Crystal.
[30a] *Guinier, A.*, J. Phys. Rad. **23**, 791-794 (1962), Les zones de segregation dans les solutions solides.
[30b] *Guinier, A.*, X-Ray Diffraction in Crystals, Imperfect Crystals and Amorphous Bodies W.H. Freeman & Co. San Francisco, London (1963).
[31] *Heine, S.*, Makromol. Chem. **48**, 205 (1961), Diskussionsbeitrag zur Berechnung des Streuverhaltens am biegsamen Faden bei der Röntgenkleinwinkelstreuung.
[32] *Heine, S., Kratky, O., Porod, G., Schmitz, P.J.*, Makromol. Chem. XLIV-XLVI, 682-726 (1961), Eine verfeinerte Theorie der Röntgenkleinwinkelstreuung des verknäuelten Fadenmoleküls und ihre Anwendung auf Cellulosenitrat in Lösung.
[33] *Heine, S., Kratky, O., Roppert, I.*, Makromol.Chem. **56**, 150-168 (1962), Lichtstreuung und Röntgenkleinwinkelstreuung von statistisch verknäuelten Fadenmolekülen, berechnet nach der „Monte-Carlo-Methode".
[34] *Heine, S.*, Makromol. Chem. **71**, 86-109 (1964), Über den Einfluß des ausgeschlossenen Volumens und einer verschieden dichten Belegung mit Streuzentren auf das Streuverhalten von Irrflugketten und die Folgerungen für frühere Streukurven-Berechnungen bei Fadenmolekülen.

[35] *Hight, R., Schmidt, P.W.*, Bull. Am.-Phys. Soc. **2**, 340, Small-Angle Scattering from Ellipsoids of Revolution.
[36] *Hosemann, R.*, Z. f. Elektrochem. Ber. d. Bunsenges. f. phys. Chem. **58**, 271-280 (1954), Analyse der Kleinwinkelstreuung mittels Faltungsoperationen.
[36a] *Hosemann, R.*, Die Naturwissenschaften, **41**, 440-446 (1954), Parakristalline Strukturen.
[36b] *Hosemann, R.*, Zur Struktur und Materie der Festkörper, Diskussionstagung der Sektion für Kristallkunde der Deutschen Mineralogischen Gesellschaft Mai 1951, S. 127-222.
[37] *Hosemann, R.*, Z. Elektrochem. **60**, 412 (1956), Bemerkung zur Arbeit von V. Gerold: Zur Auswertung der Kleinwinkelstreuung mittels Fourieranalyse.
[38] *Hosemann, R.*, Z. Elektrochem. **60**, 188 (1956), Zur Theorie der Kleinwinkelstreuung.
[39] *Hosemann, R., Joerchel, D.*, Koll. Z. **152**, 49 (1957), Modellversuche zur kontinuierlichen und diskontinuierlichen Kleinwinkelstreuung.
[40] *Hosemann, R., Motzkus, F.*, Makromol. Chem. **59**, 79 (1960), Analyse der kontinuierlichen Kleinwinkelstreuung amorpher kolloider Systeme.
[41] *Hosemann, R., Motzkus, F.*, 4. Intern. Kongreß Elektronenmikroskopie Berlin 1958, Verhandlungen Springer-Verlag, 743-745 (1960), Polydispersität kolloider Systeme.
[42] *Hosemann, R., Bagchi, S.N.*, North-Holland Publ. Comp. Amsterdam (1962), Direct Analysis of Diffraction by Matter.
[43] *Hyväringen, L.P.*, Ann. Acad. Sci. Fennicae AVI, **45**, 10 (1960), The coherent scattering of X-Rays in the direction of the primary beam.
[44] *Jan, J.P.*, Z. angew. Math. Phys. (Schweiz) **14**, 1-11, Small-Angle Scattering of X-Rays.
[45] *Kirste, R., Porod, G.*, Kolloid-Z. u. Z. f. Polymere **184**, 1-7 (1962), Röntgenkleinwinkelstreuung an Kolloiden Systemen – Asymptotisches Verhalten der Streukurven.
[46] *Kirste, R.*, Z. Phys. Chem. N.F. **36**, 265-279 (1963), Röntgenkleinwinkelstreuung an fadenförmigen Makromolekülen. Der Einfluß des Fadenquerschnittes.
[47] *Kirste, R.G.*, Z. Phys. Chem. N.F. **42**, 351-357 (1964), Röntgenkleinwinkelstreuung an Fadenmolekülen. Abhängigkeit von der Elektronendichteverteilung im Fadenquerschnitt.
[48] *Kirste, R.G.*, Z. phys. Chem. N.F. **42**, 358-366 (1964), Röntgenkleinwinkelstreuung an Fadenmolekülen. Berechnung der Streukurven von Helices.
[49] *Kirste, R.G., Wunderlich, W.*, J. Polym. Sci. (b) **3**, 851-854 (1965), The determination of the thermodynamic parameters of solutions of polymer coils from X-Ray Small-Angle measurements.
[50] *Kirste, R.G., Wunderlich, W.*, Makromol. Chem. **87**, 60 (1965), Röntgenkleinwinkelstreuung an Fadenmolekülen in Lösung. Zum Problem der Elimination der Lösungsmittelstreuung.
[51] *Klimanek, P.*, Ann. Phys., Lpz. **14**, 71-77 (1964), Zur Auswertung der kontinuierlichen Röntgenkleinwinkelstreuung dreiachsiger Ellipsoide.
[52] *Knapp, H.*, Z. angew. Phys. 9,233-9 (1957), Anwendung der Röntgenkleinwinkelstreuung zur Untersuchung technischer Präparate.
[53] *Kratky, O.*, Z.f. Elektrochem., Ber. d. Bunsenges. f. phys. Chem. **60**, 245-261 (1956), Bestimmung der Gestalt von korpuskularen und fadenförmigen Makromolekülen nach der Röntgenkleinwinkelmethode.
[54] *Kratky, O., Porod, G.*, Z. Physik. Chem. **7**, 236-241 (1956), Einfache Betrachtungen über interpartikuläre Interferenzeffekte bei der Röntgenkleinwinkelstreuung.

[55] *Kratky, O.,* Die Makromolekulare Chemie, XXXVA, 12-48 (1959), Ergebnisse der Röntgenkleinwinkelstreuung bei der Bestimmung der Größe und Gestalt von Makromolekülen in Lösung.

[56] *Kratky, O.,* Angew. Chemie, **72,** 467-482 (1960), Diffuse Röntgenkleinwinkelstreuung. Bestimmung von Größe und Gestalt von Kolloidteilchen und Makromolekülen.

[57] *Kratky, O.,* Z. f. analytische Chem. **181,** 480-481 (1961), Messung der Absolutintensität der Röntgenkleinwinkelstreuung von Kolloidteilchen und Makromolekülen zur Bestimmung ihrer Größe und Gestalt.

[58] *Kratky, O.,* Moderne Methoden der Pflanzenanalyse, herausgeg. v. Linkens und Tracey, Springer-Verlag, Berlin, Göttingen, Heidelberg, S. 336 (1962), Diffuse Röntgenkleinwinkelstreuung.

[59] *Kratky, O.,* Kolloid-Z. u. Z. f. Polymere, **182,** 7-24 (1962), Das Studium gelöster Fadenmoleküle mittels der Röntgenkleinwinkelmethode.

[60] *Kratky, O.,* Progress in Biophysics. Pergamon Press London, **13,** 105-173 (1963), X-Ray Small-Angle Scattering with Substances of Biological Interest in Diluted Solutions.

[61] *Kratky, O.,* Z. analyt. Chem. **201,** 161 (1964), Die Messung der Absolutintensität der diffusen Röntgenkleinwinkelstreuung – ein Verfahren zur „Wägung" in makromolekularen Systemen.

[61a] *Kratky, O.,* Nachr. Akad. Wiss. Göttingen, math.-phys. Kl. 1966, 123–188, Nr. 6, Extreme Anwendungen des Röntgenkleinwinkelverfahrens zum Studium von Kolloiden und Makromolekülen.

[62] *Kronmüller, H., Seeger A., Wilkens, M.,* Z. Phys. **171,** 291-311 (1963), Depolarisation und Kleinwinkelstreuung von Neutronen durch Gitterfehler in ferromagnetischen Kristallen.

[63] *Lambert, M., Guinier, A.,* J. Phys. Rad. **17,** 420 (1956), Sur l'Élargissement d'un Faisceau de Rayons X par Traversée d'une Matiere Hétérogène.

[64] *Letcher, J.H., Schmidt, P.W.,* J. Appl. Phys. (USA) **37,** 649-55 (1966), Small-Angle X-Ray Scattering Determination of Particle Diameter Distributions in Poly-Disperse Suspensions of Spherical Particles.

[64a] *Lutts, A.,* Advanc. X-Ray Anal. 6, 25-42 (1963), The X-Ray Investigation of Precipitation in Supersaturated Solid Solutions.

[65] *Luzzati, Acta Cryst.* **10,** 136-138 (1957), Interpretation Geometrique de la Diffusion aux Petits Angles d'un Faisceau de Rayons X de Section Infiniment Haute et Étroite.

[66] *Luzzati, V.,* Acta Cryst. **10,** 643 (1957), Diffusion Centrale Multiple des Rayons X par la Matiere Heterogene. I. Etude Théorique.

[67] *Luzzati, V.,* Acta Cryst. **10,** 136–138 (1957), Interpretation Geometrique de la Diffusion aux Petits Angles d'un Faisceau de Rayons X de Section Infiniment Masses et Correction du Polychromatisme.

[68] *Luzzati, V.,* Acta Cryst. **11,** 843 (1958), Determination du Rayon de Gyration et du Volume d'une Particule par la Diffusion des Rayons X aux petits Angles, lorsque le Faisceau incident est infiniment haut et étroit.

[69] *Luzzati, V.,* Acta Cryst. **13,** 935-45 (1960), Interpretation of Absolute Measurements of X-Ray Central Scattering in Point-and Linear Collimation: Solutions of Globular and Rod-like Particles.

[70] *Luzzati, V.,* X-Ray Optics and X-Ray Microanalysis, S. 133 New York Academic Press (1963).

[71] *Malmon, A.G.*, Acta Cryst. **10**, 639 (1957), Small-Angle X-Ray Scattering Functions for Ellipsoids of Revolution and Right Circular Cylinders.

[72] *Mering, J., Tchoubar-Vallat, D.*, C.R. Acad. Sci. B. (France) **262**, 1703-6 (1966), Small-Angle Scattering of X-Rays by Concentrated Systems.

[73] *Miller, A., Schmidt, P.W.*, J. math. Phys. **3**, 92-6 (1962), Small-Angle X-Ray Scattering from Randomly Oriented Cylinders of Arbitrary Cross-Section.

[74] *Mittelbach, P., Porod, G.*, Acta Physica Austriaca, 14, 185-211 (1961), Zur Röntgenkleinwinkelstreuung verdünnter kolloider Systeme. Die Berechnung der Streukurven von Parallelepipeden.

[75] *Mittelbach, P., Porod, G.*, Acta Physica Austriaca. **14**, 406-439 (1961), Zur Röntgenkleinwinkelstreuung verdünnter kolloider Systeme VI. Die Berechnung der Streukurven von elliptischen Zylindern und Hohlzylindern.

[76] *Mittelbach, P., Porod, G.*, Acta Physica Austriaca, **15**, 122 (1962), Zur Röntgenkleinwinkelstreuung verdünnter Systeme VII. Die Berechnung der Streukurven von dreiachsigen Ellipsoiden.

[77] *Mittelbach, P.*, Acta Phys. austr. **19**, 53-102 (1964), Zur Röntgenkleinwinkelstreuung verdünnter kolloider Systeme. VIII. Diskussion des Streuverhaltens regelmäßiger Körper und Methoden zur Bestimmung von Größe und Form kolloider Teilchen.

[78] *Mittelbach, P., Porod, G.*, Kolloid-Z. u. Z. f. Polymere **202**, 40 (1965), Zur Röntgenkleinwinkelstreuung kolloider Systeme. Die mittleren Durchschußlängen und die Kohärenzlänge eines kolloiden Systems, Kennzahlen zur Ermittlung von Teilchenform und Polydispersitätsgrad.

[79] *Mittelbach, P., Porod, G.*, Kolloid-Z. u. Z. f. Polymere **203**, 162 (1965), Zur Röntgenkleinwinkelstreuung kolloider Systeme.

[80] *Mittelbach, P.*, Kolloid-Z. u. Z. f. Polymere, **206**, 152–159 (1965), Einige spezielle Bestimmungsmethoden von Form und Polydispersität kolloider Teilchen in verdünnter Lösung mittels Röntgenkleinwinkelstreuung.

[80a] *Motzkus, F.*, Acta Cryst. **12**, 773 (1959), Untersuchung kolloider Systeme auf Partikelgröße und Polydispersität mit Hilfe der Röntgenkleinwinkelstreuung.

[81] *Motzkus, F., Hosemann, R.*, Makromol. Chem. **39**, 96 (1960), Röntgenographische Bestimmung der Polydispersität und Partikelgröße.

[81a] *Patou, C., Khan, R.*, C.R. Acad. Sci., Paris, Ser. A.B., **264B**, No. 17, 1275-8, (1967) Detection of a simple small scattering angle by the vector method. Procedure for the sum of two second consecutive differences.

[82] *Peterlin, A.*, J. Polym. Sci. **47**, 403-415 (1960), Light Scattering and Small-Angle X-Ray Scattering by Macromolecular coils with finite persistence length.

[83] *Peterlin, A.*, Makromol. Chem. **87**, 152 (1965), Small-Angle Scattering by a three component system.

[84] *Pigin, V.M., Terminasov, J.S., Tusov, L.V.*, Kristallografia **10**, 311 (1965), Transl.: Sov-Phys.-Crystallography **10**, 253-257 (1965), Intensity of Double Intergrain Reflections of X-Rays for Very Small Scattering Angles.

[85] *Plavnik, G.M., Rovinskii, B.M.*, Fiz.Tverd. Tela, **2**, 1099-1106 (1960), Soviet Physics-Solid State **2**, 934-1000 (1960), Investigation of the Sub-microscopic Structure of Slightly absorbing Materials by a Method of „Multiple Small-Angle Scattering of X-Rays".

[86] *Porai-Koshits, E.A., Filipovich, V.V.*, Izd. A. N. SSSR Moskau, S. 7 (1958), Some new possibilities in the small-angle X-ray scattering method. Methods of Investigation the Structure of Highly Disperse and Porous Bodies.

[87] *Reinhold, Chr., Fischer, E.W., Peterlin, A.*, J. Appl. Phys. **35**, 71-74 (1964), Evaluation of Small-Angle X-Ray Scattering of Polymers.

[88] *Schmidt, P.W.*, Acta Cryst. **11**, 674 (1958), The Small-Angle X-Ray Scattering from Polydisperse Solutions of Ellipsoidal Particles.

[89] *Schmidt, P.W., Hight, R. jr.*, J. appl. Phys. **30**, 866-71 (1959), Calculation of the Intensity of Small-Angle X-Ray Scattering at relatively large scattering angles.

[90] *Schmidt, P.W.*, J. Math. Phys. **7**, 1295-1299 (1966), Small-Angle X-Ray Scattering from Rods and Platelets.

[90a] *Schmidt, P.W.*, J. Math. Phys. (N.Y.) 8 (3) 475-7 (1967), Calculation of intersect distribution functions in small angle x-ray scattering.

[91] *Seeger, A.*, Z. Naturf. **11a**, 724 (1956), Über die Erforschung der Versetzungsdichte und Versetzungsanordnung in plastisch verformten Kristallen mit Hilfe der Kleinwinkelstreuung von Röntgenstrahlen.

[92] *Seeger, A.*, Act. Met. **5**, 24 (1957), Die Ursache der Kleinwinkelstreuung von Röntgenstrahlen in plastisch verformten Metallen.

[93] *Seeger, A.*, J. appl. Phys. **30**, 629 (1959), Small-Angle Scattering from Dislocations in Deformed Single Crystals.

[94] *Seeger, A., Kröner, E.*, Z. Naturf. **14a**, 74 (1959), Theorie der Kleinwinkelstreuung von Röntgenstrahlen und Neutronen durch innere Spannungen in festen Körpern, insbesondere durch Versetzungen.

[95] *Seeger, A., Rühle, M.*, Ann. Phys. **7**, 216 (1963), Zur Theorie der Kleinwinkelstreuung von Röntgenstrahlen und Neutronen durch Versetzungsringe.

[96] *Shashkov, O.D., Biunov, N.N.*, Fiz. Metall. i Metalloved. **16**, 681-685 (1963), Berechnung der Intensitätsverteilung gestreuter Röntgenstrahlen in der Nähe eines reziproken Gitterpunktes für gealterte Al-Ag-Legierung im Zonenstadium und die Bestimmung der Dimensionen der Guinier-Preston-Zonen.

[97] *Smoluchowski, R., Li, Y.Y.*, Phys. Rev. **94**, 866 (1954), On the Theory of X-Ray Small-Angle Scattering.

[98] *Soule, J.L.*, J. Phys. Radium **18**, 90A-102A (1957), The Determination of Specific Surfaces and Interfaces by Small-Angle Scattering of X-Rays.

[98a] *Springer, T., Schmatz, W.*, Bull. Soc. Fr. Min. Crist. 90, 428–435 (1967), Small Angle Scattering with Neutrons.

[99] *Stokes, A.R.*, Proc. Phys. Soc. **75**, 489-97 (1960), The Theory of Light Scattering and X-Ray Low-Angle Scattering by semi-stiff chain Moelcules.

[99a] *Synecek, V.*, J. Phys. Rad. **23**, 828-9 (1962), On the Spatial Distribution of Isotropic Guinier-Preston-Zones.

[100] *Tchoubar-Vallat, D., Méring, J.*, C. R. Acad. Sci. **261**, 3096-3099 (1965), Low Angle Scattering of X-Rays by Dilute Suspensions of Particles. Determination of the Distribution of Chords.

[101] *Tchoubar-Vallat, D., Méring, J.*, C. R. Acad. Sci., Paris **261**, 3361-3363 (1965), Diffusion centrale des rayons X par des systemes dilués de particules. Détection de la présance des arêtes.

[101a] *Tchoubar-Vallat, D., Méring, J.*, C. R. Acad. Sci. Paris, Ser. A. B. **263**, B(17) 981-4 (1966), Central scattering of X-Rays used to determine the porosity of concentrated systems.

[102] *Toman, K.*, Acta Cryst. **8**, 587 (1955), The Structure of Guinier-Preston-Zones. I. The Fourier Transform of the Diffuse Intensity Diffracted by a G.-P. Zone.

[103] *Tsvankin, D.Ya.*, Vysokomol. soyed. **6**, 2078-82 (1964), Transl.: Polymer Sci. USSR **6**, 2304-2309 (1964), Diffraction on a Linear System of Crystallites: Long Period in Polymers-I.

[104] *Tsvankin, D.Ya.*, Vysokomol. soyed. **6**, 2083-89 (1964), Transl.: Polymer Sci. USSR **6**, 2310-2322 (1964), Diffraction on a Linear System of Crystallites: Long Periods in Polymers-II.

[104a] *Tsvankin, D.Ya*, Kristallografia, **12**, 555-559 (1967), Beugung an linearen Systemen von Teilchen mit beliebigem Formfaktor.

[104b] *Vonk, C.G., Kortleve, G.*, Kolloid-Z. u. Z. Polym. **220**, (1), 19-24 (1967), X-Ray Small-Angle Scattering of bulk polyethylene. II. Analysis of the scattering curve.

[105] *Warren, B.E.*, Acta Cryst. **12**, 837-41 (1959), Small-Angle Intensities from double Reflections in Powder Samples.

[106] *Warren, B.E.*, Z. f. Kristallogr. **112**, 255-262 (1959), Small-Angle Scattering from Large Volumes.

[107] *Weigel, D., Renouprez, A., Boris, Imelik*, J. chim. phys. **62**, 125-130 (1965), Application de la diffusion centrale des Rayon X a l'etitude des solides poreux. I. Presentation, synthese et perfectionnement des theories de la diffusion centrale des rayons X.

[107a] *Zhurkov, S.N., Betekhtin, V.I. Slutsker, A.I.*, Fis. Metall. i. Metalloved. **17**, 564 (1964), Das zeitliche Verhalten der Festigkeit von Zweiphasenlegierungen auf Aluminium-Grundlage.

[107b] *Vainshtein, B.K.*, Diffraction of X-Rays by Chain Molecules. Elsevier Publ. Comp. Amsterdam (1966).

Solutions, liquids, colloidal particels

[108] *Anderer, F.A., Kratky, O., Lo, R.*, Z. Naturforschg. **19b**, 906-916 (1964), Untersuchung des gelösten Tabakmosaikvirus-Proteins mittels der Röntgen-kleinwinkelstreuung unter Verwendung der Absolutintensität.

[109] *Auleytner, J., Lefeld, M.*, Bull. Acad. Polon. Sci. Cl. **3**, 291-4 (1957), Anisotropic Small-Angle Scattering of X-Rays in Graphite.

[110] *Bale, H.D., Schmidt, P.W.*, J. Phys. Chem. **62**, 1179-84 (1958), Small-Angle X-Ray Scattering from Aluminium Hydroxyd Gels I.

[111] *Bale, H.D., Schmidt, P.W.*, J. chem. Phys. 31, 1612-18 (1959), Small-Angle X-Ray Scattering from Aluminium Hydroxyd Gels II.

[112] *Bielig, H.J., Kratky, O., Steiner, S., Wawra, H.*, MH. Chem. **94**, 989 (1963), Röntgenkleinwinkelmessungen an Ferritin in Lösung.

[113] *Bielig, H.J., Kratky, O., Rohns, G., Wawra, H.*, Tetrahedron Letters **38**, 2701 (1964), Röntgenkleinwinkeluntersuchung von Apoferritin in Lösung.

[114] *Bonse, U., Hart, M.*, Z. Phys. **189**, 151-162 (1965), Small-Angle X-Ray Scattering by Spherical Particles of Polystyrene and Polyvinyltoluene.

[115] *Brady, G.W.*, J. Chem. Phys. **32**, 45 (1960), Cluster Formation in Perfluoroheptane -i-Octane Systems near the Consulute Temperature.

[116] *Brady, G.W., Petz, Y.I.*, J. Chem. Phys. **34**, 332 (1961), Clustering in the critical region.

[117] *Brady, G.W., Frisch, H.L.*, J. Chem. Phys. **35**, 2234 (1961), Some further observations on the critical region.

[118] *Bragg, R.H., Corvin, I., Buttrey, J.W.*, J. appl. Phys. **31**, 1183 (1960), Small-Angle Scattering Investigation of Ludox-Mixtures.

[119] *Bragg, R.H., Hammond, M.L., Robinson, I.C., Anderson, P.L.*, Nature **200**, 555 (1963), Small-Angle Scattering by Pyrolytic Graphite.

[120] *Buttrey, J.W.*, J. Chem. Phys. **26**, 1378 (1957), Small-Angle X-Ray Scattering from the Low Carbon Paraffins.

[120a] *Cabrini, A., Celotti, G., Zanneti, R.*, Comitato Nazionale Energia Nucleare RT/MET (68) 1, Roma 68, Carakterizzazione per diffrazione dei raggi x a baso angolo di ossido di Torio colloidale.

[121] *Chu, B.*, J. Chem. Phys. **42**, 426-429 (1965), X-Ray Study of Critical Opalescence of Polystyrene in cyclohexane.

[122] *Chu, B.M., Pallesen, W.P., Kao, W.P., Andrews, D.E., Schmidt, P.W.*, J. Chem. Phys. **43**, 2950 (1965), Critical Opalescence of a Fluorocarbon-Hydrocarbon Binary Liquid Mixture: Natural Perfluoroheptan. Isooctane.

[122a] *Chu, B., Creti, D.M.T.*, J. Chem. Phys. 71, 6, 1943-46 (1967) Small angle X-ray scattering from Macroreticular Sulfonic and Cation exchange Resin-Amberlyst 15

[122b] *Clarke, A. L.*, J. Sci. Instr. 44, 383–384 (1967), Density Determinations on Small Liquid Samples.

[123] *Cleemann, J.C., Kratky, O.*, Z. f. Naturforschung, **15b**, 467-535 (1960), Größe, Gestalt und Solvatation des Edestinmoleküls aus dem Studium der Röntgenkleinwinkelstreuung.

[124] *Damaschun, G.*, Tagungsbericht der 3. Jahrestagung der Biochemischen Gesellschaft der DDR, S. 6-10, Suhl (1966), Einige Probleme bei der Untersuchung von Eiweißmolekülen mittels der Röntgenkleinwinkelstreuung.

[125] *Davidova, M.A., Plavnik, G.M.*, Isvestia Akad. Nauk SSSR, OTN, Metallurgia i Toplivo **4**, 185-187 (1959) , Untersuchung der Submikriporosität der Kohlen aus dem Kusnezbecken mit Hilfe der Röntgenkleinwinkelstreuung.

[126] *Davidova, N.A., Plavnik, G.M.*, Isvestia Akad. Nauk SSSR, OTN, Metallurgia i Toplivo 6, 150-155 (1960), Die Anwendung der Methode der Röntgenkleinwinkelstreuung auf die Untersuchung von submikroporösen Kohlen.

[127] *Dembo, A.T., Sosfenov, N.I., Feigin, I.A.*, Kristallografia **11**, 581 (1966), Untersuchung der Lösungen von Transportribonukleinsäure (s-RNS) mittels Röntgenkleinwinkelstreuung.

[127a] *Dembo, A.T., Sosfenov, N.I., Feigin, L.A.*, Sov. Phys. Crystallography, **11**, 508-513 (1967), Study of Solutions of Transfer Ribonucleic Acid (s-RNA) by Means of Small-Angle X-Ray Scattering.

[127b] *Dorosh, A.K.*, Zh. Prikl. Spektrosk., 6, No. 4 348-50 (1967), Low-angle maxima on the curves of X-Ray Scattering intensity in electrolytes.

[127c] *Dorosh, A.K., Skyshevskij, A.F.*, Zh. Strukt. Khim. 8, (2) 348-50 (1967), Low-angle maxima on the curves of X-Ray Scattering intensity in electrolytes.

[128] *Dragsdorf, R.D.*, J. appl. Phys. **27**, 620 (1956), Small-Angle X-Ray Scattering.

[129] *Eeles, W.T.*, Nature, **188**, 287-9 (1960), Small-Angle X-Ray Scattering by Pile-Irradiated Graphite.

[129a] *Feigin, L.A.*, Kristallografiya, **12**, 274-80 (1967), Absolute intensity of Small-Angle X-Ray Scattering with slit systems and calculation of molecular weight of macromolecules.

[129b] *Fedorov, B.A., Aleshin, V.G.*, Vysokomolekul. Soedin, **8**, 1506-12 (1966), Theory of Small-Angle X-Ray Scattering by Long Rigid Macromolecules in Solution.

[130] *Furukawa, K.*, Rep. on Prog. in Phys. **25**, 430 (1962), Radial distribution curves of liquids by diffraction methods.

[130a] *Hight jr., R., Higdon, W.T., Schmidt, P.W.*, J. chem. Phys. **33**, 1656-61 (1960), Small-Angle X-Ray Scattering Study of Sodium Montmorillonite Clay Suspensions.

[131] *Hight jr. R., Higdon, W.T., Darley, H.C.H., Schmidt, P.W.*, J. chem. Phys. **37**, 502-10 (1962), Small-Angle X-Ray Scattering from Montmorillonite Clay Suspensions. II.

[132] *Holasek, H., Kratky, O., Mittelbach, P., Wawra, H.*, J. Molec. Biol. 7, 321 (1963), Small-Angle X-Ray Scattering of Bence-Jones Protein.

[133] *Holasek, H., Kratky, O., Mittelbach, P., Wawra, H.*, Biochem. Biophys. Acta **79**, 76 (1964), Small-Angle Scattering of Bence-Jones Protein.

[134] *Hosemann, R., Kreutz, W.*, Die Naturwissenschaften **53**, 298–304 (1966), On the Tertiary Structure of the Protein Layers of Chloroplasts.

[135] *Kanig, G., Karge, H.*, J. colloid and Interface Sci. **21**, 649-663 (1966), Volumetric and Electronmicroscopic Investigation of the Melting and Freezing of Organic Gels.

[136] *Kasai, N., Kakudo, M., Watasa, T.*, Technol. Rep. Osaka Univ. **8**, 443-53 (1958), Study on the Structure of finely divided Solids by X-Ray Small-Angle Scattering Particle Size Determination of Silica Gels.

[137] *Kasai, N.*, Technol. Rep. Osaka Univ. **10**, 833-7 (1960), The Study on the Structure of Finely Divided Solids by X-Ray Small-Angle Scattering. II. Particle Size Determination of Carbon Black.

[138] *Kirste, R., Kratky, O.*, Z. f. Phys. Chem. Neue Folge, **31**, 363 (1962), Die Bestimmung der Persistenzlänge von gelöstem Polymethylmethacrylat aus der Röntgenkleinwinkelstreuung in verschiedenen Lösungsmitteln.

[138a] *Kirste, R.G.*, J. Polym. Sci. Part C, **16**, 2039-48 (1967), New calculations for Small-Angle X-Ray Scattering of filamentary molecules. Determination of the shape of segments.

[139] *Kratky, O., Sekora, A., Pilz, I.*, Z. Naturforschg. **9b**, 803 (1954), Eine Bestätigung der Pauling-Corey'schen Helix-Vorstellung aus Röntgenkleinwinkelmessungen an nativem Seidengel.

[140] *Kratky, O., Sembach, H.*, Makromol. Ch. **16**, 115 (1955), Der Verknäuelungsgrad von gelöstem Cellulosenitrat nach der Röntgenkleinwinkelmethode (I).

[141] *Kratky, O., Porod, G., Sekora, A., Paletta, B.*, J. Polymer, Sci. 16, 163 (1955), Determination of the Shape of Gamma-Globulin by Means of the X-Ray Low-Angle Method.

[142] *Kratky, O., Sembach, H.*, Makromol. Ch. **18/19**, 463 (1956), Der Verknäuelungsgrad von gelöstem Cellulosenitrat nach der Röntgenkleinwinkelmethode (II).

[143] *Kratky, O., Breiner, R.*, Makromol. Ch. **25**, 134 (1957), Der Verknäuelungsgrad von gelöstem Cellulosenitrat nach der Röntgenkleinwinkelmethode (III).

[144] *Kratky, O., Paletta, B., Porod, G., Strohmaier, K.*, Z. f. Naturforschg. **12b**, 287-292 (1957), Zur Querschnittsbestimmung des Tabakmosaikvirus (TMV) mittels der Röntgenkleinwinkelmethode.

[145] *Kratky, O., Kreutz, W.*, Angewandte Chemie, **70**, 134 (1958), Gestaltbestimmung der Hämoglobin-Molekel mit der Röntgenkleinwinkelmethode.

[146] *Kratky, O., Sand, H.*, Kolloid-Z. **172**, 18 (1960), Röntgenkleinwinkeluntersuchungen an Naturkautschuklösungen.

[147] *Kratky, O., Kreutz, W.*, Z. f. Elektrochem. **64**, 880-886 (1960), Bestimmung von Molekulargewicht, Größe, Gestalt und Hydratation von α_2-Makroglobulin aus der diffusen Röntgenkleinwinkelstreuung.

[148] *Kratky, O., Pilz, I., Schmitz, P.J., Oberdorfer, R.*, Z. f. Naturforschg. **18b**, 180-188 (1963), Bestimmung der Größe und Gestalt des γ-Globulinmoleküls mit der Röntgenkleinwinkelmethode.

[149] *Kratky, O., Wawra, H., Pilz, I., Sekora, A., van Deinse, A.*, MH. Chem. **95**, 359 (1964), Röntgenkleinwinkeluntersuchungen an Lösungen von nativer Seide.

[150] *Kratky, O., Ledwinka, H., Pilz, I.,* Ber. d. Bunsenges. f. phys. Chem. **70,** 904-912 (1966), Röntgenkleinwinkeluntersuchungen unter Verwendung der absoluten Streuintensität an Lösungen des Azofarbstoffes Chlorantinlichtviolett 2RLL.

[151] *Kratky, O., Ledwinka, H., Pilz, I.,* MH. Chem. **97,** 922-925 (1966), Assoziation des Azofarbstoffs Chlorantinlichtviolett 2RLL in Lösung nach der Röntgenkleinwinkelmethode.

[152] *Kratky, O., Leopold, H.,* J. Colloid Interface, Sci. **22,** 197-202 (1966), X-Ray Small-Angle investigation on titanium dioxide emulsions in lenseed oil.

[153] *Kratky, O., Leopold, H., Puchwein, G.,* Kolloid-Z. u. Z. f. Polymere, **216-217,** 255-264 (1967), Molekulargewicht und Gestalt von niedermolekularen Cellulosenitraten in Lösung nach der Röntgenkleinwinkelmethode.

[154] *Kratky, O., Pilz, I., Ledwinka, H.,* MH. f. Chem. **98,** 227 (1967), Assoziation des Azofarbstoffes β-Naphtolorange in Lösung nach der Röntgenkleinwinkelmethode.

[155] *Kratky, O., Pilz, I., Ledwinka, H.,* Chimia, **21,** 96-99 (1967), Röntgenkleinwinkeluntersuchungen an Lösungen eines Anthrachinonfarbstoffes.

[155a] *Kratky, O., Ledwinka, H., Pilz, I.,* Makromol. Chem. **105,** 171-192 (1967), Röntgenkleinwinkeluntersuchungen an Lösungen von β-Naphtholorange.

[156] *Kreutz, W., Kratky, O.,* Mh. f. Chemie, **89,** 169-172 (1958), Gestaltbestimmung des Hämoglobulinmoleküls mittels der Röntgenkleinwinkelstreuung.

[157] *Kreutz, W., Menke, W.,* Z. f. Nat. Forsch. **15b,** 402-410 (1960), Strukturuntersuchungen an Plastiden, I. Bestimmung der Dicke der Proteinlamellen aus der diffusen Röntgenkleinwinkelstreuung.

[158] *Kreutz, W., Menke, W.,* Z. f. Nat. Forsch. **15b,** 483-487 (1960), Strukturuntersuchungen an Plastiden. II. Röntgenographische Untersuchungen wasserfreier isolierter Chloroplasten.

[159] *Kreutz, W., Menke, W.,* Z. f. Nat. Forsch. **17b,** 675-683 (1962), Strukturuntersuchungen an Plastiden, III. Röntgenographische Untersuchungen an isolierten Chloroplasten und Chloroplasten lebender Zellen.

[160] *Kreutz, W.,* Z. f. Nat. Forsch. **18b,** 567-571 (1963), Strukturuntersuchungen an Plastiden, IV. Über das zweidimensionale Gitter in der Proteinlamelle.

[161] *Kreutz, W.,* Z. f. Nat. Forsch. **18b,** 1098-1104 (1963), Strukturuntersuchungen an Plastiden, V. Bestimmung der Elektronendichte-Verteilung längs der Flächennormalen im Thylakoid der Chloroplasten.

[162] *Kreutz, W.,* Z. f. Nat. Forsch. **19b,** 441-446 (1964), Strukturuntersuchungen an Plastiden, VI. Über die Struktur der Lipoproteinlamellen in Chloroplasten lebender Zellen.

[163] *Kreutz, W.,* Nature, **206,** 1358-1359 (1965), Sub-structure of Quantasomes.

[164] *Kreutz, W., Weber, P.,* Die Naturwissenschaften, **53,** 11-14 (1966), About the Proteinstructure of Quantasomes.

[165] *Kuroda, H.,* J. Coll. Sci. **12,** 496 (1957), X-Ray Small-Angle Scattering of Carbon Blacks.

[166] *Lambert, M. Guinier, A.,* C.R.Acad. Sci. **241,** 1057-9 (1955), Broadening of a Beam of X-Rays in Passage through Heterogeneous Materials.

[167] *Luzzati, V., Nicolaieff, A., Mason, F.,* J. Molec. Biol. **3,** 185 (1961), Structure de l'Acide Désoxycribonnclérique en Solution Étude par Diffusion des Rayons X aus Petits Angles.

[168] *Luzzati, V., Witz, H., Nicolaieff, A.,* J. Molec. Biol. **3,** 367 (1961), Détermination de la Masse et des Dimensions de Protéines en Solution par la Diffusion Centrale des Rayons X mésurée à l'Echelle Absolute: Exemple du Lysozyme.

[169] *Luzzati, V., Witz, H., Nicolaieff, A.*, J. Molec. Biol. **3**, 379 (1961), La Structure de la Sérum Albumine de Boeuf en Solution à pH 5,3 et 3,6: Étude par Diffusion Centrale Absolue des Rayons X.

[170] *Matuyama, E.*, Nature, **188**, 218-9 (1960), Small-Angle Scattering of X-Rays from deformed Natural Graphite.

[171] *Pigin, V.M., Terminasov, Yu.S., Tuzov, L.V.*, Kristallografiya, **10**, 311–316 (1965), Transl.: Soviet Phys. Cryst. **10**, 253-257 (1965), Intensity of Double Intergrain Reflections of X-Rays for very Small Scattering Angles.

[172] *Plavnik, G.M., Feigin, L.A.*, Dokl. Akad. Nauk, SSSR, **161**, 395 (1965), Anwendung der Röntgenkleinwinkelstreuung zur Untersuchung der Dispersität von feinverteiltem Graphit.

[173] *Reiss-Husson F., Luzzati, V.*, J. Colloid Interface, Sci. **21**, 534 (1966), Small-Angle X-Ray Scattering Study of the Structure of Soap and Detergent Micelles.

[174] *Renouprez, A., Bottazzi, H., Weigel, D., Imelik, Boris*, J. chim. Phys. **62**, 131-136 (1965), Application de la diffusion centrale des rayons X à l'étitude des solides poreux. II. Déscription et réglage d'un appareillage adapté à la diffusion centrale des rayons X.

[175] *Roscoe, C., Thomas, J.M.*, Carbon, 4, 383-90 (1966), Revelation of Small-Angle Boundaries and Forest Dislocations in Graphite Monocrystals.

[176] *Rossmann, M.P.*, Acta Cryst. **13**, 221-226 (1960), The Accurate Determination of the Position and Shape of Heavy Atom Replacement Groups in Proteins.

[176a] *Rothwell, W. S.*, J. appl. Phys. 39, 1840–45 (1968), Small-Angle X-Ray Scattering from Glassy Carbon.

[177] *Schmidt, P.W.*, J. Dairy Science **45**, 266 (1962), Small-Angle Scattering from Proteins.

[178] *Siegel, L.A.*, J. chem. Phys. **29**, 1091-6 (1958), Small-Angle X-Ray Scattering from Solutions of Aerosolot in Non-aqueous Media.

[179] *Siota, Y.*, Sci. Rep. Tohoku Univ. First Ser. **41**, 8-14 (1957), Particle Size Determination by Small-Angle Scattering.

[180] *Stirpe, D., Tompson, C.W.*, J. Chem. Phys. **36**, 392 (1962), Diffraction of X-Rays by Liquid Neon.

[180a] *Stoecker, W. C.*, Anal. Chem. 39, 628–632 (1967), Use of a simple small angle scattering device to determine particle size distributions of thoria sols.

[181] *Thomas, J.E., Schmidt, P.W.*, J. Chem. Phys. **39**, 2506 (1963), X-Ray Study of Critical Opalescence in Argon.

[181a] *Tchoubar-Vallat, D.*, C.R. Acad. Sci. B (France) **263**, 1030-2 (1966), Low Angle Scattering X-Ray by Cubic Particles of Magnesium Oxide.

[181b] *Tchoubar-Vallat, D., Mering, J.*, C.R. Acad. Sci. Paris Ser. A.B. **263**, B(17) 981-4 (1966)

[182] *Vainshtein, B.K., Feigin, L.A.*, Dokl. Akad. Nauk SSSR, **161**, 1444 (1965), Über den Ordnungsmechanismus der Moleküle der „löslichen" Ribonukleinsäure in wässriger Lösung.

[183] *Vasina, A., A., Lednev, V.V., Lemazhikhin, B.K.*, Biochimia, **31**, 720 (1966), Molecular characteristic of pepsine in solution and forces stabilizing compact pepsine globula,

[184] *Warren, B.E., Bodenstein, P.*, Acta Cryst. **18**, 282-286 (1965), The diffraction pattern of five particle carbon blacks.

[185] *Wunderlich, W., Kirste, R.G.*, Ber. Bunsenges. Chem. **68**, 646-652 (1964), Röntgenkleinwinkelstreuung an isotaktischem und syndiotaktischem Polymethylmethacrylat in Lösung.

[185a] *Wunderlich, B.*, Makromol. Chem. **108**, 315-17 (1967), Comparison of Zimm diagrams measured by light scattering and x-ray small-angle scattering in the same system. Poly (methyl methacrylate) with molecular weight of 500,000 in acetone.

Solid polymers, glasses

[186] *Anderson, F.R.*, J. Appl. Phys. **35**, 64 (1964), Morphology of Isothermally Bulk-Crystallized Linear Polyethylene.

[187] *Andrichenko, Yu.D., Druzhinina, T.V., Zubov, Yu.A., Konkin, A.A., Tsvankin, D.Ya.*, Vysokomol. Soyed. 7, 2126-2131 (1965), Transl. in: Polymer Sci. USSSR, 7, 2330-2336 (1965), Study of the Structure and Properties of Polyethylene Fibres.

[187a] *Arakawa, T.*, U.S.Dept. Comm. AD 463881. Avail. CFSTI, 114p (1965), Extended-chain polymer crystals.

[188] *Arlie, J.P., Spegt, P.A., Skoulios, A.E.*, Makromol. Chem. **99**, 160 (1967), Étude de la cristallisation des polymères. I Structure lamellaire de polyoxyéthelène de faible masse moléculaire.

[189] *Arlie, J.P., Spegt, P., Skoulios, A.*, Makromol. Chem. **104**, 212 (1967), Étude de la cristallisation des polymères. II. Structure lamellaire et repliement des chaînes du polyoxyéthylène.

[190] *Arnold, H.*, Kolloid-Z. **157**, 111 (1958), Die Kristallisation von Terylen im Kleinwinkeldiagramm.

[191] *Baltá Calleja, F.J., Bassett, D.C., Keller, A.*, Polymer, **4**, 269-279 (1963), A Study of X-Ray Long Periods Produced by Annealing Polyethylene Crystals.

[192] *Baltá Calleja, F.J., Hosemann, R., Wilke, W.*, Makromol. Chem. **92**, 25-50 (1966), Die Struktur von rekristallisiertem und verstrecktem Polyäthylen als Modell für lineare Hochpolymere.

[193] *Baltá Calleja, F.J., Hay, I.L., Keller, A.*, Kolloid-Z. **209**, 128-135 (1966), Diffraction Effects in Single Crystals and Spherulites of Poly (Ethylene Oxide).

[194] *Baltá Calleja, F.J., Hosemann, R., Wilke, W.*, J. Polym. Sci. Untersuchung über die Beziehungen zwischen Langperiode und Kettenlänge in Polyäthylenoxydkristallen.

[195] *Barnes, W.J., Price, F.P.*, Polymer **5**, 283 (1964), Morphology of Polymer Crystals: Screw Dislocations in Polyethylene, Polymethylene Oxide and Polyethylene Oxide.

[195a] *Basset, D.C.*, Polymer, **5**, 457 (1964), On the Chemistry of Polymer Chain Folds.

[196] *Belavtseva, E.M., Petrov, J.M., Tsvankin, D.J.*, Vysokomolekul. Soedin. **6**, 684 (1964), Übers. in: Polymer Sci. USSSR, **6**, 750 (1964), The Structure of Cellulose Treated With Phosphorungstic acid.

[197] *Belbeoch, B., Guinier, A.*, Makromol. Chem. **31**, 1 (1959), Structure a Grande Echelle du Polyethylene.

[198] *Beresford, D.R., Bevan, H.*, Polymer **5**, 247 (1964), The Effect of Tension and Annealing on the X-Ray Diffraction Pattern of Drawn 6 -6 Nylon.

[199] *Bingham, B.E.M.*, Makromol. Chem. 77, 139-153 (1964), AStudy of the Fine Structure of Regenerated Cellulose Fibers.

[199a] *Blais, P., Manley, R.St.J.*, J. Polym. Sci, Part A-2, **4**, 1022-4 (1966), Crystallization of isotactic polystyrene from solution.

[199b] *Blais, P., Manley, R. St. J.*, J. Macromol. Sci. Phys. 1, 525–566 (1967), X-ray long periods in bulk crystalline polymers.

[199c] *Blundell, D. J., Keller, A., Connor, T. M.*, J. Polym. Sci. A-2,5, 991–1012 (1967), Investigation of the fold-surface problem in polyethylene single crystals with the nitric acid oxidation technique.

[200] *Bonart, R., Hosemann, R.*, Koll. Z. **186**, 16 (1962), Fibrillarstrukturen in kaltverstrecktem linearem Polyäthylen.

[201] *Bonart, R., Grimm, W., Hosemann, R., Höhling, J., Pfefferkorn, G.*, Biochim. et Biophys. Acta **66**, 132-136 (1963), Röntgenkleinwinkelstreuung an kranken menschlichen Meniskusfasern.

[202] *Brown, R.G., Eby, F.K.*, J. Appl. Phys. **35**, 1156 (1964), Effect of Crystallization Conditions and Heat Treatment on Polyethylene: Lamellar Thickness, Melting Temperature and Density.

[203] *Brumberger, H., Debye, P.*, J. Phys. Chem. **61**, 1623 (1957), Low-Angle X-Ray Scattering by Glasses.

[204] *Brumberger, H., Kratky, O., Mittelbach, P.*, Mh. f. Chem. **95**, 1600-1608 (1964), Studium der Röntgenkleinwinkelstreuung von Nylon-6 unter Verwendung der absoluten Intensitätsmessung.

[204a] *Buchmann, D.R., Miller, R.L.*, J. Polymer Sci. Part **B5**, (9) 771-2 (1967), Significance of sizes inferred from Small-Angle X-Ray studies.

[205] *Burge, R.E., Randall, I.T.*, Proc. Roy. Soc. **A233**, 1-16 (1955), The Equivalence of Electron-Microscope and X-Ray Observations on Collagen Fibers.

[206] *Caspar, D.L.D., Franklin, R.E.*, Nature **177**, 928 (1956), Radial Density Distribution in the Tabacco Mosaic Virus Particle.

[207] *Cartz, L.*, Nature **180**, 1115 (1957), Low-Angle X-Ray Observations on Glass.

[207a] *Corneliussen, R., Peterlin, A.*, Makromol. Chem. **105**, 193-203 (1967), The Influence of Temperature on the Plastic Deformation of Polyethylene

[208] *Damaschun, G., Jupe, K.*, Plaste und Kautschuk, **7**, 298-300 (1960), Untersuchung der Füllstoffverteilung in Silikongummi mit Hilfe der Röntgenkleinwinkelstreuung.

[209] *Damaschun, G., Füller, H.*, Zool. Jb. Physiol. Bd. **71**, 415-428 (1965), Röntgenographische Untersuchungen über die Chinintextur der Cuticula von Chilopoden.

[210] *Dijkstra, A., Kortleve, G., Vonk, C.G.*, Kolloid-Z. **210**, 121-123 (1966), X-Ray Small-Angle Scattering of Bulk Polyethylene.

[211] *Dismore, P.F., Statton, W.V.*, Polymer Letters **2**, 1113-1116 (1964), Chain Folding in Oriented 66-Nylon Fibers.

[212] *Dismore, P.F., Statton, W.O.*, J. Polym. Sci. Part. C. **13**, 133 (1966), Chain Folding in Oriented Nylon 66 Fibers.

[213] *Dismore, P.F., Statton, W.O.*, Symp. on Small-Angle Scattering from Fib. and Partially Ordered Systems, Detroit 1965 (N.Y.: Intersci, Publ. 1966) Chain Folding in Oriented Nylon 66 Fibers.

[213a] *Dobb, M.G., Fraser, R.D.B., MacRae, T.P.*, IIIrd. Intern. Wool Textile Conf. **1**, 95 (1965), The Structure of the Keratin Filament.

[214] *Eppe, R., Fischer, E.W., Stuart, H.A.*, J. Polymer Sci **34**, 721 (1959), Morphologische Strukturen in Polyäthylen, Polyamiden und anderen kristallisierenden Hochpolymeren.

[215] *Ericson, L.G., Tomlin, S.G.*, Proc. Roy. Soc. A, **252**, 197-216 (1959), Further Studies of Low-Angle X-Ray Diffraction Patterns of Collagen.

[216] *Fedorov, B.A., Ptizin, O.B.*, Dokl. Akad. Nauk SSSR, **153**, 882 (1963), Transl. in: Dokl. Physical. Chem. **153**, 1067 (1963), Determination of the Transverse Dimensions of Macromolecules from the X-Ray Scattering at Small-Angles.

[217] *Fischer, E.W.*, Ann. N.Y. Acad. Sci. 89, 620 (1961), Thermodynamical Explanation of Large Periods in High Polymer Crystals and Drawn Fibers.
[218] *Fischer, E.W., Schmidt, G.F.*, Angew. Ch. 74, 551 (1962), Über Langperioden bei verstrecktem Polyäthylen.
[219] *Fischer, E.W.*, Faserforsch. u. Textiltechn. 15, 545-554 (1964), Schmelz- und Rekristallisationsvorgänge bei Polyäthylen-Einkristallen.
[220] *Fischer, E.W., Hinrichsen, G.*, Kolloid-Z. u. Z. f. Polymere 213, 28-38 (1966), Untersuchungen zum Schmelzverhalten des verstreckten Polyäthylens mit Hilfe der Differential-Thermo-Analyse.
[221] *Fischer, E.W., Hinrichsen, G.*, Kolloid-Z. u. Z. f. Polymere 213, 93-109 (1966), Schmelz- und Rekristallisationsvorgänge bei Polyäthylen-Einkristallen.
[221a] *Fischer, E. W., Goddar, H., Schmidt, G. F.*, Kolloid-Zs. u. Zs. f. Polym. 226, 30–40 (1968), Über Zusammenhänge zwischen der Röntgenkleinwinkelstreuung und der morphologischen Struktur verstreckter Hochpolymerer.
[222] *Frank, F.C., Keller, A., O'Connor, A.*, Phil. Mag. 3, 64 (1958), Deformation Processes in Polyethylene Interpreted in Terms of Crystal Plasticity.
[223] *Franklin, R.E.*, Nature 175, 379 (1955), Structure of Tobacco Mosaic Virus.
[224] *Franklin, R.E., Klug, A.*, Biochim. Biophys. Acta 19, 403 (1956), The Nature of the Helical Groove on the Tobacco Mosaic Virus Particle, X-Ray Diffraction Studies.
[224a] *Gallot, B., Skonlios, A.*, Kolloid-Zs. u. Zs. f. Polym. 222, 51–55 (198), Structure des savons alcalins, IV. Disavons de Li, Na, K, Rb et Cs.
[225] *Geil, P.H.*, Thesis, Univ. of Wis. (1956), Application of Small-Angle X-Ray Scattering to the Determination of the Structure of Macromolecules.
[226] *Geil, P.H.*, J. Polymer Sci. 47, 65 (1960), Morphology of an Acetal Resin.
[227] *Geil, P.H.*, Bull. Am. Phys. Soc. 7, 206 (1962), Recrystallisation of Melt-Crystallized Polyethylene During Annealing.
[228] *Geil, P.H.*, Polymer, 4, 404 (1963), Primary Nucleation of Poly-3,3-bischloro-methyloxacyclobutane Single Crystals.
[228a] *Geil, P.H.*, Polymer Single Crystals. Interscience Publ. New York (1963).
[229] *Geil, P.H.*, J. Polym. Sci. (A) 2, (1964), Polymer Deformation, II Drawing of polyethylene single crystals 3813-3833, III Annealing of drawn polyethylene single crystals and fibers 3835-3855, IV Drawing of nylon 6 and polyoxymethylene 3857-3866.
[230] *Geil, P.H., Anderson, F.R., Wunderlich, B., Arakawa, T.*, J. Polymer Sci. 2, 3707-3720 (1964), Morphology of Polyethylene Crystallized from the Melt Under Pressure.
[231] *Geil, P.H.*, Symposium on Small-Angle Scattering from Fibrous and Partially Ordered Systems, Detroit 1965 Interscience Publishers, 1966 pp. 149-63. Small-Angle X-Ray Scattering From Bulk Crystalline Polymers.
[232] *Geil, P.H.*, J. Polymer Sci. C13, 149-163 (1966), Small-Angle X-Ray Scattering From Bulk Crystalline Polymers.
[232a] *Geil, P.H.*, J. Polym. Sci. Part C, 20, 109-15 (1967), Polymer crystallization.
[233] *Glenz, W., Kilian, H.G., Müller, F.H.*, Kolloid-Z. u. Z. f. Polymere 206, 104 (1965), Feinstruktur und Überstruktur von partiell kristallisierten Netzwerken des Polyäthylens.
[234] *Goganov, D.A., Porai-Koshits, E.A.*, Dokl. Akad. Nauk SSSR 167, 1266 (1966), Über die flüssigkeitsähnliche Natur der chemisch inhomogenen Strukturen von schwach alkalischen Natriumsilikat-Gläsern.

[234a] *Grell, M.*, Kem. Kozlem. **26**, (1-2) 41-55 (1966), Small-Angle X-Ray Scattering and its practical application in the investigation of polymer structures.

[235] *Gromov, A.E., Slutsker, A.I.*, Vysokomol. Soedin, **4**, 247 (1963), Strukturuntersuchungen von Polyäthylen mit Hilfe von Röntgenstreuungsmethoden im Klein- und Weitwinkelbereich.

[236] *Gromov, E.A., Slutsker, A.I.*, Vysokomolekul. Soedin, **7**, 546 (1965), Transl. in: Polymer Sci. USSSR **7**, 604 (1965), Change in the Supramolecular Structure of Crystallizing Polymers on Orientation.

[237] *Grosskreutz, J.C.*, Biochim. Biophys. Acta, **38**, 400-409 (1960), The Physical Structure of Wheat Protein.

[237a] *Hay, I.L., Keller, A.*, J. of Mat. Sci. **2**, 538-558 (1967), A Study on Orientation Effects in Polyethylene in the light of Crystalline Texture, Part 2, Correlation of the Molecular Orientation with that of the Textural Elements.

[237b] *Hay, I. L., Kawai, T., Keller, A.*, J. Polym. Sci. Part C, 16, 2721–31 (1967), Orientation effects in polyethylene in the light of crystalline texture.

[238] *Hearle, J.W.S.*, J. Appl. Polym. Sci. **7**, 1175 (1963), The Fine Structure of Fibers and Crystalline Polymers. I. Fringed Fibril Structure.

[239] *Heikens, D.*, J. Polymer Sci. **35**, 139 (1959), A Quantitative Investigation on the X-Ray Small-Angle Scattering of Cellulose Fibers. Part I. The Concept of Scattering Power and a Method for Its Determination in Electron Units.

[240] *Heise, R., Kilian, H.G., Müller, F.H.*, Kolloid-Z. **213**, 12 (1966), Struktur von Polytetrafluoräthylen.

[241] *Hendus, H., Schnell, G., Thurn, H., Wolf, K.*, Erg. d. exakten Naturwiss. **31**, 220-380 (1959), Neuere physikalische Untersuchungen an Hochpolymeren.

[242] *Hendus, H.*, Ergeb. Exakt. Naturwiss. **31**, 331-380 (1959), Röntgenographische und elektronenmikroskopische Strukturuntersuchungen.

[243] *Hendus, H.*, Kolloid-Z. **165**, 32 (1959), Zur Deformation von Polyäthylen.

[244] *Hendus, H., Illers, K.H., Ropte, E.*, Kolloid-Z. u. Z. f. Polymere **216-217**, 110-119 (1967), Strukturuntersuchungen an Styrol-Butadien-Styrol-Blockcopolymeren.

[245] *Hermans, P.H., Heikens, D., Weidinger, A.*, J. Polymer Sci. **35**, 145 (1959), A Quantitative Investigation on the X-Ray Small-Angle Scattering of Cellulose Fibers. Part II. The Scattering Power of Various Cellulose Fibers.

[246] *Hermans, P.H., Weidinger, A.*, Makromol. Chem. **39**, 67 (1960), Absolute Measurements of X-Ray Scattering at Low-Angles in Crystalline Polymers.

[247] *Hess, K., Kiessig, H., Hanssen, E.*, Die Naturwissenschaften **39**, 135-136 (1952), Die Samenproteine der Gramineen und ihre Wandlungen beim Teigen und Backen.

[248] *Hess, K.*, J. Colloid. Sci. Suppl. **1**, 135 (1964), Über Langperioden-Interferenzen bei synthetischen Fasern und über ein neues Fasermodell.

[249] *Hess, K.*, Kolloidchemie makromolekularer Naturstoffe, **18**, 5 (1958), Die neue Auffassung über die Ultratextur von Faserstoffen und ihre experimentellen Begründungen.

[250] *Hess, K., Güttner, E., Mahl, H.*, Kolloid-Z. **168**, 37 (1960), Die elektronenmikroskopische Darstellung der großen Längsperiode bei Perlon und ihre Beziehungen zur Kollagenstruktur.

[251] *Heyn, A.N.J.*, J. appl. Phys. **26**, 519 (1955), Small Particle X-Ray Scattering by Fibers. I. Size and Shape of Microcrystallites. II. Radial Distribution of Microcrystallites.

[252] *Hirai, N., Hikasa, J., Oka, M., Kobayashi, M.,* Chem. high Polymers, (Tokyo), **22,** 590-596 (1965), Die Struktur der Einkristalle von verzweigten Polyäthylenen. I. Der Einbau der Seitenketten von Hochdruckpolyäthylen in den kristallisierten Bereich.

[253] *Hirai, N., Yamashita, Y., Matsuhata, T., Tamura, Y.,* Rept. Res. Lab. Surface Sci. Okayama Univ. **2,** 1 (1961), The Thickening of Lamellar Single Crystals of Polyethylene by heat Treatment.

[254] *Hirai, N., Mitsuhata, T., Yamashita, Y.,* Chem. High Poly. (Japan) **18,** 33 (1961), Thickening of Polyethylene Single Crystals under Heat Treatment.

[254a] *Hirami, M.,* Makromol. Chem. **105,** 296-299 (1967), Dependence of the Long Period of Nylon 6 on Annealing Temperature.

[255] *Hoffmann, L.C., Statton, W.O.,* Nature **176,** 561 (1955), Structure in Vitreous Silicates as shown by Low-Angle X-Ray Scattering.

[256] *Hoffmann, J.D., Weeks, J.J.,* J. Chem. Phys. **42,** 4301 (1965), X-Ray Study of Isothermal Thickening of Lamellae in Bulk Polyethylene at the Crystallization Temperature.

[257] *Höhling, H.J., Pfefferkorn, G., Hosemann, R., Wilke, W.,* Kolloid-Z. **210,** 118-121 (1966), Bestimmung struktureller Veränderungen degenerierter menschlicher Achillessehnen durch kombinierte röntgenographische und infrarotspektroskopische Untersuchungen

[258] *Hosemann, R.,* Z. Elektrochem. **58,** 923 (1955), Bemerkung zur Arbeit von *O. Kratky* und *G. Porod* „Zur Kleinwinkelstreuung der Cellulose".

[259] *Hosemann, R., Bonart, R.,* Fortschr. Miner. **38,** 59 (1960), Über den parakristallinen Charakter der Langperiodeninterferenzen.

[260] *Hosemann, R., Bonart, R.,* Makromol. Chem. **39,** 105 (1960), Modellversuche zur Deutung der Röntgen-Langperiodeninterferenzen.

[261] *Hosemann, R., Bonart, R.,* Struktur u. biolog. Funktion der Eiweiße 14-37 (1962), Beitrag zur parakristallinen Struktur von Fibroinen.

[262] *Hosemann, R.,* Polymer **3,** 349 (1962), Crystallinity in High Polymers, especially Fibers.

[263] *Hosemann, R.,* J. appl. Phys. **34,** 25-41 (1963), Crystalline and Paracrystalline Orders in High-Polymers.

[264] *Hosemann, R.,* Pergamon Press 35-53 (1963), Structure of organic solids and new organic polymers.

[265] *Hosemann, R.,* Chemiefasern D 2047, E. 34, 123, 174, 284, 369 (1963), Kristallinität in Hochpolymeren, besonders Fasern.

[266] *Hosemann, R., Wilke, W.,* Faserforschg. und Textiltechn. **11,** 521 (1964), Die parakristalline Struktur des Polyäthylens.

[267] *Hosemann, R., Wilke, W., Balta Calleja, F.J.,* Acta Cryst. **21,** 118-123 (1966), Twist-Korngrenzen und andere parakristalline Gitterstörungen in Polyäthylen-Einkristallen.

[268] *Hosemann, R., Lemm, K., Wilke, W.,* Molecular Crystals **1,** 333-362 (1967), The paracrystal as a model for liquid crystals.

[269] *Hosemann, R.,* Combined Analysis of Small-Angle Scattering of reflections (000) and (hkl). Small-Angle X-Ray Scattering. Ed. H. Brumberger, Gordon and Breach (1967).

[270] *Illers, K.-H., Hendus, H.,* Kolloid-Z. u. Z. f. Polymere **218,** 56 (1967), Lamellendicke und Röntgenkleinwinkelperioden von Polyäthylen.

[271] *Jagodzinski, H.*, Z. Elektrochem. **65**, 313-321 (1961), Röntgenkleinwinkelstreuung an Chrysotil-Asbest.

[272] *Janeschitz-Kriegel, H., Kratky, O., Porod, G.*, Z. f. Elektrochemie, **56**, 146-154 (1962), Röntgenkleinwinkelmessungen an porösen Hydratzellulosefäden.

[272a] *Kambour, R.P.*, Werkstoffe und Korrosion **18**, 393-400 (1967), Die Rolle des „Crazing" beim Bruchmechanismus von glasartigen Polymeren.

[273] *Kantola, M., Kahköhnen, H.*, Ann. Acad. Sci. Fenn. **AIV**, 137 (1963), Small-Angle X-Ray Investigation of the Orientation of Crystallites in Finuish Coniferous and Decidous Wood Fibers.

[274] *Kantola, M.*, Faserforsch. u. Textiltechn. **15**, 587-590 (1964), Röntgenographische Untersuchungen über die Orientierung der Kristallite in Holzfasern.

[275] *Kasai, N., Fujiwara, S., Morioka, S., Kurose, H., Kakudo, M., Watase, T.*, J. Chem. Soc. Japan **64**, 55 (1961), The Fine Texture of Cold Drawn Polyethylene.

[276] *Kawai, T.*, Makromol. Chem. **84**, 290 (1965), Molecular Fractionation and Thickening of Lamellar Crystals during Isothermal Crystallization.

[277] *Kawai, T.*, Kolloid-Z. **201**, 15-20 (1965), Melting Points of Polyethylene Crystals and the Relation between Molecular Length and Chain Folding.

[277a] *Kawai, T., Iguchi, M., Tonami, H.*, Koll. Zs. Z. f. Polym. **221**, (1) 28-40 (1967), Crystallization of Polyethylene under Orientation.

[278] *Kawai, T.*, Kolloid Z. **201**, 104-111 (1965), On the Thickening Mechanism of Polymer Single Crystals on Annealing.

[278a] *Kawai, T., Matsumoto, M., Kato, M., Maeda, H.*, Kolloid-Zs. u. Zs. f. Polym. 222, 1–10 (1968), Crystallization of Polyethylene in Steady-State Flow.

[278b] *Kawai, T., Goto, T., Maeda, H.*, Kolloid-Zs. u. Zs. f. Polym. 223, 117–127 (1968), Fold Structure of Polyethylene Single Crystals.

[279] *Keller, A., O'Connor, A.*, Nature, **180**, 1289 (1957), Large Periods in Polyethylene: The Origin of Low-Angle X-Ray Scattering.

[280] *Keller, A., Maradudin, A.*, J. Phys. Chem. Solids **2**, 301 (1957), Diffraction of X-Rays by fibres consisting of small crystals: Application of theory to polyamides.

[281] *Keller, A., O'Connor, A.*, Disc. Faraday Soc. **25**, 114 (1958), Study of Single Crystals and their Association in Polymers.

[282] *Keller, A.*, Kolloid Z. **165**, 34 (1959), Bemerkungen zur Kleinwinkelstreuung beim Strecken von Polyäthylen.

[283] *Kiessig*, Koll. Z. **152**, 62 (1957), Die Bedeutung von Langperioden-Interferenzen für die Struktur von Hochpolymeren.

[284] *Kiessig, H.*, Papier **12**, 118 (1958), Die röntgenographischen Untersuchungen der großen Periode bei Cellulose.

[285] *Kilian, H.G.*, Kolloid-Z. u. Z. f. Polym. **189**, 23 (1963), Kristallisation von Copolymeren des Äthylens.

[286] *Kilian, H.G.*, Faserforsch. u. Textiltechn. **15**, 537-542 (1964), Zusammenhang zwischen Kristallitgrößenverteilung und parakristalliner Störung in den Kristallgittern von partiell kristallisierten Copolymeren des Äthylens.

[287] *Kilian, H.G.*, Kolloid-Z. u. Z. f. Polymere **205**, 7-18 (1965), Gesetzmäßigkeiten der Überstruktur von kristallisierten linearen Copolymeren.

[288] *Kitaigorodskii, A.I., Tsvankin, D.Ya., Petrov, Yu.M.*, Vysokomol. Soedin, **3**, 1428 (1961), Langperioden in enanthischen Fasern.

[289] *Kitaigorodskii, A.I., Tsvankin, D.Ya., Petrov, J.M.*, Vysokomolekul Soedin. **5**, 1062 (1963), Transl. in: Polymer Science USSR **5**, 118 (1964), Long Periods in Polyethylene terephtalate Films.

[290] *Kniess, F., Kratky, O.,* Monatshefte f. Chemie, **90,** 506-509 (1959), Intensitätsänderungen im Weit- und Kleinwinkelbereich des Röntgendiagramms von Polytetrafluoräthylen durch Einwirkung von Röntgenstrahlen.

[291] *Kobayashi, K., Kurokaua, M.,* Nature, **196,** 538-9 (1962), Small-Angle Diffraction of Polyethylene.

[291a] *Korfleve, G., Vonk, C. G.,* Kolloid-Zs. u. Zs. f. Polym. 225, 124 (1968), X-Ray Small-Angle Scattering of Bulk Polyethylene III. Results.

[292] *Kratky, O., Porod, G.,* Z. f. Elektrochem. **58,** 918-923 (1954), Zur Kleinwinkelstreuung der Cellulose.

[293] *Kratky, O., Sekora, A.,* Z. Naturforsch. **9b,** 505 (1954), Auffindung einer Längsperiodizität im Röntgenkleinwinkelbild einer jodierten Kunstseide.

[294] *Kratky, O., Sekora, A., Pilz, I.,* Monatshefte f. Chemie, **86,** 379-384 (1955), Über Bildung und Stabilität der beiden Modifikationen von Naturseide.

[295] *Kratky, O.,* Transactions of the Faraday Society **52,** 558-570 (1955), An X-Ray Investigation of Silk Fibroin.

[296] *Kratky, O., Porod, G.,* Die Physik der Hochpolymeren **III,** 192-232 (1955), v.H.A. Stuart, Springer-Verlag Berlin Form und Größe der kristallinen Bereiche.

[297] *Kratky, O., Sembach, H.,* Angewandte Chemie, 67, 603-606 (1955), Röntgenkleinwinkelmessungen an Cellulose.

[298] *Kratky, O., Sekora, A., Zahn, H., Fritze, E.R.,* Z. f. Naturforschung, **10b,** 68-72 (1955), Kleinwinkel-Röntgeninterferenzen bei nitrierten Faserkeratinen.

[299] *Kratky, O.,* Monatshefte für Chemie, **87,** 269-280 (1956), Zur molekularen Morphologie des Seidenfibroins.

[300] *Kratky, O., Sekora, A., Breiner, R.,* Makromolekulare Chemie, **22,** 115 (1956), Röntgenographische Studien zur übermolekularen Struktur von Vinyon N.

[300a] *Kratky, O.,* Trans. Far. Soc. 52, 558 (1956), An X-Ray Investigation of Silk Fibroin.

[301] *Kratky, O., Porod, G.,* Z. f. Elektrochem. **60,** 188-190 (1956), Zur Kleinwinkelstreuung der Cellulose.

[302] *Kratky, O., Sekora, A., Breiner, R.,* Angew. Chemie, **68,** 619 (1956), Röntgenographische Studien zur übermolekularen Struktur von Vinyon N.

[303] *Kratky, O., Breiner, R.,* Makromol. Chem. **26,** 92-95 (1957), Röntgenographische Studien zur übermolekularen Struktur von Vinyon N.

[304] *Kratky, O., Lauer, M., Ratzenhofer, M., Sekora, A.,* Collagen, herausge. v. N. Ramanathan, Interscience Publishers John Wiley Sons, N.Y.-London, Symposium Nov. 1960, Dependence on Age of the X-Ray Diagram of Human Tendon Collagen.

[305] *Kratky, O., Schmitz, P.J., Schier, K.,* Monatshefte f. Chem. **93,** 321-323 (1962), Riesenperioden in gestrecktem Polyäthylen.

[306] *Kratky, O., Sekora, A., Szpak, N.,* Monatshefte für Chemie, **93,** 1450-1452 (1962), Nichtkontinuierliche Verschiebung des Kleinwinkelmaximums beim Tempern von isotaktischem Polypropylen.

[307] *Kratky, O.,* Internat. Ser. of Monographs on Elmagn. Waves **5,** 459-476 (1963), Absolute Intensity of Small-Angle X-Ray Scattering in Solid High Polymer Research.

[308] *Kratky, O., Schwarzkopf, K., Schier,* Monatshefte f. Chemie, **94,** 714 (1963), Die Absolutmessung der Kleinwinkelstreuung von linearem Polyäthylen bis zu Braggschen Werten von 15800 A.

[309] *Kratky, O., Miholic, G.,* J. Polym. Sci. **C2,** 449 (1963), Small-Angle X-Ray Investigations with Absolute Intensity Measurements on Regenerated Air Swollen Cellulose.

[310] *Kratky, O.*, International Series of Monographs on Electromagnetic Waves, **5**, 459 (Proceedings of the Interdisciplinary Conference on Electromagnetic Scattering (Potsdam, New York) Edited by Milton Kerker, Pergamon Press, Oxford-London-New York-Paris (1963), Absolute Intensity of Small-Angle X-Ray Scattering in Solid High Polymer Research.

[311] *Kratky, O., Miholic, G.*, Monatshefte f. Chemie, **94**, 151-161 (1963), Röntgenkleinwinkeluntersuchungen an regenerierten, porös getrockneten Cellulosefäden.

[312] *Kratky, O., Mittelbach, P., Sekora, A.*, Kolloid-Z. u. Z. f. Polymere, **200**, 1 (1964), Die Röntgenkleinwinkelstreuung von Azetylzellulosefolien, gefärbt mit 1-4-Diaminoanthrachinon.

[313] *Kratky, O.*, Pure and Appl. Chem. **12**, 483-523 (1966), Possibilities of X-Ray Small-Angle Analysis in the Investigation of Dissolved and Solid High Polymer Substances.

[314] *Krigbaum, W.R., Godwin, R.W.*, J. Chem. Phys. 43, 4523-4524 (1965), Direct Measurements of Molecular Dimensions in Bulk Polymers.

[315] *Krigbaum, W.B., Balta, Y.I., Via, G.H.*, Polymer 7, 61 (1966), A reversible change in Long Period Spacing with Temperature.

[316] *Liedberg, D.J., Smid, R.K., Bergeron, C.G.*, J. Amer. Ceram, Soc. 49, 80-3 (1966), Microseparation in Lead Borate Glasses.

[317] *Mandelkern, L., Worthington, C.R., Posner, A.S.*, Science **127**, 1052 (1958), Low-Angle X-Ray Diffraction of Fibrous Polyethylene.

[318] *Mandelkern, L., Posner, A.S., Diorio, A.G., Roberts, D.E.*, J. Appl. Phys. **32**, 1509-1517 (1961), Low-Angle X-Ray diffraction of crystalline nonoriented polyethylene and its relation to crystallisation mechanisms.

[319] *Marikhin, V.A., Slutsker, A.I., Yastrebinskii, A.A.*, Fiz. Tverd. Tela 4, 2534-2538 (1962), Transl.: Sov. Phys. Solid State 4, 1858 (1963), Investigation of the Structure of Oriented Polyethyleneterephtalate (Lavsan).

[320] *Marikhin, V.A., Slutsker, A.I., Jastrebinskii, A.A.*, Dokl. Akad. Nauk SSSR **153**, 303 (1963), Der Einfluß von Einlagerungen auf die übermolekulare Struktur orientierter Polymerer.

[321] *Marikhin, V.A., Slutsker, A.I., Yastrebinskii, A.A.*, Fiz. Tverd. Tela 7, 441-445 (1965), Transl. Soviet Phys. Solide State 7, 352-355 (1965) Variation of Small-Angle X-Ray diffraction intensity during contrasting of polymers.

[321a] *Mihaly, G.*, Kem. Kozlem. **26**, 41-55 (1966), Small-Angle X-Ray Scattering and its practical application in the investigation of polymer structures.

[322] *Mnyukh, Yu.V., Belavtseva, E.M., Kitaigorodskii, A.I.*, Dokl. Akad. Nauk SSSR, 133, 1132 (1960), Morphologie der Molekülpackung in linearen Polyäthern.

[323] *Moore, R.S., Gieniewski, Ch.*, J. Polym. Sci. Part C **13**, 55 (1966), Quantitative Studies of Ringed Spherulite Deformation in Polyethylene Films.

[323a] *Nakajima, A., Hamada, F., Hayashi, S., Sumida, S.*, Kolloid-Z. u. Z. f. Polym. 222, 10–16 (1968), Effect or Solvent on Single Crystal Formation from Dilute Polyethylene Solution.

[323b] *Nakajima, A., Hayashi, S.*, Kolloid-Z. u. Z. f. Polym. 225, 116 (1968), Lamellar Thickniss of Polyethylene Single Crystal Isothermally Crystallized in Dilute Solution.

[324] *Nukushima, Y., Itoh, Y., Fischer, E.W.*, Polymer Letters 3, 383 (1965), Nachweis des partiellen Schmelzens von Polyäthylen-Einkristallen mit Hilfe der Röntgenkleinwinkelstreuung.

[325] *Ochainski, D.*, Plaste und Kautschuk, **12**, 645-651 (1965), Bestimmung der Abmessungen geordneter Bereiche in teilkristallinen Hochpolymeren aus dem Röntgendiagramm unter Berücksichtigung der Gitterstörungen.

[326] *O'Leary, K., Geil, P.H.*, J. Macromol. Sci (Phys) **B 1** (1) 147-160 (1967), Reversible Long Period Change during the Annealing of Crystalline Polymers.

[326a] *Panteleyev, M. V., Tsvankin, D., Ya., Shlenskii, O. F.*, Polymer Science USSR, 8, 2274–2280 (1966), Structural Changes During Stretching of Oriented Polyethylene Films.

[327] *Peterlin, A., Meinel, G.*, J. appl. Phys. **36**, 3028-3033 (1965), Thermodynamic Properties of Drawn Linear Polyethylene.

[327a] *Peterlin, A.*, Amer. Chem. Soc., Div. Polymer Chem. Preprints **7**, (1) 109-10 (1966), Plastic deformation of polyethylene, Mechanism and properties.

[327b] *Plavnik, G. M., Sinitsyna, G. M., Vlodavets, I. N.*, Probl. Fiz.-Khim.Mekh. Voloknistykh Poristykh Dispersynkh Strukt. Mater., Mater, Konf., Riga 1965, 103–17 (pub. 1967) (Russ.).

[328] *Pollack, S.S., Robinson, W.H., Chiang, R., Flory, P.J.*, J. Appl. Phys. **33**, 237-238 (1962), X-Ray diffraction of linear polyethylene crystallized at 131 °C.

[329] *Porai-Koshits, E.A., Andreyew, N.S.*, Nature **182**, 335 (1958), Low-Angle X-Ray Scattering by Glasses.

[330] *Porai-Koshits, E.A., Andreyew, N.S.*, J. Soc. Glass. Tech. **43**, 235-261 (1959), Low-Angle X-Ray Scattering by sodium borosilicate glasses.

[331] *Porod, G.*, Fourth International Congress of Biochemistry 1958 **IX** Physical Chemistry of High Polymers of Biological Interest, Pergamon Press, London, New York, Paris, Los Angeles (1960), Die röntgenographische Erforschung großer Perioden bei Cellulose.

[332] *Porod, G.*, Makromolekulare Chemie, **XXXV**, 1-25 (1960), Anwendung und Ergebnis der Röntgenkleinwinkelstreuung in festen Hochpolymeren.

[333] *Porod, G.*, Fortschr. Hochpolym.-Forsch., **2**, 363-400 (1961), Anwendung und Ergebnisse der Röntgenkleinwinkelstreuung in festen Hochpolymeren.

[334] *Posner, A.S., Mandelkern, L., Worthington, C.R., Diorio, A.F.*, J. appl. Phys. **31**, 536, (1960), Low-Angle X-Ray Diffraction of Fibrous Polyethylene.

[335] *Ranby, B.G., Brumberger, H.*, Polymer, **1**, 399 (1960), Observations of the Chain Folding in Crystalline Polymers.

[336] *Rothe, H.*, Kolloid-Z. **151**, 155 (1957), Der Einfluß der Kristallitbreite auf die Form der Langperioden-Interferenzen bei vollsynthetischen Faserstoffen.

[337] *Rothe, H.*, Faserforschung u. Textiltechnik, **8**, 244, (1957), Zur Frage der Langperiodeninterferenzen an synthetischen Faserstoffen.

[338] *Ruscher, Chr. Walenta, E.*, Faserforschung und Textiltechnik, **18**, 78-83 (1967), Röntgenkleinwinkelstreuung an Polyacrylnitrilfasern.

[339] *Salovey, R., Basset, D.C.*, J. Appl. Phys. **35**, 3216-3221 (1964), Irradiation of Annealed Polyethylene Crystals.

[340] *Schiller, C., Mering, J.*, C.R. Acad. Sci., Paris, Ser. A,B 264 B (3), 247-50 (1967), Diffusion centrale des rayons X par des carbons graphitales. Déviation de la de Poral

[340a] *Schultz, J. M., Robinson, W. J., Pound, G. M.*, J. Polym. Sci. A-2, 511–533 (1967), Temperature-Dependent X-Ray Small-Angle Scattering from Melt-Crystallized Polyethylene.

[341] *Sella, C.*, Beitrag IB 7, Symposium über Makromoleküle Wiesbaden (1959) Study of Polyethylene by Diffraction of X-Rays at Small-Angles.

[342] *Sella, C.*, Compt. rend. **248**, 1819 (1959), Etude des Polyethylene par diffraction des rayons X aux petits angles.

[343] *Seto, T., Hara, T.*, Rep. Progr. Polymer Phys. Japan **9**, 207 (1966), Structure of Non-Crystalline Regions in Drawn Polyethylene.

[344] *Seto, T., Tajima, Y.*, Jap. J. Appl. Phys. **5**, 534 (1966), Observation of Kink Bands in Oriented Polyethylene.

[345] *Slutsker, A.I., Gromov, A.E., Pschezhetskii, V.S.*, Fis. Tverd. Tela, **6**, 456 (1964), Struktur und Festigkeit nadelförmiger Polyoxymethylenkristalle, die nach der Methode der gerichteten Polymerisation hergestellt wurden.

[346] *Smith, D.C.*, Ind. Eng. Chem. **48**, 1161 (1956), Molecular structure of Marlex polymers.

[347] *Statton, W.O., Hoffmann, L.C.*, Nature (London) **176**, 561 (1955), Structure in Vitreous Silicates as Shown by Low-Angle Scattering of X-Rays.

[348] *Statton, W.O.*, J. Polym. Sci. **22**, 385-397 (1956), Crystallite Regularity and Void Content in Cellulose Fibers as Shown by Small-Angle X-Ray Scattering.

[349] *Statton, W.O., Godard, G.M.*, J. appl. Phys. **28**, 1111 (1957), Tridirectional X-Ray Patterns of Oriented Film at wide and Small-Angles.

[350] *Statton, W.O.*, ASTM Special Technical Publication No. 247 (1958), The Use of X-Ray Diffraction and Scattering in Characterization of Polymer Structure.

[351] *Statton, W.O.*, J. Polymer Sci. **28**, 423 (1958), Higher Orders of Long Period X-Ray Diffraction in Polyethylene Fibers.

[352] *Statton, W.O.*, J. Polymer Sci. **41**, 143 (1959), Polymer Texture The Arrangement of Crystallites.

[353] *Statton, W.O., Hoffmann, L.C.*, J. appl. Phys. **31**, 404 (1960), Structure in Vitreous Silicate Fibers as Shown by Small-Angle X-Ray Scattering.

[354] *Statton, W.O., Geil, P.H.*, J. Appl. Polymer Sci. **3**, 357 (1960), Recrystallization of Polyethylene during Annealing.

[355] *Statton, W.O.*, J. Appl. Phys. **32**, 2332 (1961), Rate of Recrystallization of Polyethylene Single Crystals.

[356] *Statton, W.O.*, J. Polymer Sci. **58**, 205 (1962), Microvoids in Fibers as Studied by Small-Angle Scattering of X-Rays.

[357] *Statton, W.O.*, Newer Methods of Polymer Characterization ed. B. Ke, Interscience 1964, Small-Angle X-Ray Studies of Polymers.

[358] *Stenius, Ake*, Svensk Papperstidning, 1-17 (1954), The General Discussion on Cellulose, I. The Fibrillar Structure of the Wood Cellulose Fibre, II. The Molecular Order and the Chemical Nature of the Wood Cellulose Fibre.

[359] *Sterling, C.*, J. Polymer Sci. **56**, 10 (1962), A Low-Angle Spacing in Starch.

[360] *Stern, F.*, Trans Faraday Soc. **51**, 430 (1955), Dependence on Moisture Content of the Small-Angle X-Ray Scattering Power of Cellulose Fibers.

[361] *Stuart, H.A.*, Ann. New York Acad. Sci. **83**, 3, (1959), Problems of High-Polymer Crystallinity.

[362] *Swanbeck, G., Thyresson, N.*, Acta Dermato-Venereologica, **41**, 289-296 (1961), An X-Ray Diffraction Study of Scales from Different Dermatoses.

[362a] *Suzuki, Y., Sakurada, I.*, Nippon Hoshasen Kobunshi Kenkyu Kyokai Nempo **Z**, 25-32 (1965-66), Small-Angle X-Ray studies on polyethylene obtained by gas-phase polymerization of ethylene.

[363] *Takagi, Y., Hattori, H., Nukushina, Y.*, Chem. High Polymers Japan, **21**, 398 (1964), Untersuchungen über das Verstrecken von Polyamidfasern. V. Umwandlung des Kristallzustandes beim Verstrecken.

[363a] *Takayanagi, M., Imada, K., Kajiama, T.*, J. Polym. Sci. C, **15**, 263-80 Disc. 280-1 (1966), Mechanical properties and fine structure of drawn polymers.

[364] *Tanaka, K., Seto, T., Hara, T., Tajima, Y.*, Rep. Progr. Polymer Phys. Jap. **7**, 63 (1964), Structure and Plasticity of Oriented Polyethylene.

[365] *Tomlin, S.G., Worthington, C.R.*, Proc. Roy. Soc. **A 235**, 189 (1956), Low-Angle X-Ray Diffraction patterns of Collagen.

[366] *Tsukiyama, H.*, J. Sci. Hiroshima Univ. Ser. A-II, **25**, 261-270 (1961), X-Ray Study on the Effect of Heating on Structures of Nylon 6.

[366a] *Tsvankin, D. Ya.*, Vysokomol. Soedin., Ser. A 9, 2668–2671 (1967), Low angle x-ray diagrams and structure of oriented films of polyethylene.

[367] *Vogel, W.*, Phys. Status Solidi 14, 255-286 (1966), Neue Strukturmodelle aus Glas und ihre Beziehung zu den physikalischen und chemischen Eigenschaften.

[367a] *Vonk, C. G., Kortleve, G.*, Kolloid-Z. u. Z. f. Polym. 220, 19–24 (1967), X-Ray Small Angle Scattering of Bulk Polyethylene.

[368] *Weinberg, D.L.*, J. Appl. Phys. **33**, 1012 (1962), Surface Effects in Small-Angle X-Ray Scattering.

[368a] *Wunderlich, W.*, Makromol. Chem. 108, 315–317 (1967), Comparison of Zimm diagrams measured by light scattering and x-ray small angle scattering in the same system. Poly (methyl methacrylate) with molecular weight of 500,000 in acetone.

[369] *Zahn, H., Pieper, W.*, Koll. Z. 180, 97 (1962), Molekülängenunabhängige Langperioden in Kleinwinkelröntgenogrammen von Oligomeren.

[370] *Zannetti, R., Ferrero, A., Ferracini, E., Fishera, A.M.*, Gazetta Chimica Italiana 96, 786-802 (1966), Studio delle zone d.ordine nel polipropilene isotattico.

[370a] *Zannetti, R., Martelli, A., Fichera, A.M.*, Gazz. Chim. Ital. 97, (4) 452-69 (1967) Order zone study of isotactic polypropylene. II. Small-Angle X-Ray diffraction at 20-200.

[370b] *Zannetti, R., Fichera, A., Celotti, G., Ferrero Martelli, A.*, Europ. Pol. J. 4, 399-411 (1968). A study of the Order Zones in isotactic Polypropylene III: General interpretation of the S.A. Scattering.

[371] *Zarzycki, J., Nauchin, F.*, Phys. Chem. Glasses, 8, 11-20 (1967), Study of kinetics of the metastable phase separation in the lead oxide – boron trioxide system by Small-Angle Scattering of X-Rays.

[371a] *Zarzycki, J., Naudin, F.*, C.R. Acad. Sci. Paris, Ser. A.B., 265 B, 1456–1459 (1967), Spinodal decomposition of a boric oxide-lead oxid-alumina glass demonstrated by small angle x-ray diffraction.

[372] *Zhurkov, S.N., Marikhin, V.A., Slutsker, A.I.*, Fis. Tverd. Tel. 1, 1159 (1959), Soviet Physics-Solid State 1, 1080 (1960), A Study of the Submicroscopic Porosity of Deformed Polymers.

[373] *Zhurkov, S.N., Slutsker, A.J., Yastrebinskii, A.A.*, Doklady Akad. Nauk SSR **153**, 303-305 (1963), Effekt of stress on the supermolecular structure of oriented polymers.

[374] *Zhurkov, S.N., Slutsker, A.I., Yastrebinskii, A.A.*, Fiz. Tverd. Tela, 6, 3601-3607 (1964), Transl. in: Soviet Phys. Solid State 6, 2881-2886 (1965), Relation between elastic deformation and structure of oriented polymers.

[375] *Zubov, Yu.A., Markova, G.S., Kargin, V.A.*, Vysokomol. soyed. **5**, 1171 (1963), Transl. in: Polymer Sci. USSR **5**, 234 (1964), X-Ray Studies of Polyethylene, Polycaproamide and Polyethyleneterephtalate Fibers.

[376] *Zubov, Yu.A., Tsvankin, D.Ya.*, Vysokomol. Soedin. 6, 2131-2138 (1964), Bestimmung der Größe der Kristallite, der amorphen Bereiche und des Kristallinitätsgrades mit Hilfe der Langperiode.

[377] *Zubov, J.A., Tsvankin, D.J., Markova, G.S., Kargin, V.A.*, Vysokomolecul. Soedin. 6, 406 (1964), Transl. in: Polymer Sci. USSR 6, 450 (1964), The problem of long periods in polypropylene fibres. I. Effect of orientation and heat treatment (annealing) on the size of the long periods.

[378] *Zubov, Yu.A., Tsvankin, D.Ya., Markova, G.S., Kargin, V.A.*, Dokl. Akad. Nauk SSSR 157, 948 (1964), Temperaturabhängigkeit der Langperiode in orientierten Polymeren.

[379] *Zubov, J.A., Tsvankin, D.J.*, Polymer Sci. USSR, 7, 2028 (1965), Orig.: Vysokomol. Soed. 7, 1848-1856 (1965), The Variation with Temperature of the Long Period in Oriented Polymers-II.

Pure metals

[380] *Atkinson, H.H., Lowde, R.D.*, Phil. Mag. **2**, 589 (1957), Small-Angle Scattering from Deformed Metals.

[381] *Atkinson, H.H.*, Phil. Mag. **3**, 476-88 (1958), Small-Angle Scattering from cold worked and fatigued metals.

[382] *Atkinson, H.H., Smallmann, R.E., Westmacott, K.H.*, J. of Appl. Physics. **30**, 646 (1959), Small-Angle Scattering of X-Rays from Neutrons Irradiated Copper.

[382a] *Beeman, W.W., Kaesberg, P., Anderegg, J.W., Webb, M.B.*, Handbuch der Physik **32**, 440 Springer-Verl. (1957), Small-Angle Scattering from Cold-Worked Metals.

[382b] *Betekhtin, V., Slutsker, A.I.*, Sov. Phys. Solid State **4**, 94-98 (1962), Study of the disorientation of mosaic blocks by measurements of Small-Angle X-Ray Scattering.

[383] *Betekhtin, V.I., Slutsker, A.I.*, Fis. Metall i. Metalloved. **13**, 615 (1962), Untersuchung der Orientierung der Mosaikblöcke im Aluminium.

[384] *Betekhtin, V.I., Slutsker, A.I.*, Fiz. Metallov Metallovedenie (USSR) **21**, 358-61 (1966), Transl.: Phys. Metals Metallography (GB) **21**, 3, (66/67), The Relative Proportion of Intra- and Intergranular Double X-Ray Reflections in Polycrystalline Metals.

[384a] *Franks, A., Holden, J.*, Nature, **176**, 1022 (1955), Investigation of the fatigue of metals by X-Ray Scattering.

[385] *Fricke, H., Gerold, V.*, J. appl. Phys. **30**, 661 (1959), Experiments on Double Bragg Reflections in Deformed and Undeformed Metal Foils.

[386] *Gonser, U., Fujita, F.E.*, Physica, **24**, Supplem. 177-8 (1958), Small-Angle Scattering of X-Rays by a Deuteronirradiated Germanium Crystal.

[386a] *Grosskreutz, J.C., Rollins, F.R.*, J. appl. Phys. **30**, 668 (1959), Small-Angle X-Ray Scattering from Copper and Aluminium Under Cyclic Stress.

[387] *Guentert, O.J.*, Phys. Rev. **138**, A 732-36 (1965), Angular distribution of speculary reflected X-Rays from thin films.

[388] *Hofer, E.M., Chollet, L.F., Hintermann, H.E.*, J. Electrochem. Soc. (USA) **112**, 1145-7 (1965), Defects in the Structure of Electro-Deposited Copper.

[389] *Kalikhman, V.L., Umanskij, J.S.*, Fis. Tverd. Tela, **3**, 331-335 (1961), Transl.: Sov. Phys. Solid State **3**, 238-240 (1961), Determination of the Orientation of Diffusion Submicropores in Brass by the Method of Small-Angle Scattering.

[390] *Neynaber, R.H., Brammer, W.G., Beeman, W.W.*, J. appl. Phys. **30**, 656 (1959), On The Mechanism of the Small-Angle X-Ray Scattering from Cold Worked Metals.

[391] *Nishchirii, V.G., Terminasov, Yu.S.*, Fiz. Metallov Metallovedenie, **21**, 33-42 (1966), Transl.: Phys. Metals Metallography **21**, (1966), A Low-Angle X-Ray Diffraction Study of the Structure of Fatigued Nickel.

[392] *Pines, B.J., Kusnezova, R.N.*, Fis. Tverd. Tela **3**, 1475 (1961), (Sov. Phys. Solid State **3**, 1070-1076 (1961), Variation of the Submicroporosity in Electrolytic Metallic Films with Heating and Loading.

[393] *Pines, B.J., Kusnezova, R.N.*, Fis. Tverd, Tela **4**, 1247 (1962), (Sov. Phys. Solid State **4**, 914-917 (1962)), Alternation of the Submicroporosity in Electrolytic Iron Films after Annealing under Load.

[394] *Pines, B.J., Kusnezova, R.N.*, Fis. Tverd. Tela **7**, 961 (1965), (Sov. Phys. Solid State **7**, 775-778 (1965)), On the Question of the Absolute Value of Submicroporosity Developed in Electrolytic Films After Annealing and under Load.

[394a] *Plavnik, G.M., Robinskij, B.M.*, Fis. Tverd. Tela **2**, 1099 (1960), Sov. Phys. Solid State **2**, 994-1000 (1960), Investigation of the Submicroporosity of Low-Absorption Materials by the Method of Multiple Small-Angle Scattering of X-Rays.

[395] *Robinson, W.H., Smoluchowski, R.*, J. appl. Phys. **27**, 657-8 (1956), Low-Angle X-Ray Scattering by Surface Defects.

[395a] *Robinson, W.H., Smoluchowski, R.*, J. Appl. Phys. **30**, 617 (1959), Small-Angle Scattering of X-Rays by Plastically Deformed Single Crystals.

[396] *Schilling, W., Schmatz, W.*, Phys. stat. sol. **4**, 95-101 (1964), Kleinwinkelstreuung an neutronenbestrahltem Kupfer.

[397] *Seeger, A., Gerold, V., Rühle, M.*, Z.f. Metallkunde **54**, 493 (1963), Nachweis von dreidimensionalen Leerstellenagglomeraten in abgeschreckten Kupfereinkristallen mit Hilfe der Kleinwinkelstreuung von Röntgenstrahlen.

[398] *Smallman, R.E., Westmacott, K.H.*, J. appl. Phys. **30**, 603-616 (1959), Structure of Quenched and Irradiated Metals.

[399] *Stork, A., Christ, J., Schmatz, W.*, Z. angew. Phys. **18**, 468-471 (1965), Eine Untersuchung zur magnetischen Kleinwinkelstreuung von langsamen Neutronen an Versetzungen in Nickel.

[400] *Thomas, K., Franks, A.*, J. appl. Phys. **30**, 649 (1959), Study of X-Ray Scattering from Fatigued Metals.

[401] *Warren, B.E.*, Phys. B. 41 (4) 847 (1962), Aust. J. Phys. **13**, 376-383 (1960), Small-Angle Intensities from Double Bragg Reflections in Cold-Worked Metals.

[402] *Webb, M.B., Beeman, W.W.*, Acta Metallurgica 7, 203 (1959), Double Bragg-Scattering in Cold-worked Metals.

[403] *Wild, R.L., Ogier, W.T., Nickel, J.C.*, Bull. Am. Phys. Soc. **2**, 340 No. 7 Paper C6, Small-Angle X-Ray Scattering from Plastically Deformed Cu and Ni.

[404] *Zhurkov, S.N., Betekhtin, V.I., Petrov, A.I., Slutsker, A.I.*, Fis. Metall. i. Metalloved. **18**, 270-276 (1964), Die Veränderung der Orientierung der Blöcke in Metallen beim Fließen.

Alloys Al – Zn

[405] *Akopjan, R.A., Tusov, L.V.*, Fis. Metall. i. Metalloved. **20**, 361-367 (1965), Untersuchung der Frühstadien der Alterung einer Al-Zn-Legierung nach der Methode der Röntgenkleinwinkelstreuung.

[406] *Bonfiglioli, A.F.*, J. Phys. Rad. **23**, 817-819 (1962), Formation et Réversion des zones de Guinier-Preston.

[407] *Bonfiglioli, A.F., Guinier, A.*, Acta Metallurgica (USA) **14**, 1213-24 (1966), The Structure of G.P.-Zones in Al-Zn Alloys at the First Stage of Formation.

[408] *Gerold, V., Schweizer, W.*, Z. Metallkde., **52**, 76 (1961), Die Kinetik von Entmischungsvorgängen in übersättigten Aluminium-Zink-Mischkristallen.

[409] *Gerold, V.*, Phys. stat. sol. **1**, 37 (1961), Die Zonenbildung in Aluminium-Zink-Legierungen.

[409a] *Gould, R.W., Starke, E.A.*, jr., Advan. X-Ray Anal. 9, 59-73 (1966), Observations of G-P zone reversion in Al-Zn-Mg alloys by Small-Angle Scattering and transmission electron microscopy.

[410] *Graf, R.*, Compt. rend. **242**, 1311 (1956), Etude aux rayons X de phénomènes de précipitation dans l'alliage Al-Zn-Mg a 7 % de Zn et de 3 % de Mg.

[411] *Graf, R.*, Compt. rend. **244**, 337 (1957), Etude aux rayons X de phénomènes de précipitation dans l'alliage Al-Zn-Mg a 9 % Zn et 1 % Mg (AZ9G1).

[412] *Graf, R.*, Compt. Rend. **249**, 1110 (1959), Quelques observations sur les phénomènes des réversion dans l'alliage Al-Zn à 10 % de zinc. Influence d'un écrouissage sur la décomposition de la solution solide obtenue par réversion.

[413] *Graf, R., Genty, B.*, Compt. Rend. Acad. Sci. Paris, **251**, 2517 (1960), Étude aux rayons X et au microscope électronique de la précitation dans un alliage Al-Zn à 40 % de zinc.

[414] *Graf, R.*, J. Phys. Rad. **23**, 819-822 (1962), Etude de la Précipitation dans un Alliage Al-Zn à 30 % de Zn.

[415] *Herman, H., Cohen, J.B.*, Nature, 191, 63 (1961), Resistivity Changes due to Formation of G.P. Zones (Clusters rich in Solute).

[416] *Herman, H., Cohen, J.B., Fine, M.E.*, Acta Metallurg. 11, 43-56 (1963), Formation and Reversion of Guiner-Preston Zones in Al-5,3 at. % Zn.

[417] *Hirano, K.*, J. Phys. Soc. Japan, **10**, 995 (1955), Aging Process in Quenched Al-Zn Solid Solutions.

[418] *Johnson, A.A., Hughes, E.J., Barton, P.W.*, J. Inst. Metals, **94**, 186-87 (1966), The Solves Curve for G.P. Zones in Al-Zn Alloys.

[419] *Merz, W., Anathasam, T.R., Gerold, V.*, Phys. status solidi 8, K5-K8 (1965), Struktur und Eigenschaften von Aluminium-Zinkmischkristallen mit Guinier-Preston-Zonen.

[420] *Merz, W., Gerold, V.*, Z. Metallkde, **57**, 607-615 (1966), Strukturelle Untersuchungen der Ausscheidung in Al-Zn-Legierungen.

[421] *Rognlic, M.*, Electron Microscopy A, 209-210 1964, (G.P. zones in an Al-Zn-alloy.

[422] *Tusov, L.V.*, Kristallografia, **10**, 51 (1965), Engl. Übers.: Sov. Phys. Cryst. **10**, 39-42 (1965), Method of Determining the Dimensions of Guinier-Preston-Zones in Al-Zn Alloys.

Al – Cu

[423] *Baur, R., Gerold, V.*, Z. Metallkde. **52**,671, (1961), Entmischungsvorgänge im System Aluminium-Silber.

[424] *Baur, R., Gerold, V.*, Acta metallurgica (USA) **10**, 637-45 (1962), The Existence of a Metastable Miscibility Gap in Aluminium-Silver Alloys.

[425] *Belbeoch, B., Guinier, A.*, Acta Met. **3**, 370 (1955), Relation entre les structures et les proprietes des alliages Al-Ag pendant le durcissement structural.

[426] *Gerold, V.*, Z. Metallkde. 46, 623 (1955), Über die Aushärtung von Al-Ag-Legierungen, IX. Röntgenographische Untersuchungen über die Kalthärtung.
[427] *Freise, E.J., Kelly, A., Nicholson, R.B.*, Acta Met. 9, 250 (1961), Guinier-Preston Zones in an Aluminium-Silver Alloy.
[428] *Guinier, A.*, J. Metals 8, 673 (1956), Precipitation Phenomena in Supersaturated Solid Solutions.
[429] *Jan, J.P.*, J. appl. Phys. 26, 1291-7 (1955), Small-Angle X-Ray Scattering from Precipitates in Cold-worked Al-Ag and Al-Zn.
[430] *Kantola, M., Kähkönen, H.*, Ann. Acad. Sci. Fennicae, A VI. Nr. 173 (1965), Small-Angle X-Ray Investigation of the Precipitation in an Al-Ag Alloy.
[431] *Sato, S., Kelly, A.*, Acta Metall. 9, 59-61 (1961), X-Ray Small-Angle Scattering from Guinier-Preston-Zones in Deformed Al-Ag Single Crystals.
[432] *Synecek, V., Sebo, P.*, J. Phys. 14, 622-628 (1964), On the configuration of Guinier-Preston Zones in Al-Ag and Al-Zn alloys.

Al – Ag

[433] *Baur, R.*, Z. Metallkde. 57, 368-74 (1966), Clustering in Aluminium Copper Alloys. III. Qualitative X-Ray Investigations on Nucleation and Growth of the Θ-Phase in an Aluminium 2 At. % Copper Alloy.
[434] *Baur, R., Gerold, V.*, Z. Metallkde, 57, 181-186 (1966), Entmischungsvorgänge im System Aluminium Kupfer. I. Quantitative röntgenographische Bestimmung der Größe und Menge von G.P. Zonen I.
[435] *Gerold, V.*, Z. Metallkde. 45, 593-599 (1964), Röntgenographische Untersuchungen über die Aushärtung einer Al-Cu-Legierung mit Kleinwinkel-Schwenkaufnahmen.
[436] *Gerold, V.*, Acta Cryst. 11, 238 (1958), The Structure of Guinier-Preston Zones in aluminium-copper alloys.
[437] *Silcock, J.M., Heal, T.J., Hardym, H.K.*, J. Inst. Metals 82, 239 (1953-54), Structural Ageing Characteristics of Binary Al-Cu Alloys.
[438] *Toman, K.*, Acta Cryst. 10, 187 (1957), The Structure of Guinier-Preston Zones. II. The Room Temperature Ageing of the Al-Cu Alloy.

Other alloys

[439] *Nagorsen, G., Averbach, B.L.*, Met. Rep. 11 (7) 1960 (Mass. Inst. of Techn.) Small-Angle Scattering in Gold-Nickel Alloys.
[440] *Kalikhman, V.L., Umanskij, J.S.*, Dokl. Akad. Nauk SSSR 132, 108 (1960), Untersuchung des Anfangsstadiums der Porenbildung in den Legierungen L 62 und N80CH20 mit der Methode der Röntgenkleinwinkelstreuung.

Anomalous surface reflection

[441] *Guentert, O.J.*, J. appl. Phys. 36, 1361 (1965), Study of the Anomalous Surface Reflection of X-Rays.
[442] *Nigam, A.N.*, Phys. Rev. 138, A 1189-91, Origin of Anomalous Surface Reflection of X-Rays.
[443] *Warren, B.E., Clarke, J.S.*, J. appl. Phys. 36, 324 (1965), Interpretation of the Anomalous Surface Reflection of X-Rays.
[444] *Yoneda, Y.*, Phys. Rev. 131, 2010 (1963), Anomalous Surface Reflection of X-Rays.

Experimental technique

[445] *Beeman, W.W., Neynaber, R.H.,* Am. Phys. Soc. No. 17 Washington 1954, Phys. Rev. **95**, 617 (1954), Equipment for the Measurement of very small angle X-Ray-Scattering Cross-Sections.

[446] *Bergman, M.E., Fankuchen,* Rev. Sci. Instr. **20**, 696 (1949), Modification of X-Ray Diffraction Microcamera to permit Study of long spacings.

[447] *Bolduan, E.A., Bear, R.S.,* J. appl. Phys. **20**, 983 (1949), Effective Use of Collimating Apertures in Small-Angle X-Ray Diffraction Cameras.

[448] *Bonse, U., Hart, M.,* Conference on Small-Angle X-Ray Scattering. *H. Brumberger,* Ed. New York: Gordon and Breach Science Publ. 1966.

[449] *Bonse, U., Hart, M.,* Report 382, issued by the Materials Science Center. A New Tool for X-Ray Small-Angle Scattering and X-Ray Spectroscopy. The Multiple Reflection Diffractometer.

[450] *Bonse, U., Hart, M.,* Appl. Phys. Let. 7, 238 (1965), Tailless X-Ray Single-Crystal Reflexion Curves obtained by Multiple Reflection.

[451] *Bonse, U., Hart, M.,* Z. f. Phys. **189**, 151 (1966), Small-Angle X-Ray Scattering by Sperical Particles of Polystyrene and Polyvinyltoluene.

[451a] *Brady, G.W.,* Rev. Sci. Instrum. **38**, 6, 736-9 (1967), Liquid metal sample holder for low-angle X-Ray diffraction.

[451b] *Brumberger, H., Alexandropoulos, N.G.,* Rev. Sci., Instr. **38**, No. 11 1579-80 (1967), High temperature sample cell for the Kratky small angle X-Ray camera.

[452] *Damaschun, G.,* Naturwiss. **51**, 378 (1964), Ein lichtstarker Monochromator zur Untersuchung der Kleinwinkelstreuung von Röntgenstrahlen.

[453] *Damaschun, G.,* Exp. Techn. Phys. **13**, 224-230 (1965), Zur Kollimation von Röntgenstrahlen unter Ausnutzung der Totalreflexion III. Ein lichtstarker Monochromator zur Untersuchung der Röntgenkleinwinkelstreuung.

[454] *Damaschun, G., Müller, J.,* Z. Naturforsch. **20a**, 1274 (1965), Die Messung der Absolutintensität der Röntgenkleinwinkelstreuung durch Schwächung des Primärstrahles mit Absorptionsfiltern nach vorheriger Monochromatisierung durch Totalreflexion.

[455] *Eins, S., Unangst, D.,* Z. Naturforschung 17a, 198-202 (1962), Über die Neukonstruktion einer Röntgenkleinwinkelkamera vom Kratky-Typ mit großem Auflösungsvermögen.

[456] *Fiedler, H.,* Naturwiss. 44, 85-6 (1957), Eine variable Röntgenkleinwinkelkamera einfacher Bauweise.

[457] *Gromov, A.E., Slutsker, A.I.,* Pribori i technika Eksperimenta **3**, 165 (1964), Eine Mikrostrahlkammer für die Untersuchung der Röntgenstreuung bei kleinen Winkeln.

[458] *Hagström, S., Siegbahn, K.,* J. Ultrastructure Res. **3**, 401-419 (1960), A Small-Angle X-Ray Scattering apparatus using a spherically bent crystal.

[458a] *Heine, S.,* Makromol. Chem. 103, 289–290 (1967), Automatic graphic recording of x-ray small angle diffraction curves.

[459] *Henke, B.L., Du Mond, J.W.,* J. Appl. Phys. **26**, 903 (1955), Submicroscopic Structure Determination by Long Wavelength X-Ray Diffraction.

[460] *Henke, J., Schulze, G.E.R.,* Z. Naturf. **12a**, 346 (1957), An improved Frame Camera (Rahmenkammer) for X-Ray low-Angle Scattering.

[461] *Jagodzinski, H., Wohlleben, K.,* Z. Elektrochem. 64, 212-216 (1960), Eine neue Kleinwinkelkamera mit fokussierenden Monochromatoren.

[461a] *Jellinek, G.*, Zs. f. Instrumentenkunde 75, 31–47 (1967), Zur Konstruktion optimaler Blendensysteme für die Röntgenkleinwinkelstreuung. I. Photographische Kammer mit zwei Lochblenden.

[461b] *Jupe, K.*, Z. Naturforsch. **21a**, 1997-2000 (1966), Eine Methode zur Verbesserung der Monochromatisierung bei Röntgenkleinwinkel-Experimenten.

[462] *Kahovec, L., Weiß, H.*, Monatshefte f. Chemie, **93**, 335-347 (1962), Schwärzungsbestimmung bei Röntgenkleinwinkelaufnahmen durch automatische Zählung der Silberkörner.

[463] *Kheiker, D.M., Feigin, L.A., Yakovlev, I.I.*, Kristallografiya **10**, 447-449 (1965), Transl.: Sov. Phys. Cryst. **10**, 372-4 (1965), A Small-Angle X-Ray Diffractometer with an Asymmetric Focussing Monochromator.

[464] *Kratky, O.*, Zschr. f. Elektrochem. **58**, 49-53 (1954), Neues Verfahren zur Herstellung von blendenstreuungsfreien Röntgenkleinwinkelaufnahmen I.

[465] *Kratky, O., Sekora, A.*, Monatshefte f. Chemie, **85**, 660 (1954), Neues Verfahren zur Herstellung von blendenstreuungsfreien Röntgenkleinwinkelaufnahmen II.

[466] *Kratky, O.*, Kolloid-Z. 144, 110-120 (1955), Neues Verfahren zur Herstellung von blendenstreuungsfreien Röntgenkleinwinkelaufnahmen III.

[467] *Kratky, O.*, Z. f. Elektrochemie, 62, 66-73 (1958), Neues Verfahren zur Herstellung von blendenstreuungsfreien Röntgenkleinwinkelaufnahmen IV.

[468] *Kratky, O.*, Z. f. Elektrochem. **62**, 73-77 (1958), Neues Verfahren zur Herstellung von blendenstreuungsfreien Röntgenkleinwinkelaufnahmen V.

[469] *Kratky, O., Kahovec, L., Werner, H.*, Z. f. Elektrochem., Ber. d. Bunsenges. f. phys. Chem. 63, 64-70 (1959), Mehrfachphotometrierung, ein Verfahren zur genauen Vermessung von Röntgenkleinwinkelaufnahmen.

[470] *Kratky, O., Wawra, H.*, Mh. Chem. **94**, 981 (1963), Messungen der Absolutintensität der diffusen Röntgenkleinwinkelstreuung durch mechanische Schwächung des Primärstrahles bei Anwendung der Impulszähltechnik.

[471] *Kratky, Ch., Kratky, O.*, Z. f. Instrkde. 72, 302-304 (1964), Ein einfach programmierbares Schrittschaltwerk für die Messung der Röntgenkleinwinkelstreuung.

[472] *Kratky, O., Leopold, H.*, Makromol. Chem. **75**, 69-74 (1964), Messung und Unterdrückung der Blendenstreuung am Kollomationssystem für Röntgenkleinwinkeluntersuchungen.

[473] *Kratky, O., Pilz, I., Schmitz, P.J.*, J. Colloid Interf. Sci. 21, 24-34 (1966), Absolute Intensity Measurement of Small-Angle X-Ray Scattering by Means of a Standard Sample.

[474] *Leopold, H.*, Elektronic, 14, 359 (1965), Programmierbare Messeinrichtung für Röntgenkleinwinkelstreukurven.

[475] *Luzzati, V., Baro, R.*, J. Phys. Rad. 22, 186 A-188 A (1961), Description of a Small-Angle X-Ray Diffraction Camera with Linear Collimation.

[476] *Mitra, G.B., Maitra, J.C.*, Indian J. Phys. 36, 335-43 (1962), Construction and Working Principles of the Banerjee Camera for Studying Small-Angle X-Ray Scattering.

[477] *Ruck, H., Kouris, M., Manley, R.St.J.*, J. Ultrastructure Res. 3, 46-50 (1959), A Multipurpose Fiber and Crystallinity X-Ray Diffraction Camera.

[478] *Schulze, G.E.R., Henke, Y.*, Exper. Techn. der Phys. **5**, 180-183 (1957), Further Development of the Limiting Chamber For the Recording of Small-Angle X-Ray Scattering.

[478a] *Siegbahn, K., Hagström, S.*, X-Ray Microscopy and X-Ray Microanalysis. Elsevier Publ. Comp (1960), 467–471. Small Angle Scattering Apparatus with a Point-Focusing Monochromator.

[479] *Slutsker, A.I., Egorow, E.A.*, Transl.: Instr. exper. Techn. (USA) **5**, 788-94 (1960), Apparatus for the Measurement of Small-Angle X-Ray Scattering.

[480] *Teare, P.W.*, Brit. J. appl. Phys. **11**, 287-289 (1960), Method of recording Low-Angle X-Ray Scattering when intensity scattered by specimen changes rapidly with time.

[481] *Tusov, L.V., Akopjan, R.A.*, Savodskaja Laboratoria **30**, 622 (1964) Röntgenkamera für die photographische Registrierung der Kleinwinkelstreuung.

[482] *Unangst, D.*, Exp. Techn. Phys. **12**, 304 (1964) Zur Kollimation von Röntgenstrahlen unter Ausnutzung der Totalreflexion. I. Allgemeine Betrachtungen über Kreiszylindrische Kollimatoren und ein Ausblick auf ihre Anwendung in der Faseroptik.

[483] *Unangst, D.*, Exp. Techn. Phys. **12**, 320 (1964) Zur Kollimation von Röntgenstrahlen unter Ausnutzung der Totalreflexion II. Experimentelle Untersuchungen an gezogenen Glaskappilaren mit kreisförmigem Querschnitt.

[484] *Unangst, D.*, Z. f. Naturforsch. **20a**, 1366-1367 (1965) Zur Verkleinerung der Störstrahlung beim Kratkyschen Blendensystem für die Untersuchung der Röntgen-Kleinwinkel-Streuung.

[485] *Unangst, D., Damaschun, G.*, Optik und Spektroskopie aller Wellenlängen, Akademie-Verlag Berlin, S. 308 (1962) Kollimation durch Totalreflexion bei Röntgenfeinstrukturaufnahmen.

[486] *Unangst, D., Siegel, W.*, Exp. Techn. Phys. **11**, 275 (1963) Zur Leistungsfähigkeit und Verbesserung von Rundblendensystemen für die Untersuchung der Röntgenkleinwinkelstreuung.

[487] *Wassberg, G., Siegbahn, K.*, Ark. Fys. **14**, 1-15 (1958) Small Angle Scattering of X-Rays.

[488] *Weinberg, D.L.*, Rev. Sci. Instr. **34**, 691 (1963) Absolute Intensity Measurements in Small Angle X-Ray Scattering.

[489] *Worthington, C.R.*, J. Sc. Instr. **33**, 66 (1956) Small Angle X-Ray Diffraction Unit.

[490] *Zhurkov, S.N., Slutsker, A.I.*, J. techn. Fis. **27**, 1392 (1957) Transl.: Sov. Phys. Techn. Phys. **2**, 1287-89 (1957) Very-low-angle Scattering of X-Rays by Submicroscopic Imperfections.

Methods of correction of experimental scattering curves

[491] *Chu, B., Tan Creti, D.M.*, Acta. Cryst. **18**, 1083 (1965) Infinite Slit Height Corections in Small Angle X-Ray Scattering.

[492] *Fedorov, B.A., Feigin, L.A., Dembo, A.T.*, Kristallografia **10**, 788 (1965) Berücksichtigung der Kollimatorkorrektur bei der Kleinwinkelstreuung von Röntgenstrahlen. Der Fall eines „unendlich hohen Spaltes".

[493] *Filipooich, V.N.*, Zh. tekh. Fiz. 27, 1029-44 (1957) Collimation Correction in Low-Angle X-Ray Scattering. Übers.: Sov. Phys. Techn. Phys. **2**, 5-8, 938-953 (1957).

[494] *Gerold, V.*, Acta Cryst. **10**, 287 (1957) Neue Methoden zur Eliminierung des Spalteinflusses von röntgenographischen Kleinwinkelaufnahmen (graphisch).

[495] *Heine, S.*, Acta Physica Austriaca **16**, 144 (1963) Die Entschmierung von Röntgen-Kleinwinkel-Streukurven mit einer elektronischen Rechenanlage.

[496] *Heine, S., Roppert, J.*, Acta Physica Austriaca **15**, 148 (1962) Die Behandlung des Problems der Entschmierung von Röntgen-Kleinwinkelstreukurven mittels einer elektronischen Rechenanlage.

[497] *Heine, S.*, Makromol. Chemie **103**, 289-290 (1967) Automatische graphische Darstellung von Röntgenkleinwinkel-Streukurven.

[498] *Knapp, H.*, Kolloid, Z. **142**, 163 (1955) Ein einfaches Entschmierungsverfahren für Röntgenkleinwinkel-Untersuchungen mit Hilfe der neuen Kratkyschen Kamera.

[499] *Kratky, O., Porod, G.*, Z. Skala, Acta Phys. Abstr. **13**, 76 (1960) Verschmierung bei Röntgenkleinwinkeldiagrammen.

[499a] *Krigbaum, W.R., Godwin, R.W.*, Rev. Sci. Instr. **38**, 398-404 (1967) Theoretical Main Beam Profiles for the Kratky Small Angle Camera.

[499b] *Lake, J.A.*, Acta Cryst. **23** (2) 191-4 (1967), An Interative Method of Slit-correcting Small-angle X-Ray Data.

[500] *Mazur, J., Wims, A.M.*, J. Res. Natl. Bur. Std. **A 70**, 467-471 (1966) Formal Solution for Slit Correktions in Small Angle X-Ray Scattering.

[501] *Ruland, W.*, Acta Cryst. 17, 138-142 (1964) Fourier Transform Methods for the Silt-height Correction in Small Angle Scattering.

[502] *Schmidt, P.W.*, Acta Cryst. **8**, 772 (1955) A New Method for Calculating the Effect of the Collimating System on the Small Angle X-Ray Scattering Pattern.

[503] *Schmidt, P.W., Height jr, R.*, Acta Cryst. **13**, 480 (1960) Slit Hight Corrections in Small-Angle X-Ray Scattering.

[504] *Schmidt, P.W.*, Acta Cryst **19**, 938-942 (1965) Collimation Corrections in Small Angle X-Ray Scattering.

[505] *Schulze, G.E.W., Diele, S., Peil, J.*, Acta Phys. Austriaca **24**, **2**, 129-34 (1966) A Numerical Method for the Unscrambling of X-Ray Small-Angle Scattering Diagrams.

[506] *Shchedrin, B.M., Feigin, L.A.*, Kristallografiya USSR, **11**, 159-163 (1966) Transl.: Soviet Phys. Cryst. (USA) **11**, 166-168 (1966) Calculation of the Collimation Correction in Small-Angle X-Ray Scattering. The Case of Finite Apertures.

[507] *Synecek, V.*, Acta Cryst. **13**, 378 (1960) A Method of the Intensity Distribution Measurement of the Small Angle Scattering of X-Rays Eliminating the Influence of the Imperfect Collimation.

[508] *Synecek, V.*, Acta Cryst. **15**, 642 (1962) Slit-High Correction in Small Angle Scattering without Spherical Symmetry.

[509] *Synecek, V., Simerska, M.*, Czech. J. Phys. **10**, 240-6 (1960) Rapid Graphical Determination of the Radial Intensity Distribution of the Small-Angle Scattering of X-Rays from the measured Data.

[510] *Tusov, L.V., Pigin, V.W.*, J. Techn. Fis. **34**, 2028 (1964) Transl.: Sov. Phys. Techn. Phys. **9**, 1560-67 (1964) Collimation Distortions of Small-Angle Scattering X-Ray Diagrams, and how to Eliminate them when Using a Primary Beam of Circular Cross Section.

[511] *Umanskii, Yu.S., Chirikov, N.N.*, Fiz. Metall. i. Metallov. 16, 480-481 (1963) Korrektur für die Konvergenz bei der Röntgenkleinwinkelstreuung.

Different topics

[512] *Baranov, V.G., Volkov, T.I., Shepelevskii, A.A.*, Vysokomol. Soedin., Ser. A **9**, (9), 1876-83 (1967) Effect of Polydispersity of Spherulites on Small-Angle Scattering of Polarized Light.

[512a] *Bassett, G.A., Keller, A.*, Phil. Mag. 9, 817 (1964) Low-Angle Scattering in an Electron Microscope: Application to Polymers.

[513] *Beebe, E.V., Coalson, R.L., Marchessault, R.H.*, J. Polym. Sci., Part C 13, 103 (1966) Characterization of Cellulose Gels by Small Angle Light Scattering.

[513a] *Berry, G.C., Nomura, H., Mayhan, K.G.*, J. Prolym. Sci., A-2, 5, (1), 1-21 (1967), Dilute Solution of an Polycarbonate in Good and Poor Solvents.

[514] *Budyanskii, G.M.*, Yadernaya Fiz. 1, 224-228 (1965) Transl.: Sov. J. Nucl. Phys. 1, 155-158 (1965) Multiple Scattering of a Narrow Beam of Fast Neutrons.

[515] *Coalson, R.L., Marchessault, R.H., Peterlin, A.*, J. Polym. Sci Part C 13, 123 (1966) Small Angle Scattering by a Three-Component System. Testing the Theory for Light Scattering.

[516] *Christ, J.*, Phys. stat. solidi 7, 537-576 (1964) Kleinwinkelstreuung von langwelligen Neutronen an Versetzungen in kaltverformtem Kupfer.

[516a] *Drahos, V., Delong, A.*, Slaboproudy Obz. 27, (8), 494-500 (1966) Small-Angle Diffraction in a Transmission Electron Microscope.

[517] *Ernst, V.*, Nucl. Phys. A 94, 528-36 (1967) Intensity Shift in Small Angle Multiple Scattering to Transversely Polarized Electrons.

[518] *Ferrier, R.P., Murray, R.T.*, J. Royal Microscopical Soc. 85, 323-335 (1966) Low-Angle Electron Diffraction.

[519] *Fink, M., Kessler, J.*, Z. Phys. 196, 1-15 (1966) Absolute effective cross-section for small-angle

[519a] *Kolyadin, A.I., Ageeva, L.E., Tyutikova, L.P.*, Fiz. Tverd. Tela 8, (11), 3254-9 (1966), Low-Angle Light Scattering in Ruby and Corundum Single Crystals.

[520] *Mahl, H., Weitsch, W.*, Naturwiss. 47, 301-2 (1960) Small-Angle Diffraction with Electron Beams.

[513b] *Bettelheim, F. A.*, J. Polym. Sci. A-2,5 1043–1053 (1967), Low-Angle Light Scattering of Ionotropic Gels.

[514a] *Clough, S. B., Stein, R. S.*, J. Appl. Phys. 38, 4446–4450 (1967), Scattering of Light by Ringed Spherulites Containing Biaxial Crystals.

[519b] *Mader, S., Herd, S. R.*, J. Appl. Phys. 38, 2396–2397 (1967), Electron Diffraction from Optical Gratings and Latex Spheres.

[521] *Mahl, H., Weitsch, W.*, Z. Naturf. 15a, 1051 (1961) Kleinwinkelbeugung mit Elektronenstrahlen.

[522] *Moore, R.S., Gieniewski, Ch.*, J. Polym. Sci., Part C, 13, 95 (1966) A New Technic for Observing Light-Scattering. Pattern from Polymer Films.

[523] *Samuels, R.J.*, J. Polym. Sci. Part C, 13, 37 (1966) Small-Angle Light Scattering from Deformed Spherulites. Theory and its Experimental Verification.

[524] *Shifrin, K.S.*, Izv. Akad. Nauk SSSR, Fiz. Atmos. Okeana, 2, 9, 928-32 (1966) Essential Range of Angles of Scattering in Measuring Particle Size Distribution by the Small-Angle Method.

[525] *Smart, J., Burge, R.E.*, Nature, Lond. 205, 1297 (1964) Small Angle Electron Diffraction Pattern of Spheres and Viruses.

[526] *Stein, R.S., Erhart, P., van Aartsen, J.J., Clough, S., Rhodes, M.*, J. Polym. Sci. Part C, 13, 1 (1966) Theory of Light Scattering from Oriented and Fiber Structure.

[526a] *Tompsett, M.F., Heitage, M.B., Grigson, C.W.B.,* Nature, **215**, (5100), 498-9 (1967) Small Angle Filtered Electron Diffraction from Growing Films.

[527] *Wade, R.H., Silcox, J.,* Phys. Stat. Sol. **19**, 57-62 (1967) Small Angle Electron Scattering from Vacuum Condensed Metallic Films I. Theory.

[528] *Wade, R.H., Silcox, J.,* Phys. Stat. Sol. **19**, 63-76 (1967) Small Angle Scattering from Vacuum Condensed Metallic Films II. Experimental Results.

[529] *Wallach, M.L.,* J. Polym. Sci. Part C, **13**, 69 (1966) Light Scattering from Polymer Films.

[530] *Yeh, G.S.Y., Geil, P.H.,* J. Mater Sci. **2**, (5), 457-69 (1967) Selected Area Small-Angle Electron Diffraction.

General View on Molecular Packing

A. I. Kitajgorodskij *)

With 22 figures

1. Introduction

The present paper deals with crystals built from molecules.

The geometrical peculiarity of a molecular crystal is self-evident. If it is possible to single out such groups of atoms in a crystal in which a distance from each atom of the group to at least one atom of the same group is significantly smaller than the distance to the adjacent atoms of other groups, the crystal is said to be molecular. Thus, for example, in hydrocarbon crystals, spacings between H atoms in different molecules are not less than 2.2-2.4 Å, whereas distances from these atoms to chemically-bonded C or N atoms are about 1 Å. Intramolecular spacings between bonded C atoms are 1.2-1.5 Å; at the same time, the atoms of different molecules are at least 3.3 Å apart. The order of difference between intramolecular and intermolecular distrances in two-atom O and N molecules is about the same.

Organic molecules containing hydroxyl (OH) and amine (NH_2) groups display a tendency to form so-called hydrogen bonds. In a hydrogen-bonded structure, two O atoms, or one O atom and one N atom, or two N atoms of adjacent molecules are so arranged that the proton is situated approximately on a straight line drawn between these two atoms. In this case, the difference between the intramolecular and intermolecular distances is somewhat smaller: the proton positioned between two O atoms lies I Å from the O atom of the same molecule, and 1.6-1.8 Å from that of a different molecule. But in this case, too, the molecule may be quite unambiguously defined.

Speaking about molecular crystals we shall mean mainly crystals of organic substances. Only very few inorganic compounds such as nitrogen or oxygen crystals, or molecules built from nitrogen and phosphor atoms form molecular crystals. There are inorganic substances which may only formally be classified as molecular crystals, since their intramolecular and intermolecular distances do not differ by more than 5-10 %. As to organic substances, they are all molecular crystals, with the obvious exception of organic salts. The class of organic compounds is infinite, and, therefore, physics of molecular crystals is physics of organic crystals.

*) Institut of Elemento-Organic compounds, Akademij of Sciences of USSR, Moscow, USSR.

The greater part of the work on the structure of organic crystals has been devoted to problems of the chemical composition of a molecule. The research has been concentrated on bond lengths and valence angles, the mechanism of association of atoms into a molecule, stereochemical configurations and conformation. As to mutual molecular orientations in a crystal, this problem has been dealt with only because information on mutual arrangement of molecules facilitates structural analysis.

A lack of interest in the structure of an organic crystal and very few publications which attempt to interrelate the arrangement of molecules in a crystal with crystal properties could be justified but only as long as organic substances were treated as dissolved chemical reagents. In recent years, however, research workers have addressed themselves seriously to problems associated with solid organic substances. Synthetic polymeric compounds have come to the fore, peculiar features of solid-state reactions have been observed and, finally, and this is perhaps most important, it is becoming obvious that numerous biological processes are most intimately correlated with the mutual disposition of organic molecules in protein and nucleic acid crystals.

The author of this paper began studies of regularities in the mutual orientation of organic molecules in a crystal as long as 25 years ago [1]. At the first stage of these studies, a simple geometrical model was offered for interpretation of crystal structures. It was found that if we bound a molecule by van der Waals' radii, as was first suggested by *Mack* and *Magat* [2, 3], an organic crystal can be represented as a close packing of solid molecules. This geometrical model and its aplicability for predicting the structure of crystals are dealt with in my book [4].

The principle of close packing of molecules in a crystal quite logically suggests the idea of describing the energy of molecular interactions by the sum of the interactions of the atoms that build up these molecules. This idea underlies a new refined model which I would term a physical model. The physical model of an organic crystal has greater predictive abilities than the geometrical model because with this model, it is possible to calculate a crystal structure more accurately and, besides, to evaluate quantitatively the thermodynamic properties of a crystalline compound.

In this paper, I shall try to give a brief outline of the state of the problem of molecular packing in an organic crystal, with major emphasis on the physical model. It is not my intention to prove the validity nor discuss various applications of the geometrical crystal model, as these subjects have been given a comprehensive treatment in the above-mentioned publication [4], but some general remarks may be called for.

2. Geometrical model of an organic crystal

The mutual orientation of molecules is characterized by the shortest distances between the atoms of adjacent molecules. In most instances, the packing of molecules is determined by the interaction between H atoms, or the interaction of H atoms with atoms of other elements.

In early X-ray analysis, the coordinates of H atoms were left out of the scope of research and the tables which presented the results listed only distances between the C atoms of adjacent molecules, which is absolutely insufficient for determining the type of packing.

Recent papers report the coordinates of H atoms obtained in computing the least R-factor by the least-squares method. These data should be treated with caution. As a rule, the values of valence bond lengths of an H atom derived by X-ray diffraction analysis are considerably underrated. Apart from such systematic errors, X-ray analysis is associated with large random errors. In determining proton coordinates, particular attention should be given to neutron diffraction studies. The nuclear magnetic resonance technique offers many potentialities so far largely unexplored. However, only in rare cases is it necessary to resort to experimental analysis, because the a priori localization of H atoms does not involve any particular difficulties.

Systematic studies of gas molecules have furnished a great body of information on the lengths of a C-H, O-H, etc. bonds which enables prediction of bond lengths in a majority of compounds which have not yet been studied. Moreover, data obtained in gas molecule experiments can, with a high degree of certainty, be extended to the crystalline state in molecular crystal studies. The crystalline field has no effect whatsoever on bond lengths and influences but slightly valence angles. The only material effect of the crystalline field is that it changes the conformation of a molecule whenever the possibility of rotation about single bonds presents itself. The effect of the crystalline field will be discussed below, therefore, I will restrict myself to pointing out that this effect does not handicap the a priori determination of the coordinates of H atoms, since in our analysis of packing we proceed from the considerations of molecular conformation in a crystal.

After the positions of all atoms in a molecule have been determined by appropriate methods, we can pass on to the analysis of molecular packing. The fundamental result of such analysis is that the shortest distances between the atoms of the same chemical elements vary quite insignificantly, this being the graphic evidence that a crystal can be to some approximation described by a geometrical model.

The geometrical model is constructed as follows. We start from analysing spacings between the atoms of the nearest molecules to find the shortest interatomic distances for all molecular pairs (for example, for molecules related by a translation along the axis b, axis c and by the symmetry operation of the double screw axis for the group $P2_1/a$). These are "determining contacts". Then, we select the values of intermolecular atom radii whose sums show the closest agreement with experimental data. These intermolecular radii are the mean radii for a given structure. With the aid of these radii, a volume model of the molecule can be constructed. It is obvious that since the sums of the mean intermolecular radii slightly differ from the actual distances, the model will constitute a packing in which some atom pairs slightly overlap, while other pairs do not touch each other. It appears that it will always be possible to effect ideal packing (i.e. packing in which no molecules are suspended in empty space and none overlap) by minor translational and rotational shifts of the molecules. In my book many examples are cited which show that molecules are usually in contact with 12 adjacent molecules, sometimes, the number being 10 or 14. The molecules in such a crystal are packed very closely: the projections of one molecule are inserted in the hollows in another, i. e. adjacent molecules dovetail.

The difference between the ideal and actual packings is very small. For example, for a naphthelene crystal, the ideal packing with coordination number of 12 in an experimentally observed cell at room temperature is obtained if we take a radius of 1.76 Å for carbon, and a radius of 1.18 Å for hydrogen. The orientations of molecules in the ideal and experimentally observed structures do not differ by more than 2-3°. A fact essential for the X-ray diffraction analysis technique is that the ideal packing which can be derived from strictly geometrical considerations, is described by such a structural model as can be employed for initial calculation of structure amplitudes.

The mean values of intermolecular radii vary, though within narrow limits, from structure to structure [1]).

The studies of these differencies are of limited interest and are warranted only when similar structures are dealt with, in particular, structures that form homologous series. Generally, these differences can be attributed to the inconsistency of the

---

[1]) The mean values of intermolecular radii for a number of structures studied by 1952, are reported in my book referred to above. Unfortunately, research data accumulated during the last few years have not been given systematic geometrical treatment. It should be emphasized that this work is by no means restricted to compiling a list of the shortest distances which are smaller than a certain arbitrarily chosen limit. For conformity of the model with the geometrical principle, the distances used for deriving the average figures should refer to the "determining contacts" of atoms only, i. e. the shortest spacings between the atoms of all pairs of adjacent molecules.

model with the molecular interaction energy formula, as well as to different roles of molecular vibrations in different crystals. Different characteristic temperatures and the differences between melting points and room temperature at which most experiments are made motivate a somewhat cautious approach to geometrical conclusions about molecular interaction.

Discrepancies between the ideal and actual packing patterns and variations in the mean intermolecular radii from structure to structure can be interpreted on the basis of the physical model to be described below.

Within the framework of the geometrical model, it is worthwhile not so much to investigate differences between distances, as to use average figures for describing packing densitiv. The same intermolecular radii can be used for a large group of compounds, and the volume of a molecule calculated from these figures. X-ray diffraction experiments have given the volume per molecule in a crystal. The ratio of the former volume to the latter will be called a molecular packing coefficient.

It would be of use to know the following regularities. The packing coefficients for the majority of crystals are within 0.65 to 0.77, i. e. of the same order as the close packing coefficient of spheres and ellipsoids. If the shape of a molecule is such that no packing can be effected with a packing coefficient above 0.6, it can be predicted that a drop of the temperature of the liquid will cause vitrification of the substance. Another interesting regularity is the following: morphotropic changes associated with loss of symmetry are accompanied by an increase in packing density.

Here is one of illustrative examples. The crystals of $Sn(C_6H_5)_4$, $Sn(C_6H_4CH_3)_4$ and $Sn(C_6H_4OCH)_4$ are tetragonal. Their packing coefficients are, respectively, 0.70, 0.68 and 0.62. The $Sn(C_6H_4OC_2H_5)_4$ crystal is monoclinic and has a packing coefficient of 0.67. Loss of symmetry is balanced by an increase in packing density.

Another example showing the physical meaning of the packing coefficient is as follows. The moduli of compressibility of tolane, dibenzyl and stilbene crystals are, respectively, 4.07; 4.54; 6.50 (in 10^{10} dyn/cm^2), their packing coefficients being 0.69; 0.71; 0.72. Thus, for analagous structures, compressibility is inversely related to the packing coefficient.

The analysis of all features of molecular packing in an organic crystal, i.e. the symmetry of arrangement, angles of tilt, the relation between packing density and properties of the crystal supports very well the idea of close packing. It would not be, of course, feasible to consider all possible packing patterns of molecules in cells of different dimensions and different symmetry. Nevertheless, the statement that of all conceivable structures, the actual structure is one of most closely-packed appears quite realistic.

Zorky and *Poraj-Koshits* [5] have made an attempt to verify this hypothesis within the framework of the geometrical model for a two-dimensional case. They have calculated all possible packings and found only few packing patterns with great density. Experimentally observed structures have been found to be among the closset-packed structures. It seems, that the assertion that the actual packing has the highest packing density is accurate to about 0.01 of the packing coefficient.

Close packing can exist if molecular coordination number is sufficiently high. The experimental evidence is that coordination number is usually 12; sometimes a specific shape of a molecule provides packing with coordination numbers of 10 and, naturally, 14.

In their turn, high coordination numbers seem to be determined by appropriate symmetry of a crystal. In the above publication, the author made an attempt to predict all possible space groups in organic crystals on the basis of the close packing principle. The prediction procedure consisted, first of all, in determining the symmetry of two-dimensional layers which provided conditions for packing of molecules into a layer with coordination number of 6, the molecules being arbitrarily tilted relative to the axes of the layer cell. In a general case, there are only two such layers of molecules of arbitrary shape: an oblique cell layer with inversion centres, and a layer with a rectangular cell built up by translation and the second-order screw axis parallel to the translation axis. The next operation was to select space groups in which these layers are possible and superpose so as to yield high coordination numbers. It is obvious, for example, that the superposition of layers with the aid of a mirror symmetry plane is here excluded.

From these considerations, only six space groups were found possible for molecules occupying a general position in a crystal. It is these groups that are most frequently encountered among the structures studied.

From the viewpoint of close packing requirements, a remarkable predominance of the space group $P2_1/c$ in organic chemical crystallography becomes obvious. It is only in this group that the closest-packed layers can be built on all the three planes of the cell.

The groups $P2_1$ and $P2_12_12_1$ without a symmetry centre are also among the most densely packed. They are quite logically to be found mostly in the cases of asymmetrical molecules [1]).

As is known, high-symmetry molecules sufficiently frequently form crystals in which these molecules occupy special positions with a lower number of degrees of freedom or even without degrees of freedom (hexamethylenamine, di-p-xylylene).

---

[1]) These three groups rank first in the list of space groups compiled by Nowacki (Acta Cryst. **21**) and cover half of all organic substances studied so far.

It is clear that in this case close packing is somewhat hampered, because the symmetry of a special position implies certain mutual orientations of the molecules. However, closest packing is completely feasible in one case – when a molecule occupies a centrosymmetrical position in a crystal. In this case, similarly to a molecule in a general position, closely-packed layers can be formed with coordination number of 6 for an arbitrary tilt of the molecule axes to the axes of the layer cell. Here we have again an oblique cell layer with symmetry centres, and a rectangular cell layer displaying symmetry of layer bc of the space group $P2_1/c$.

The space group $P2_1/c$ retains its dominant position in a crystal in this case, too, but now there are two molecules in the cell.

Since the preservation of the centre of symmetry in a crystal does not involve lower packing density, this symmetry element is always present in a crystal. For example, molecules with *mm m* symmetry lose, as a rule, their symmetry planes in a crystal and retain the inversion sentre (a common naphthalene structure). The others side of the same story is the impossibility of the crystal with a centrosymmetric molecule in the general position.

The preservation of other symmetries in a crystal is undoubtedly associated with a lower packing density. The analysis of concrete cases shows that the preservation of second-order axis symmetry in a crystal or occupation of the mirror symmetry plane by a molecule may cause a 0.02-0.03 decrease in the packing coefficient. It is obvious that the geometrical model cannot account for this decrease. Using this model, however, it is possible to predict space groups which provide the highest packing density under this supplementary condition. We have derived these groups and found that, in full agreement with experiment for molecules located on symmetry planes the first place is occupied by the group Pnma, whereas for molecules which show the symmetry of the second-order rotation axis the best groups are A2a and Pbcn.

It is not difficult to compile a list of space groups possible for close packing of molecules which retain the symmetry of any of point groups in a crystal.

It should be emphasized that in all known cases when a molecule preserves in a crystal high symmetry at the expense of a certain decrease in the packing density, this decrease is not large. If a small decrease is impossible, symmetry is partially or completely lost.

There are practically no exceptions from these rules. In other words, we do not know any organic crystal structures with packing coefficients below 0.6-0.7; in most cases, the closest packings are realized; if a molecule preserves high symmetry in a crystal, crystallization occurs in one of the space groups providing the best conditions for packing. As an example, we have considered all structures of organic

crystals described in the "Structure Reports' of 1952-1956. Of the 315 structures considered, 268 (86 %) belong to the closest-packed structures, 14 retain high symmetry in the optimum space groups, 9 are disordered structures. There are 10 structures in which the close packing requirements are, so to say, overfulfilled. These structure have more than one molecule in a general position. 7 or 8 structures are doubtful cases which need verification, and the remaining structures are peculiar rarely encountered packings in which molecules either occupy two nonequivalent positions of different symmetry, or are in a general position in crystals showing tetragonal or hexagonal symmetry.

Whereas the latter examples enable close packing despite the restrictions imposed by high symmetry of the crystal, the instances when molecules occupy two or more independent positions (for example, bi-phenylene: 4 molecules in a general position, two in symmetry centres) entail an increase in the number of degrees of freedom per cell and, consequently, can ensure packing of the highest density. It would be of interest to disclose the failure of a "simple" packing for these elegant structures, for example, to show that all conceivable cells of biphenylene with symmetry $P2_1/c$ $Z=2$ give packing of lower density as compared with that of experimentally observed structures.

Thus, we can state that the geometrical model produces results which are in excellent agreement with experiment.

The reasons for this excellent agreement of the geometrical model with experiment need some explanation. As will be shown in further exposition (section 8), the geometrical model describes with a sufficient degree of accuracy the effects of the tendency for minimization displayed by the potential energy of molecular interaction. The trend to retain symmetry must be accounted for by the trend of free crystal energy for minimization and must be first of all governed by enthropy requirements. It can be stated that at absolute zero, crystal structures are in a much better agreement with the geometrical model than at 300 °K at which experiments are usually made. It is true that in a number of instances we observe phase transitions at low temperatures with the result that the molecule loses its symmetry in a crystal. But it is equally obvious that very often no polimorphic changes occur at low temperatures for kinetic reasons, to say nothing of the fact that the behaviour of substance at temperatures below liquid nitrogen temperature has been examined in very rare cases only.

The geometrical model is unable to explain why a molecule preserves symmetry in a crystal (except for symmetry $\bar{1}$), neither can it explain why it is only very rarely that more than one molecule occupies a general position [1]). The geometrical mo-

[1]) This does not refer to numerous structures in which molecules are dimeric due to hydrogen bonds.

del fails to explain scatter of intermolecular distances in one structure and from crystal to crystal. This model relates the structure to crystal properties only in terms of a packing coefficient, i. e. qualitatively. Nevertheless, the model is valuable because, first, it provides graphic representation of the mutaul orientations of molecules in a crystal, and, second, it is an aid in calculation of unknown structures.

A number of workers have successfully used analysis of molecular packing in a crystal with a view to formulating a crude structural model. Preliminary calculations of a crude model can be carried out before the analysis of X-ray diffraction intensities. At the present time it has become possible to employ electronic computers [6] (earlier, molecular models had been used for the purpose) for geometrical analysis [4], in other words, for calculating possible orientations of molecules compatible with their shape from a known size and symmetry of a unit cell. For simple structures, a unique solution is obtained; in more complicated instances, several solutions are possible, but, anyhow, the number of possible orientations can always be quite definitely determined. Calculated structures possible from the geometrical point of view can be analyzed for intensities and, thereby, a correct solution may be obtained. There is also another alternative [7, 8]: minimalization of a certain function which is the sum of the conventional R-factor and the expression which reaches a minimum for geometrically correct solutions. This procedure facilitates and speeds up solution of the problem.

3. Physical model

For interpreting structural stability and properties of organic crystals we must proceed one step further from the geometrical model. It is absolutely unrealistic to try to calculate a general expression for crystal free energy which is the key for the solution of all problems in the field of thermodynamics without some simplification. We shall, therefore, formulate a simplified model and try to prove that it offers promising advantages for the solution of the stated problems [9, 10].

Let us consider the free energy of a crystal as the sum of potential energy of interaction between particles and free vibrational energy. Let us also assume that both components may be subdivided into two parts: inter- and intramolecular:

$$U + u + F + f$$

Consider first the vibrational part of the free energy. It is a well known fact that the spectrum of intramolecular vibrations depends but slightly on the phase state of the substance. In two polymorphic modifications, in whose crystals molecules

occupy different positions with respect to each other, shifts of the infrared spectrum lines responsible for intramolecular vibrations are within experimental error. Thus, in structural analysis, i.e. in comparing different possible packings we can disregard the intramolecular portion of free energy. In other words, the volume or pressure derivatives of the intramolecular parts of the thermodynamic functions at constant temperature equal to zero: $\left(\frac{\partial f}{\partial V}\right)_T = 0$.

The crystalline portion of the thermodynamic functions may be explicitly presented for enthropy and heat capacity at constant volume by calculating intramolecular components using conventional oscillator formulae from data on normal intramolecular vibration spectra. Comprehensive experimental information is, of course, required, that is, not only data on heat capacity at constant pressure within the entire temperature range, but also the same relationships for the expansion and compressibility.

Table I lists data for a naphthalene crystal calculated from the following expressions (specific heat c_p from [11], expansion factor from [12] and volume compressibility from measurements, performed in the author's laboratory:

$$c_v^{cr} = c_p - c_v^{mol} \qquad S^{cr} = S - S^{mol}$$

$$E^{cr} = \int_0^T c_v^{cr}\, dT \qquad \Delta U = \int_0^T (c_p - c_v)\, dT$$

$$F = U_0 + \Delta U + F^{vib}$$

Here $U = U_0 + \Delta U$ is intermolecular interaction energy (lattice binding energy); U_0 – lattice binding energy at absolute zero, and ΔU – increment of lattice binding energy due to thermal expansion.

For low temperatures, the values of ΔU are not quite accurate, since compressibility has been calculated only down to nitrogen temperatures and then extrapolated. The values of F may include a large additive error, because U_0 measured by sublimation heat is experimentally derived with low accuracy.

Nevertheless, accumulated data are sufficiently typical and, therefore, deserve attention. From the c_v^{kp} temperature curve we can infer that lacking the anharmonic effect the tendency of aproaching to the value about 12 $\frac{cal}{mole}$ would be obvious. This means that at appropriate temperatures almost uniform energy distribution over the degrees of freedom is provided: in contrast to an atom, a molecule has six degrees of freedom – three translational and three rotational frequen-

odynamic functions of naphthalene crystal

$\alpha \cdot 10^6$ 1 / deg	$\beta \cdot 10^{10}$ cm^3 / erg	$C_p - C_v$ cal / mole.deg	C_v^{mol} cal / mole.deg	C_v cal / mole.deg	C_v^{cr} cal / mole.deg	S cal / mole.deg	S^{mol} cal / mole.deg	S^{cr} cal / mole.deg	ΔE cal / mole	ΔU cal / mole
100	0.089	0.05	0.001	2.56	2.56	0.99	0	0.99	14.6	0.5
140	0.096	0.38	1.13	9.66	8.53	7.6	0.21	7.4	277	8
150	0.104	0.7	3.9	13.7	9.8	14.05	1.43	12.6	686	29
170	0.113	1.1	7.2	17.0	9.8	19.4	3.2	16.5	1142	65
220	0.125	2.1	11.0	20.8	10.8	24.9	5.3	19.6	1608	126
250	0.139	3.1	14.8	24.9	10.11	29.8	7.7	22.1	2082	231
325	0.155	5.5	19.5	28.4	8.9	35.0	10.6	24.4	2563	397
425	0.178	9.4	24.4	30.6	6.2	40.1	13.9	26.2	3043	694
550	0.208	15.2	28.7	31.7	3.0	45.1	17.8	28.0	3522	1179

and β have been obtained by extrapolation.

cies. Another feature specific for molecular crystals is the appreciable contribution of expansion work to the total free energy. It is necessary to point out that vibrational free energy values are much smaller than U_0, which equall to

$$16700 \frac{\text{cal}}{\text{mole}} .$$

The above subdivision of the thermodynamic functions into the intermolecular and intramolecular parts seems advantageous because for interpreting many properties, molecules may be treated as hard molecules. We believe that these assumptions can be successfully used for explaining structural stability, thermal expansion and elasticity of organic crystals.

For a crystal composed of hard molecules attempts can be made at solving the dynamic problem using the conventional lattice dynamic technique (see section 9 below). To enable comparison of the theoretically obtained results with experiment, it is worthwhile to consider the characteristic temperature of a crystal derived from thermodynamics experiment.

To introduce the thermodynamic characteristic temperature, we shall represent the crystalline portion of entropy by the Debye interpolation expression for a particle with six degrees of freedom:

$$S^{cr} = -\ 6R\ln\left[1 - \exp\left(-\frac{\theta}{T}\right)\right] + 8RD\left(\frac{\theta}{T}\right) .$$

Entropy is a function of volume and temperature. The characteristic temperature depends on the same variables. If experiment shows that the characteristic temperature varies within narrow limits depending on the parameters of the state, we

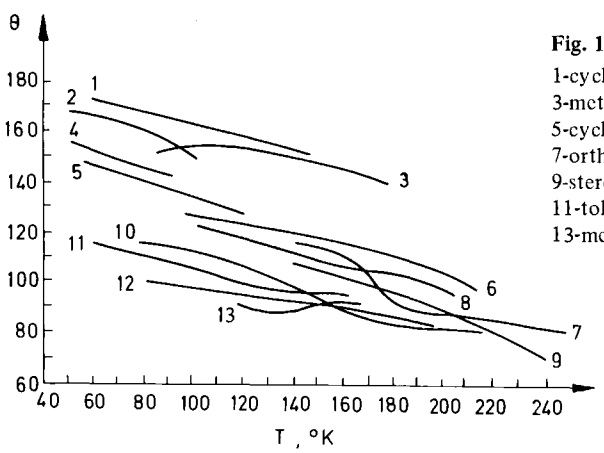

Fig. 1
1-cyclopropane; 2-ethylene; 3-methyl chloride; 4-butane; 5-cyclopenthane; 6-pyromedine; 7-ortho-xylene; 8-para-xylene; 9-sterene; 10-ethylbenzene; 11-toluene; 12-para-fluorotoluene; 13-meta-xylene

can employ harmonic approximation. If θ is a function of volume alone and is explicitly independent of temperature, this implies that quasi-harmonic approximation can be used. The accuracy of these approximations may be estimated from our data calculated for the naphthalene crystal.

As can be seen from Table I, the characteristic temperature does not varies significantly. However, a drop of θ with temperature must be taken into account. This phenomenon is sufficiently typical as evidenced by the figure taken from publication [13] (see Fig. 1).

A drop of θ with temperature can well be expected from quasi-harmonic approximation. As temperature rises, the volume of a unit cell expands,distances between the equilibrium positions increase, and the frequency spectrum is shifted towards low frequencies. However, an experimentally observed drop of the characteristic temperature is smaller than that which would occur exclusively due to thermal expansion. And, indeed, in a general case we have

$$\left(\frac{\partial\theta}{\partial T}\right)_p = \left(\frac{\partial\theta}{\partial T}\right)_v + \alpha V \left(\frac{\partial\theta}{\partial V}\right)_T .$$

In quasi-harmonic approximation $\left(\frac{\partial\theta}{\partial T}\right)_V = 0$. But $\alpha V\left(\frac{\partial\theta}{\partial V}\right)_T$ can be estimated experimentally, as $\left(\frac{\partial\theta}{\partial V}\right)_T = \frac{\alpha}{\beta \cdot \frac{\partial S}{\partial\theta}}$. The figures of the table show that $\left(\frac{\partial\theta}{\partial T}\right)_V \neq 0$.

It can be shown that the explicit temperature dependence of θ is reversed (anharmonicity which increases with temperature causes a rise in the characteristic temperature), and, consequently, the quasi-harmonic effect is made less prominent.

A more detailed discussion of the characteristic temperature of organic crystals would lead the discussion too far from the subject of my article which is molecular packing. The information presented above is sufficient for treating the problem of structural stability.

[14] was the first work to point out that the crystalline portion of the thermodynamic values can be described by the Debye function for particles with six degrees of freedom. Later, however, this model was unjustly ignored and it was suggested that translational and torsional vibrations should be handled separately [15]. I do not think this is justified, because translations contain optical branches as well.

4. Energy of interaction of molecules in a crystal. Atom – atom potentials

Since no electrons are exchanged in the interaction of saturated molecules, this appreciably facilitates the calculation of the potential energy of a molecular system. However, any satisfactory practical solution of this problem using rigorous quantum-mechanical techniques encounters unsurmountable difficulties. Despite these difficulties, it seems quite feasible to elaborate a semi-empirical method for calculating molecular interaction energy in a crystal lattice. A number of simplifying hypotheses must necesserily be made and, in fact, the only criterion of the validity of the semi-empirical method is its ability to predict structure and properties for a sufficiently large class of substances.

The studies on the interaction of molecules which are being carried out by *K. V. Mirskaya* and myself are based on the atom-atom potential method which implies additivity of molecular interaction energy with respect to the atoms that build up these molecules [16, 17]. The principal advantage of this method for studying organic substances is that it permits selection of atom-atom potentials from experimental data only for few representatives of a class of compounds with subsequent application of the curves thus obtained for predicting the properties of all the other compounds of this class. Thus, for example, if C-C, C-H and H-H interaction potentials are known, it is possible to calculate the properties of a vast class of hydrocarbons.

The atom-atom potential method may neglect electrostatic interactions in a molecular crystal which are due to permanent multipole moments in a molecule. Such interactions do not play any important role in the lattice. This fact (although in cases when molecules have high dipole moments) is not self-evident and must be demonstrated by straightforward calculations to be given in section 5.

A vast body of experimental data can be employed to verify the method and the potential curves obtained. Such physical parameters as the elasticity tensor, expansion tensor and normal crystal vibration spectrum can be used for the purpose. However, the most straight forward verification and, consequently, the initial checking stage, is calculation of sublimation heat and crystal structure. This technique may be applied to select the optimum atom-atom potential curves to be used in calculation of other properties of crystals.

Molecular interaction in a crystal includes dispersion attraction, repulsion due to overlapping of electron shells (the sum total of these interactions will be called van der Waals'interactions), and electrostatic interactions, provided the molecules have permanent multipole moments.

Calculations of attraction energy are usually based on London's theory developed in 1930 [18]. According to this theory, the attraction energy of two spherically symmetrical particles located at long distances compared with their sizes, is inversely proportional to the 6th power of the distance between their centres. Till now London's formula $U = -Ar^{-6}$ was applied to whole molecules (first of all, to the monoatomic molecules of rare gases). The constants A are derived either from approximate empirical London's and Slater-Kirkwood's formulae [19], making use of the ionization and polarizability potentials, or by quantum-mechanical techniques. In the latter case, additional assumptions should often be made which obscure the causes of errors in the results obtained. Repulsion energy is calculated from reciprocal power relationships (Br^{-n} or exponential $Be^{-\alpha r}$) first used by *Born* and *Pauling* for ion repulsion. The constants B, n, α are selected empirically.

On account of such different approaches to calculation of different portions of molecular interaction energy, the results obtained for one pair of molecules are, as a rule, inapplicable for another. A question which now arises is as follows: would it be possible to formulate a more general model which could be used with the same parameters for calculating a vast range of substances.

The fact that molecules form close packings in an organic crystal and that the atom of each molecule tends to locate itself between the atoms of the adjacent molecule and as close as possible to this molecule, suggests the additivity of not only molecule-molecule but also atom-atom interaction energy. The validity of the additivity assumption can be accurately estimated only by checking the theory, but proceeding from the analysis of the non-additivity effects carried out by *Axilrod, Teller* [20] and *Wojtala* [21] it can be concluded that these effects must be negligible in calculating lattice binding energy.

For describing interaction between non-bonded atoms of different molecules, it is profitable to use 6-exp potential, i.e. London's formula for atom attraction and the exponential law for repulsion. This formula must be applicable much more rigorously to atoms than to whole molecules or groups or groups of atoms. This is because, first, the mean value of the dipole moment for a stationary state in the electron system of an atom is always zero which cannot be stated for a group of atoms. Second, precision X-ray diffraction analysis shows that excellent agreement with experiment can be achieved by making calculations with isotropic atom factors of X-ray scattering, and that electron density patterns can be represented with the accuracy of the experiment as superposition of spherically symmetrical atoms. From the point of view of polarizability, atoms can also be considered almost isotropic. And, finally, the ratio of the size of a particle to a distance between the particles is always more fabourable for atoms, even at the shortest distances observed in a crystal, than for whole molecules or any group of atoms.

A purely empirical approach to selection of the A, B and α constants both for long and short distances seems to be the most feasible way of determining the analytic expression of interatomic potentials. Studies of molecular, and, in particular, organic crystals can furnish a great deal of relevant information, since the main peculiarity of organic compounds is that vast classes of substances are built from a very limited number of atom varieties.

At the first stages of our studies it can be safely assumed that the atoms of one chemical element interact independently of the type of molecules they compose, and the specific interaction of an atom in a given molecule can be, if necessary, taken into account by assuming that each atom is the superposition of a neutral atom and a certain residual electric charge accommodated in the centre of the atom. Then electrostatic interaction of two molecules can be calculated by using the classical multipole expansion technique. The other portion of the interaction energy (named Van der Waals' interaction) which does not depend on the localized charge distribution in molecules is determined by interaction between neutral atoms.

The constants A, B, α of the 6-exp potential of neutral atom interaction can readily be expressed through the following three parameters: equilibrium distance r_0, potential well depth U_0 and second derivative at the point of minimum D.

r_0 and U_0 can easily be included in the potential formula which assumes the following form:

$$U(r) = \frac{U_0}{6-\alpha r}\left(-\frac{\alpha r_0^7}{r^6} + 6e^{-\alpha(r-r_0)}\right).$$

As to α, it is related to all the three physical parameters through the following equation:

$$\frac{Dr_0}{U_0} = \frac{6(\alpha r_0)^2 - 42\,\alpha r_0}{6-\alpha r_0}.$$

It is worthwhile to compare analytical and experimental data with respect to these physical parameters, because, first of all, their magnitudes lie within a rather narrow interval, and, secondly, each parameter is particularly sensitive to certain properties. Namely, equilibrium distances are mainly responsible for lattice constants, potential well depths – for sublimation heat, and the parameter D – for molecular vibration frequencies and the crystal elasticity tensor.

Preliminary calculations have shown that as could well be expected the values of r_0 exceed the mean distances between the nearest atoms of adjacent molecules which we find in crystals by approximately 15 %. In the works by the author and *K. V. Mirskaya* [17], the values used for C . . . C, C . . . H and H . . . H interactions are – 3.8 Å, 3.3 Å, 2.8 Å.

The parameters U_0 have not yet been carefully studied. At any rate, it can be said that their values do not differ much for different pairs of atoms and lie in the vicinity of 0.06 kcal/mole. The values of the product of the parameters αr_0 also vary insignificantly, namely, within 12-16.

At present there appears to be no need to complicate molecular interaction energy calculations by allowing for noncentrality of atom-atom potentials. At the same time, the attempts at using atom-atom potentials for calculating barriers to rotation of one part of a molecule with respect to the other about single bonds show that atom interaction energy depends on the angle between the interatomic distance and the valence bonds.

This dependence compelled some authors to introduce in the calculation scheme an additional energy component which is interpreted as bond interaction energy. However, this inclusion is redundant. In order to obtain the correct values of internal rotation barriers for ethane and analagous molecules, it is quite sufficient to make a reasonable assumption (which is independently confirmed by the experience of organic chemical crystallography) about the equilibrium radius of a monovalent atom depending on the angle with a valence bond.

Assuming r_0 equal to α and $\frac{\alpha}{\epsilon}$ along and across the bond respectively, we have calculated energy of interaction between the H atoms of an ethane molecule from our 6-exp potential expression. The only supplementary condition is: the equilibrium radius is assumed equal to

$$r_0 = \frac{a}{2}\left[(\epsilon \sin^2\psi_1 + \cos^2\psi_1)^{-\frac{1}{2}} + (\epsilon \sin^2\psi_2 + \cos^2\psi_2)^{-\frac{1}{2}}\right]$$

where: ψ_1 and ψ_2 are angles between the interatomic vector and the bonds. A new parameter appears in the equation. For $\epsilon = 0.82$ the experimental value of the barrier to rotation is estimated at 3 kcal/mole.

It is quite sufficient to introduce such ellipticity for H atoms. Interaction between C atoms can be thought to remain central – there is no conflict with experiment.

As to hydrogen bond, it is reasonable to include it in our atom-atom potential model in the following way. All interactions are determined according to the above formulae, except for the interaction of a H atom associated with an O/or N/atom through hydrogen bond. For this atom pair we introduce a potential with two minima. At a long distance, dispersion interaction occurs; as the distance between the atoms becomes shorter, we obtain the minimum of "conventional" interaction. With further approach, the atoms cross a low barrier and get into the other minimum – hydrogen bond minimum.

If we leave aside the problem of investigating the configuration of a hydrogen bond potential, its expression can be included in a general formula in the simplest form by truncating the classical van der Waals' potential curve for O and H atoms at a certain point g left of the minimum. A potential well for hydrogen bond can be described by a parabola, with the junction of the curves at the point g. Thus, the potential of the following form is suggested for hydrogen bond:

$$U_{O\ldots H} = -\frac{A}{r^6} + Be^{-\alpha r} \qquad r_g < r < \infty$$

$$U_{O\ldots H} = U_0 + a\,(r - r_0)^2 \qquad 0 < r < r_g$$

For U_0 and r_0, we can take relevant figures reported in the literature, for example, $U_0 = 3$ kcal/mole and $r_0 = 1.6$ Å, a being equal to $a = \frac{U_g - U_0}{(r_g - r_0)^2}$. The parameter of the proposed curve is the curve junction coordinate r_g. This value determines also U_g and, consequently, the height and the coordinate of the barrier which separates the two minima on the curve representing the oxygen – hydrogen potential.

It appears obvious that the arbitrary configuration of the potential will but slightly affect the results of the calculation of optimum molecular conformations or packings. Of course, if it is required to study the configuration of the hydrogen bond potential with greater accuracy, a curve with two or three free parameters should be chosen.

Among other things, our atom-atom potential model owes its success to the fact that the dependence of hydrogen bond energy on the O–H. . . O angle is effected automatically. It can be easily seen that a deflection of this angle from 180° at constant O–H and H . . . O distances results in a sharp rise of energy due to O atom repulsion. In this way, using our "universal" potential and assuming the equilibrium radius for oxygen equal to 1.46 Å, we obtain the energy loss of 0.05 kcal/mole for a 160° angle, 0.15 kcal/mole for a 140° angle, and above 1 kcal/mole for 100-120° angles.

This calculation takes into account steric interaction of O atoms alone. Actual energy loss may be higher than the above figures. This calculation scheme has not yet been used for determining molecular interaction energy.

5. Energy of electrostatic interaction

Calculation of electrostatic interaction energy in a molecular crystal is a very laborious job not only on account of slow convergence of the lattice sums, but also due to large variations in lattice space symmetry and in the ratios of unit cell parameters. All this makes calculation of the lattice sums in a general form nonfeasible.

The multipole energy values reported in the literature are, as a rule, derived on computers and refer to concrete crystals. It would be of interest, however, to estimate, at least approximately, without cumbersome calculations for many particular crystals, the maximum electrostatic contributions to lattice binding energy, and also to determine the dependence of the magnitude of these contributions on the mutual orientation of multipoles and space symmetry of a lattice.

To solve these problems, dipole centres were located in lattices with dense spheric packing and different space symmetry was imposed on the orientation of the dipole vectors, without changing the mutual arrangement of the dipole centres [22]. The interaction energy of the dipoles related through the vector **r** and oriented in the directions $\mathbf{S}_1$ and $\mathbf{S}_2$ was calculated from classical equation:

$$\epsilon_\mu = \mu^2 \left\{ \frac{\mathbf{S}_1 \mathbf{S}_2}{|\mathbf{r}|^3} - \frac{3(\mathbf{S}_1\mathbf{r})(\mathbf{S}_2\mathbf{r})}{|\mathbf{r}|^5} \right\}$$

where μ – the dipole moment of a molecule. Lattice binding energy was represented by a conditionally convergent alternating series – the sum of the interaction energies of the dipole taken as the origin of coordinates with all other lattice dipoles.

In the above publication the expressions were derived which define electrostatic lattice energy versus the orientation of the original dipole vector for several space groups most commonly encountered in molecular crystals ($P\bar{1}$, **P1**, $P2_1$, Pa, A2, Aa, $P2_1/c$, $P2_12_12_1$, $P2_122_1$, $Pca2_1$, $Pna2_1$).

These analytical relationships have been used for constructing polar maps which graphically represent the orientation dependence of electrostatic energy, including the regions of the most favourable orientations of molecules in a lattice from the viewpoint of its electrostatic energy. A comparison of the analytical expressions and polar maps for different space groups makes it possible to assess the effect of crystal lattice symmetry on the electrostatic energy of the lattice in its "pure form".

Below are given a formula and a polar map for the group $P2_1/c$. The electrostatic energy of the lattice showing such symmetry is

$$E_\mu = 0.86 \frac{\mu^2}{a^3} [-3 + (2\sqrt{2}x + Z)^2]$$

where a is the shortest distance between the dipole centres, and x, φ, Z represent direction cosines of the original dipole. The substitution of the Cartesian coordinates in the above formula by the spherical coordinates θ, φ yields a polar diagram for the group $P2_1/c$ which is given in Fig. 2. Here, the polar distance θ is measured from the axis z which is perpendicular to the drawing plane and coincident with the normal to the dense layers in a three-layer spherical packing of the lattice under consideration (φ is measured from the axis parallel to [110] of the cubic lattice).

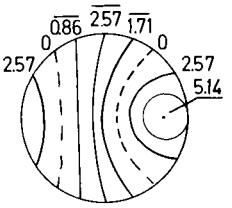

Fig. 2
Numbers denote energy in μ^2/a^3

These expressions allow approximate estimation of possible electrostatic contributions of different molecular crystals to the lattice binding energy. Several examples of such estimations are listed in Table 2.

Table 2. Approximate values of dipole interaction energy in some crystal lattices

Compound	Symmetry	μ, D	E, kcal/mole	
			min.	max.
Nitro-benzene $C_6H_5NO_2$	$P2_1/c$	3.96	-2.8	5.6
Nitro-anthracene $C_{14}H_9NO_2$	$P2_1/a$	3.96	-1.5	3.0
m-dinitro-benzene $C_6H_4(NO_2)_2$	$Pbn2_1$	3.96	-2.3	0
Acenaphthene-quinone $C_{10}H_2(CO_2)_2$	$P2_12_12_1$	4.90	-3.6	0.3

For nitro-benzene, apart from approximate estimation, we have made straightforward calculations by summing energy in the lattice up to about 50 Å. The sum converges to E_μ = 1.4 kcal/mole which falls into the range given in the table. The heat of sublimation for the above compounds is about 20 kcal/mole. It can be seen that dipole interactions do not play a major role in the lattice even if the dipole

moment is large. For crystals whose molecules have moments below 1D, for instance, for hydrocarbons, the contribution of the dipole moment to the lattice binding energy must be negligible.

The same procedure has been adopted to estimate the quadrupole contribution to the lattice binding energy of a molecular crystal. Publication [23] gives a general dependence of quadrupole interaction energy in a crystal lattice on the angles of quadrupole tilts to the symmetry elements for the same row of clossest-packed spheres lattices of low symmetry as for dipole interactions. The interaction energy of two quadrupoles with an axially or cylindrically symmetrical charge distribution has been calculated from formula:

$$\epsilon_Q = \frac{3}{16}\frac{Q^2}{r^5}\left\{1 + 2(\mathbf{S}_1\mathbf{S}_2) - 5(S_{1r}^2 + S_{2r}^2) - 20\,S_{1r}S_{2r}(\mathbf{S}_1\mathbf{S}_2) + 35\,S_{1r}^2S_{2r}^2\right\}$$

where r is a vector connecting the quadrupole centres; the unit vectors $\mathbf{S}_1$ and $\mathbf{S}_2$ characterize the directions of the quadrupole axes relative to the lattice axes; S_{1r} and S_{2r} are projections of $\mathbf{S}_1$ and $\mathbf{S}_2$ on r ; and Q is a scalar which determines the quadrupole moment tensor of the axial quadrupole. To cite an example, we write an equation for the energy of a quadrupole lattice showing symmetry $P2_1/c$ as a function of the angles θ and φ formed by the quadrupole located at the lattice point (000) with the lattice axes:

$$E_Q = \left(\frac{1}{2}\right)\left(\frac{Q^2}{a^5}\right)\,[1.33 - \sin^2\theta\,(6.67 + 11.47\,\sin^2\varphi) + \sin^4\theta\,(5.84 - 4.22\,\sin^2\varphi +$$

$$+ 15.67\,\sin^4\varphi) + \sin^3\theta\cdot\cos\theta\cdot\cos\varphi\,(4.70 - 6.91\,\sin^2\varphi)\,].$$

Here, a is again the shortest distance between the lattice points. A corresponding polar diagram is shown in Fig. 3.

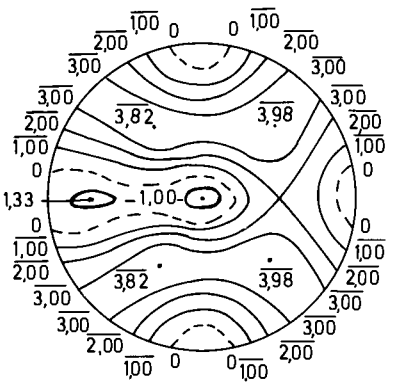

Fig. 3
Numbers denote energy in Q^2/a^5

Using the above equation, we have measured the magnitude of quadrupole lattice energy for naphthalene. The minimum and maximum possible values of such energy have been estimated at -0.7 and 0.2 kcal/mole, respectively. This result is confirmed by *Craig* et al. [28] who report the magnitude of -0.4 kcal/mole. It is self-evident that the contribution of quadrupole energy to the total naphthalene lattice energy which has been experimentally determined at -16.7 kcal/mole, is insignificant.

The following example illustrates to what extent electrostatic interactions can influence the establishment of an equilibrium crystal structure. Calculation of changes in van der Waals' interaction energy in an anthracene crystal caused by variation of the Eulerian angle θ (an angle between the normal to the molecular plane and the crystal axis z) yields the curve U (θ) shown in Fig. 4. If an anthracene molecule had a dipole moment of 4D, it would be necessary to include the electrostatic component E_μ (upper curve) in this curve in order to obtain total lattice energy. In this case, the position of the minimum on the curve U(θ) would shift by not more than 0.5°. Generally speaking, electrostatic energy seems to be in most cases a rather slowly varying function of the structure parameters. Calculations show that even in the region of the fastest variations of dipole energy as a function of these parameters, it fails to shift the position of van der Waals' energy minimum by more than 1–1.5°, and quadrupole energy – by more than 0.3° which is, of course, negligible from the viewpoint of packing effects.

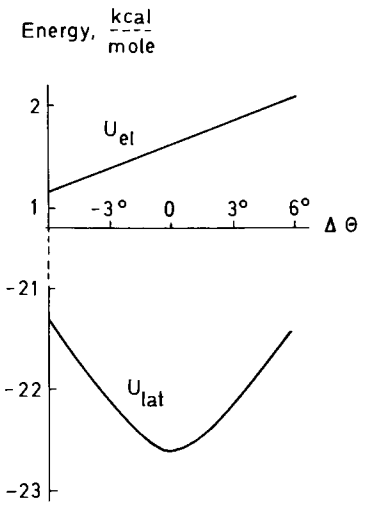

Fig. 4

6. The calculation of structure and properties with the help of atom-atom potentials

Since the electrostatic energy contribution to the lattice binding energy of a molecular crystal is not determining, the problem of calculating this energy should be reduced to studies of van der Waals' interactions.

In an atom-atom approximation, van der Waals' lattice binding energy referred to one molecule is given as the sum of energies over all interatomic vectors relating the atoms of one molecule (k-number of atoms in a molecule) to all atoms of the adjacent molecules:

$$U = \frac{1}{2} \sum_{i=1}^{k} \sum_{j=k+1}^{\infty} (-Ar_{ij}^{-6} + Be^{-\alpha r_{ij}}).$$

In a general case, the lattice sums Σr_{ij}^{-6} and $\Sigma e^{-\alpha r_{ij}}$ must be derived by direct summation which is feasible when computers are employed. As van der Waals' energy rapidly decreases with distance, it is sufficient to restrict distances to 15-20 Å. Calculations on a number of organic crystals show that a lattice energy error that arises in this case does not exceed 1 %. It is important to point out that for many practical purposes the radii of summation can be taken considerably smaller.

In the course of physical processes involving deformations, thermal expansion, compression, etc. the size and shape of a unit cell, mutual arrangement of molecules and, consequently, crystal lattice potential energy may undergo certain changes. To allow for these changes, we define lattice binding energy as a multidimensional function of the lattice spacings a, b, c unit cell angles α, β, γ, Eulerian angles θ, φ, ψ describing the position of the molecule relative to the crystal axes, and the coordinates of the centre of gravity of this molecule X, Ψ, Z:

$$U = U(a, b, c, \alpha, \beta, \gamma, \theta, \varphi, \psi, X, \Psi, Z).$$

It can be assumed in most cases (see section 8) that at variations of the above parameters, the arrangement of atoms in the molecule is stable.

Knowing the configuration of such a multidimensional surface, we can calculate a number of physical properties of crystals. Thus, lattice binding energy at the energy surface minimum point determined accurate to within zero-point oscillation energy, equals to the heat of sublimation of a crystal at absolute zero. The zero-point energy contribution for the majority of molecular crystals does not exceed 1-2 %

of the heat of sublimation. The abcissae of the energy surface minimum define the equilibrium structure of a crystal at absolute zero. According to approximate estimations for molecular crystals, the effect of zero-point oscillations on establishment of the equilibrium structure which manifests itself in certain expansion of the lattice as against its size under overall static equilibrium, is negligible. The second derivatives of lattice energy density with respect to deformations at the energy surface minimum determine crystal elasticity factors at 0 °K. On the basis of the procedure for calculating the potential energy of molecular interaction, we can solve the problem of determining the spectrum of intermolecular oscillations in a crystal and then characteristic temperature, crystalline portion of free energy and its derivatives over the state parameters.

Other problems in the field of molecular crystal physics can also be resolved to an atom-atom approximation. These problems are: studies of reorientation motions of molecules in a lattice, calculation of surface energy in different crystallographic directions, etc. Nonetheless, the advantages offered by this method may be used only after quantitative verification of the underlying assumptions.

Hydrocarbon crystals are a very convenient object for checking the accuracy of an atom-atom approximation when applied to molecular crystals. As has been stated above, the contributions of electrostatic interaction and zero-point oscillations to the heat of sublimation and equilibrium structure of these crystals can be neglected, and, therefore, the lattice binding energy surface corresponding to van der Waals' interaction energy alone, must describe the actual properties of crystals with a high degree of accuracy.

For calculating the interaction energy of hydrocarbon molecules one can use three interatomic potential curves CC, CH, HH whose parameters are given on the page 16. Programmes have been elaborated [17] for computing lattice binding energy at any point of an energy surface; unidimensional, two-dimensional, etc. cross-sections of this surface; the positions of surface minima in any of these cross-sections and the position of the total surface minimum over all the variables [24], for crystals showing symmetry not below monoclinic and having one independent molecule in a unit cell.

Below are given the results [17] obtained in calculations of heat of sublimation and equilibrium structures for hydrocarbon crystals. Sublimation heat has been estimated at 2.4 kcal/mole for methane, 15.5 for adamantane, 10.5 for benzene, 16.5. for naphthalene and 21.7 for anthracene, the respective experimental values being 2.4, 12.7, 10.0, 16.7, 22.6 kcal/mole. An important thing about these results is that the same interatomic potentials are applicable for measuring the cohesion energy of crystals composed of molecules of a different chemical composition.

And, in fact, the only property common for the molecules under consideration is that they are built from the atoms of the same elements. As to other characteristics of these molecules – size, shape, valence bond saturation – they are quite different.

Analytically derived structural characteristics of a crystal lattice must be consistent with experimental data at least in the following aspects. First of all, this agreement must refer to the equilibrium orientations of molecules in a lattice if the unit cell parameters are preset at definite environmental conditions. The selected potential curves show the following. In all the one-dimensional cross-sections of the lattice energy surface over Eulerian angles calculated for benzene, naphthalene, anthracene and polyethylene, the energy variation curves display a minimum in the vicinity of the experimental point, the discrepancy between the analytical and experimental figures not exceeding 2-3°. The potential surface minimum calculated at simultaneous variation of all the three Eulerian angles for naphthalene, has the abcissae of 29, 44 and 295°, whereas the respective experimental figures are 29, 40 and 296°. The calculations have also demonstrated – in full agreement with experiment – very weak dependence of the equilibrium orientations of molecules in a lattice on the temperature variations in the unit cell parameters. Eulerian angles remain practically independent of small deformations in a crystal, for instance, when the unit cell parameters vary within ± 0.1 Å of the initial values. The equilibrium molecular orientations derived are also almost insensitive to minor variations in the constants of the C-C, C-H and H-H potential curves. Studies on the role played by different atoms in the establishment of angle equilibrium show that in the crystals already investigated, the sum of CH and HH interactions is mainly responsible for equilibrium, while C atom interaction energy in the vicinity of the equilibrium point varies so slowly that it practically does not affect the position of a minimum on the energy curve. It is further obvious that if the potential curves have been correctly chosen, the minimum in any energy surface cross-section over the unit cell parameters a, b or c must lie several tenths of angstrom left of the experimental values of the parameters obtained for room temperatures. In the above publication [17], the calculated parameters of a unit cell were in satisfactory agreement with experiment (Fig. 5).

Finally, the coordinates of the total energy surface minimum over all the variables must be compatible with a crystal structure at absolute zero. There is certain experimental evidence that in this case, too, atom-atom potentials describe a crystal lattice structure with a sufficient degree of accuracy.

In [24] a series of calculations were made on a benzene crystal with a view to determining the position and depth of the lattice energy surface minimum as a function of the unit cell parameters and Eulerian angles and studying the configuration

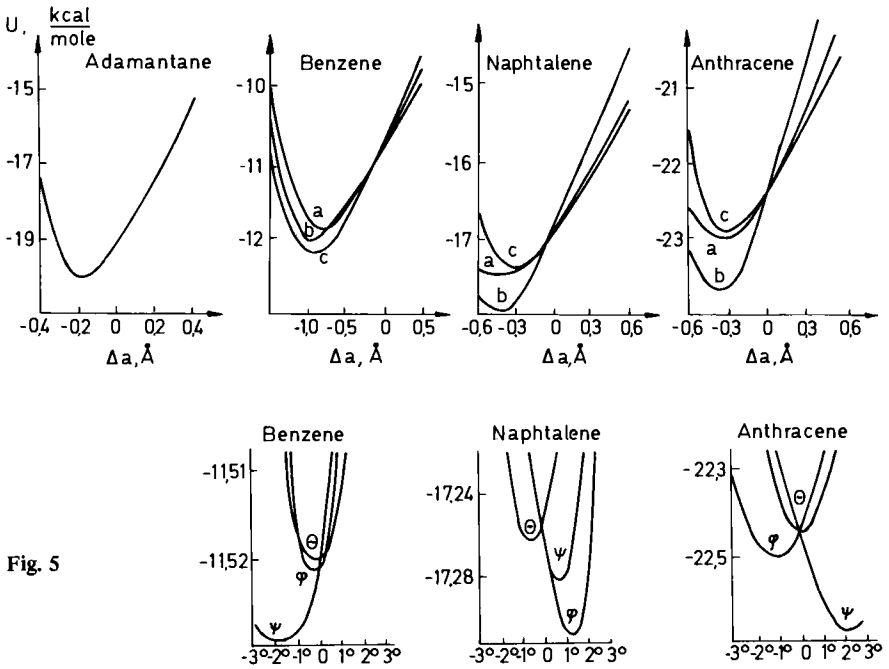

Fig. 5

of this surface in the vicinity of the minimum. In these calculations, the authors used structural data reported by *Cox, Cruickshank* and *Smith* [25] and the data on the thermal expansion tensor for benzene [26, 27]. The summation radius in lattice energy calculations was taken equal to 15 Å. In this case the lattice energy calculation error does not exceed 1 %. The relationship between this value and the summation radius for benzene is shown in Fig. 6.

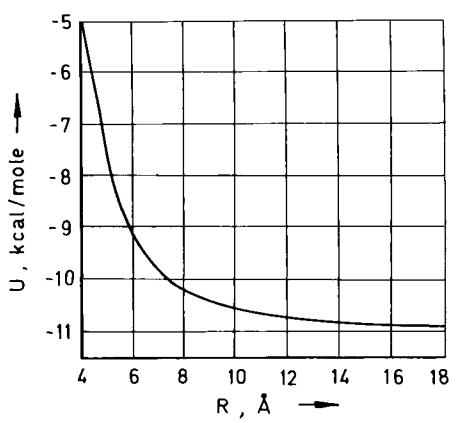

Fig. 6
Crystalline benzene lattice energy versus summation radius

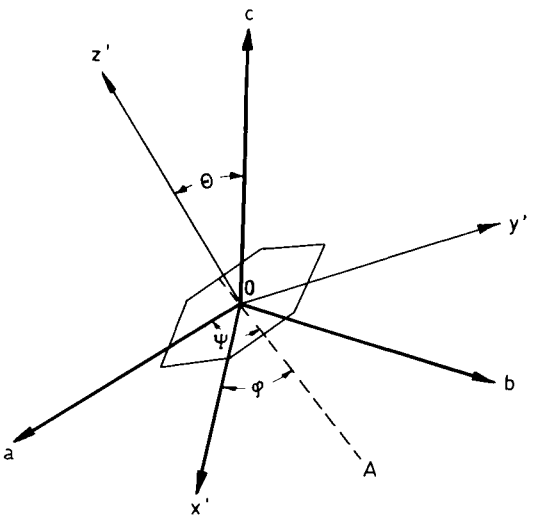

Fig. 7
Benzene molecule coordinate system oriented with respect to the crystal coordinate system. θ, φ, ψ – Eulerian angles

Let us determine the arrangement of benzene molecules in a lattice of Pbca symmetry with four molecules in a unit cell with the lattice parameters a = 7.46, b = 9.666, c = 7.033 Å corresponding to the structure of this crystal at –3 °C [25]. C-H bond lengths are taken equal to 1.08 Å.

Assume that we do not know the values of the angles θ, φ, ψ which describe the rotation of the coordinate system x', y', z' associated with the molecule, with respect to the coordinate system of the crystal (Fig. 7). For initial calculations, one assumes these angles equal to zero (then the original molecule lies entirely on the ab plane). By varying the mutual arrangement of the molecules so that the angle passes through all values from 0 to 180°, one derives the lattice energy variation curve in this process (Fig. 8a). As could well be expected, this curve is symmetrical relative to $\theta = 90°$ and displays two equivalent minima, –8.4 kcal/mole deep, out of which we chose, for instance, the lefthand minimum with the abcissa = 24°. Further, we fix $\theta = 24°$ and find the optimum arrangement of the molecules with the angle ψ varying from 0 to 180° (Fig. 8b). Then, we determine the curve $U(\varphi)$ (Fig. 8c) for each of the two symmetrically independent minima $\psi = 20°$ and $\psi = 90°$ with a similar depth (–9.4 and –8.8 kcal/mole, respectively). In both cases, the optimum molecular arrangement is provided at the angles φ close to 0, 60, 120°, etc. (in the 0-360° range there are six equivalent positions obtained due to a benzene molecule having the sixth-order symmetry axis; let any of these angles be selected, for example, $\varphi = 180°$).

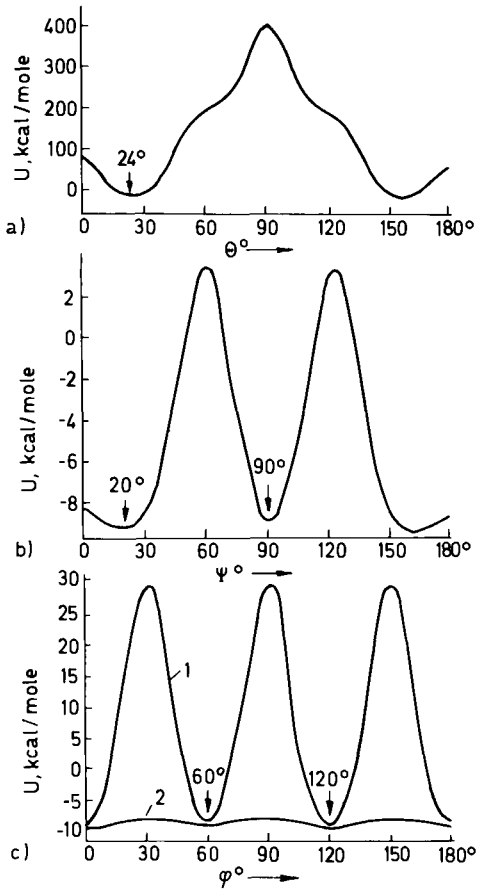

Fig. 8
Determination of the equilibrium orientation of molecules in the crystal lattice with specified parameters of the unit cell:
a) $U(\theta)$ with $\varphi = 0°$; $\psi = 0°$;
b) $U(\psi)$ with $\theta = 24°$, $\varphi = 0°$;
c) $U(\varphi)$ with $\theta = 24°$ and $\psi = 20°$ /I/ and $\psi = 90°$ /2/

In this way, steepest descent has generated two sets of Eulerian angles ($\theta = 24°$, $\varphi = 180°$, $\psi = 20°$ and $\theta = 24°$, $\varphi = 180°$, $\psi = 90°$) which we consider as approximations for more accurate calculation of the quilibrium structure. Further minimization is achieved by varying all Eulerian angles simultaneously. In the first case, the minimum abcissae represent 22°, 180°, 20° and the ordinate gives -9.6 kcal/mole. In the second case, the equilibrium angles θ, φ, ψ are, respectively, 47.6°, 178° and 104.7°, while the value of energy at the minimum point is -11 kcal/mole. Thus, the second of the two possible structures appears more profitable from the energy point of view, whereas the first local minimum of the surface $U(\theta, \varphi, \psi)$ is not only less deep, but also, as can be observed in Fig. 8b, c, less distinct, so that a molecular arrangement corresponding to this minimum would probably be

unstable. In fact, the experimentally observed structure shows good agreement with the second structure we have calculated, the experimental figures being: $\theta = 47.3°, \varphi = 178°$ and $\psi = 107.5°$.

This calculation can be regarded as a physical justification of molecular packing prediction by means of geometrical analysis performed within the geometrical scheme, for example, using volume models [4].

For comparison with Fig. 8 below are given one-dimensional cross-sections $U(\theta)$, $U(\varphi)$, $U(\psi)$ through a surface point corresponding to the deepest minimum (Fig. 9).

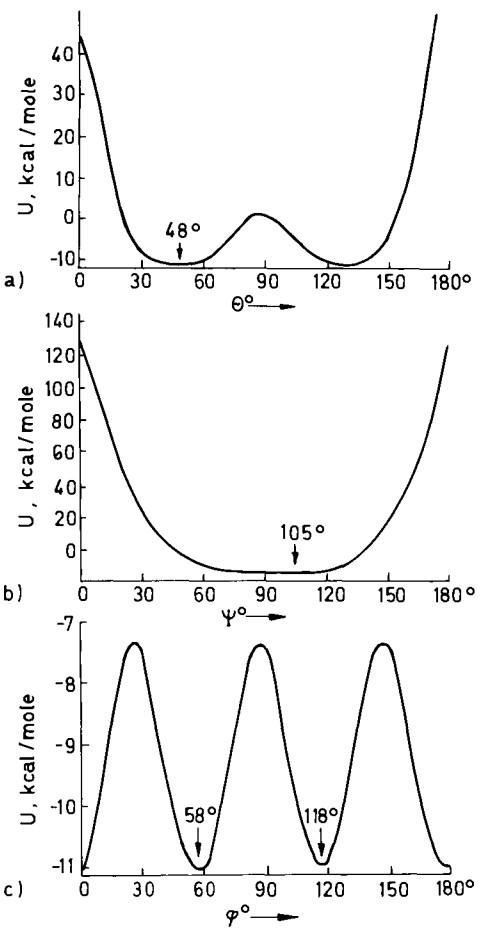

Fig. 9
Unidimensional sections of energy surface $U(\theta)$, $U(\varphi)$, $U(\psi)$ near the equilibrium point for a broad range of Eulerian angles

It would be of interest to investigate which of the three types of interaction – CC, CH or HH – makes the main contribution to the establishment of equilibrium molecular orientation in a crystal. The analysis of the contributions of atoms of different chemical elements evidences that equilibrium in a benzene crystal depends mainly on CH and HH interactions (Fig. 10). Even when neither U_{CH} nor U_{HH} separately passes a minimum in the vicinity of an equilibrium, it is the sum total of these interactions that is responsible for equilibrium structure. As to C atom interaction energy in the vicinity of an equilibrium, it varies so slowly that practically does not affect the position of the total minimum on the energy curve. This result is consistent with the well known fact that in a benzene crystal there are many intermolecular CH and HH contacts as compared with C atom contacts. This makes us doubt the validity of the conclusion arrived at by *Craig* et al [28] that only repulsions between H atoms are of importance for molecular orientations, because interaction between C and H atoms was not considered in the above publication.

To examine crystal structure at absolute zero it is required to find a minimum of the surface $U(a, b, c, \theta, \varphi, \psi)$ over all the six variables. According to their physical

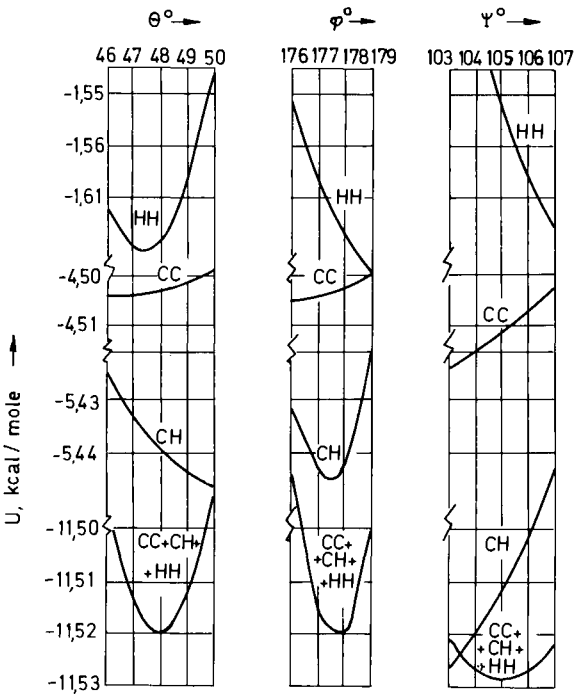

Fig. 10
Contributions of C-C, C-H H-H interactions to the establishment of equilibrium orientation of molecules in a crystal

meaning, these variables can logically be divided into two groups – the Eulerian angles θ, φ, ψ and the lattice parameters a, b, c so that each group could be minimized separately.

Since the accuracy of locating a minimum on the energy surface depends on the accuracy of energy calculation at each surface point and parameter derivatives in determining the direction of steepest descent, we do not obtain absolutely equal minimum coordinates when descending to a minimum from different surface points. Therefore, in order to locate a minimum, descent from different surface points in the neighbourhood of the minimum was used with subsequent averaging of the results obtained [24].

Thus, the minimum location procedure consists of the following steps. Knowing the lattice parameters at several temperature points, one finds corresponding minima in the three-dimensional cross-section $U(\theta, \varphi, \psi)$ for each of the points. This is, by the way, a method which can be used for calculating changes in the orientation of molecules relative to crystallographic axes at different lattice deformations, caused, for example, by a temperature drop. Table 3 presents calculated equilibrium Eulerian angles at three selected temperatures. Lattice parameters for this calculation have been taken from [25] and [27]. The bracketed figures are the experimental values of an angle between the normal to a molecular plane and the axis c (angle θ). These calculations demonstrate weak dependence of the equilibrium Eulerian angles on temperature-determined changes in the lattice parameters, which is in full agreement with experiment.

Table 3. Equilibrium orientation of molecules in benzene crystal at different temperatures

°C	Lattice parameters			Eulerian angles		
	a	b	c	θ	φ	ψ
-3°	7.46	9.67	7.03	47.6 / 48.1 /	178.0	104.7
-55°	7.44	9.55	6.92	47.1 / 47.1 /	178.2	104.0
-135 °	7.39	9.42	6.81	46.7 / 46.6 /	178.2	104.2

After fixing the equlibrium molecular orientation thus obtained at each selected point we continue descent to a minimum varying the lattice parameters a, b, c; then average the results of several descents over the lattice parameters and make final descent over Eulerian angles with the averaged values of a, b, c. The values of a, b, c averaged over the three descents for a benzene crystal have been estimated at 7.24, 9.41, 6.77, equilibrium Eulerian angles being equal to 47.5°, 178.5°, 103.9°.

In order to make the calculated coordinates of the energy surface minimum comparable with experimental data, we extrapolate structural data at low temperatures to the absolute zero. The extrapolation results and the lattice parameters calculated for the potential surface minimum are given in Table 4.

Table 4. Parameters of benzene unit cell at absolute zero

Lattice parameters	Theoretical data	Experiment	
		[26]	[27]
a	7.24	7.27	7.36
b	9.41	9.43	9.32
c	6.77	6.71	6.75

It can be seen that analytical and experimental results are compatible to within 1-1.5 %.

Good agreement of calculated and experimental data on lattice parameters and Eulerian angles testifies to the fact that the selected equilibrium distances between C-C, C-H and H-H atom pairs on the interatomic potential curves which are mainly responsible for the results of equilibrium structure calculation, are sufficiently close to the actual values. On the other hand, the lattice binding energy of a benzene crystal at a energy surface minimum has been found to be -11.73 kcal/mole, experimental heat of sublimation being 10-10.5 kcal/mole [52]. This result cannot be considered satisfactory, the more so that for other hydrocarbons studied, the values of lattice binding energy at a potential surface minimum are also below experimentally derived values of heat of sublimation.

It has been convincingly shown that heat of sublimation mainly depends on the potential well depth on the interatomic curves. On the C-C, C-H and H-H curves considered above, the depths of all potential wells were assumed equal to 0.067 kcal/mole. If we decrease the potential well depth on the C-H curve down to 0.057 kcal/mole and on the H-H curve to 0.048 kcal/mole without changing the position of the minima, lattice binding energy, at a surface minimum for instance, for benzene, will be equal to -10.5 kcal/mole which is in good agreement with experiment.

It is not the intention of the author to offer just now the final confirmation of our atom-atom potentials. It is necessary first both to consider a larger number of examples and to use data on intermolecular vibration frequencies and elasticity tensors which determine the third constant of the potentials – their curvature. Nevertheless, the suggested changes in potentials are sufficiently probable,as in this case the tendency for better agreement between analytical and experimental values of heat of sublimation is observed also for anthracene, liphenyl, adamantane and polyethylene crystals.

It is apparent from what has been said above that the lattice binding energy surface of a molecular crystal which is a function of the lattice parameters and mutual molecular orientations displays a large number of minima having different configurations and depths. In most cases, however, only one minimum corresponds to the actual crystal structure (leaving aside possible statistical disorder in molecular arrangement, polimorphism, etc.). For interpretation of many physical processes in crystals and also for selection of the appropriate mathematical technique of minimum location, it is essential to know the characteristics of the potential surface configuration in the vicinity of this minimum, namely, potential well width, the steepness of the potential hole walls, presence of "roughness", minor local minima, etc. This information can be obtained by calculating the value U as a function of all or some of the variables a, b, c, θ, φ, ψ on which this value depends, with appropriate selection of steps for these variables.

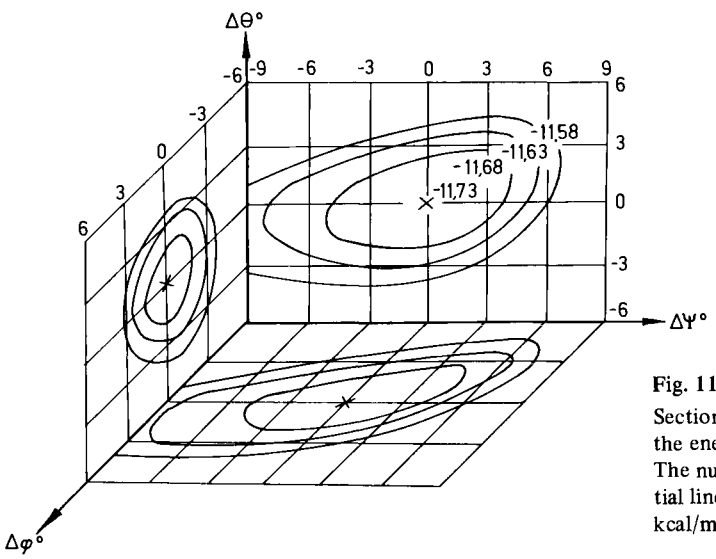

Fig. 11
Section U (θ, φ, ψ) through the energy surface minimum. The numbers on equipotential lines denote energy in kcal/mole

Fig. 11 shows the three main projections of the three-dimensional energy surface cross-section U (θ, φ, ψ) for a benzene crystal through the energy minimum with respect to all variables. The cross-section has been calculated with a 3° step in the range of the angles θ, φ, ψ varying within ± 9° of the equilibrium values. Besides, 1°–step calculations have been made in the immediate vicinity of the minimum to investigate the surface near the minimum in finer details. In this range, the three-dimential potential hole has rounded edges and gently slopes towards the variation of the angle ψ (in the vicinity of a minimum $\partial U/\partial\psi = 0.011$

kcal/mole. deg), the wall towards θ and φ becoming steeper ($\partial U/\partial\theta = 0.018$, $\partial U/\partial\varphi = 0.023$ kcal/mole. deg). The cross-section displays no peculiarities (local minima, "roughness") in the entire range of Eulerian angle variations. It should be emphasized that this range covers all possible amplitudes of angular molecular vibrations in a lattice which, for example, in a benzene crystal vary from 2.5 to 7.9°[27] in the ring plane, depending on the temperature.

In cases when lattice deformations do not entail changes in the space group and mutual molecular orientation, lattice binding energy is a 3-dimentional function of the unit cell lattice spacings U(a, b, c). The three main cross-sections of this surface U(a, b), U(a, c) and U(b, c) through the energy minimum with respect to all the variables calculated with a 0.5 Å step are shown in Fig. 12. The surface U(a, b, c) differs from the surface U(θ, φ, ψ) in that it can have essentially only

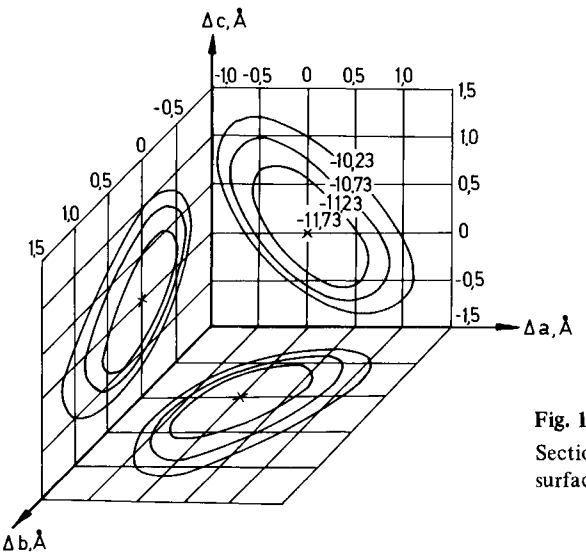

Fig. 12
Section U(a, b, c) through the energy surface minimum

one minimum whose position is determined by the size and orientation of molecules in the lattice and by the selection of interatomic potential curves. The configuration of the surface is similar to that of the interatomic potential – it rises steeply from the equilibrium point towards the decreased lattice spacings, i.e. intermolecular distances, and more gently in the opposite direction. According to calculations of a cross-section with a smaller step (0.1 Å), the surface U(a, b, c) in the vicinity of the minimum is rather flat: variations in the lattice parameters of about 0.1 Å cause lattice binding energy to change by about several hundredths of a kcal/mole. Further on, the potential well becomes steeper. If all the benzene lattice parameters increase simultaneously, which corresponds to transition from

a minimum to a point near the melting temperature (270 °K), the lattice binding energy has been shown to vary by about 0.6 kcal/mole, that is within quite reasonable limits.

The foregoing discussion reviewed the results obtained in the author's laboratory.

Our ideas to represent lattice binding energy as the sum of atom-atom potentials and to calculate molecular packing by varying the arrangement of molecules in a cell have been used by several workers in other countries.

From the viewpoint of these considerations, the structure of a hexamethylbenzene crystal has been studied [29]. This structure is a convenient object for calculations because the compound is crystallized in a group PI with one molecule in a cell. The authors have calculated the potential energy of a crystal as a function of rotational degree of freedom only. It has been found that in three-dimensional energy distribution, the deepest minimum very well describes the actual molecular array in a crystal.

The authors of work [30] have carried out structural analysis on a number of dicarboxylic acids and calculated the lattice binding energy of these crystals. Their purpose was to check the euristic possibility of the closest packing principle for predicting molecular packing patterns. Their calculations have been made on meso-β–β' dimethyladipinic acid. The analysis has yielded the only structure possible from the closest packing considerations. The same result has been derived in lattice binding energy calculations by the atom-atom potential method. This result confirmed by subsequent studies of the structure proves once more that organic crystal structure is predictable.

In [31] molecular packing in a crystal was calculated by minimizing crystal energy with respect to the positions of the molecules using the steepest descent technique. Minimization involves variation of three translational parameters which determine the coordinates of the molecule centre, three orientational parameters, 6 or less lattice constants and, if necessary, parameters describing rotation about single bonds in a molecule.

The validity of the potential functions in the (6-exp) form with parameters specified in section 4 and that given in [33] was verified. In order to avoid cumbersome calculations, the summation was made only until the interatomic distances exceed the position of the potential function minimum by more than 2 Å. It has been noted that this mode of computation affects appreciably the magnitude of lattice binding energy and but slightly molecular packing. Good results were obtained for naphthalene (calculated C atom positions differ from experiment by about 0.04 Å), anthracene and phenanthrene crystals; the results for 1, 3, 5-triphenylbenzene are somewhat worse.

The programme developed in [31] can be used for selecting interatomic potential functions which represent the actual crystal structure with the highest accuracy. In this work it is emphasized that it is of extreme importance to more accurately select constants in the non-bonded interaction potentials. The attempts at approaching the solution of this problem are made by the same author in his subsequent work [32].

Publication [32] deals with the problem of finding the parameters A, B and α in the (6-exp) potentials defining non-bonded C-C, C-H and H-H interaction. The value of α in the C-C potential is assumed equal to 3.60 $Å^{-1}$ from data on an inter-layer distance and compressibility for graphite. The same parameter in the H-H potential is taken from the quantum-mechanical calculation of the repulsion of two H_2 molecules made by the author and assumed equal to 3.74 $Å^{-1}$. The constant α for C-H interactions is the average of these two values. The constant B_{HH} is taken to be 4000 kcal/mole on the basis of Urey-Bradley's spectroscopic force constant data, lattice vibration analysis and quantum-mechanical calculations. The other five constants are determined by the least squares method from 77 experimental equations which include crystal structure and sublimation heat terms for 9 aromatic hydrocarbons and elasticity constants for some of them.

The interatomic potential parameters obtained as a result of these calculations reproduce benzene, naphthalene and anthracene structures accurate to within approximately 0.05 Å with respect to C atom positions and 1 % with respect to the lattice constants. Errors in the elasticity constants for benzene and naphthalene are much larger than experimental error.

In this calculation, the position of the repulsion and attraction centre for the H atom was shifted by 0.07 Å towards the C atom along the C-H valence bond. It is perhaps due to this shift that the equilibrium distance r_0 on the author's curve turned out to be much larger (about 3.2 Å) than the value assumed in our calculations.

The two publications to be discussed below are attempts to go beyond the framework of the atom-atom potential model and interpret molecular crystal structure by taking into account the electron stucture of a molecule.

In [28, 34], the authors consider the effect of different components of intermolecular interaction energy on molecular orientation in aromatic hydrocarbon crystals. Dispersion energy of attraction is calculated "using polarizability of molecules as a whole without allowing for individual contributions of C-C and C-H bond electrons". Apart from geometrical terms which describe the lattice, van der Waals' energy equation also incorporates the molecular constants A^{Ky} defining energy transitions in free molecules. These constants can only to some approximation be

determined from experimental molecular polarizability components, and the results for dispersion energy can be widely different, depending on the assumptions used. It should be pointed out, through, that the major role for solving the packing problem is played by variations of energy caused by angular shifts of molecules which can be estimated by lattice sum variations, rather than the absolute magnitude of the energy. A repulsion potential is taken into account only for the closest neighbours with overlapping electron clouds and is written as the sum total of three components $U_{rep} = U_1(H - H) + U_2(C - H) + U_3(C - C)$, depending on interactions between individual atoms; detailed calculations were made for H atoms only. The authors employed two expressions to describe a repulsion potential: a formula containing an exchange integral, and the exponential components of the total interatomic (6-exp) potential. The authors also estimated the quadrupole contributions to the lattice binding energy of naphthalene and benzene crystals. It was found that these contributions are negligible and do not affect the establishment of an equilibrium structure in a crystal.

Though this technique is undoubtedly interesting, it is obvious nonetheless that it cannot be generally applied for predicting the structures and properties of organic crystals. The consistent atom-atom potential method appears to me the only technique suitable for such calculations.

The lattice binding energy of a benzene crystal was calculated with a view to assessing the relative contributions of the σ– and π–electrons to attractive energy [35]. The total lattice binding energy is evaluated by summing pair-wise interactions of whole molecules. The formula for the dispersion energy of attraction between molecules used by the authors is different from the classical London equation in that the former includes the molecule polarizability tensor and angular components which define mutual orientation of molecules. In energy calculations, the authors determined the exchange integral for two orbitals which belong to the repulsion centres (H-H and H-C atoms). Nevertheless, the proportionality factors in the exchange integral equations were calculated from experimental data.

The correctness of the calculations is checked by comparing the calculated and experimental values of the lattice binding energy; however, agreement between them is far from satisfactory ($2\,U_{theor} = -17.55$ kcal/mole, $2\,U_{exp} = -21.3$ kcal/mole).

7. Condition of structural stability of organic crystal and the principle of close packing

The actual structure of a crystal is characterized by minimum free energy. To explain why a crystal has a specific molecular packing pattern means to show that all packings other than actual display higher free energy.

In this discussion I would disregard the effects of the crystalline field on the shape of a molecule and intramolecular vibrations. Generally speaking, these effects are insignificant and will be considered in the next section.

If the mutual molecular orientation is given, free energy can be calculated on the basis of a law governing intermolecular interaction. Crystal free energy is a function of the symmetry and size of the unit cell, the coordinates of the centre of gravity of the molecule and Eulerian angles which define molecular orientation.

The condition of stability of a crystal structure which implies that free energy variations must be zero can be written as:

$$\delta F = \delta U + \delta F^{vib}$$

At absolute zero, intermolecular free energy equals to zero-point vibrational energy, i.e. about 0.2 kcal/mole. Variation of this value from structure to structure do not exceed hundredths of kcal/mole. Since the potential well depth is much larger than that, crystal structure at absolute zero must be consistent with minimum energy of intermolecular interaction, in other words, a stable structure must satisfy the following condition:

$$\delta F = \delta U = \frac{\partial U}{\partial R_i} \delta R_i + \frac{\partial U}{\partial \varphi_i} \delta \varphi_i + \frac{\partial U}{\partial a_i} \delta a_i$$

where: R_i are radii-vectors of the centres of molecules, φ_i – Eulerian angles and a_i – unit all parameters.

If our consideration is restricted to centrosymmetrical structures of the naphthalene type, the first term of this equation is omitted. Crystals of monoclinic symmetry exhibit a seven-dimensional energy surface. Modern computers make the construction of such a surface quite feasible. This problem has been partially solved by us for rhombic benzene (see above), and by other workers for triclinic hexamethylbenzene [29]. In both instances, the energy surface (meaning, of course, the part of the surface which corresponds to the symmetry of only one of possible space groups) displays one deep minimum which is associated with the actual structure.

Comprehensive investigation of a lattice binding energy surface including consideration of different symmetries has intrinsic interest because it helps understand the phase diagram of a solid-state substance. The energy surface must show very many minima. Shallow minima are of no interest as they cannot generate a structure on account of thermal fluctuations. First of all, we choose the lowest-lying minimum among all deep minima. This minimum should correspond to a structure which is stable at absolute zero. Other deep minima lying above the lowest minimum represent actual high-temperature modifications only if they correspond to minimum free energy.

Let us consider two minima: the deepest minimum with energy U_0 and the minimum that follows the deepest one and has higher energy U_1. At absolute zero the stable structure U_0 and the metastable structure U_1 are characterized by the parameters-abcissae of the potential well bottoms. As temperature rises, the figurative point shifts along the edge of the wells. At a certain temperature T, lattice binding energies become $U_0 + \Delta U_0$ and $U_1 + \Delta U_1$, and the vibrational parts of free energy F_0 and F_1. A polymorphic change occurs if the total free energy of structure I becomes equal to the total free energy of the structure stable at 0°, i.e. if

$$U_0 + \Delta U_0 + F_0 = U_1 + \Delta U_1 + F_1 .$$

Only very few potential wells, if any, can satisfy this condition. It is clear from the above discussion that a polymorphic change is possible only if the free vibrational energy of the unstable structure increases with temperature faster than that of the stable structure. This condition is, however, not sufficient, because the crystal may melt before the loss in the potential energy has been balanced.

It is known that heat required for a polymorphic transition (but not for a transition into a rotational crystalline state to be discussed below) rarely exceeds 1 kcal/mole. It may be supposed that free vibrational energy also rises during this transition by approximately the same value. It means that if a structure stable at absolute zero is represented by a potential well lying deeper than the others by the above value, no polymorphic changes can occur in this substance.

As was shown in section 6, the coordinates of a minimum are only slightly displaced effect of crystal heating, the minima of the energy surface are representative of all structures possible in the substance, several of these being the actual structures. In other words, each actual structure is given by its own minimum on the energy surface of our model.

As was shown in section 6, the coordinates of a minimum are only slightly displaced by electrostatic interaction. This means that mutual molecular arrangement is characterized by a minimum of the energy surface calculated by means of the atom-atom potential model. Of course, this minimum may not necesserily be the

deepest, but only one of the deepest. But this is of no importance. The fact that any crystal structure has its own minimum on the energy surface which represents the sum total of atom-atom interactions is suggestive of the close packing principle [36]. Only one additional simplifying assumption is required in this case – it is necessary to consider molecules as being absolutely rigid, i.e. to substitute the repulsive portion of the curve by a vertical line. In this case, a trend for minimization of the potential energy is evidently analagous to the requirement of locating a maximum number of atoms at the closest distances to each other.

8. Effect of crystalline field on the shape of molecule

In order to correctly estimate the objective nature of X-ray diffraction technique for studying organic crystals and to understand differences in experimental definitions of interatomic distance parameters and valence angles, one must have a clear idea of the effect of the crystalline field on the structure of a molecule.

If we consider a molecule to be sufficiently labile, the condition of crystal structure stability must be written not in the form given in the previous section, but as

$$\delta F = \delta U + \delta F^{vib} + \delta E$$

where δE denotes molecular energy variation. It means that when evaluating comparative advantages of several different packing patterns, it is necessary, strictly speaking, to estimate variations in the energy of the molecules themselves.

It is self-evident that these variations cannot be too large. It may perhaps seem at first glance that where high accuracies are implied the effect of the crystalline field must by all means be taken into account. If this were true, it would immensely complicate the problem of calculating an appropriate structure by energy minimization: the number of parameters would greatly increase if the parameters of the molecule itself have to be added to the lattice parameters.

The solution of our problem is considerably facilitated by the fact that in most cases it is not necessary to allow for the effect of the crystalline field whatsoever, while in certain specific instances it is sufficient to consider only the parameters associated with rotation of the parts of the molecule about a single bond.

There are two principal consequences of the influence of the crystalline field on the shape of a molecule: deviation from an optimum conformation, and selection of one of possible conformations.

Below is given the explanation of the concept of the conformation of an organic molecule.

The configuration of the potential energy of atom interaction in a molecule is a multi-dimensional surface in a space of geometric parameters defining the mutual arrangement of the atoms. Each well on such a surface represents a certain constuction of atoms which is called the conformation of the molecule. If thermal motion does not bring the figurative point beyond the well, the term "conformation" is equivalent to "configuration". Sometimes, two or more potential wells are separated by barriers which are commensurable with kT. Then, the molecule can exist in several distinct conformations. It would be appropriate to term this molecule flexible in order to distinguish it from a rigid molecule which possesses only one conformation.

We shall first consider molecules having only one conformation and try to answer the following question: what is the difference between the geometry of these molecules in a crystal and the geometry of free molecules? A great body of experimental information which is now available can help evaluate the extent of molecular deformations under the effect of the crystalline field. There are four approaches to the solution of this problem. First, we may compare the structure of gaseous and crystal molecules; second, make comparative study of the geometries of crystallographically independent molecules in the same crystal; third, analyze the structure of a molecule whose symmetry in a crystal is lower than the symmetry of a free molecule; and, finally, we may compare molecules of different polymorphic modifications.

Here are a few examples. Studies of gaseous benzene molecules have established that the structure of a benzene molecule is a regular plane hexagon formed by C atoms with a distance of 1.397 ± 0.001 Å between the carbon atoms, and the length of the C-H bond equal to 1.084 Å. X-ray diffraction analysis of crystals yields the following values for this molecule: bond lengths – 1.379, 1.374, 1.378 Å; valence angles – 119°50′, 120°42′, 119°28′.

A phenanthrene molecule occupies a general position in a crystal. At the same time it is obvious that this molecule exhibits at least second-order axis symmetry. The direct experimental results are shown in Fig. 13a. The equivalent angles differ by several degrees, the difference between the equivalent distances ranges from 0.01 to 0.03 Å.

The figure also shows experimentally determined sizes of the two halves of an acenaphthene molecule (Fig. 13b). The molecules in a crystal occupy two independent positions with mirror symmetry. The order of difference is here the same as above.

The above data are typical enough. A question which now arises is as follows; should these differences be ascribed to experimental errors or do they reflect actual differences in the molecular structure caused by the effect of the crystalline field?

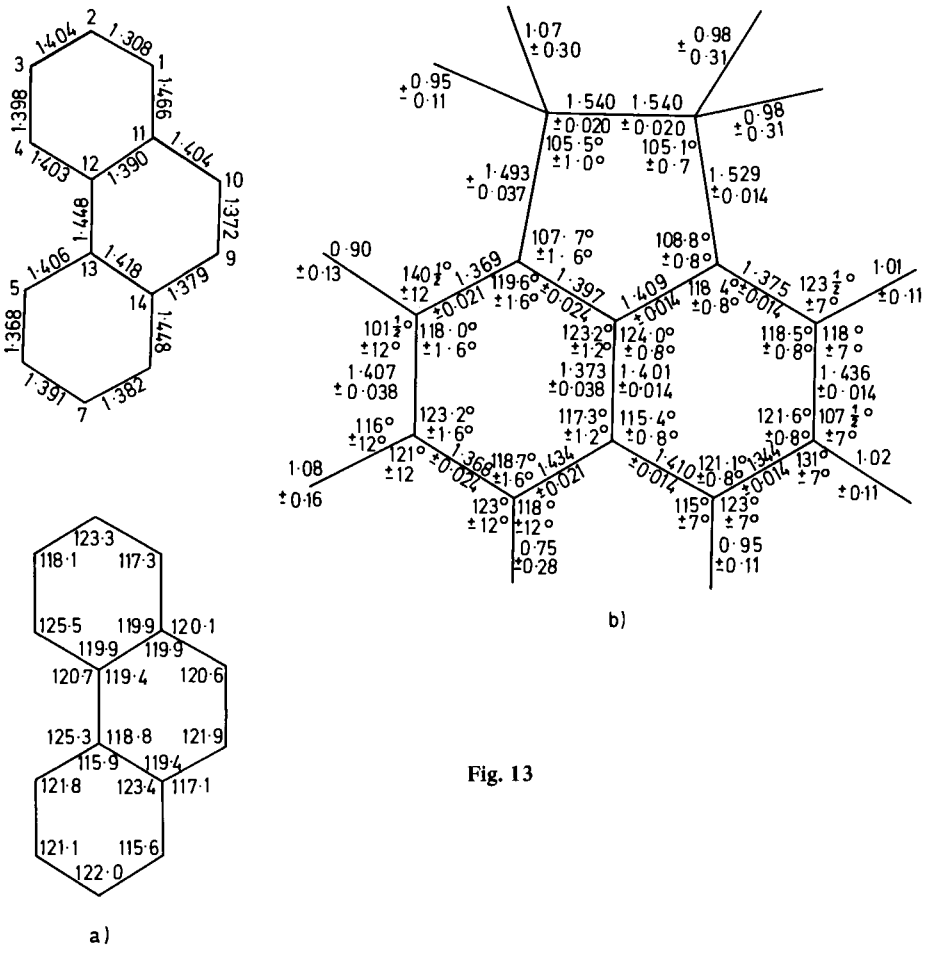

Fig. 13

It will be now shown by simple calculations that in all these cases the difference is due to experimental errors or artifacts.

For each concrete case it would be necessary to point out the following. If the atoms are displaced so as to eliminate distortions, the molecular energy is bound to reduce by ΔE, and the lattice binding energy to increase by ΔU. The distortion of a molecule may be energetically justified if $|\Delta E| \approx |\Delta U|$. On the contrary, distortion is impossible if $|\Delta E| \gg |\Delta U|$. Strictly speaking, changes in free energy rather than in potential energy should be calculated. Nevertheless, the contribution of minor distortions to variations in molecular vibrations seems to be quite insignificant.

ΔE can be calculated for each concrete case using, for example, the mechanical model of a molecule, while ΔU is estimated by means of the atom-atom potential scheme.

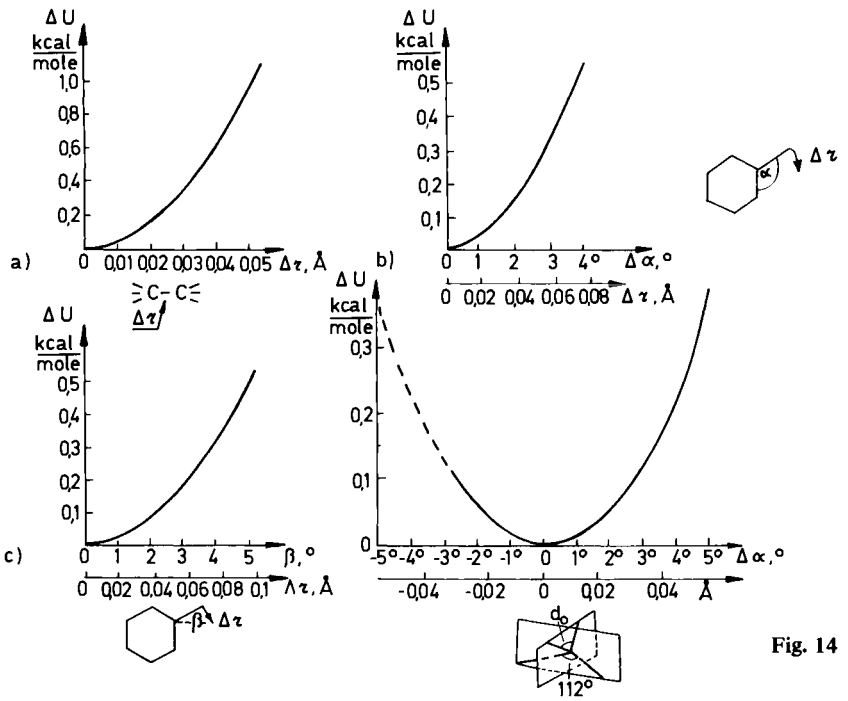

Fig. 14

It is, however, by no means necessary to discuss concrete cases. It is quite sufficient to consider curves given in Fig. 14. The figure shows changes in molecular energy which are caused by changes in C-C bond length (a), displacement of a H atom in an aromatic molecule on a plane and perpendicular to the plane (b, c), and changes in an HCH angle in an aliphatic molecule (d).

For comparison, we have taken a typical example of a benzene crystal and calculated variations of the lattice binding energy caused by the displacement of different C and H atoms various sides of their true positions. The results have indicated that a 0.03 Å displacement of an atom from its true position always changes the lattice binding energy by less than 0.01 kcal/mole. In other words, in the scale of the figure which illustrates the energy of molecular distortion at the expence of variations in bond lengths, the curve describing lattice binding energy variations practically coincides with the X-axis.

Thus, we arrive at the following conclusion: the crystalline field does not affect bond lengths. It should be pointed out, by the way, that from my point of view, the best measure of the accuracy of X-ray diffraction analysis of organic crystals is discrepancies in bond lengths which must be equal from the chemistry viewpoint. With this criterion applied, there seems to be no experiment which could claim accuracy above 0.01 Å.

The mechanical model of an organic molecule which has been successfully used by us and other workers for calculating optimum conformations of free molecules [39, 40] embodies the assumption that molecular energy may be subdivided into binding energy, valence angle elasticity energy and non-bonded atom interaction energy.

Interaction between binding energy and other molecular energies is quite insignificant, though in [40] it is proved that the mechanical model can also be reliably applied for interpreting different bond lengths in hydrocarbons; roughly speaking, the larger the repulsion of corresponding groups of non-bonded atoms, the larger are bond lengths. In our physical model, as is indicated by the above numerical example, valence-bond energy can be disregarded.

It now remains to discuss possible effects of the crystalline field on the sum of the two components: valence angle energy plus non-bonded interaction energy. (We have called this sum molecular strain energy.)

Where these two components do not interact, the situation is clear. From the same figure it follows that the changes in the valence angles are not balanced by a gain in the lattice binding energy.

The results are equally obvious a priori in cases when changes in a moleculare are associated only with variations of the distances between the non-bonded atoms, i. e. in the case of rotation about the single bond. Here, the major role is played by the steepness of the potential well representing the conformation of the molecule. Cases may be encountered when the non-bonded atoms of a molecule in an optimum conformation are located at distances close to equilibrium distances. The steepness of the potential well near an equilibrium will then be small, and the amount of interaction between the atoms of the two parts of the molecule will be of the same order as the interactions between the non-bonded atoms of adjacent molecules. In these conditions, the crystalline field is obviously quite able to cause considerable rotation of the parts of the molecule about the single bond. Therefore, calculation of an optimum structure should involve not only consideration of variations in the packing pattern, but also of changes in the molecular energy which must be expressed in terms of angular rotation about the single bonds. If the distance between non-bonded atoms descreases as the molecule rotates, relevant energy quickly rises. After the parts of the molecule have rotated at a certain angle, intramolecular repulsion is balanced by the crystalline field forces.

Thus, the crystalline field can bring a molecule out of the optimum conformation by means of rotation about a single bond, but only if a free molecule has not been strained. On the other hand, if the optimum conformation of a free molecule exhibits an appreciable decrease in the distances between nonbonded atoms, this molecule is rigid with respect to the crystalline field, because the conformational well is very steep.

We have considered molecular changes caused either by variations of valence angles, or changes in the distances between non-bonded atoms.

If conformational changes are determined by some parameter whose variation brings about a change in both energy components, one must be very cautious in assessing the effect of the crystalline field. A change of the valence angle may be unfavourable as such, but it is possible to imagine such cases when the competition between valence angle elasticities and non-bonded interactions will be settled by the effect of the crystalline field.

As a hypothetical example for illustration, consider a substituted benzene molecule. Under the effect of interaction between the substituents, the valence bonds that link them with the benzene ring may go out of the benzene ring plane. A gain in the non-bonded interaction energy is offset by the distortion of the valence angles. But the crystalline field always compresses a molecule. Therefore, a molecule may become flat in a crystal.

In such cases an a priori statement not founded on calculations may prove to be erroneous. When searching for an optinum crystal structure, one must not only vary the cell parameters and the degrees of freedom of the entire molecule, but also the internal parameter (in our example, it is an angle or angles formed by the out-of-plane bonds).

A classical example of the influence of the crystalline field on a molecular conformation is biphenyl which is non-planar in a gaseous state and planar in a crystal. The flattening of the molecule involves loss of the ortho-atom repulsive energy, and, on the contrary, an increase of the conjugation energy of the benzene rings and of packing density (planar systems are more convenient for packing).

Molecules displaying relatively easy rotation of the benzene rings are generally good objects for studies on this problem.

The example is publication [41] which reports the results of the calculation of the structure of a 2-bromo-I.I-p-tolylethylene crystal. The observation has been made that a phenyl ring located close to the bromine atom is turned 67° out of the ethylene plane, while the second phenyl ring is 24° out-of-plane. Calculations have shown that an optimum conformation is obtained at angles of 45° and 35°, respectively. Using the formula of the atom-atom potential model given above in para 4, the authors have calculated the energy of interaction of a given molecule with adjacent

molecules as a function of these rotation angles. It has been found that, with due allowance for molecular packing, the optimum ring rotation angles are 67° and 25°, which is fully compatible with experiment.

To summarize, it must be emphasized once again that the crystalline field does not change the bond lengths of organic molecules. Valence angles remain constant if these changes do not cause an increase in other intramolecular energies. The major effect of the crystalline field on the shape of a molecule consists in providing rotations about single bonds which are favourable for packing. However, these rotations can take place only if the optimum conformation of the molecule is unstrained.

As the crystalline field compresses the molecule, then, other conditions being equal, a conformation in which the molecule occupies the least volume, is selected.

If the energies of several conformations of one molecule differ to a more or less considerable degree, the crystal is composed of optimum molecules. The reason is that in this case large possibilities are provided for formation of different packing patterns, and, therefore, a decrease of the molecular energy by 2-3 kcal/mole can hardly be balanced by an increase of the lattice binding energy.

9. Lattice dynamics

In most cases, heat motion in a molecular crystal is manifested in vibrations of atoms near an equilibrium. These vibrations can be subdivided into intra- and intermolecular vibrations, usually, with a considerable interval between the two groups. Intermolecular vibrations occur at frequencies of 100 cm^{-1} and lower; the frequency of intramolecular vibrations ranges from 200–300 cm^{-1} to higher frequencies. The amplitudes of the vibrations are also quite different.

There is no doubt that intermolecular vibrations interact with lowest-frequency intramolecular deformational vibrations. However, this interaction cannot be too large. Therefore, the division of the thermodynamic functions into the intramolecular and intermolecular components adopted in our physical model is justified to some approximation whose accuracy is not yet known.

The experimental values of the thermodynamic functions minus intramolecular parts which can be calculated from the data available on the spectrum of normal intramolecular vibrations using the oscillator formulae, gives the crystalline portions of free energy, enthropy, heat capacity, etc. These crystalline components depend on the intermolecular vibration spectrum.

It will not introduce a large error in our calculations if the above subtraction is performed with intramolecular spectra obtained for the gaseous state. Experiment shows that differences in the vibrational frequencies of molecules in different aggregate states do not exceed 0.1 % for high frequencies and 3-5 % for low frequencies. The magnitude of an error arising in the crystalline components of the thermodynamic functions due to neglecting the effect of the crystalline field on the molecular frequencies is usually less than 1 %.

Disregarding the interaction between the frequencies and the effect of the crystalline field on these frequencies, we can consider a molecule as being rigid and, knowing the law of molecular interaction, solve the problem of lattice dynamics.

A crystalline molecule has six degrees of freedom: three translational motions and three vibrations about an equilibrium.

Consider a molecule at a certain moment of vibration. All Z molecules are brought out of an equilibrium state. The position of each molecule is defined by six displacements (three of which are linear and three angular). The total number of "coordinates" which describe the arrangement of molecules in a cell is 6Z.

It can be easily shown by conventional mathematical treatment that 6Z frequencies ω which are a function of the wave vector $\mathbf{k}$ obey equation:

$$| T_{SS'} - \delta_{SS'} \omega^2 | = 0$$

where S indexes 6Z "coordinates" of the cell. Here

$$T_{SS'} = \sum_{h} \lambda^{h}_{SS'} e^{i\mathbf{k}\mathbf{R}^{h}_{SS'}} .$$

The index h identifies the number of the cell with respect to the cell taken as zero. $\mathbf{R}^{h}_{SS'}$ denotes the radiusvector connecting the "centres" of two molecules. The problem is solved by calculating the coefficients $\lambda^{h}_{SS'}$ which are

$$\lambda^{h}_{SS'} = \frac{\partial^2 U}{\partial t_S \cdot \partial t_{hS}} .$$

The interaction energy U which can be calculated by means of atom-atom potentials must be differentiated with respect to all pairs of coordinates of all the molecules. As the amount of interaction quickly decreases with distance, it appears practically sufficient to consider one molecule and its closest neighbours. The coordinates t_S for one molecule are $\sqrt{m}u_1, \sqrt{m}u_2, \sqrt{m}u_3, \sqrt{I_1}\Omega_1, \sqrt{I_2}\Omega_2, \sqrt{I_3}\Omega_3$. Here u_1, u_2, u_3 are linear displacements along the axes, while $\Omega_1, \Omega_2, \Omega_3$ – designate rotations about these axes. The axes of coordinates are the major inertia axes of each molecule.

After determining all the frequencies ω (**k**), we proceed to calculation of the eigenvectors of each normal vibration:

$$\Delta_{Sm} = |T_{SS'} - \delta_{SS'}\omega_m^2|_S ,$$

both indexes passing values from 1 to 6Z.

If a molecule occupies a general position in a crystal, each normal vibration of this molecule is the combination of translational and orientational motions. If a molecule is centrosymmetrical, its orientational and translational motions are readily distinguishable. For instance, the lattice dynamics of a naphthalene crystal is represented by 12 dispersion hypersurfaces (a frequency is a function of the wave vector). For $\vec{k} = 0$ 6 of these 12 frequencies are translational and 6 orientational. In its turn, each group 0f 6 frequencies is composed of symmetrical and antisymmetrical vibrations. It should be remembered that the space group is preserved at symmetrical vibrations. Out of six translational motions, three are acoustic, i.e. their frequencies vanish when the wave vector is zero (for a wave of an infinite length).

Optical frequencies measured in Raman spectrum experiments are frequencies for infinite-length waves. However, on account of the forbiddance laws, only 6 orientational frequencies can be observed.

The above procedure for lattice dynamics calculation has been evoled in [42]. As to vibrational frequency calculation by means of atom-atom potentials, [43] is the first work where vibrational frequencies were calculated as a function of the wave number (for a direction (010)) for naphthalene and anthracene crystals. The calculated results show good agreement with experiment (Fig. 15). The above calculations have been made using atom-atom potentials in the form given in para 4.

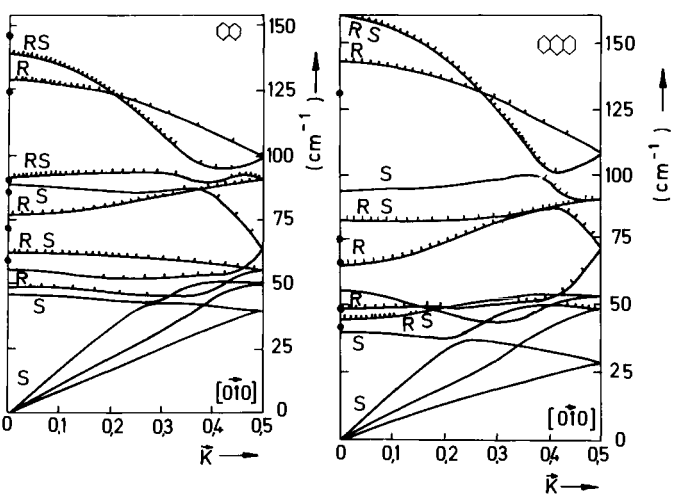

Fig. 15
The black circles denote experimental data, R rotations; S – symmetric mode

The eigenvectors of vibrations were also determined in [43]. Many earlier workers proceeded from the assumption that molecules in a crystal vibrate harmonically about their inertia axes. But there are no reasons whatsoever to expect such results. It is clear that the major vibrational axes are determined by the crystalline field. It has been found that in a naphthalene crystal the major vibrational axes for low-frequency anti-symmentrical vibrations form two 30° angles with the principal inertia axes. The axes running along the long molecular axis have been found to be close to each other.

In the work cited above frequencies were evaluated for a certain single unit cell. An attempt can be made at estimating to a quasi-harmonic approximation the temperature dependence of vibration frequencies. In this approximation, as is known, frequencies are regarded as functions of the cell size.

The temperature dependence of the mean square frequency of the intermolecular vibration spectrum was determined in [44]. The value ω^2 is known to equal the characteristic temperature accurate to the magnitude of a factor close to unity. This calculation has been made for an adamanthane crystal. In this case, too, the results are in reasonable agreement with experiment.

On the basis of a frequency spectrum it is, of course, possible to calculate the average amplitudes of molecular vibrations which determine the values of the temperature factor in X-ray diffraction analysis. However, comparison with experimental data is not so easy, because the intensities of diffraction spots depend on a variety of factors, including intramolecular vibrations.

So far we have discussed vibrational motions of molecules. But these are not the only kind of motions possible. The nuclear magnetic resonance technique has confirmed earlier predictions about reorientational motions of molecules in a crystal. These motions can occur if reorientation barriers are only of the order of the value of kT. In other words, a molecule can be reoriented only if it has a suitable shape – disc, sphere, cylinder.

Reorientation of molecules is quite compatible with a rigorous order in a crystal. X-ray analysis gives a clear picture of electron density with fixed average positions of the atoms. If molecules are reoriented so that any succeeding position of a molecule cannot be distinguished from its previous position, this reorientation will produce no effect whatsoever on X-ray diffraction experiment.

For illustration, consider benzene and hexamethylbenzene crystals. The molecules are reoriented by rotation about the 6th-order axis of the molecule.

The reorientation frequency must satisfy the following relationship:

$$\omega_c = \omega_0 e^{-\frac{U}{kT}}$$

where U denotes the activation energy of reorientational motions. As temperature rises, the reorientation frequency gradually goes up starting from zero. At a sufficiently typical barrier height (about 3 kcal/mole), the number of reorientiational transitions amounts approximately to 10^5 per second at 85 °K, and 10^8 per second at 170 °K [45]. The frequency of benzene molecular vibrations is about 10^{12}. It is thus obious that most time a molecule exists in the state of vibrations. Even at a temperature approaching the melting temperature, there will be one reorientational transition for a thousand or so vibrations. It follows that thermodynamic values for ordered crystals are insensitive to molecular reorientation.

It has been said in the preceding sections that information on reorientation of molecules in a crystal is obtained from the analysis of line widths in nuclear magnetic resonance. Usually, proton resonance is observed. At low temperatures, substance gives a wide line; at a certain temperature the molecular reorientation frequency becomes equal to the line width. According to theoretical investigations, under such a condition the width of the line must quickly and appreciably reduce.

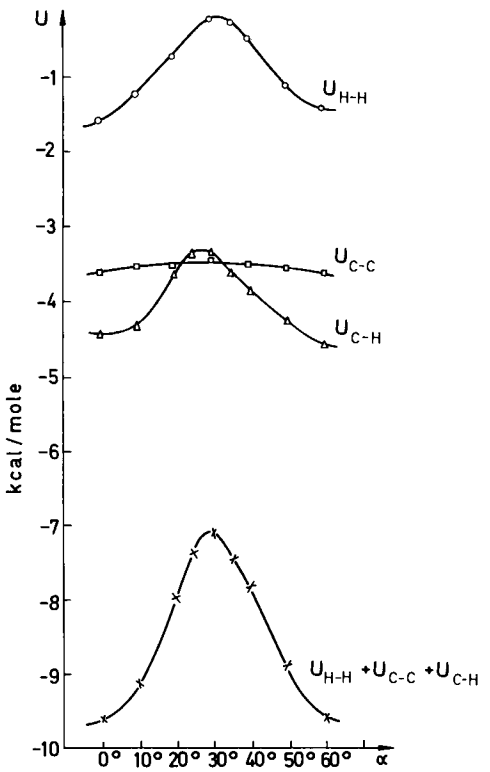

Fig. 16
Energy of interaction between one rotating molecule and its stationary neighbours. The diagram shows the cumulative curve and also the behaviour of energy components which are due to interaction of atoms of different varieties.

The moment of narrowing of the nuclear magnetic resonance line is often erroneously associated with a phase transition. This is not so: the temperature of line narrowing is the temperature at which this method starts to "discern" reorientation of molecules.

In view of the fact that reorientation is a rare phenomenon, discussion of reorientation in terms of the geometrical or physical model should amount to consideration of the rotation of a molecule, its neighbouring molecules being at rest. Whether or not reorientation is possible can be roughly estimated without mathematical treatment, by analyzing the compression of atoms formed when the molecule turns from one equilibrium state to another. If at a certain moment of rotation the intermolecular distance between the closest atoms is decreased, for example, twice, no rotation can surely occur.

With atom-atom potentials, one can relatively easily calculate the energy curve corresponding to reorientation rotation.

We have carried out such calculations for a benzene crystal. The results are shown in Fig. 16. The barrier is formed when the molecule turns about 30° from an equilibrium. The height of the barrier is close to 3 kcal/mole, which corresponds to the experimentally observed value.

10. Crystals with disorder elements

The arrangement of molecules established by X-ray diffraction analysis is the arrangement averaged over all the crystal cells. If there is certain disorder in the molecular arrangement, inherent in a crystal, the X-ray technique detects "the average molecule" by superposition of all molecules located in the same crystallographic position of the average unit cell.

One of the elementary and most common examples of this kind of disorder is formation of centrosymmetrical crystals by molecules without a symmetry centre. Such crystals are, for instance, p-chloro-bromo-benzene, p-nitro-chloro-benzene and azulene (hydrocarbon consisting of a five-member ring conjugated with a seven-member ring).

In such crystals, the average molecule is actually obtained by centrosymmetric superposition of two molecules with half-weight atoms. If we construct a hypothetic space lattice of average cells (for all the three above crystals this is a $P2_1/c$ lattice with two molecules in a unit cell), the space lattice will have an equal number of points with molecules facing the opposite directions.

It is quite evident that such a disordered crystal can be formed only if the inversion of a molecule by the symmetry centre of the average crystal cell entails minimum loss of energy.

For illustration, we have made simple calculations for an azulene crystal by means of the atom-atom-potential model.

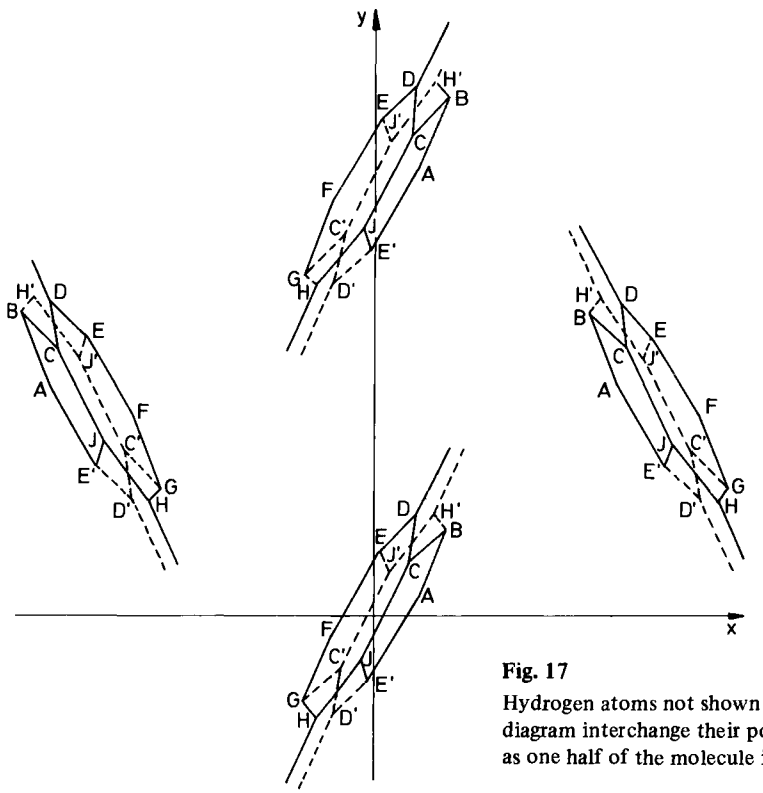

Fig. 17
Hydrogen atoms not shown in the diagram interchange their positions as one half of the molecule is inverted

Fig. 17 represents the average molecule of the average cell of an azulene crystal in the form given in publication [46]. We have added the coordinates of H atoms to this drawing. The structure of a crystal is very similar to naphthalene crystal structure. It can be easily seen that the inversion of the molecule (a half of the average molecule) by the symmetry centre practically does not change the contacts between the molecules of the ab layers. We have considered all possible versions of the mutual arrangement of azulene molecules to the closest neighbour approximation on the ab plane. The calculations have demonstrated that 23 arrangement

patterns are not favourable because they are associated with a higher energy than the interaction energy of molecules located so as to form a regular non-centrosymmetric lattice ($P2_1$). 7 arrangement versions, however, have been found to be more favourable, two cases involving energy which was 0.4 kcal/mole lower than that of an ordered crystal.

The following point is also worthy of note: all molecular arrangement patterns are associated with interaction energies lying within 1 kcal/mole. At the same time, configurational enthropy for distribution over two positions RTln2 at room temperature is 0.42 kcal/mole.

The calculations show that, first, no second-order phase change should be expected, because preservation of order in the same lattice of molecular centres is much less favourable. Second, loss in the lattice binding energy on account of unavoidable unfavourable arrangements in an azulene crystal may apparently be compensated for by an increase of enthropy.

Of course, the above example in no way proves that azulene must necessarily crystallize into disordered crystals. For proving this, it would be required to apply the usual procedure – that is, to show that all other conceivable azulene structures are "worse" than the experimentally observed disordered structure. Nevertheless, it has been demonstrated that our physical model offers correct interpretation of the phenomenon of disordered structure formation.

A very interesting class of disordered structures are hexasubstitution benzene derivatives. Using for substitution halogen atoms, methyl groups and other small substituents, one can obtain a large number of isomorphous crystals of the hexachlorobenzene type (ordinary centrosymmetric monoclinic structure with two molecules in a unit cell).

According to the results of the X-ray diffraction and nuclear quadrupole analysis conducted in the author's laboratory [47, 48], orientational distributions of molecules may considerably differ from one crystal to another. Since the average molecule is centrosymmetric, there are three independent positions in a crystal over which the benzene ring substituents are distributed.

In some cases, the situation is quite simple. For instance, a monobromo-pentachloro-benzene molecule has 1/6 of the Br atoms and 5/6 of the Cl atoms in each position. If two ortho or meta- Cl atoms in a hexachlorobenzene molecule are substituted by Br atoms, there will be 1/3 of the Br atoms and 2/3 of the Cl atoms in each positions. Like in many other similar cases, the average molecule displays here 6/mmm symmetry. Such a situation in which the distribution of substituents is dictated by the symmetry of a free molecule is not obligatory. Let us see the behaviour of tetrachloro-p-dibromo-benzene molecules. The average molecule has

mmm symmetry. One of the orientations is strongly preferred: 2/3 of the molecules are oriented similarly, while the remaining molecules are equally distributed between two other positions. Surely there must be cases in which different probabilities correspond to all the three positions.

We want to emphasize that molecules in disordered crystals of this type may exhibit both uniform and non-uniform positional distribution of molecules.

Another subject of interest is the investigation of shortrange order in the arrangement of differently oriented molecules. However, no work seems to have been done to study this problem.

Molecules of disordered organic crystals exhibit the same motions as do those in quite ordered crystals. Some molecules only vibrate about an equilibrium (p-nitrochloro-benzene, azulene), others reorient about one of their axes. In the case of small substituents, all hexasubstitution benzene derivatives are probably capable of reorientation. The phenomenon of reorientation in such molecules containing protons has been shown by French workers [49, 50, 51] using the nuclear magnetic resonance technique.

11. Rotational crystalline state

Crystals with disorder elements which have been discussed in the foregoing section give good-quality X-ray pictures representing hundreds of reflections. It means that variations of the size and shape of the unit cells with respect to the average value do not exceed too much those for conventional ordered systems. This has been confirmed by our calculations for an azulene crystal: there is but a slight difference in the energy of various mutual arrangements of molecules in unit cells of the same size. A characteristic structural feature of disordered crystals of this type is that the inversion of a molecule causes partial transposition of the atoms; at any rate, certain important geometrical elements of the molecule – planes or axes – are aligned.

We have considered structures in which disorder is brought about by a relatively small number of different orientations, while order is retained with respect to a normal to its plane. It is quite probable that other structures of the same type exist, for example, well-ordered low-symmetry structures in which disorder is caused by rotations about the long molecular axis.

It should be pointed out that there may be both static and dynamic versions of disordered crystals of this kind. In this case, molecular reorientations do not generate any structural peculiarities. More than that, no effect is produced on the thermodynamic properties of the crystals. If the nuclear magnetic resonance method were not available, no proofs of molecular reorientations could have been furnished.

Any classification is always arbitrary to a certain extent. Nevertheless, one can safely distinguish between the above disordered crystals and a relatively wide class of substances commonly called plastic crystals by British authors. What we would like to emphasize is that we are speaking about a very peculiar state of the substance which always has its own domain of existence in the phase diagram. Therefore, we prefer the term rotational crystalline state. The specific features of these substances discovered by *Timmermans* have been described in detail in various reviews [52], therefore, I would only like to point to the following two peculiarities: high-symmetry cells typical of sphere and cylinder packings, and the existence of not more than 10 reflections on X-ray photographs, that is, the scatter of the unit cell sizes within 1 or even 2 Å. The rotational crystalline state is characteristic of molecules of almost spherical shape, for instance, methane and ethane derivatives with small substituents, or molecules of a shape close to a cylinder – paraffin type molecules.

There may be two cases when a low-symmetry molecule occupies a high-symmetry position in a crystal: first, when all orientations with respect to the crystal axes are equiprobable (the average molecule displays sphere or cylinder symmetry), and second, when a molecule has several fixed orientations derived by the crystal symmetry elements from one arbitrary orientation. In the latter case, an asymmetric molecule will be located at the points of a cubic face-centered lattice in 48 distinct orientations, a centrosymmetric molecule in 24 orientations, a molecule showing D_{3h} symmetry in 8 positions, etc.

No matter which of the above hypotheses may be correct, plastic crystals obviously have pronounced short-range order in the arrangement of the molecules or even a domain structure in which individual ordered domains are transferred into each other at the expense of "erroneously" located molecules. It is also evident that the short-range order is quite labile, because reorientation of molecules takes place in absolutely all substances in the rotational crystalline state.

The existence of short-range order can be deduced from many facts (see reviews [52]). First of all, the maximum diameter of a molecule is always much larger than the average size of an effective sphere, the difference reaching 1 Å. Secondly, nuclear magnetic resonance analysis shows that a barrier to reorientation amounts to several kcal/mole, and that most time each molecule exists in the state of vibrations around an equilibrium and only sometimes jumps from one equilibrium state to another.

Since the main subject of this paper is packing of molecules, we now come back to the molecular packing problems. Although much work has been done in this field, the following two problems of prime importance have not yet been solved: the nature of short-range order remains obscure, and no data is available for proving the presence or absence of orientations fixed with respect to the crystal axes.

Satisfactory compatibility of the entropy involved in transition from the ordered state into the rotational crystalline state with a configurational gain in the entropy is often taken as the evidence of a finitness of the number of molecular orientations in a crystal. Thus, from the symmetry considerations, a bicycloheptane molecule must occupy 24 different positions in order to simulate the symmetry of a cubic cell point [52], page 93. The transition enthropy has been estimated at $R\ln 24 = 6.3$ cal/deg. mole which agrees with the experimental figure. In our opinion, we can hardly rely on such comparisons. It is clear that the vibration amplitudes of molecules in the rotational crystalline state are considerably larger than those in an ordinary crystal. Therefore, a substantial portion of the transition enthropy should be attributed to the freedom of motion.

Nonetheless, the hypothesis about certain preferred orientations with respect to the crystal axes seems to be sufficiently logical, despite the fact that the more spherical a molecule is, the lower is the probability of orientations fixed with respect to the axes of the crystal.

It has already been pointed out above that the short range order problem has not yet been investigated.

For solving this interesting problem within the framework of any of the two models described in the test it would be profitable to state the problem of mutual molecular arrangement in a group of several molecules. It would be worthwhile to consider this problem for two molecules, three molecules and for 1 coordination sphere, that is, a group of 13 molecules (one central molecule and 12 neighbours). Appropriate calculations can be carried out in terms of the geometrical model or by evaluating the minimum energy with the help of the atom-atom potential method.

The problem for two (as well as for three) molecules can be formulated as follows: to find the optimum arrangement of a pair of molecules whose centres are located at an average distance established by an X-ray experiment.

Calculations for a group of molecules comprising a coordination sphere will be illustrated on linear paraffins. As is known, at temperatures approaching melting temperatures, paraffin crystals undergo a polymorphic change and pass into the rotational crystalline state which is a close packing of cylinders with an appropriate effective diameter.

We know what arrangement of a group of seven molecules (one central molecule and 6 neighbours) is optimum from the point of view of potential energy. This arrangement is packing into a rectangular cell with a screw symmetry axis typical of organic chemical crystallography. In other words, it is the packing which existed with long-range order before the polymorphic change has occured. Let us superimpose this packing on a hexagonal packing. From Fig. 18 it follows that there may be 6 different ways of such superposition. Thus, the proposed model is constructed of identical domains oriented in 6 different ways with respect to the crystal axes. The average hexagonal cell formed by superposition of six rectangular cells will naturally be somewhat smaller than the experimentally observed cell. It can be supposed that a material increase of the cell volume which accompanies the transition of the molecule to the rotational crystalline state is associated with the transition layers which must necesserily exist in the such model of a crystal. Knowing the potential and free energy of the domains we could try predict the most probable molecular arrangement by constructing possible transistion layers.

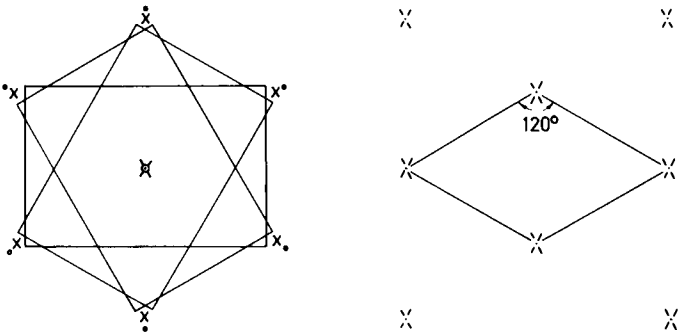

Fig. 18

The point of the hexagonal cell is located in the centre of the triangle formed by the closest points of three rectangles. Two of these are derived by rotating the original rectangle through 60° (240°) and 120° (300°), respectively.

The same procedure could be applied to determine the most probable arrangement of molecules in the closest sphere packing under the assumption that on the packing plane (plane (111) of the face-centered cubic lattice) there exist small ordered regions where molecular arrangement is goverened by the same law of symmetry as on the ab plane of the space group $P2_1/a$ or $P2_1$.

12. Hydrogen bonds in crystals

This aspect of organic chemical crystallography has not yet been a subject of systematic investigation. Information about the nature of hydrogen bonds in certain crystalline compounds has been obtained, so to speak, as a by-product of other research.

Although some spectral data appear to indicate hydrogen bonds with atoms of a number of elements, molecular crystals display bonds only with oxygen and nitrogen atoms. These bonds are sufficiently strong: there is indirect evidence to the effect that the energy of each bond is of the order of 3 kcal/mole.

Now that significant progress has been made in the computation of lattice energies by means of atom-atom potentials it would be well in order to carry out a systematic investigation of the sublimation heats of hydrogen-bonded organic crystals. The experimental value of the lattice energy minus the interaction energy calculated for all atom pairs yields the total energy of hydrogen bonds (for the purpose of these calculations we "forget" the proton responsible for the hydrogen bonds). An interesting program of systematic research into a class of compounds which contain hydroxyl, hydroxyl and carbonyl, hydroxyl and amino groups etc. is still awaiting its enthusiast.

It seems well justified to extend the atom-atom approximation for lattice energies to the case of hydrogen bonds, as is done in section 4.

The hydrogen bond parameters appear to vary insignificantly from one molecule to another. However, it can reasonably be expected that accurate results on the molecule packing will be obtained even if we assume these parameters to be practically constant or, at most, differentiate between hydrogen atom parameters in the hydroxyl-hydroxyl and hydroxyl-carbonyl bonds (the literature data suggest a sufficiently pronounced difference in the equilibrium values of hydrogen bonds in the two groups).

The formation of each hydrogen bond involves a significant loss of energy and it is, therefore, obvious that such structures will display a tendency to saturate all hydrogen bonds. If any possible bond fails to form this is due only to geometric restrictions.

Experimental evidence indicates that, as a rule, nature succeeds in building up a unit cell in which a new hydrogen bond would but slightly affect the molecular packing density. The simultaneous satisfaction of the requirement of maximum packing density (or the equivalent minimization condition for the sum of atom-atom potentials associated with conventional interactions) and the tendency for

maximum saturation of hydrogen bonds is facilitated by the fact that minor bends of a hydrogen bond link entail low energy losses. This conclusion is confirmed by the shape of the atom-atom potential for hydrogen bonds that has been suggested by the author (see para 4) and absence of correlation between proton deviations from the bond link and the bond length [53].

The geometries of saturated hydrogen bonds may be quite different depending on the arrangement of donor and acceptor groups in the molecule.

While a pair of molecules cannot produce more than two hydrogen bonds, hydrogen-bonded molecules can form either dimers or rings, or infinite chains. Formally speaking the former case corresponds to the formation of a large crystalline „molecule". If there are three such possible bonds, three-dimensional cage structures may be built up from any number of molecules.

When hydrogen bonds are responsible for the formation of rings or cages structures and the interaction of these structures is due to dispersion forces, hydrogen bonding may lose some of its characteristic properties (for example the melting temperature does not rise).

If molecules can have three hydrogen bonds the resultant structure may also fall into clusters of chains or two-dimensional layers. In this case, too, a number of crystal properties will be determined by van der Waals' forces rather than by hydrogen bonds as the former bind clusters of chains and layers of molecules to form a crystal.

Finally, with four hydrogen bonds, double layers and three-dimensional arrays can be built up. In the latter case the hydrogen bonds become critical for the crystal properties as any disintegration of a crystal requires their breaking.

13. Two-component systems. Solid solutions

Investigations of the structure of organic system solid solutions were started in the authors laboratory over ten years ago. The objective was to grow solid solution monocrystals [54], make precision measurements of unit cells as a function of solution composition [55-57] and measure the effective temperature factor of X-ray interference [57, 58]. In some cases electron density series were constructed [55, 59, 60].

This research was primarily aimed at examining solubility conditions and changes in crystals caused by the insertion of impurity molecules.

The results obtained also included data on the distribution pattern of impurity molecules in the matrix lattice. The principal objects of research were crystals of simple derivatives of aromatic compounds.

Organic solid solutions are substitutional solutions. This follows immediately from the trend of the curves of unit cell volume versus impurity concentration (Fig. 19). If the impurity molecule is larger than the matrix molecule the cell volume grows; otherwise, the cell decreases in size.

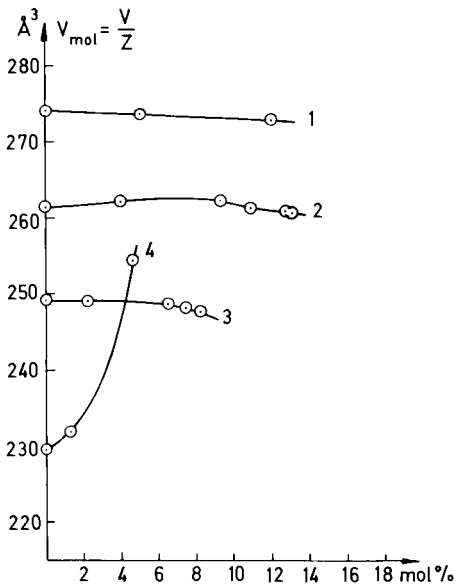

Fig. 19
1-stilbene in dibenzene; 2-diphenylmercury in tolane; 3-tolane in diphenylmercury; 4-anthracene in acridine

As early as the initial stage of the work it was seen that two molecules must be very similar in shape in order to produce a solid solution. If we assume that the matrix molecule is replaced by an impurity molecule (the shape of the unit cell remaining unaltered) then even with the most advantageous positioning of the impurity molecule the distances between the closest atoms of the matrix molecule and the impurity molecule may be such as would result in appreciable energy losses.

These losses can be easily estimated using the atom-atom potential curves. For a rough assessment it will suffice to remember that if two or three interatomic distances are reduced some thirty per cent, no solid solution is possible. Such is the situation when the impurity molecule is larger than the host molecule. Energy losses due to the introduction of smaller molecules into the lattice will obviously be smaller (the atom interaction curve descends less steeply towards distances

larger than the equilibrium distance), and, indeed, the examination of experimental results indicates that with other conditions being equal, the solubility limit is higher if the matrix molecules are larger than the impurity molecules [61].

Energy losses can be calculated with sufficient precision. However the results should not be taken too literally. When an impurity molecule enters the lattice the latter is distorted, and the numerical results for the undistorted lattice are, therefore, maximal.

For more accurate calculations of energy losses due to an impurity molecule it would be necessary to know the principal trend of strain diminishing.

Nevertheless, the geometrical interpretation of a cell which contains an impurity molecule has a distinct physical meaning. Thus, for example, an examination of the replacement of an anthracene molecule by an acridine molecule suggests that the replacement should result in a shorter axis a and a longer axis b which is confirmed by experiment [56].

It stands to reason that the packing coefficient expressed in the geometrical model in terms of shorter distances and in the physical model in terms of interaction energy losses is not the only parameter to be considered. In the general case solubility conditions should be defined as follows [62]: when a molecule of crystal A is substituted by a molecule of substance B the free energy of crystal A changes. These changes are as follows: firstly, an impurity molecule causes lattice energy changes which may be termed lattice strains; consequently, the free energy changes by ΔU; secondly, the free energy decreases by $T\,|\Delta S_c|$ where $\Delta S_c = R[(1-x)\ln(1-x) + x \ln x]$ represents configuration entropy; thirdly, the substitution changes the vibration spectrum free energy by ΔF_{vib} and finally, account should be taken of possible changes in the impurity molecule conformation as the molecule enters into a solid solution. If the conformation energy difference is equal to ΔE, the solution free energy will differ from that of the pure component by $x \cdot \Delta E$ where x denotes impurity concentration.

Thus, if a solid solution of B in A is formed, its free energy may be defined as

$$F_A + \Delta U_{lat} + \Delta F_c + \Delta F_{vib} + x \cdot \Delta E .$$

At a given temperature either a mixture with free energy $x F_B + (1 - x)F_A$ or a solid solution may be formed. For a solution to be formed its energy should be lower, i.e.

$$F_A + \Delta U_{lat} - T\,|\Delta S_c\,| + \Delta F_{vib} + x \cdot \Delta E < x F_B + (1 - x)F_A .$$

As both parts of the inequality include free intramolecular energy (which is not affected by molecular interactions), we have

$$\Delta U_{lat} - T \mid \Delta S_c \mid + \Delta F_{vib} + x \cdot \Delta E < x\,(F_B^{cr} - F_A^{cr})\,.$$

where F^{cr} is the "crystalline" part of the free energy. Assuming that for low concentrations ΔF_{vib}^{cr} is also proportional to concentrations we derive

$$T \cdot \mid \Delta S_c \mid > \cdot \Delta U + x \cdot \Delta f_{vib}^{cr} + x(F_A^{cr} - F_B^{cr}) + x \cdot \Delta E$$

i.e. the configuration effect of mixing should exceed the total contribution of the following four factors:

1) strain energy;

2) free energy variation due to changes of the crystal lattice vibration spectrum;

3) additive changes of the crystalline part of the free energy;

4) energy of impurity molecule conformation changes.

These four parameters determine the solubility conditions.

Thus, solid solution formation may be obstructed by the following factors.

1) large strains due to the fact that the impurity molecule cannot be accommodated at normal distances;
2) higher free energy of molecular lattice vibrations which may occur if the substitution of the impurity molecule increases the vibration frequency of the molecules and lowers the characteristic temperature of the crystal;
3) the crystal B (substance to be dissolved) has a substantially smaller crystalline part of the free energy than the crystal A;
4) conformation change energy ΔE required for the geometric conformity of molecules to be solved with solvent molecules is too large.

It is evident that the solubility conditions depend primarily on the lattice energy. Let us, for example, consider one per cent solubility. Dividing both parts of the inequality by 0.01 we obtain

$$3 \text{ kcal/mole} > \Delta U + \Delta f_{vib}^{cr} + \Delta F.$$

However, free energies have magnitudes of several kcal/mole. Their differences will always be substantially smaller than 3 kcal/mole. At the same time, lattice energy variations will exceed this value already with two or three intermolecular distances enlarged 25-30 %.

The lattice energy is equivalent to the packing coefficient unless hydrogen bonds are involved. As has been demonstrated by experiment, molecules capable of forming hydrogen bonds do not produce solid solutions with molecules which are unable to form such bonds. The reason is quite obvious as the breaking of one hydrogen bond involves an energy loss of about 3 kcal/mole. It appears highly improbable that such losses could be compensated for by free energy variations. This remark does not apply to the situation when molecules can form hydrogen-bonded dimers. Such molecules as β-naphthol enter into solid solutions with naphthalene. In this case the number of hydrogen bonds in the pure component and in the solid solutions may remain the same.

Thus, in the absence of hydrogen bonds (and also in the case of such substances as β-naphthol) it may be claimed that the proper geometry is not only a necessary but also a sufficient condition of solubility.

If the molecules are substantially different in shape the entire mechanism of solubility and its limit will depend on geometric factors. With the molecular shapes essentially similar, the process will obviously be controlled by differences in the free energies of the components, and variations of the vibrational free energy which occur as an impurity molecule enters its host crystal.

In most cases discussed above, dynamic disorder in a crystal is augmented by the addition of impurity molecules [57]. In this situation impurity molecules reduce the vibrational free energy and do not affect solubility.

We have found that impurity molecules may reduce vibrations in the following systems (an X-ray diagram of a doped crystal is better than that of the pure component. The improvement is such as would be achieved by holding the crystal at a lower temperature): diphenyl-mercury-tolane (tolane side), and p-dibromobenzene -p-diiodobenzene (with small additions of the first component) [57, 58].

Thermodynamic studies of such systems may be of great interesc.

Examples of genuine solid solutions are the following systems investigated in our laboratory: dibenzyl-stilbene [55], acridine-anthracene [56], p-diiodobenzene p-dibromobenzene [57]. In these systems the cell volume changes with impurity concentration in conformity with the requirements of the geometrical substitution model.

Alongside with such systems there are others in which the unit cell volume is practically independent of impurity concentration gwroth. At the same time such solid solutions are single-phase systems – monocrystals, and their contamination with impurities, for example the presence of β-Cl-naphthalene in naphthalene has been confirmed not only by our measurements of the crystal melting temperatures but also by the results of microanalysis (with an accuracy of ± 0.02 %). Thus, for

x = 6.5 % β-Cl-naphthalene in naphthalene the discrepancy between the unit cell volume reduction computed with the cell size assumed constant and the experimental measurements of the unit cell reduction is equal to 1.5 Å. For x = 3 % 1,8 dinitronaphthalene in 1,5-dinitronaphthalene this value is -4.7 Å. Such solutions have been termed by us interblock solid solutions, the implication being that impurity molecules are disposed in some oriented fashion on the block interfaces. For example, β-Cl-naphthalene molecules can replace naphthalene molecules in block interface unit cells with Cl atoms protruding like "frills" beyond the blocks. Evaluations of the size of such blocks whose entire surfaces are overlain by impurity molecules yield reasonable values. Solid solutions of β-Cl-naphthalene in naphthalene and 1,8-dinitronaphthalene in 1,5-dinitronaphthalene [63, 64] are not unique examples of systems with interblock solubility.

There is some indirect evidence acquired by examining luminiscence and absorption spectra of impurities which leads us to believe that a molecule geometrically unable to enter the matrix crystal lattice may nevertheless adjust itself to the lattice using or producing imperfections of the latter. Of special interest are in this regard the results obtained from the studies of aromatic molecules added in small quantities to molten paraffins. When this system solidifies the impurity molecules are uniformly surrounded by the matrix molecules as is evidenced by sharp quasiline spectra (the Shpolsky effect) [65]. The contribution of partial geometric correspondence to this effect is quite obvious. Thus, for example, especially sharp spectra are produced by anthracene solved in heptane (the linear dimensions of the molecules are identical) [66].

The importance of the partial geometric correspondence of impurity and matrix molecules in the production of luminiscent systems was convincingly demonstrated by *Belikova* and *Belyaev* [67].

We have discussed the conditions for partial solubility of organic molecules. The conditions for continuous solution formation are described in the author's book. It is shown that if molecules are not asymmetric (i.e. if there are no left-hand or right-hand molecules) a necessary condition for the formation of continuous solid solutions is the identity of the space groups and the equal number of molecules in the cell, while a sufficient condition is the similarity of the structures of the two pure components. In terms of our physical model it means that on the multidimensional energy surface both pure components and all intermediate solid solutions are associated with the same potential well.

14. Binary Crystals. Molecular Compounds

In a number of instances it is possible to obtain crystals built up from molecules of two kinds, equivalently oriented in all crystal cells. Such crystals are called crystals of molecular compounds. Their composition ratios are 1 : 1 or 2 : 1; more complex systems are rare.

It will be emphasized that the formation of such a crystal does not necessary indicate the presence of some specific forces acting between the "compound's" molecules. Moreover, the word "compound" in this context is admittedly not the best term.

The free energy of a binary crystal is obviously lower that the mean energy of monomolecular crystals. The packing of a bimolecular crystal may well be denser (the potential energy of interaction is lower) than the packing of the components. An example of this kind is apparently the molecular compound of triphenyl methane and benzene. The structure of this crystal is not yet known, but from a purely geometrical point of view it would be natural to expect that the benzene molecules make it easier for the unsuitably shaped triphenyl methane molecules to pack more densely.

Molecules capable of producing hydrogen bonds can be more often expected to form bimolecular crystals. It has been noted above that in this case the optimal structure should meet both the requirement of dense packing and the tendency to the maximum saturation of hydrogen bonds. It can hardly be surprising that in a number of instances nature copes with this formidable task with outstanding success by combining two different molecules in one crystal. Examples of such crystals (with no new component added to the interaction energy) are numerous both among aliphatic compounds (fatty acids) and aromatic substances such as the meta-and-para cresol system.

Optical spectroscopy and radiospectroscopy have provided physical data on the special interaction of molecules of bimolecular crystals containing a molecule with nitrogroups as one of the components [68]. The molecule with a strong dipole moment is believed to polarize the molecule of the other component. This pair of molecules has a lower energy of electrostatic interaction. Some results seem to show that the electric charge may be transferable from one molecule to the other.

The structure of many binary crystals of this type has been fully investigated. The principal result of this work demonstrates that the packing principles of the molecules is not different from that in pure compound monocrystals. Not infrequently

component molecules alternate to make up stacks. In the crystal of anthracene and symmetric trinitrobenzene the molecular planes are practically parallel [69]. Similar stacks of molecules are found in the crystal where instead of anthracene one of the components is paraiodoaniline but the molecules are inclined with respect to the stack axis (see [41]).

In the series of bimolecular crystals with 4,4′-dinitrodiphenyl as the polarizing component the component molecules are tilted 90°. There are apparently a number of possibilities for reducing the electrostatic energy of interaction.

Of specific importance is the fact that in all such cases the distances between the non-bonded atoms of adjacent molecules do not decrease.

Frolova and the author established in their early work [70] that even in binary crystals where one can reasonably expect the contribution of additional interaction energy molecular packing, is in no way different from that in monomolecular crystals. This conclusion was arrived at by calculating the packing coefficients for bimolecular crystals and their components. The results are listed in the table below, taken from this less known paper.

Thus, it appears that the main energy component – the sum of atom-atom potentials – remains practically constant. A bimolecular crystal is apparently formed due to the fact that the mixing of dipole molecules with molecules having induced dipole moments causes the electrostatic component of the interaction energy to decrease. It seems doubtful that the charge transfer may affect the lattice energy.

It would be interesting to test these conjectures experimentally, i.e. to make thermodynamic measurements and calculations of the lattice energy.

A large group of crystals built up from molecules of two or more varieties fall in the class of so-called clathrate compounds, based on hydrogen bonds. Hydrogen-bonded molecules produce various cage structures with hollows of different size. Such hollows may be filled by molecules of another variety. The interaction of molecules which fill hollows with those of the frame structure can be interpreted both in terms of a geometrical or a physical model. It is, for example, possible to compute the packing coefficient of the smaller molecule in a cage structure. As follows from such calculations, impurity molecules do not push "the prison walls" further apart. In some instances inserted molecules are elegantly accommodated in the frame hollows and execute only minor motions about the position of equilibrium. In other instances, as has been shown both by X-ray diffraction analysis and by thermodynamic studies, the inserted molecule is in a state of free rotation.

Table 5

Compounds		Packing coefficient of bimolecular crystal	Packing coefficient	
A	B		A	B
Naphthalene + trinitrobenzene		0.72	0.70	0.64
Ditto + trinitrochlorobenzene		0.68	0.70	0.65
Ditto + trinitrophenol		0.68	0.70	0.65
Ditto + α-trinitrotoluene		0.68	0.70	0.63
Ditto + γ-trinitrotoluene		0.78	0.70	0.62
Acenaphthene-trinitrophenol		0.68	0.70	0.65
Ditto + α-trinitrotoluene		0.64	0.70	0.63
Ditto + β-trinitrotoluene		0.63	0.70	0.70
Ditto + γ-trinitrotoluene		0.63	0.70	0.62
Phenanthrene-trinitrobenzene		0.71	0.68	0.64
Ditto + trinitrochlorobenzene		0.7	0.68	0.65
Ditto + trinitrophenol		0.56	0.68	0.65
Ditto + α-trinitrotoluene		0.70	0.68	0.63
Ditto + β-trinitrotoluene		0.65	0.68	0.70
Fluorene + α-trinitrotoluene		0.67	0.69	0.63

Very interesting work on clathrate compounds with water layers around large molecules and the problem of crystal hydrates as a whole merit special attention. Important results of great interest have been obtained by *Jeffrey* et al. [71]. It is our impression that the problem could be dealt with in a more comprehensive and productive manner if hydrogen bonds were investigated in terms of atom-atom potentials for some elementary cases.

15. Structures of Crystal Polymers

Conformations of macromolecules in crystals are governed almost exclusively by intramolecular interactions. It can be calculated that variations of the molecular packing coefficient within rather broad limits will cause an energy change of not more than several hundred calories per monomeric link (for example, per CH_2 group in polyethylene). Meanwhile conformation transitions require as a rule energy changes one order of magnitude higher. At the same time the molecular packing coefficients of most polymers change very insignificantly and remain within 0.70-0.73 at room temperature.

However, if the potential surface in the vicinity of the minimum is a plateau or a valley or if two local minima are separated by rather low barriers, the intermolecular forces may affect the conformation and the real configuration will, therefore, not lie at the principal energy minimum. Exceptions are apparently most numerous among crystals of natural macromolecules where intermolecular hydrogen bonds may occur. Unfortunately, for the time being, these conclusions are based only on conjectures for while conformation calculations are bound to give quantitative estimates, such calculations for biopolymers are outside of today's researcher's capabilities. It is believed that in the none too distant future they will become feasible.

Thus, when investigating conformation theoretically we may in most cases consider a polymer molecule as being free, while problems of molecular packing in crystals can be treated independently. Conformations of any steroregular polymers can, at least in principle, be derived by straightforward calculations (without statistics). In such polymers adjacent links (or pairs or other combinations of links) are identical and the displacement angle of each links in relation to its neighbour is quite definite and recurs along the chain. Such macromolecules will, therefore, form regular spirals.

Formulae relating the spiral parameters (spiral radius ρ, translation along the chain d and rotation angle θ in transition from one monomeric unit to the next) with the parameters of the primary structure – bond lengths, valence angles and rotation angles were first derived in [72]. Later these formulae were generalized to make them applicable to chains of any structure [73]. Thus, at the present time equilibrium configuration calculations for macromolecules can be easily compared with results obtained by X-ray diffraction analysis which provides data on the spiral parameters.

To measure valence angles and rotation angles, it is necessary to minimize the potential function which will enable one to determine spiral parameters uniquely. Even unsophisticated evaluations of macromolecule conformations using the rigid sphere model (atoms are modelled by spheres, with their minimum overlapping regarded as the figure of merit) often give accurate values of spiral parameters. These results are described in detail in [75]. However, a number of other authors calculated conformation making use of semiempirical potentials of interaction between non-bonded atoms. Calculated results for isotactic and syndiotactic polypropylene are reported in [74], for isotactic poly-α-olefins and polyaldehydes, syndiotactic polypropylene and poly-1,2-butadiene – in [76], polytetrafluorethylene in [77], for polyethylene, polytetrafluoro – and chloroethylene, polymethylene oxide and polyethylene oxide – in [78], polyethylene, polytetrafluorethylene, polyisobutylene, polyvinylidenchloride, polyoxymethylene and isotactic polypropylene – in [79] and for polyethylene – in [80].

Most of the authors of the publications listed above use the following computation procedure. In accordance with *Eyring* [81], a i-th coordinate system is selected such that the X-axis is oriented along the main chain bond, the Y-axis-in the plane of three atoms of the main chain and the Z-axis is directed so as to provide for the right-hand screw rotation of the coordinate system; the system is referenced on the i-th atom of the main chain (Fig. 20). Using the relationship $X_{i-1} = AX_i + B$ where X-coordinate vectors and A and B – matrices,

$$A = \begin{pmatrix} -\cos\alpha & -\sin\alpha & 0 \\ \sin\alpha \cdot \cos\varphi & -\cos\alpha \cdot \cos\varphi & -\sin\varphi \\ \sin\alpha \cdot \sin\varphi & -\cos\alpha \cdot \sin\varphi & \cos\varphi \end{pmatrix}; \quad B = \begin{pmatrix} l \\ 0 \\ 0 \end{pmatrix}$$

(φ–rotation angle, α–valence angle in the main chain and l–bond length), the atom coordinates are transformed to the (i-I)-th system. Similarly, the atom coordinates are transformed from the (i-1)-th system to (i-2)-th system and so on. If n links are considered the procedure is repeated n times. Then the distances between the non-bonded atoms are calculated and substituted into the expressions for the corresponding potentials, thus giving the energy of non-valence interactions as a function of the valence angles and the rotation angles.

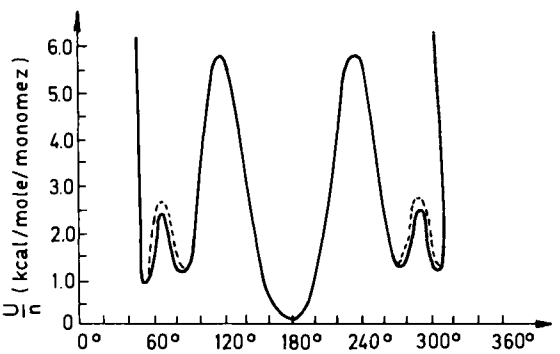

Fig. 20

Optimal conformations reported in the papers cited above were found by plotting level lines (or equipotential lines), with the valence angles fixed and the rotation angles being varied. It is quite obvious that rotation angles are the main conformation parameters, but it would also be informative to obtain a complete solution of the minimization problem allowing all independent variables to vary (the problem has never been so formulated).

With valence angles fixed for one-atom chains (–M–) ∞ it is possible to derive one-dimensional potential curves, as has been done in [80] for polyethylene

(Fig. 20); two-dimensional level lines will be required for two-atom chains $(-M_1-M_2-)_\infty$. For the purpose of illustration, mention may be made of the equipotential curves for polyvinylidenchloride $(-CH_2-CHCl-)_\infty$ reported in [79] (Fig. 21).

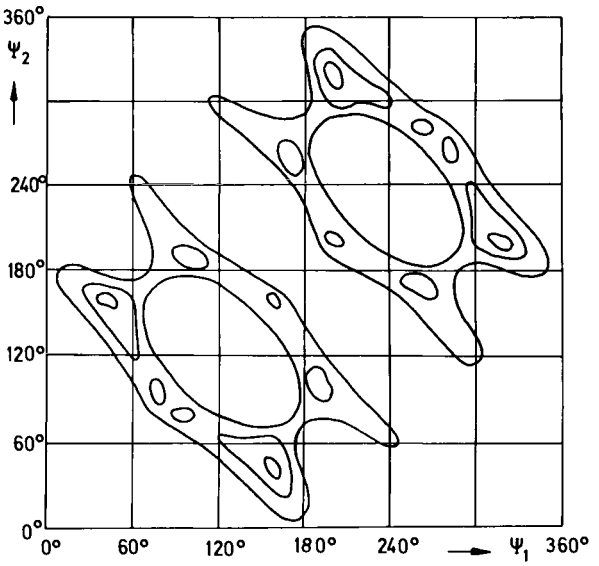

Fig. 21

It is noteworthy that an infinite number of links ($n = \infty$) should be taken if accurate solutions of the problems are to be obtained. Then if $\lim_{n \to \infty} (U/n)$, i.e. the limit of strain energy per monomeric unit exists (the theorem of its existence for the functions of the type discussed has not yet been proved) optimal conformation can be computed with any desired accuracy (provided, of course, the computation parameters are properly selected). In practice, however, only relatively few links (4-6) are taken into account as in the computation procedure described above, the computation time requirement increases geometrically with the number of links.

We shall now discuss some computation results.

The potential function for polyethylene (Fig. 20) has three deep local minima at $\varphi = 180°$, 85° and 55° the first minimum being somewhat deeper than the other two. In real crystals only a flat zigzag is realized ($\varphi = 180°$) which has long been known from X-ray studies. Spiral conformation ($\varphi = 55°$ or 85°) cannot be realized in a crystal not only because its intramolecular energy is somewhat higher but

also in view of the fact that spirals are usually associated with less dense packing – an obvious disadvantage from the point of view of energy.

The equipotential lines of Fig. 21 have been drawn on the assumption that C-C, C-H and C-Cl bond lengths are 1.54 Å, 1.00 Å and 1.78 Å, respectively, and CCC valence angles equal 114° (generally speaking, vinyl polymers with non-equivalent adjacent monomeric units (polyvinylidenchloride) will have two different CCC valence angles). A similar diagram has been constructed for CCC angles = 120 °. It will be noted at this point that although the energies in the two cases are substantially different, the minima practically coincide. This example goes to show that minima can be successfully found from the main conformation parameters – angles of rotation around the bond.

The deepest minimum (Fig. 21) falls at rotation angles $\varphi_1 = 165°$ and $\varphi_2 = 30°$ which is in good agreement with experiment. An X-ray analysis of polyvinylidenchloride performed by the authors has revealed that rotation angles around two non-equivalent C-C bonds should be close to 0° and 160°.

Let us take one other example. The potential function of polytetrafluoroethylene $(-CF_2-CF_2-)_\infty$ for various rotation angles (Fig. 22) was derived in [77]. The CCC angle in the chain was taken equal to 116°, the C-C and C-F bond lengths – to 1.54 Å and 1.38 Å, respectively, and the FCF angle – to 110°. The treatment which made use of the potential curve of *Mason* and *Kreevoy* [82] included only F . . . F interactions. As follows from Iwasaki's calculations the local minima are associated with the rotation angles of 60°, 90° and 165° or angles symmetrical to 180°, which are typical of enantiomorphic conformations. The deepest minimum corresponds to the spiral conformation with K = 2.17 where K is the number of monomeric units in one turn. According to structure data [83], the polytetrafluoroethylene spiral has at 20 °C 13 monomeric units in 6 turns (K = 2.18). The ease of the clockwise spiral transformation into a counter-clockwise spiral at room temperature may be attributed to the low rotational barrier height at $\varphi = 180°$.

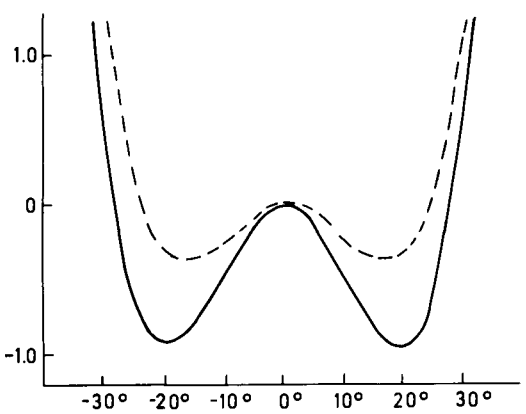

Fig. 22

The above examples indicate general agreement between experimental data and nearly all computed conformations of stereoregular polymers. However, results reported by different authors have been obtained on the basis of different approaches and potential curves.

Thus, [76] takes into account non-bonded interactions controlled by the orientation of adjacent links $\left(\frac{U_0}{2}\right)(1 + \cos 3\varphi)$ where U_0 represents a constant approximately equal to the height of the barrier to internal rotation.

We believe that it would be more advantageous to use the dependence of the atom-atom potential on the angle between the atom distance and the valence bond (see para 4).

Several authors disregarded electrostatic interactions and nevertheless obtained correct results. *Iwasaki* asserts that electrostatic interactions in polytetrafluoroethylene (dotted line in Fig. 22) do not affect significantly the equilibrium configuration. It appears that to a first approximation they may be included in the potential functions for non-valence interactions. All this is in full agreement with para 5.

The fact that calculations of polymer optimal conformations are relatively insensitive to the assumptions used and the parameters adopted gives good reason to expect that calculated results may provide in many cases (and especially with appropriate parametrization) more structural information about stereoregular polymers than is available from experiment.

If the conformation of a linear molecule is known, it is fairly simple to determine the packing of such molecules. And, indeed, geometric treatment consists only in the examination of possible rotations about the molecular chain and relative translations along the axis.

In the case of simple molecules such as polyethylene, the geometric problem involves no difficulties at all. As is shown in the author's book, only three structures – those with rhombic, monoclinic and triclinic subcells – are compatible with the close-packing principle. Two of them (rhombic and monoclinic) have been observed experimentally. The same problem is easily solved energetically by minimizing the chain interaction energy.

The author understands that the close packing principle and the computation of the minimized sum of atom-atom potentials are used with advantage by Italian authors (*Corradini* et al.) in order to determine optimum packings of polymer chains in crystals.

Similar problems for non-linear polymers are obviously much more difficult to tackle but further efforts of researchers will undoubtedly provide a clue to their solution.

References

[1] *Kitajgorodskij, A. I.*, J. Phys. USSR, **9**, 351, 1945.
[2] *Magat, M.*, Z. Phys. Chem., B, **16**, 1, 1932.
[3] *Mack, E.*, J. Amer. Chem. Soc., **54**, 2141, 1932.
[4] *Kitajgorodskij, A. I.*, Chemical Organic Crystallography, New York: Consultants Bureau, 1959.
[5] *Zorky, P. M., Poraj-Koshits, M. A.*, Kristallografija, 6, 655, 1961.
[6] *Leiserowitz, L., Rabinovich, D.* and *Schmidt, G. M. J.*, Abstracts of the Communications of the Seventh International Congress of Crystallography, Moscow, USSR, 1966, 8.62.
[7] *Gelfand, I. M., Vul, E. B., Ginsburg, S. L., Fedorov, Yu. G.*, Metod ovragov v zadachakh rentgenostrukturnogo analiza, Izd. Nauka, Moscow, 1966.
[8] *Bertinotti, A.*, Abstracts of the Communications of the Seventh International Congress of Crystallography, Moscow, USSR, 1966, 8.13.
[9] *Kitajgorodskij, A. I.*, Kristallografija, 7, 195, 1962.
[10] *Kitajgorodskij, A. I.*, Koreshkov, B. D., Solid State Physics (Russ.), 8, 62, 1966.
[11] *Timmermans, J.*, Physico-chemical constants of pure organic compounds, 1950.
[12] *Ryjenkov, A. P., Kozhin, V. M.*, Kristallografija (in print).
[13] *Kitajgorodskij, A. I., Koreshkov, B. D., Pikus, E. L.*, Solid State Physics (Russ), 7, 2843, 1965.
[14] *Lord, R. C., Ahlberg, I. E.* and *Andrews, D. H.*, J. Chem. Phys., **5**, 649, 1937.
[15] *Cruickshank, D. W. I.*, Acta Cryst., **9**, 1010 (1956).
[16] *Kitajgorodskij, A. I.*, Tetrahedron **9**, 183 (1960); **14**, 230 (1961); Doklady Acad. Sci. USSR, **137**, 116, 1961.
[17] *Kitajgorodskij, A. I., Mirskaya, K. V.*, Kristallografija 6, 507, 1961; 9, 174, 1964.
[18] *London, F.*, Zeits. Phys. Chem. **B11**, 222, 236, 1930; F. London, Zeits. Phys. **63**, 245, 1930.
[19] *Slater, J., Kirkwood, J.*, Phys. Rev., 37, 682, 1931.
[20] *Axilrod, B. M., Teller, E.*, J. Chem. Phys., **11**, 299, 1943.
[21] *Wojtala, V. J.*, Acta Phys. Polonica, **25**, 27, 1964.
[22] *Kitajgorodskij, A. I.*, Mirskaya, K. V., Kristallografija, **9**, 634, 1964.
[23] *Kitajgorodskij, A. I., Mirskaya, K. V.*, Kristallografija, **10**, 162, 1965.
[24] *Kitajgorodskij, A. I., Mirskaya, K. V., Tovbis, A. B.*, Kristallografija (in print).
[25] *Cox, E. G., F. R. S., Cruickshank, D. W. I., Smith, I. A. S.*, Proc. Roy. Soc. **A247**, 1, 1958.
[26] *Kozhin, V. M., Kitajgorodskij, A. I.*, J. Phys. Chem. (Russ.), **29**, 2075, 1955.
[27] *Bacon, G. E., Curry, N. A., Wilson, S. A.*, Proc. Roy. Soc. **A279**, 98, 1964.
[28] *Craig, D. P., Dobosh, R. A., Mason, R., Santry, D. P.*, Disc. Far. Soc., **40**, 110, 1965.
[29] *Giglio, E.* and *Liquori, A.*, Abstracts of the Communications of the Seventh International Congress of Crystallography, Moscow, USSR, 1966, 8.37.
[30] *P. Corradini, Avitabile, G., Ganic, P.* and *Martuscelli, E.*, Abstracts of the Communications of the Seventh International Congress of Crystallography, Moscow, USSR, 1966, 8.26.
[31] *Williams, D. E.*, Science, **147**, 605, 1965.
[32] *Williams, D. E.*, J. Chem. Phys. **45**, 3770, 1966.
[33] *Craig, D. P., Mason, R., Pauling, P., Santry, D. P.*, Proc. Roy. Soc. **A286**, 98, 1965.
[34] *Bartell, L. S.*, J. Chem. Phys. **32**, 827, 1960.

[35] *Banerjee, K., Salem, L.*, Molec. Physics, **11**, 405, 1966.
[36] *Kitajgorodskij, A. I.*, Acta Crystl. **18**, 585, 1965.
[37] *J. Trotter*, Acta Cryst., **16**, 605, 1963.
[38] *Ehrlich, H. W. W.*, Acta Cryst. **10**, 699, 1957.
[39] *Kitajgorodskij, A. I., Dashevsky, V. G.*, Theoretical and Experimental Chem., **3**, 35, 1967; **3**, 43, 1967 (Russ.).
[40] *Bartell, L. S., Jacob, E. J.* and *Bradford Thompson, H.*, Influence of Non-bonded Interactions on Molecular Geometry and Energy: Calculations for Hydrocarbons Based on Urey-Bradley Field (Preprint).
[41] *Casalone, G. L., Mariani, C., Mugnoli, A.* and *Simonetta, M.*, Acta Cryst. **22**, 228, 1967.
[42] *Kitajgorodskij, A.*, Journ. de Chim. Physique, **1**, 9, 1966.
[43] *Pawley, G. S.*, Phys. Stat. Sol., **20**, 347 (1967).
[44] *Kitajgorodskij, A. I., Koreshkov, B. D., Kulkin, A. G.*, Solid State Physics (Russ.), 7, 643, 1965.
[45] *Waugh, J. S., Fedin, E. I.*, Solid State Physics (Russ.), 4, 2233, 1962.
[46] *Robertson, J. M., Shearer, H. M., Sim, G. A.* and *Watson. D. G.*, Acta Cryst. **15**, 1 1962.
[47] *Khotsynova, T. L., Babushkina, T. A., Semin, G. K.*, Zhurnal Strukturnoj Khimii, 7, 634, 1966 (Russ.).
[48] *Khotsynova, T. L., Robas, V. I., Semin, G. K.*, Proceedings of the All-Union Conference on Investigation of Solid State Properties by Magnetic Resonance Methods, Krasnoyarsk (1964): Sb. "Radiospektroskopiya tverdogo tela", Moscow, Atomizdat, 233, 1967.
[49] *Eveno, M., Meinnel, J.*, Journ. de Chim. Phys., **1**, 108, 1966.
[50] *Balcon, Y., Meinnel, J.*, Journ. de Chim. Phys., **1**, 114, 1966.
[51] *Brot, C., Darmon, I.*, Journ. de Chim. Phys., **1**, 100, 1966.
[52] Physics and Chemistry of the Organic Solid State, Vol. 1, Ed. by *Fox, D., Labes, M. M., Weissberger, A.*, Interscience Publ. 1963.
[53] *Fuller, W.*, J. Phys. Chem., **63**, 1705, 1959.
[54] *Kitajgorodskij, A. I., Myasnokova, R. M.*, Dokl. Akad. Nauk USSR, **129**, 380, 1959.
[55] *Kolosov, N. I.*, Kristallografija, **3**, 700, 1958.
[56] *Myasnikova, R. M., Kitajgorodskij, A. I.*, Kristallografija, **3**, 160, 1958.
[57] *Kitajgorodskij, A. I., Lyan Dun-chey*, Kristallografija, **5**, 238, 1960.
[58] *Samarskaya, V. D., Myasnikova, R. M., Kitajgorodskij, A. I.*, Kristallografija, **11**, 855, 1960.
[59] *Lyan Dun-chey, Struchkov, Yu. T.*, Izvestija Akad. Nauk USSR, **6**, 1010, 1960 (Russ.).
[60] *Samarskaya, V. D., Myasnikova, R. M., Kitajgorodskij, A. I.*, Kristallografija (in print).
[61] *Kitajgorodskij, A. I., Mnyukh, Yu. V.*, Vysokomolekulyarnye Soedineniya, **1**, 128, 1959 (Russ.).
[62] *Kitajgorodskij, A. I.*, Zhurnal Strukturnoj Khimii, **1**, 324, 1960.
[63] *Kitajgorodskij, A. I., Mjasnikova, R. M.*, Kristallografija, **5**, 247, 1960.
[64] *Kitajgorodskij, A. I., Mjasnikova, R. M.*, Kristallografija, **5**, 638, 1960.
[65] *Shopolskij, E. V.*, Uspekhi Fizicheskikh Nauk, **68**, 51, (1959); 71, 215 (1960); 77, 321 (1962); **80**, 255 (1963), (Russ.).
[66] *Bolotnikova, T. N., Klimova, L. A., Nertzesova, G. N., Utkina, L. F.*, Optika i spektroskopija, **21**, 420, 1966 (Russ.).
[67] *Belikova, G. S. Belyaev, L. M.*, Sb. "Rost Kristallov" vol. 111, Akademizdat, Moscow, 1961, 316 p. (Russ.).
[68] *McGlynn, S. P., Boggus, I. D.*, JACS **80**, 5096, 1958.

[69] *Brown, D. S., Walwork, S. C.,* Acta Cryst. 17, 168, 1964.
[70] *Kitajgorodskij, A. I., Frolova, A. A.,* Izvestija Sektora Fiziko-Khimicheskogo Analiza Akad, Nauk USSR, XIX, 309, 1949 (Russ.).
[71] *Jeffrey, G. A., Jordan, T., McMullan, R. K.,* Abstracts of the Communications of the Seventh International Congress of Crystallography, Moscow, USSR, 1966, 8.54.
[72] *Shimanouchi, T., Mizushima, S.,* J. Chem. Phys., **24**, 707, 1955.
[73] *Birshtein, T. M.,* Vysokomolekulyarnye Soedineniya, 5, 1675, 1963 (Russ.).
[74] *Natta, G., Corradini, P., Ganic, P.,* J. Polymer Sci. **58**, 1191, 1962.
[75] *Bunn, C., Holmes, D.,* Disk. Faraday Soc., No. 25, 95, 1958.
[76] *Borisova, N. P., Birshtein, T. M.,* Vysokomolekulyarnye Soedineniya, **5**, 279, 1963 (Russ.).
[77] *Iwasaki, M.,* J. Polymer Sci. **A1**, 1099 (1963).
[78] *Magnasco, V., Gay, G., Nicora, C.,* Nuovo Cim., **34**, 1263, 1964.
[79] *Santis, P. de., Giglio, E., Liquori, A. M., Ripamonti, A.,* Nuovo Cim., 26, 616 (1962); J. Polymer Sci. **A1**, 1383 (1963).
[80] *Scott, R. A., Scheraga, H. A.,* J. Chem. Phys. **44**, 3054, 1966.
[81] *Eyring, H.,* Phys. Rev., **39**, 746, 1932.
[82] *Mason, E. A., Kreevoy, M.,* J. Amer. Chem. Soc., **78**, 5808, 1955.
[83] *Bunn, C.,* Howells, Nature, 174, 549, 1954.

Subject index

Absolute measurement of small angle scattering 137
Absolute intensity measurement, particle volumes 113
Absorbing crystals, rocking curves in Bragg case 26
Absorption by weak beams 79
– of electrons by crystals 72
Accidental interactions of weak and strong beams 86
Activation energy, reorientational 222
Al-Cu-alloys 139
Amorphous macrostructures 118
Amplitudes of waves in excited wave field, Laue case 17
Anomalous absorption 20, 25, 32, 63
–, Borrmann effect 1
–, Laue case 18
Anomalous dispersion 4
Anpassung (adaption) 57
Atom – atom potentials, analytical form 188
Azulene, molecular disordering in crystals 224

Backfolding of chain molecules 131
Band theory, relation to dynamical theory 65
Benzene, crystal structure 199
–, energy surfaces in crystals 205
–, unit cell at absolute zero 204
Bethe, dynamical theory of diffraction 55
Binary molecular crystals 237
Biological fibers 138
Biphenyl, molecular conformation in crystal and vapour 217
Bloch wave 5, 57
Boltzmann-statistics 109
Borrmann effect, dependence on temperature 20
–, equations and physical interpretation 19
Borrmann fan 33
–, energy distribution and wave fields excited by divergent beams 31
Boundary conditions in Maxwell's equations 2, 17
Braggwindows in small angle scattering 135
Bulk polymers, low angle scattering from 138

Carbon black, analysis of small angle scattering 115, 137
Cell edge fluctuation, effect on small angle scattering 121
Chain conformation in polymers 131, 138
Chloroplasts, lamellar structure 124, 134
Clathrate compounds 238
Close packing, possible space groups 179
Collagen, structure 121, 138
Collimation errors in small angle scattering 104
Colloidal structure factors 133
Complex potential, Bethe theory of scattering 62
Convergent-beam patterns 75
Convolution polynom 120
Coordination statistics, convolution polynom 120
Critical point, liquid structure 137
– temperature of solution 137
Crystal rotation method in electron diffraction 76
Crystals, free energy of 181
– index of refraction for x-rays 35
–, phase diagram and potential energy surface 211
Crystalline polymers, structures of 239

Debye-Waller factor 5, 20, 24, 80
Dicarboxylic acids, lattice energies 207

Diffraction by a slit 46
–, generalized form of the theory 40
Diffraction theory, analytical solution of equations 40
–, general solution for incident plane wave 45
–, general solution for incident spherical wave 43
–, numerical integration of equations 40
–, traverse topographs 46
Discontinuous reflections in polymers 122
Dislocation density in nickel 139
– rings in metals 138
Dispersion energies, London theory 187
Dispersion surface 12, 18, 23, 44, 60
– and incident plane polarisation 13
–, Ewald sphere 7
–, relation to Poynting vector 13
–, the two beam case 12
Double Bragg-reflections 139
Double refraction of wave fields, in crystals 32
–, experimental observations 34
Dynamical structure potentials 65
Dynamical theory, fundamental equations 2, 9
–, present applications 49

Equal-thickness fringes in electron micrographs 75
Ewald construction, small angle scattering 102
Ewald wave 1, 6, 8, 9, 12
Excitation error (Anregungsfehler), Bragg equation 59
Excited wave fields, tie points 16
Extinction distance, two-beam case 63
– and diameter of dispersion surface 16
– in the Bragg case 25
Extinction-line contours 75

Ferromagnetic metals 139
Folding (convolution) products, small angle scattering 102
Friedel's law, failure of 90
Fringe micelle model, scattering from polymers 131
Fundamental equations of electron diffraction 56

Glasses, small angle scattering from 138
Grain boundaries in ultrafibrils of polyethylene 129
Graphite, small angle scattering 137
g_{sr}-values in small angle scattering 122
Guinier approximation for scattering by globular particles 110
Guinier-Warren-plot 111, 127
Guinier-Preston zones 107, 134, 139
Guinier Preston II Zones 139

Hexahalobenzenes, crystal structures and disorder 225
Hexamethylbenzene, crystal structure 207
High diluted systems, small angle scattering from 137
Hydrocarbon crystals, heats of sublimation 196
Hydrogen bonds in organic systems 173
–, atom – atom potential of 189, 190
Hydrogen bonded crystals 230

Inner surface of colloidal systems 116
Integrated intensity in the dynamical theory 22
Integrated intensities, expressions for the dynamic and kinematic theories 28
Intensity function, small angle scattering 102, 104, 121

Dipolar interaction energies 191
Interference multiple refraction 60, 75
Intermolecular energies and shapes of molecules 212
Intermolecular radii 176
Intermolecular vibrations 218

Keratin, small angle intensity function 121
Kossel-Möllenstedt patterns 75

Lamellae, small angle scattering from 116

Lamellar systems, small angle scattering 124, 134
Lattice δ-function in electron scattering 56
Lattice energy, calculation of 195
Long range order in paracrystals 119

Macromolecules, conformation of in crystals 239
Many-beam effects in dynamical theory 83
Mean absorption coefficient in two beam case 63
Mechanical model of an organic molecule 216
Metals, small angle scattering 138
Metallic alloys, Guinier-Preston zones 139
Microcrystallites in chloroplasts 134
Molecular crystals, packing 173
–, electrostatic interaction energy in 191
–, lattice disordering 223
–, molecular vibrational frequencies 220
Molecular interactions, atom – atom potentials 186
– packing coefficient 177
Molecular vibrations, eigenvectors of 221
Molecular vibrational frequencies, quasi-harmonic approximation 221
Molecules, close packing of 174
Multiple small angle scattering 116

Naphthalene, crystalline thermodynamic functions 182
N-beam approximation, dynamical theory 58
Neutron scattering by deformed metals 138
Neutron small angle scattering 139
Non-absorbing crystals, rocking curves and integrated intensities 25
Non spherically symmetric structures, small angle scattering from 119

Optical potential and electron scattering 68
Organic crystals, characteristic temperature of 185
–, determining contacts 176
–, dipolar interaction energies 192
–, geometrical models of
–, lattice dynamics 218
–, molecular reorientations 221
–, physical models 181
–, potential surface minima 197
–, principle of close packing 210
–, quadrupole interaction energies 193

Paracrystals, theory of 119
Paracrystalline lattice factor 120
Paracrystalline lattices 108
Paracrystalline layer structures 132
Paraffin hydrocarbons, rotational crystalline state 229
Particle amplitudes, continuous small angle scattering 108
– factor 109–111
– scattering factor 109
– shape function 109
Patterson-function 103
Pendellösung, fringes 28, 30
– effect, measurements of 21
Pendellösung fringes, plane and spherical waves 37
Perfect crystals, propagation of real waves in 29
Phases of Structure Amplitudes 90
Plastic crystals, short-range order in 227
Point defects 139
Polydisperse systems 113
Polydispersity 113
Polyethylene 124, 127
Polystyrene 129
Porphyrin ring 136
Porods formulae, scattering by particles 112
Propagation of real waves in crystal lattices 7
Pseudo-kinematical theory 79, 93

Q-correlationfunction, small angle scattering 103
Q-function, small angle scattering 103
Quasi-harmonic approximation in molecular crystals 185

Real waves, angular amplification and departures from Bragg's law 30
Reciprocal space, relationship of tie points in dynamical theories 11
Relativistic corrections in dynamical theory 94
Rocking curve 21, 24
–, intrinsic 35

Scattering amplitude in small angle analysis 102
Scattering-matrix theories 61
Shape amplitude in small angle scattering 106, 117
Shape function in low angle diffraction 105, 121, 133
Silica gel, particle size 137
Simultaneous reflections, anomalous effects of 84
Smecal defects 139
Smectic and nematic superstructures 132
Solid solutions, effects of impurity concentration 232
–, free energy of 233
–, interblock 236
–, molecular vibrations in 235
–, solubility conditions 231
–, two component systems 231
Step dislocations 138
Strain distributions 138
Structure potential in dynamical theory of diffraction 56
Supermolecular correlation in polymers 131
Systematic interactions, correction of structure potentials 86

Thermodynamic characteristic temperature 184
Thin crystals, rocking curves 27
Tie-point 12, 16, 60
–, characterisation of 6
Tobacco mosaic virus, small angle scattering from 137
Trial and error methods, shapes of particles 117
Two-beam case in dynamical theory 61, 63
Twofold Bragg reflexions 138

Ultrafibrils 125, 127
Umweganregung 84

Van der Waals' radii 174

Wave-fields 6, 23
– in perfect crystals, of plane wave limited by a slit 48
– in the dynamical theory 57
–, properties of 8
Wave propagation, in crystalline medium-wave fields 5
–, in homogenous dielectric medium 3
Wave vectors, boundary conditions 14
–, – and reflection and transmission 14
–, – in the Bragg case 23
–, – on the exit surface 20

X-ray diffraction, dynamical theory of 1

Yoshioka theory of electron diffraction 68

Acta METALLURGICA

Published for the Board of Governors of Acta Metallurgica, sponsored by the American Society for Metals, The American Institute of Mining, Metallurgical and Petroleum Engineers, and the American Society for Testing and Materials **Editor: Bruce Chalmers,** Harvard University, Cambridge, Mass.

Publishes theoretical and experimental studies emphasizing those aspects of the science of materials concerned with the relationship between the structure of solids and their properties (mechanical, electrical, magnetic, optical and chemical) and with the thermodynamics, kinetics and mechanisms of the processes which can occur within the material. Letters to the Editor now published separately in Scripta Metallurgica. Abstracts in language of article, English, French and German.

Volume 17 (1969) £ 30.0.0 $ 75.00 DM 300,–
Monthly
2 years (1969–1970) £ 54.0.0 $135.00 DM 540,–
Single copy £ 3.0.0 $ 7.50 DM 30,–

Pergamon Press Ltd. · Headington Hill Hall · Oxford OX3 OBW

Pergamon Press Inc. · Maxwell House · Fairview Park · Elmsford, New York 10 523

Friedr. Vieweg + Sohn GmbH · 3300 Braunschweig · Postfach 185